

UNIVERSITY of SOUTHAMPTON
SCHOOL of ENGINEERING SCIENCES
SHIP SCIENCE

Modelling of Excitation and Response Induced by Impact:
An Investigation for Slamming of Mono- and Multi-Hulled Vessels

M.Phil. Thesis

Supervisor : Prof.P.Temarel

Research Student: S. Demirtas



16/10/2005

ABSTRACT

Waves, winds and currents can cause specific environmental effects that a marine structure has to withstand. Amongst these, wave action is the fundamental source of load on the marine structure. In order to ensure safety, operability, economy and design-life duration of a marine structure, theoretical estimates of wave loads and structural response play an increasingly important role in the overall design process.

The interaction between a structure and a fluid medium is of great concern in numerous engineering problems, e.g., slamming of ships in rough seas, vibration of water retaining structures under earthquake loading etc. All these dynamic problems include the interaction, which takes place between the structure and surrounding fluid. It is of practical importance to estimate the effect of the induced fluid loading on the dynamic state of the vibrating structure. If the vibration takes place in a relatively low-density fluid, such as air, in comparison with the structural material, in most situations, the loading will have a comparatively small influence on the vibration. However, when the vibrating structure is in contact with a fluid which has a comparable density, such as water, the fluid loading which depends on the structural surface motions will significantly alter the dynamic state of the structure from that of the in vacuo vibration. In other words, the equations of structural and fluid motions are inexorably linked. Therefore, development, improvement and application of numerical techniques for analyzing such an interaction become one of the most important activities of naval architecture researchers.

The following document is about the interaction mentioned above and particularly studied on the slamming issue and its main characteristic, transient excitation and response.

A dry analysis is presented on simple beams, idealized SWATH ship as a preamble to a future wet deck slamming analysis and plates (unstiffened and stiffened). As the basis of subsequent harmonic and transient analyses, modal characteristics of each system is studied and in conjunction with the results obtained from these, responses on frequency and time domain are calculated in this document.

In the following part of the thesis beams and plates are analysed under transient excitation, since this is the basis for modelling the excitation and response induced by slamming. Results are produced and compared both using theoretically established convolution method and ANSYS (transient analysis with full and mode superposition methods).

Realistic stiffened plates and their equivalent flat plates are also studied and analysed in the subsequent sections. Difficulties encountered during the structural modelling (finite element modelling) are briefly outlined, with particular emphasis to the importance of the selection of appropriate finite elements.

Table of Contents

| | |
|---|----|
| ABSTRACT | 2 |
| Table of Contents | 3 |
| List of Figures | 5 |
| List of Tables | 12 |
| Nomenclature | 14 |
| Acknowledgements | 16 |
| 1. INTRODUCTION | 17 |
| 1.1. Aims and Objectives | 17 |
| 1.2. Layout of the Thesis | 18 |
| 2. BACKGROUND and LITERATURE SURVEY | 20 |
| 2.1. Rigid Body Analysis | 21 |
| 2.1.1. Two-Dimensional Hydrodynamics | 25 |
| 2.1.2. Three-Dimensional Hydrodynamics | 31 |
| 2.2. Hydroelasticity | 33 |
| 2.2.1. Two-Dimensional Hydroelasticity | 37 |
| 2.2.2. Three-Dimensional Hydroelasticity | 39 |
| 2.3. Slamming | 42 |
| 2.4. Stiffened Flat Plates | 54 |
| 2.4.1. Orthotropic Plate Approximation | 55 |
| 2.4.2. Grillage Approximation | 57 |
| 2.4.3. Plate and Beam Idealizations | 57 |
| 3. PERIODIC RESPONSE of UNIFORM BEAMS | 64 |
| 3.1. Modal Analysis of Beams | 64 |
| 3.1.1. Free-Free Uniform Beam | 66 |
| 3.1.2. Pinned-Pinned Uniform Beam | 67 |
| 3.2. Numerical Modal Analysis of Beams | 67 |
| 3.2.1. Free-Free Uniform Beam | 68 |
| 3.2.2. Pinned-Pinned Uniform Beam | 69 |
| 3.3. Determination of Generalized Coordinates | 71 |
| 3.4. Analytical Calculation of the Beam Deflections | 75 |

| | |
|---|-----|
| 3.5. Comparison of Numerical Results with Theoretical Calculations on the Frequency Domain | 77 |
| 3.5.1. Undamped Condition | 77 |
| 3.5.2. Damped Condition | 78 |
| 3.6. Discussion | 80 |
| 4. DRY ANALYSIS of a SWATH | 83 |
| 4.1. Modelling of a Uniform Idealised SWATH Ship by ANSYS | 83 |
| 4.1.1. Modal Analysis of the Idealised SWATH Ship by ANSYS | 87 |
| 4.2. Comparison of FEA Results with an Existing Study on the Similar Model SWATH and Discussion | 89 |
| 5. THEORETICAL and NUMERICAL MODELLING of TRANSIENT ANALYSIS | 90 |
| 5.1. Impulse Excitation | 90 |
| 5.1.1. Response to an Impulse | 90 |
| 5.1.2. Response to a General Forcing Condition-Arbitrary Excitation | 93 |
| 5.2. Transient Response of the Beams | 93 |
| 5.2.1. Methodology | 95 |
| 5.2.2. Pinned-Pinned Uniform Beam | 96 |
| 5.2.3. Free-Free Uniform Beam | 102 |
| 5.2.4. Conclusive Remarks | 104 |
| 5.3. Transient Response of the Flat Unstiffened and Stiffened Plates | 105 |
| 5.3.1. Theory of Plates | 105 |
| 5.3.2. Transient Response | 106 |
| 5.3.3. Verification of Modal Analysis | 107 |
| 5.3.4. Analysis of Plates (6m x 12m) | 110 |
| 5.3.5. Analysis of a Realistic Plate (Tanker Bottom Forward end) | 124 |
| 5.3.6. Equivalent Flat Plate | 143 |
| 5.3.7. Conclusive Remarks | 150 |
| 6. CONCLUSIONS | 152 |
| 7. RECOMMENDATIONS FOR FURTHER WORK | 155 |
| REFERENCES | 156 |
| APPENDIX – A – Complementary figures relating to beam analysis | 171 |
| APPENDIX – B – Complementary figures relating to plate analysis | 174 |

List of Figures

| | |
|--|----|
| Figure 1 Six degrees of freedom for rigid body motions..... | 21 |
| Figure 2 Coordinate system..... | 23 |
| Figure 3 The hull slice | 26 |
| Figure 4 Stiffened plate (Tanaka et al., 1998) | 55 |
| Figure 5 Orthotropic plate idealization (Bedair,2 1997)..... | 56 |
| Figure 6 A beam in bending(Rao, 1995) | 64 |
| Figure 7 Free-free uniform beam..... | 66 |
| Figure 8 Pinned-pinned uniform beam..... | 67 |
| Figure 9 2D-Elastic beam element used in the FE modelling of the beams..... | 68 |
| Figure 10 Mode shapes and natural frequencies of free-free uniform beam-ANSYS.68 | |
| Figure 11 Comparison of natural frequencies obtained theoretically and numerically for F-F beam..... | 69 |
| Figure 12 Mode shapes and natural frequencies of pinned-pinned uniform beam- ANSYS..... | 69 |
| Figure 13 Comparison of natural frequencies obtained theoretically and numerically for P-P beam..... | 70 |
| Figure 14 FEA model of the uniform pinned-pinned beam..... | 76 |
| Figure 15 Theoretical and numerical comparisons of forced-undamped nodal responses at node 5 (F at node 11), using 5,10 and 17 modes in the harmonic mode superposition method-Both the amplitude and zoomed in plots shown respectively | 77 |
| Figure 16 Theoretical and numerical comparisons of forced-damped (dmp.r.=0.01) nodal responses at node 5 (F at node 11), using 5,10 and 17 modes in the harmonic mode superposition method- Both the amplitude and zoomed in plots shown respectively | 78 |
| Figure 17 Theoretical and numerical comparisons of forced-damped (dmp.r.=0.01) nodal responses at node 5 (F at node 12), using 5,10 and 17 modes in the harmonic mode superposition method-Both the amplitude and zoomed in plots shown respectively | 79 |

| | |
|--|----|
| Figure 18 Comparison of amplitudes obtained from harmonic excitation-ANSYS (F at node 12) with and without damping (dmp.r.=0.01) | 79 |
| Figure 19 Comparison of amplitudes obtained from harmonic excitation-analytical (F at node 12) with and without damping (dmp.r.=0.01) | 79 |
| Figure 20 Comparison of amplitudes (at node 7) obtained from ANSYS (F at node 11) using different damping ratios-Both the amplitude and zoomed in plots shown respectively | 80 |
| Figure 21 Comparison of amplitudes (at node 7) obtained from 17 mode harmonic superposition (F at node 11) using different damping ratios-Both the amplitude and zoomed in plots shown respectively..... | 80 |
| Figure 22 BEAM44 3-D Tapered unsymmetric beam (ANSYS Elements reference) | 84 |
| Figure 23 SHELL63 Elastic shell (ANSYS Elements reference)..... | 85 |
| Figure 24 Comparison of offset and non-offset element application, based on the real constant descriptions | 85 |
| Figure 25 Visualization of elements in the model, based on the real constant descriptions | 86 |
| Figure 26 Finite element idealization of the SWATH model..... | 86 |
| Figure 27 Comparison of the natural frequencies of the SWATH-like vessel modeled by Wu and the similar one modeled in this document..... | 89 |
| Figure 28 Unit impulse (Rao, 1995) | 91 |
| Figure 29 Impulse response function (Rao, 1995)..... | 91 |
| Figure 30 Arbitrary forcing function (Rao, 1995) | 92 |
| Figure 31 Impulse at arbitrary time (Rao,1995) | 92 |
| Figure 32 Conversion of a continuous function into a discrete one | 95 |
| Figure 33 Pinned-Pinned uniform beam..... | 96 |
| Figure 34 Rectangular, triangular and sinusoidal pulses used in the transient analysis | 96 |
| Figure 35 Comparison of ANSYS results against convolution sum results using two different time intervals such as dt=0.01s. and dt=0.002s. for the transient response of the pinned-pinned beam as displacements(uz) at node 11 to a triangular impulse as shown in section 5.2.2 | 97 |

| | |
|---|-----|
| Figure 36 Convergence analysis of different number of modes in the transient response of pinned-pinned beam as displacements (uz) at node 11 under triangular impulse, using mode superposition with dmp.r.=0.01 and discrete time interval dt=0.002s..... | 98 |
| Figure 37 Comparison of analytical results against convolution sum results using two different time intervals such as dt=0.01s. and dt=0.002s. for the transient response of the pinned-pinned beam as displacements (uz) at node 11 to a sinusoidal impulse as shown in section 5.2.2..... | 99 |
| Figure 38 Convergence analysis of different number of modes in the transient response of pinned-pinned beam as displacements (uz) at node 11 under sinusoidal impulse, using mode superposition with dmp.r.=0.01 and discrete time interval dt=0.002s..... | 100 |
| Figure 39 Convergence analysis of different number of modes in the bending moment response of pinned-pinned beam at element 11 under sinusoidal impulse, using mode superposition with dmp.r.=0.01 and discrete time interval dt=0.01s..... | 101 |
| Figure 40 Convergence analysis of different number of modes in the bending moment of pinned-pinned beam at element 11 under sinusoidal impulse, using mode superposition with dmp.r.=0.01 and discrete time interval dt=0.002s..... | 102 |
| Figure 41 Convergence analysis of different number of modes in the bending moment response of the free-free beam at element 11 under sinusoidal impulse, using mode superposition with dmp.r.=0.01 and discrete time interval dt=0.01s..... | 103 |
| Figure 42 Convergence analysis of different number of modes in the bending moment response of the free-free beam at element 11 under sinusoidal impulse, using mode superposition with dmp.r.=0.01 and discrete time interval dt=0.002s..... | 103 |
| Figure 43 Uniform rectangular plate (Meirovitch, 1967) | 106 |
| Figure 44 Uniaxially stiffened clamped (fixed end) plate with single stiffener(Rikards, 2001) | 108 |
| Figure 45 Selected vibration modes of shell stiffened plate..... | 109 |
| Figure 46 Comparison of vibration mode 20 for beam and shell models (Stiffened clamped plate)..... | 110 |
| Figure 47 Geometry of the unstiffened flat plate used in the analysis | 111 |
| Figure 48 Stiffened plate models in three directions | 112 |

| | |
|---|-----|
| Figure 49 Plates with and without tripping..... | 115 |
| Figure 50 uz-displacements at node 391 for all fixed ended plate variations covered in the text (ANSYS) | 116 |
| Figure 51 Nodal responses (uz-displacements) for longitudinally stiffened beam under triangular impulse with damping ratio 0.01 and 0.5, discrete time interval $dt=0.005$ | 117 |
| Figure 52 Convergence of modes for clamped longitudinal beam-stiffened plate (Disp. UZ)..... | 118 |
| Figure 53 Convergence of modes for clamped transverse beam-stiffened plate (Disp. UZ)..... | 118 |
| Figure 54 Convergence of modes for clamped orthogonal beam-stiffened plate (Disp. UZ)..... | 119 |
| Figure 55 Comparison of responses between ANSYS and the numeric method using $dt=0.01s$. at node 507 of the orthogonal beam stiffened model..... | 120 |
| Figure 56 Comparison of responses between ANSYS and the numeric method using $dt=0.005s$. at node 507 of the orthogonal beam stiffened model..... | 121 |
| Figure 57 Comparison of responses between ANSYS and the numeric method using $dt=0.005s$. and $dt=0.001s$. respectively at node 507 of the orthogonal beam stiffened model..... | 121 |
| Figure 58 Convergence of modes for clamped longitudinal beam-stiffened plate (Strs. SX) | 122 |
| Figure 59 Convergence of modes for clamped transverse beam-stiffened plate (Strs. SX) | 122 |
| Figure 60 Convergence of modes for clamped orthogonal beam-stiffened plate (Strs. SX) | 123 |
| Figure 61 Model of tanker bottom forward end studied in ANSYS..... | 125 |
| Figure 62 First six mode shapes of the stiffened (Beam-44) tanker plate..... | 126 |
| Figure 63 Example of two merged Shell-63 stiffeners (e.g. model (2:4))..... | 127 |
| Figure 64 Some of the coupled vibration mode shapes and natural frequencies of model (4:8)..... | 128 |
| Figure 65 Some of the coupled vibration mode shapes and natural frequencies of model (4:7)..... | 129 |

| | |
|--|-----|
| Figure 66 Some of the coupled vibration mode shapes and natural frequencies of model (1:1)..... | 130 |
| Figure 67 Some of the coupled vibration mode shapes and natural frequencies of model (1:1) [*] | 131 |
| Figure 68 Contour plots of static UZ translation (Beam-44 stiffened model)..... | 132 |
| Figure 69 Contour plots of static UZ translation (model (1:1))..... | 133 |
| Figure 70 Contour plots of static UZ translation (model (1:1) [*]) | 133 |
| Figure 71 Double bottom tanker panel | 134 |
| Figure 72 Mode characteristics of double bottom panel..... | 135 |
| Figure 73 Comparison of uz-displacements obtained from numerical method and ANSYS at node 92 for stiffened tanker plate..... | 136 |
| Figure 74 Comparison of sx-direct stresses obtained from numerical method and ANSYS at node 92 for stiffened tanker plate..... | 137 |
| Figure 75 Transient response comparison of Shell63(x:x) to Beam 44 models..... | 138 |
| Figure 76 Beam44 transient response using Full Method and Mode Sup. Method.. | 140 |
| Figure 77 Convergence plots of displacements obtained by ANSYS & Numerical Method | 140 |
| Figure 78 Convergence comparison when time interval is decreased in Numerical method. F at node 198, UZ at node 198 | 141 |
| Figure 79 Convergence comparison when time interval is decreased in Numerical method. F at node 146, UZ at node 146 & 137 | 142 |
| Figure 80 Harmonic response convergence plots of Beam44 model | 143 |
| Figure 81 Static response results obtained both for original (first 2 graphs) and equivalent (last 2 graphs) plate from ANSYS..... | 144 |
| Figure 82 Node references..... | 145 |
| Figure 83 Static responses-F at 391 and F at 219 vs. various nodal responses | 145 |
| Figure 84 Comparison of modal responses for FEHBeam stiffened and equivalent plates | 146 |
| Figure 85 Original vs equivalent plate transient responses F at node 391, UZ at nodes 219,391,507,559 | 147 |
| Figure 86 Original vs equivalent plate transient responses F at node 219, UZ at nodes 219,391,507,559 | 147 |

| | |
|--|-----|
| Figure 87 Original vs. equivalent plate harmonic responses F at node 391, UZ at nodes 219,391,507,559 | 148 |
| Figure 88 Original vs equivalent plate harmonic responses F at node 219, UZ at nodes 219,391,507,559 | 149 |
| Figure 89 Comparison of ANSYS results against convolution sum results using two different time intervals such as dt=0.01s and dt=0.002s for the transient response of the pinned-pinned beam at node 11 to a rectangular impulse as shown in section 5.2.2 | 171 |
| Figure 90 Mode shapes of the pinned-pinned beam..... | 172 |
| Figure 91 Modal bending moments of the pinned-pinned beam..... | 173 |
| Figure 92 First 12 mode shapes of single stiffened (Beam44) clamped plate-24x24 mesh | 174 |
| Figure 93 First 12 mode shapes of single stiffened (Shell63) clamped plate-24x24 mesh | 175 |
| Figure 94 Mode shapes and natural frequencies of the unstiffened flat fixed ended (clamped) plate..... | 176 |
| Figure 95 Mode shapes and natural frequencies of the longitudinally stiffened (Shell99-no tripping), fixed end flat plate (Shell99)..... | 177 |
| Figure 96 Mode shapes and natural frequencies of the transversely stiffened (Shell99-no tripping), fixed end flat plate (Shell99)..... | 178 |
| Figure 97 Mode shapes and natural frequencies of the orthogonal stiffened (Shell99-no tripping), fixed end flat plate (Shell99)..... | 179 |
| Figure 98 Mode shapes and natural frequencies of the longitudinal stiffened (Beam44), fixed end flat plate (Shell99)..... | 180 |
| Figure 99 Mode shapes and natural frequencies of the transversely stiffened (Beam44), fixed end flat plate (Shell99)..... | 181 |
| Figure 100 Mode shapes and natural frequencies of the orthogonal stiffened (Beam44), fixed end flat plate (Shell99)..... | 182 |
| Figure 101 Mode shapes and natural frequencies of the longitudinal stiffened (Shell99), fixed end flat plate (Shell99)..... | 183 |
| Figure 102 Mode shapes and natural frequencies of the transversely stiffened (Shell99), fixed end flat plate (Shell99)..... | 184 |

| | |
|---|-----|
| Figure 103 Mode shapes and natural frequencies of the orthogonal stiffened (Shell99), fixed end flat plate (Shell99)..... | 185 |
| Figure 104 uz-displacements at node 391 for long., transv. and orth. stiffened plates under triangular pulse..... | 186 |
| Figure 105 UZ-displacements at node 391 for clamped long. stiffened plate using 1-25 transient mode superposition, dmp.r.=0.08, dt=0.005s. | 187 |
| Figure 106 UZ-displacements at node 391 for clamped transv. stiffened plate using 1- 25 transient mode superposition, dmp.r.=0.08, dt=0.005s. | 188 |
| Figure 107 UZ-displacements at node 391 for clamped orth. stiffened plate using 1-25 transient mode superposition, dmp.r.=0.08, dt=0.005s. | 189 |
| Figure 108 Unstiffened clamped plate uz- amplitudes and sx-stresses for nodes 391, 559,507..... | 190 |
| Figure 109 Fixed ended (FE) long. stiffened plate, uz-amplitudes at node 559 for three types of stiffening elements, numerical method dt=0.005s. | 191 |
| Figure 110 Fixed ended (FE) transv. stiffened plate, uz-amplitudes at node 559 for three types of stiffening elements, numerical method dt=0.005s. | 192 |
| Figure 111 FE orth. stiffened plate, uz-amplitudes at node 559 for three types of stiffening elements, numerical method dt=0.005s. | 193 |
| Figure 112 FE orth. stiffened plate, uz-amplitudes at node 559 for three types of stiffening elements, numerical method dt=0.001s. | 194 |
| Figure 113 FE long. stiffened plate, sx-stresses at node 559 for three types of stiffening elements, numerical method dt=0.005s. | 195 |
| Figure 114 FE transv. stiffened plate, sx-stresses at node 559 for three types of stiffening elements, numerical method dt=0.005s. | 196 |
| Figure 115 FE orth. stiffened plate, sx-stresses at node 559 for three types of stiffening elements, numerical method dt=0.005s. | 197 |
| Figure 116 FE orth. stiffened plate, sx-stresses at node 559 for three types of stiffening elements, numerical method dt=0.001s. | 198 |
| Figure 117 Modal uz-deflections at node 219 for three different stiffening directions | 199 |
| Figure 118 Modal uz-deflections at node 391 for three different stiffening directions | 200 |

| | |
|---|-----|
| Figure 119 Modal sx-direct stresses at node 391 for three different stiffening directions..... | 201 |
| Figure 120 First six mode shapes of the stiffened (Beam-44) tanker plate (Profile view)..... | 202 |
| Figure 121 7-12 mode shapes of the stiffened (Beam-44) tanker plate..... | 202 |
| Figure 122 7-12 mode shapes of the stiffened (Beam-44) tanker plate (Profile view)..... | 203 |
| Figure 123 Comparison of uz-displacements obtained from numerical method and ANSYS at node 146 for stiffened tanker plate..... | 203 |
| Figure 124 Comparison of sx-direct stresses obtained from numerical method and ANSYS at node 146 for stiffened tanker plate..... | 204 |
| Figure 125 Comparison of uz-displacements & sx-direct stresses obtained from numerical method and ANSYS at node 112 for stiffened tanker plate..... | 204 |
| Figure 126 Full method-Original vs equivalent plate transient responses F at node 391, UZ at nodes 219,391,507,559 | 205 |
| Figure 127 Full method-Original vs equivalent plate transient responses F at node 219, UZ at nodes 219,391,507,559 | 205 |
| Figure 128 Full method-Original vs equivalent plate harmonic responses F at node 391, UZ at nodes 219,391,507,559 | 206 |
| Figure 129 Full method-Original vs equivalent plate harmonic responses F at node 219, UZ at nodes 219,391,507,559 | 206 |

List of Tables

| | |
|---|----|
| Table 1 Comparison of natural frequencies (Hz) for F-F beam after numerical and analytical solutions..... | 69 |
| Table 2 Comparison of natural frequencies (Hz) for P-P beam after numerical and analytical solutions..... | 70 |
| Table 3 Generalized masses of the free-free beam (consisting of 20 finite elements) for modes 1-5 corresponding to actual modes 4-5-7-8-10 | 73 |
| Table 4 Generalized masses of the pinned-pinned beam(consisting of 20 finite elements) for modes 1-7 corresponding to actual modes 1-2-3-5-7-8-10 | 74 |

| | |
|---|-----|
| Table 5 Generalized masses of the free-free beam (consisting of 20 finite elements) for modes 1-5 corresponding to actual modes 4-5-7-8-10 | 74 |
| Table 6 Generalized masses of the pinned-pinned beam(consisting of 20 finite elements) for modes 1-7 corresponding to actual modes 1-2-3-5-7-8-10 | 74 |
| Table 7 The values of undamped case amplitudes (in meters) at node 5 (F applied at node 11) on the frequency domain between ANSYS and theory (superposition of first 5,10, and 17 modes)..... | 77 |
| Table 8 The values of damped case (dmp.r.=0.01) amplitudes (in meters) at node 5 (F applied at node 11) on the frequency domain between ANSYS and theory (superposition of first 5,10, and 17 modes)..... | 78 |
| Table 9 Comparison of natural frequencies obtained from ANSYS in this current document and the modal analysis done by Wu (1984). | 89 |
| Table 10 Natural Frequencies of the pinned-pinned beam (Hz)..... | 96 |
| Table 11 Natural Frequencies of free-free beam (Hz)..... | 102 |
| Table 12 Experimental and numerical frequencies of single stiffened clamped plate | 108 |
| Table 13 Table of the natural frequencies and the node lines for all the plate models | 113 |
| Table 14 UZ-translations at 8 different nodes (Beam-44 stiffened model)..... | 132 |
| Table 15 UZ-translations at 8 different nodes (model (1:1))..... | 133 |
| Table 16 UZ-translations at 8 different nodes (model (1:1) [*]) | 133 |
| Table 17 Natural frequencies..... | 146 |

NOMENCLATURE

The definitions of a given symbol in the document are given in this section.

-Through out the document, overdots signify differentiation with respect to time, primes signify differentiation with respect to space.

-Symbols are also defined where they appear in the text.

| | |
|-----------|--|
| A | Cross section area |
| A_{mn} | Vibration amplitude for plates |
| a_{π} | Generalised added mass |
| [a] | Generalised mass matrix |
| $B(x)$ | Sectional beam |
| b_{π} | Generalised added damping |
| [b] | Generalised damping matrix |
| c_{π} | Generalised added stiffness |
| [c] | Generalised stiffness matrix |
| D | Bending flexural rigidity for plates |
| E | Young's modulus |
| EI | Flexural rigidity |
| F, f | Force |
| G | Shear modulus |
| $G(x)$ | Shape factor |
| g | Acceleration of gravity |
| I | Moment of inertia |
| [K] | Stiffness matrix |
| k_{AG} | Shear rigidity |
| L, l | Length |
| M | Bending moment |
| [M] | Mass matrix |
| p | Pressure |
| p_r | Principal coordinate corresponding to the r^{th} mode shape |

| | |
|--------------|--|
| $\{p_r\}$ | Principal coordinate vector for six rigid body modes |
| T | Sampling period |
| t | time/thickness |
| \bar{U} | Forward speed |
| u_i | Rigid body degrees of freedom ($i=1,2..6$) |
| \mathbf{V} | Velocity vector |
| V | Shear force |
| v | Horizontal transition |
| w | Vertical transition |
| w_r | Mode shape |
| X, x | Longitudinal Cartesian coordinates axes |
| Y, y | Horizontal Cartesian coordinates axes |
| Z, z | Vertical Cartesian coordinates axes |
| α | Shear damping constant |
| β | Bending damping constant |
| Δ | Displacement |
| Δt | Time increment |
| δ | Kronecker delta |
| θ | Rotation |
| μ | Mass per unit length |
| ν | Poisson ratio |
| ν_r | Modal damping factor |
| ζ | Damping ratio |
| γ | Shear strain |
| ρ | Density |
| Φ | Velocity potential |
| ω_r | Modal natural frequency |
| Σ | Summation |
| ∇ | Gradient operator |
| ∇^2 | Laplacean operator |
| { } | Vector |

ACKNOWLEDGEMENTS

I would like to express my sincere thanks to Prof. P. Temarel for his valuable and patient inspiration and guidance throughout my work. Most of the time, he was more than a supervisor. Also many thanks; to Prof. W.G. Price for giving me the opportunity to work under the roof of this unique scientific institution and keeping interest in the work and to Dr. A. Ergin for supporting me to do this study and opening a new page in my life.

Special thanks to Dr. B. Uzunoglu, Dr. K. Yelen, Dr. S. E. Hirdaris, Dr. M. Meunier, Dr. R. Pemberton, Dr. M. Thibaudeau, Corrado Labriola and all other colleagues in the Department for their technical and moral support.

On a personal note my gratitude to my wife Yina Zheng Demirtas and Vera Thompson for being the most supportive and sharing every difficulty with me throughout my study.

Finally by no means least, the most special thanks go to my mother-Sevim Demirtas who gave me the inspiration and the support to be here today and to my dearest father-Avni Demirtas who is always in my heart.

1 INTRODUCTION

In order to ensure safety, operability, economy and design-life duration of a marine structure, theoretical estimates of loads and structural response play an important role in the overall design process. Especially in slamming, due to its severe nature, the interaction between a structure and a fluid medium is of great concern.

Therefore, modelling of excitation and response induced by impact and development, improvement and application of numerical techniques that can be used to analyze slamming on mono- and multi-hulled vessels are investigated in this document.

In the analysis, whilst allowing for local structural details, it is also important to acknowledge the effects of these details on modelling and response side of the problem, such as accuracy, simplicity or complexity. Subsequently, under the influence of these ideas, the overall aims and objectives of this study are given as in next section.

1.1 Aims and Objectives

The aim of this proposed research is to generate mathematical models for excitation and response due to impact slamming which also take into account the local structural details and material properties in mono- and multi-hulled vessels.

The objectives of this research project are mainly:

- To generate mathematical models simulating impact excitation and response whilst allowing for the influence of structural configuration and material properties, such as;
 - stiffened and unstiffened flat plates,
 - longitudinal, transversal and orthogonal stiffening,
 - stiffened and unstiffened wedge shapes of varying deadrise angles to stand for the bow visualization,

The following objectives were further envisaged, towards a PhD thesis:

- To incorporate these mathematical models in two and three dimensional fluid-structure interaction software to simulate the impact slamming of high speed mono- and multi-hulled vessels
- To investigate the possibilities of reducing impact induced loads by ways of active or passive systems (e.g. smart materials, damping mechanisms)

1.2 Layout of the Thesis

The thesis is arranged in 7 chapters. Chapter 2 is intended to give a brief background, beginning with ideal fluid equations for rigid body analysis and hydroelasticity theory for elastic bodies, and then continuing with literature survey on the problem of slamming and the modelling of stiffened plates.

In chapter 3 modal analysis of simple beams is studied using ANSYS and results are compared with theory. This work was carried out to gain a better understanding of the fundamentals in modelling “dry” dynamic analysis of beamlike structures. The modal characteristics are later used in the frequency domain response analysis of the beams.

Chapter 4 represents the dry analysis of a SWATH ship taken from the thesis of Wu (1984) and includes the comparisons between two models. This investigation was carried out to gain a better understanding of modelling the “dry” dynamic analysis of non-beamlike structures. It was the intention to use the wet deck of a twin-hulled vessel as an application of the impact model developed in this thesis.

In chapter 5 transient analyses of beams and plates is presented. Modal characteristics are obtained prior to obtaining the transient response through the mode superposition method. Impulse excitations such as triangular, rectangular and sinusoidal are applied to the beam and plate models. Transient responses are found using ANSYS FEA program and using the, so-called, numerical method (mode superposition) throughout this document. Results from these two methods are compared and studied. Towards the end of chapter 5 issues related to modelling stiffened plates are investigated. Different directional stiffeners are included in the plate FE models using shell and

beam elements. Various combinations of stiffening and finite elements are considered in the modal and transient analyses. On the other hand particular examples of stiffened plates from literature are also used for the verification of FE modelling and modal analysis. A stiffened single bottom plate of a tanker is modelled and studied to see the response of a real system. The stiffened plate is studied dynamically using different finite elements and methods. At the end of chapter 5, a preliminary equivalent plate is created to represent structurally a stiffened flat panel and static and dynamic response comparisons are presented.

Conclusions of the work carried out and recommendations for future work are given in chapter 6 and chapter 7, respectively.

2 BACKGROUND and LITERATURE SURVEY

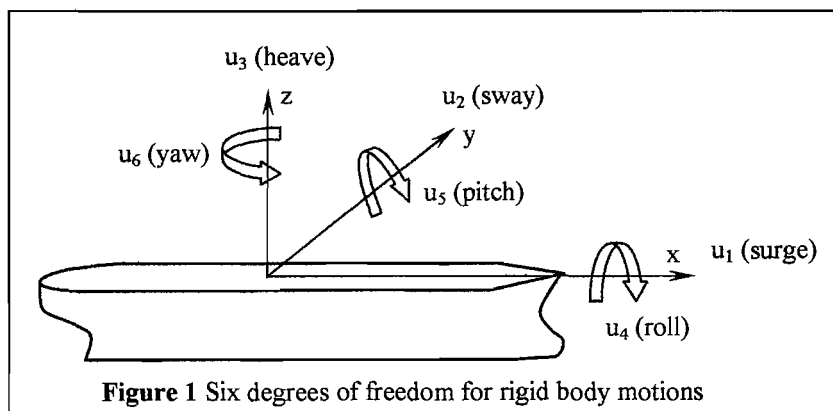
Accurate prediction of wave-induced motions and hydrodynamic loads is very important in ship design. In the design process, naval architect has to consider the initial cost, safety, reliability, operability and life duration of the floating structure. Empirical, quasi-static, hydrodynamic (i.e. rigid body analysis) and hydroelastic approaches can be the tools to analyze the interaction at different stages of the design.

Empirical rules are generally based on tests and past experience, which are costly and not open to progress. Static or quasi-static methods are used in the early stages of design (preliminary design) mainly in industry and by classification societies as a result of their simplicity.

In reality ships operate in conditions determined randomly by environment (e.g. wind, seaway etc.) which has dynamic characteristics. Traditionally the behaviour of a moving, floating structure in water can be divided into three. These are (Bishop et al, 1986); a) *manoeuvring* which deals with the behaviour of a rigid ship in calm water when it is subject to external actions caused by forced motion of rudder, stabilizer fins, propellers or thrusters. b) *Seakeeping*, which describes the responses of a rigid ship, moving or stationary, in regular sinusoidal waves or in a random seaway. In other words wave-induced motions of ships have been investigated widely under this topic. In order to predict the motions of a ship in waves, the ship is regarded as an unrestrained rigid body with six degrees of freedom. These degrees of freedom consist of three translation components, which are surge, heave and sway; and three rotation components, which are roll, pitch and yaw (Figure 1). c) *Structural theory*, based on empirical rules, which determine the loading, imposed on the structure, and then the use of structural analysis of a quasi-static nature. Since ships are treated as rigid bodies in seakeeping and manoeuvring theories, magnitudes and characteristics of bodily responses are the main interests. In other words rigid body assumption excludes the strains and stresses.

In linear hydrodynamics the unsteady motions of the ship and the fluid are assumed to be small. To be able to investigate the motions, the formulation of fluid-structure interaction is required. In this interaction, ship undergoes prescribed oscillatory motion in each of its six degrees of freedom in calm water causing radiation problem and at the same time as a result of diffraction problem incident waves act upon the ship in its equilibrium position. Evaluation of the fluid-structure interaction involves determination of added mass and damping coefficients (hydrodynamics), hydrostatic restoring coefficients and wave excitation forces and moments.

In the mid-seventies the hydroelasticity theory was developed and introduced (Bishop and Price, 1979) in order to provide more accurate predictions of the dynamic loads and responses of beamlike hulls travelling in random seas. In its most general form this approach subsumes both manoeuvring and seakeeping theories. This theory is extended to non-beamlike structures in the three dimensional hydroelasticity (Bishop et al, 1986). The advantage of hydroelasticity is that it is unified, that is to say it is capable of predicting the rigid body as well as the distortional responses of floating, fixed and submerged structures in a fluid domain.



2.1 Rigid Body Analysis

The study of wave loads, ship motions and structural responses has improved much due to the significant increase in size and speed of ships. Initially the ship hydrodynamics was studied on the roll motion of the steamships by Froude (1861). Kriloff (1896) studied the pitch and heave motions of ships with increasing power and speed. These two scientists derived differential equations of ship motions for the

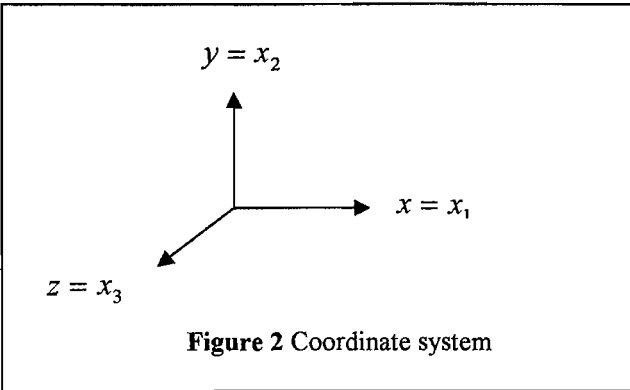
inertial and restoring forces of the ship. In their work, the pressure field of the undisturbed incident waves was considered and the resultant force on the ship has become known as the Froude-Krylov exciting force. Another major advance on the ship's hydrodynamic disturbance followed in a study by Lewis (1929) considering the added mass associated with hull vibrations in structural modes. In this study the characteristic frequency is sufficiently large, so that inertial effects are dominant and gravitational forces can be neglected. On the other hand Lewis assumed the ship hull to be slender and used a strip theory approach for the integration of the hydrodynamic force longitudinally in terms of the two-dimensional characteristics of each transverse section. This appears to be the first development of a strip theory in ship hydrodynamics (Newman, 1978). Later Haskind (1946a,b) used Green's theorem to construct the velocity potential due to the presence of the ship hull and derived the necessary Green's function or source potential. The velocity potential was decomposed into a form including separately the solution of the diffraction problem and solutions of the radiation problem for each mode of oscillatory ship motion.

According to the different treatment of the ship's hydrodynamic disturbance, theoretical studies of wave-ship interaction can be categorized into two- or three-dimensional problems to be solved in the time or frequency domain using linear or nonlinear methods. A brief overview of the methods is given in the following sections.

Idealized fluids can be analyzed mathematically by deleting stress tensor of the Navier-Stokes equation, which is generalized equation for the fluid motion. In the motion of an ideal fluid, the fundamental equations are the continuity equation and Euler's equations. The velocity vector $\mathbf{V} = (u_1, u_2, u_3)$ must satisfy the continuity and Euler's equations (Newman 1977),

$$\nabla \cdot \mathbf{V} = 0 \quad \text{or} \quad \frac{\partial u_1}{\partial x_1} + \frac{\partial u_2}{\partial x_2} + \frac{\partial u_3}{\partial x_3} = 0 \quad (1)$$

$$\frac{\partial u_i}{\partial t} + u_j \frac{\partial u_i}{\partial x_j} = -\frac{1}{\rho} \frac{\partial p}{\partial x_i} + \frac{1}{\rho} F_i \quad , \quad i = 1, 2, 3 \quad (2)$$



where, p is the normal pressure stress, ρ is the fluid density and F_i is the external force field which consist only of the gravitational force ρg acting vertically downwards.

$$\text{If } F_i = (0, -\rho g, 0) \quad \Rightarrow \quad \frac{\partial u_i}{\partial t} + u_j \frac{\partial u_i}{\partial x_j} = -\frac{1}{\rho} \frac{\partial}{\partial x_i} (p + \rho g x_2).$$

To simplify these equations, it is assumed that the motion is irrotational. An irrotational flow is one in which fluid elements moving in the flow field do not undergo any rotation. Further, if the velocity field is irrotational, it can be represented as the gradient of the scalar function ϕ , or the velocity potential. In other words, if the fluid motion is irrotational, the velocity can be derived from gradient of a scalar potential ϕ . The velocity potential ϕ exists only for irrotational flow. The reason for replacing the velocity by its potential is that the velocity can be envisaged and measured in the laboratory by experiments, whereas the velocity potential is no more than a mathematical abstraction. However, the velocity is a vector quantity with three unknown scalar components, whereas the velocity potential is a single scalar unknown from which all three-velocity components may be computed:

$$u_i = \frac{\partial \phi}{\partial x_i}, \quad (3)$$

or $\mathbf{V} = \nabla \phi. \quad (4)$

If equation (3) is substituted for the velocity vector in the continuity equation (1), the Laplace equation, which expresses conservation of fluid mass for potential flows and

provides the governing partial differential equation to be solved for the function ϕ , is attained

$$\frac{\partial}{\partial x_1} \frac{\partial \phi}{\partial x_1} + \frac{\partial}{\partial x_2} \frac{\partial \phi}{\partial x_2} + \frac{\partial}{\partial x_3} \frac{\partial \phi}{\partial x_3} = 0, \quad (5)$$

or

$$\nabla^2 \phi \equiv \frac{\partial^2 \phi}{\partial x_1^2} + \frac{\partial^2 \phi}{\partial x_2^2} + \frac{\partial^2 \phi}{\partial x_3^2} = 0. \quad (6)$$

Bernoulli's equation can be obtained by integrating the Euler's equations to give an explicit equation for the pressure. There are two flow cases for the presentation of Bernoulli's equation.

If the flow is considered to be steady, but non irrotational, then Euler's equations take the form (after omitting the time dependent terms)

$$u_j \frac{\partial u_i}{\partial x_j} = - \frac{\partial}{\partial x_i} (p / \rho + gx_2) \quad (7)$$

The pressure is obtained after integrating equations (7), as

$$p = -\frac{1}{2} \rho V^2 - \rho gx_2 + C, \quad (8)$$

where

$$V^2 = \sum u_i u_i = u^2 + v^2 + w^2. \quad (9)$$

The second form of Bernoulli's equation, valid for unsteady irrotational flows, is more useful since the flow of an inviscid fluid is generally irrotational but may be unsteady. It is obtained by substituting equation (3) in the general form of Euler equation (2) for $F_i = (0, -\rho g, 0)$,

$$\frac{\partial}{\partial t} \frac{\partial \phi}{\partial x_i} + \frac{\partial \phi}{\partial x_j} \frac{\partial}{\partial x_j} \frac{\partial \phi}{\partial x_i} = -\frac{1}{\rho} \frac{\partial}{\partial x_i} (p + \rho gx_2), \quad (10)$$

after integrating equation (10),

$$\frac{\partial \phi}{\partial t} + \frac{1}{2} \frac{\partial \phi}{\partial x_j} \frac{\partial \phi}{\partial x_j} = -\frac{1}{\rho} (p + \rho gx_2) + C(t), \quad (11)$$

the second form of Bernoulli's equation is obtained, where $C(t)$ may be chosen arbitrarily(equal to zero, deleted, etc.).

2.1.1 Two-Dimensional Hydrodynamics

Strip theory is the main tool of hydrodynamics. It gives an opportunity for a quick and reasonably accurate prediction of the wave loads. In its basic definition, strip theory is used to calculate the inertia loads and the fluid actions due to the wave-induced motions of a slender hull by dividing it into transverse strips in longitudinal direction. Hydrodynamic properties of added mass and damping are associated with each strip. The excitations induced by the waves and reciprocally experienced by the hull are evaluated using the hydrodynamic contribution of these strips.

Korvin-Kroukovsky (1955) first developed a strip theory for ship motions. Some refinements and extensive experimental comparisons were provided later by Korvin-Kroukovsky and Jacobs (1957). Grim and Schenzle (1969) generalized the strip theory to the prediction of roll, sway and yaw motions in oblique waves. Later, a range of linear strip theories has been proposed by Gerritsma and Beukelman (1964), Tasai and Takaki (1969) and probably the most cited and well-known strip theory of Salvesen et al. (1970).

The essence of strip theory is thus to reduce a three-dimensional hydrodynamic problem to a series of two-dimensional problems which are easier to solve. The major difficulty in determining the ship motions is to perform the calculations needed to find the coefficients of added mass, damping and the diffraction exciting forces, which requires the solution of difficult hydrodynamic problems.

If a body moves in an infinite ideal fluid, hydrodynamic pressure forces and moments will result which can be expressed most simply in terms of the added-mass coefficients.

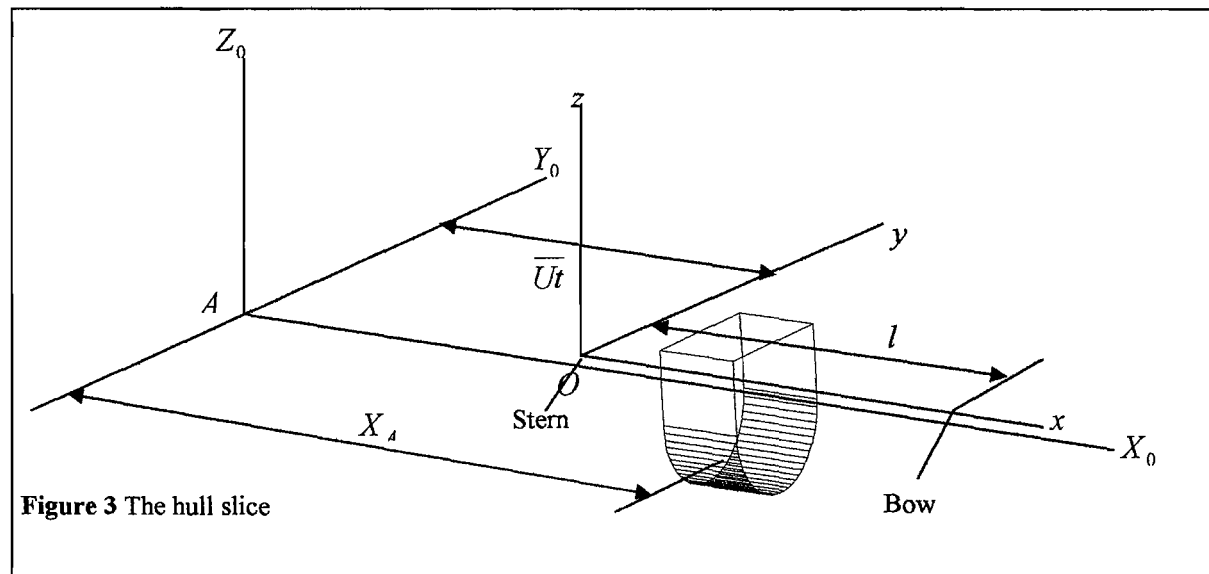
The added-mass coefficients physically represent the amount of fluid accelerated with the body. The added mass can be interpreted as a particular volume of fluid particles that are accelerated with the body. However, the particles of fluid adjacent to the body will accelerate to varying degrees, depending on their position relative to the body.

The three-dimensional added-mass coefficients can be approximated by a strip theory synthesis, in which the flow at each section is assumed to be locally two-dimensional. The flow field at any cross section of the ship may be approximated by the assumed two-dimensional flow in that strip. To obtain the total effect on the ship, the effects of all individual strips are integrated along the length. For example, the strip theory approximation for the heave added mass is

$$A_{33} = \int_L a_{33}(x)dx \quad (12)$$

where $a_{33}(x)$ is the two-dimensional added mass and L denotes that the integration is taken over the ship length.

In the process of estimation of hydrodynamic loading applied to the hull by a sinusoidal wave, fluid actions are estimated by means of strip theory. According to the theory it is thought that at some instant t , a slice of the hull lies in the plane of a slice of water. Strip theory predicts the force exerted by the fluid slice on its instantaneously coincident hull slice. In other words, strip theory seeks to predict the force applied by the strip of fluid to the hull (Bishop and Price, 1979).



In Figure 3 the thin slice of hull is normal to AX_0 , distant X_A from the origin A of the fixed axes and x from the origin O of the equilibrium axes. (Bishop and Price, 1979)

At time t , $X_A = \bar{U}t + x$

At the instant $t = 0$ when O coincided with A , $\frac{dx}{dt} = -\bar{U}$

The relative displacement of the ship and water surface is

$$\bar{z}(x,t) = w(x,t) - \zeta(x,t) \quad (13)$$

where $w(x,t)$ is the upward displacement of the section of the hull coincident with the strip and $\zeta(x,t)$ is the local surface elevation. The quantity $\bar{z}(x,t)$ is thus a measure of hull emergence at the water strip. The upward force per unit length exerted by the fluid on the hull, $F(x,t)$, is dependent upon $\bar{z}(x,t)$ and its total derivatives with respect to time.

$$F(x,t) = -\left\{ \frac{D}{Dt} \left[m(x) \frac{D\bar{z}(x,t)}{Dt} \right] + N(x) \frac{D\bar{z}(x,t)}{Dt} + \rho g B(x) \bar{z}(x,t) \right\} \quad (14)$$

$m(x)$ is the local ‘added mass’ per unit length, $N(x)$ is the local ‘fluid damping coefficient’ and the operator $\frac{D}{Dt}$ is the total derivative with respect to time; that is

$$\frac{D}{Dt} = \frac{\partial}{\partial t} + \frac{\partial}{\partial x} \frac{dx}{dt} = \frac{\partial}{\partial t} - \bar{U} \frac{\partial}{\partial x} \quad (15)$$

$$\frac{D\bar{z}(x,t)}{Dt} = \left(\frac{\partial}{\partial t} - \bar{U} \frac{\partial}{\partial x} \right) \bar{z}(x,t) \quad (16)$$

$$\frac{D^2 \bar{z}(x,t)}{Dt^2} = \left(\frac{\partial}{\partial t} - \bar{U} \frac{\partial}{\partial x} \right)^2 \bar{z}(x,t) \quad (17)$$

$$F(x,t) = -m(x) \frac{D^2 \bar{z}(x,t)}{Dt^2} - \left[N(x) - \bar{U} \frac{dm(x)}{dx} \right] \frac{D\bar{z}}{Dt} - \rho g B(x) \bar{z}(x,t) \quad (18)$$

The relative displacement $\bar{z}(x,t)$ can be eliminated by introducing the quantity $[w(x,t) - \zeta(x,t)]$. $B(x)$ is the sectional beam. In this way it is found that

$$F(x,t) = -H(x,t) + Z(x,t) \quad (19)$$

where

$$H(x,t) = m(x) \frac{D^2 w(x,t)}{Dt^2} + \left[N(x) - \bar{U} \frac{dm(x)}{dx} \right] \frac{Dw(x,t)}{Dt} + \rho g B(x) w(x,t) \quad (20)$$

$$Z(x,t) = m(x) \frac{D^2 \zeta(x,t)}{Dt^2} + \left[N(x) - \bar{U} \frac{dm(x)}{dx} \right] \frac{D\zeta(x,t)}{Dt} + \rho g B(x) \zeta(x,t) \quad (21)$$

After using equations $\frac{D\zeta}{Dt} = -i\omega\zeta$ and $\frac{D^2\zeta}{Dt^2} = -\omega^2\zeta$ related with Smith correction

we find that

$$Z(x,t) = \left\{ m(x)\omega^2 - i\omega \left[N(x) - \bar{U}m'(x) \right] + \rho g B(x) \right\} \zeta(x,t) \quad (22)$$

The strip theories mentioned above all assume unsteady potential flow analysis and they assume the ship is slender, speed is moderate and hull sections are well sided. These strip theories are low-speed theories. However, Blok and Beukelman (1984) showed that the heave and pitch results from strip theory were still satisfactory when the Froude number reached 0.57~1.4.

Conformal mapping techniques are also used in literature to derive hydrodynamic properties such as added mass and damping for each section. Lewis and multi-parameter mapping are some examples to conformal mapping techniques. Multi-parameter conformal mapping also permits the transformation of asymmetric sections to a circle, where Lewis mapping is more suitable for hull sections, which are symmetric (Westlake et al, 2000). Investigations by Kerczek et al. (1969), Westlake et al. (2000) and textbook by Newman (1977) can be studied for further information on conformal mapping techniques.

Faltinsen and Zhao (1991a,b) have presented a modified liner strip theory (high speed strip theory), where the three-dimensional free surface boundary condition is used to interrelate the two-dimensional problems at each strip. Faltinsen (1993) generalized the high-speed slender body theory of Chapman (1975) to consider the interaction between the steady and unsteady flow fields around the ship. Since the two-dimensional velocity potential satisfies a three-dimensional free surface condition and the diverging wave system generated by the ship motion is included, the high-speed slender body theory is also called 2½-D method. This is the main difference to the conventional strip theory where the two-dimensional velocity potential satisfies a linearized two-dimensional free surface condition, so that only the transverse wave system is considered.

Linear strip theories have been widely used in the literature to estimate the performance of a ship in waves, due to their computational simplicity. However when the ship forward speed gets higher, it is no longer reasonable to apply the conventional strip theory, because the fluid field near the ship hull cannot be described sufficiently as a two dimensional flow. In addition strong nonlinearity is probably the most prominent feature of high-speed vessels even in moderate sea states (Wu and Moan, 1996). More over in the extreme seas due to large ship motions the nonlinearity problem arises. When the literature is investigated there are studies in which nonlinear ship motions and structural responses have been observed.

Existing nonlinear analyses can be categorized as perturbation or time-domain simulation methods. In the perturbation method the boundary conditions or the hydrodynamic coefficients and the responses are expanded into perturbation series and a sequence of linear problems in ascending order are solved separately in the frequency domain (Jensen and Pedersen, 1979, 1981). Based on this procedure Jensen and Pedersen (1979) developed a nonlinear quadratic strip theory formulated in the frequency domain for predicting wave loads and ship responses in moderate seas. According to their observation, the first order fluid forces are identical to those of the classical linear strip theory (Gerritsma and Beukelman, 1964), while quadratic terms arise due to the nonlinearity of the exciting waves, the flare of the ship hull geometry,

and the perturbation of the two-dimensional hydrodynamic coefficients. The limitation of this nonlinear analysis is that, if the perturbation parameter is larger, the higher order corrections will not improve the linear results (Wu and Moan, 1996).

The time simulation method on the other hand is the most suitable for describing the real nonlinear problem. Furthermore there are several advantages in using time-domain analysis compared to a frequency-domain analysis. Time-domain analysis can deal with the exact instantaneous body surface for large-amplitude motions of a vessel. Most importantly transient impact is easily treated in the time-domain. Because of its advantages, at the beginning scientists worked on developing nonlinear time domain strip methods extracted directly from frequency domain strip theory formulations. Some of these attempts are presented by Mayerhoff and Schlachter (1980), Yamamoto et al. (1980), and Guedes Soares (1989). These theories are found to be weak in irregular waves due to neglecting hydrodynamic memory effects and the hydrodynamic coefficients in the equations of motion.

The time-domain solution for the free surface hydrodynamics means to solve the initial boundary problem in the time-domain. The basic work was done by Finkelstein (1957). He systematically derived various time-domain free surface Green functions. Cummins (1962) decomposed the time-domain velocity potential in to instantaneous and memory parts based on the impulsive response function, separating the ship geometry from the ship motion. Ogilvie (1964) generalized this approach by including the forward speed.

De Kat and Paulling (1989) and Fonseca and Guedes Soares (1998) studied partly nonlinear strip theories based on time-domain potential flow representation or the Fourier transform of frequency dependent transfer functions. The fluid action consists of linear and nonlinear parts. The linear fluid forces are expressed by a time convolution as discussed by Cummins (1962). The nonlinear hydrostatic restoring force and the Froude-Krylov force are calculated accurately. These approaches are verified with experimental results from model tests (Xia and Wang, 1997). Fonseca and Guedes Soares (1998) presented a time domain strip method to predict the vertical

motions and sectional induced loads of ships in large amplitude waves. Their solution is obtained in the time-domain using convolution to account for the memory effects related to the free surface oscillations.

Watanabe and Guedes Soares (1999) presented a comparison between the predictions of different non-linear time-domain codes applied to study the vertical wave induced bending moment in a container ship in waves of different steepness. Most of the methods in this study are based on strip theory formulations applied to both rigid and flexible hull formulations. In the lower wave height region the results computed from different methods are similar, however, the agreement among the computed values becomes poor in the higher wave region.

2.1.2 Three-Dimensional Hydrodynamics

The linear two-dimensional theories are computationally efficient, but since the forward speed terms are neglected in the free surface boundary condition, they are not suitable for high-speed vessels. In this sense three-dimensional approaches can incorporate forward speed effects more properly. However, strip theories are efficient in evaluating symmetric motions for slender beamlike ships, these theories fail in the case of non-beamlike and high speed vessels. The need for three-dimensional theories is parallel to the developments in the design of high-speed multi-hull vessels and other ocean structures.

In literature, in order to consider the speed and three-dimensional effects, slender body theories are proposed. In these theories fluid domain is considered to be made of two parts, which are inner fluid field and outer (far) field. The inner fluid field is treated as a two-dimensional problem matched with a three-dimensional solution for the far field. The outer solution can be constructed from a singularity distribution method, known as Green function method (Panel method). In this method the mean wetted surface, which stands for the hull boundary, is discretized into panels. The singularities, which are located in the discretized boundary, satisfy the free surface condition. After evaluating the strength of singularities (sources), these are used to determine the fluid pressure and forces acting on the hull. (Fonseca and Guedes

Soares, 1998). Based on different solutions of the inner two-dimensional problem, different kinds of slender body theories have been proposed, such as the original slender body theory (Newman, 1964), which is a low frequency theory assuming the wave length of the incident waves in the same magnitude as the ship's length, the unified slender body theory (Newman, 1978) which eliminates the limitations of original theory on the wave lengths and encounter frequency, the high-speed slender body theory (Chapman, 1975), and the new slender body theory (Yeung and Kim, 1984).

Majority of three-dimensional solutions are based on the boundary integral equation method and the unsteady potentials are solved either in the frequency or in the time-domain, using Green function methods or Rankine source methods (Fonseca and Guedes Soares, 1998). Chang (1977) is the first who successfully applied the Green function method in the frequency domain. Inglis and Price (1980), Guevel and Bougis (1982) applied the method to a ship with steady forward speed. Other investigations also carried out on this method differing in the computation of the Green function, such as Wu and Eatock-Taylor (1987) and Ba and Guilbaud (1994). On the other hand, time domain linear solutions applying Green function method were presented by Liapis and Beck (1985), King et al. (1988) and Bingham et al. (1994).

Wenyang and Yishan (1999), studied the time-domain calculation of hydrodynamic forces on ships particularly with large flare in two and three-dimensional cases. In their two-dimensional and three-dimensional time-domain free surface Green function source distribution applications on large flared ship hulls (non wall sided), it is found that the source strength diverges with the time stepping which makes the calculation fail. In their 3-D application, as an alternative to panel method, they introduced a wall sided surface which encloses the hull surface in the fluid and used Green theorem to solve the problem.

Ye and Hsiung (1999) proposed an investigation based on Cummins' potential decomposition and Chapman's wave body interaction analysis to compute the ship motion with forward speed in regular head waves. They used impulse response

functions to solve the equations of motions in the time domain. They applied the method to compute the radiation forces of a catamaran with forward speed. It was noted that the time-domain computation for ship motions is particularly important in the cases where the forward speed effect is considered.

2.2 Hydroelasticity

Ships are treated as rigid bodies in seakeeping and manoeuvring studies, with interest focused on the magnitudes and characteristics of the bodily responses as mentioned in the previous section. A ship moves as a rigid body and also distorts. The rigid body motions are investigated as if the ship does not distort. However, this set of motions is only a subset of a larger group of motions for, in reality, a ship is a flexible structure capable of distorting in an infinite number ways. There is a simplification in the assumption of a rigid body that it excludes the ideas of strains and stresses. To overcome such limitations, hydroelasticity theory was developed, based on the fact that a flexible structure distorts through applied fluid actions, along with a mathematical model founded on the scientific principles of solid mechanics and fluid dynamics (Aksu et al., 1993). Hydroelasticity theory, in which the coupled hydrodynamic and structural dynamic problems are solved simultaneously, has been introduced to determine the wave-induced motion, internal forces and stresses more accurately.

Hydroelasticity is the study of the behaviour of a flexible body moving through a liquid. (Bishop et al., 1986). This describes the behaviour of a flexible ship hull or offshore structure distorting due to the actions of external fluid loading arising from the seaway, rudder, propeller, etc. The steady state and transient responses of flexible ship structures in regular and irregular seaways can be investigated employing hydroelasticity analysis. The theory involves a description of the structure of the vessel and the fluid actions applied to it. In its most general form, it encompasses both seakeeping and structural dynamics. The hydroelasticity theory of ships is a milestone in the study of wave-structure interaction.

There are two-dimensional and three-dimensional hydroelasticity theories to predict the responses (bodily motions, deflections, bending moment, shear force, twisting moment, stresses) at any point within a flexible structure excited by regular and irregular waves approaching the structure at an arbitrary heading angle. For beam-like ship structures, both symmetric (vertical bending) and anti-symmetric (lateral bending and twisting) responses can be predicted by the two-dimensional theory as well as the influence of hull slamming assessed. For flexible structures of arbitrary shape (e.g. jack-up structure, barge, multi-hulled vessels) a general three-dimensional hydroelasticity allows responses to be evaluated and the theory includes the ability to predict transient slamming responses excited in oblique seaways (Aksu et al., 1993). The principles of both two and three dimensional hydroelasticity theories are the same. The main difference is the employment of different methods in terms of idealization of the structure and the evaluation of the fluid-structure interaction. In two dimensional hydroelasticity theory, the structure is idealized as a Timoshenko beam whilst a strip theory is used to determine the hydrodynamic coefficients and wave excitation associated with rigid body motions and distortions (Bishop and Price, 1979). On the other hand for the three dimensional theory, a finite element idealization of the structure and a panel element discretisation of the wet surface of the hull is employed. In this case a source whose strength is determined from boundary conditions is situated at the center of each panel and use is made of suitable Green's functions (Bishop et al., 1986)

Evaluation of the dynamic loads and responses using hydroelasticity theory for a vessel travelling at arbitrary heading in regular waves and irregular seaways are lead by two subsequent approaches, dry and wet analysis. The dry or in vacuo analysis, in which the structure vibrates freely in vacuo, in the absence of any structural damping or external force and the wet analysis introducing the fluid actions, which are applied as an external loading to the flexible structure.

In describing the responses, it is necessary to assign coordinates to deflections at various degrees of freedom and one particular set of generalized coordinates, having the advantage of being unambiguous and easily commended, is the set of principal

coordinates of the dry structure. Hydroelasticity theory is based on this set of principal coordinates with six coordinates describing the rigid body motions and as many generalized coordinates as necessary describing the symmetric and anti-symmetric responses. This implies that it is necessary to analyze the behaviour of the flexible structure in vacuo (dry analysis) to evaluate the principal modes of corresponding to the principal coordinates, and in the wet analysis, when the structure is in fluid, all fluid actions are treated as externally applied generalized fluid forces acting on the structure (Aksu et al., 1993).

In the dry analysis, when the floating structure is a slender hull (beam-like ships), Timoshenko beam theory, in which the rotation of the cross section is considered as the sum of the shearing angle and the rotation of the neutral axis, can be used (Bishop and Price, 1979). On the other hand, for non-beam-like vessels, linear finite-element approach is convenient to be used to describe the dynamical behaviour of dry structure in vacuo.

According to the hydroelasticity theory developed for beam-like structures, the symmetric responses, vertical displacement $w(x,t)$, bending moment $M(x,t)$ and shear force $V(x,t)$ at any point along the structure measured from the stern can be expressed by summations in the form (for free-free beam representation) (Bishop and Price, 1979)

$$w(x,t) = \sum_{r=0}^N w_r(x)p_r(t) \quad (23)$$

$$M(x,t) = \sum_{r=2}^N M_r(x)p_r(t) \quad (24)$$

$$V(x,t) = \sum_{r=2}^N V_r(x)p_r(t) \quad (25)$$

where $p_r(t)$ denotes the r^{th} principal coordinate of the principal column vector $\{p(t)\}$ of order $N+1$.

Principal coordinate $\{p(t)\}$ is a solution of the equation, if we assume the generalized values in matrices belong to dry hull

$$[a]\{\ddot{p}(t)\} + [b]\{\dot{p}(t)\} + [c]\{p(t)\} = \{F(t)\} \quad (26)$$

where $[a]$ is the generalized mass matrix, $[b]$ is the generalized damping matrix, $[c]$ is the generalized stiffness matrix, $\{p(t)\}$ is the principal coordinate representing the response and $\{F(t)\}$ is the generalized force representing input loading. $[a]$, $[b]$ and $[c]$ are diagonal matrices, $\{p(t)\}$ and $\{F(t)\}$ are column vectors.

In general two-dimensional hydroelasticity theory, the dynamic responses against the excitation (i.e. motions, distortions, shearing forces, bending moments, and twisting moments) can be determined by using techniques of modal analysis. The ship's hull is assumed to be beam-like. Its dynamic characteristics are determined in a dry-hull analysis. By treating the hull as a non-uniform Timoshenko beam and adopting a suitable process for representing the continuous structure as one with finite number of degrees of freedom, a set of principal modes and natural frequencies may be determined.

In order to describe the fluid motion around oscillating deformable structures, the interface boundary condition must be given. Price and Wu (1985) presented a linear potential flow theory of flexible marine structures, where the classical kinematic rigid body (Timman-Newman) boundary condition for seakeeping problems (Newman, 1978) was generalized as the interface boundary condition. (Xia, 1996) gave a general linear boundary condition for hydroelastic analysis of arbitrarily shaped floating structures with ideal or viscous fluids.

The complexity of ship dynamics has led to the adoption of the most basic assumptions (Bishop and Price, 1991). The structural and hydrodynamic analyses are usually performed separately. Wave-induced motions of ships have been thoroughly studied in the field of seakeeping. When wave induced internal forces and structural performances of ships are to be examined, the fluid is put aside and all the fluid loads are assumed to be prescribed, for example, by seakeeping theory. These assumptions

bring some questions to discussion; if the natural frequencies associated with elastic deflections are within the spectrum of wave loads, the structure may suffer steady state global elastic vibration, referred as springing. On the other hand if the ship undergoes slamming, it may be accompanied by transient vibration, i.e. whipping. To be able to determine these fluid-induced structural responses accurately, the coupling effects between the structural and hydrodynamic problems cannot be neglected (Xia and Wang, 1997).

2.2.1 Two-Dimensional Hydroelasticity

In the two dimensional hydroelasticity, which is also referred as unified strip theory developed by Bishop and Price (1979), fluid actions are represented by strip theories (Gerritsma and Beukelman, 1964; Salvesen, Tuck and Faltinsen, 1970), while the generalized modes are composed of the rigid motion modes and the additional dry modes of the ship structure represented as a non-uniform beam vibrating in vacuo.

Bishop et al. 1977, Bishop et al. 1980 and Bishop et al 1986 applied this method on various beamlike ships to investigate symmetric, antisymmetric and unsymmetric dynamic behaviour in waves.

Beam model brings limitations to the analysis especially in the case of multi-hull vessels such as SWATH ship. Mainly the slender ship and high speed assumptions restrict the two-dimensional theory, since strip theory particularly takes into account monohulls which usually modelled as Timoshenko beams and zero forward speed.

To overcome the limitations imposed by two-dimensional strip-beam theory, Wu, Xia and Du (1991) proposed a general slender body hydroelasticity theory by extending Newman's unified ship motion theory (Newman, 1978) to admit distortions of the ship hull. The hull is treated as a Timoshenko beam. The resulting unified theory is valid generally for all wave frequencies of practical importance.

Hermundstad et al. (1994) presented a linear hydroelastic analysis of a high speed mono-hull which is based on modal technique (using dry modes) and involves a three

dimensional free surface condition with forward speed to predict the symmetric responses. The results suggested that the hydroelastic effect in linear responses is insignificant for most high-speed vessels as far as extreme values are concerned, but it may influence fatigue life.

(Hermundstad, 1995) reported a linear hydroelastic approach based on the 2½ dimensional fluid method (Zhao and Aarsnes, 1995), which is a slender body theory for ships moving at high forward speeds. Hermundstad et al. (1999) also used a similar method, which is the generalized version of the method presented by (Faltinsen and Zhao, 1991a,b) and investigated the linear hydroelastic analysis of high speed catamarans and monohulls in regular waves. In this modified method, they properly included the hydrodynamic interactions between catamaran hulls into the theory and they avoided the numerical differentiation of the velocity potential by utilizing Tuck's theorem (Ogilvie and Tuck, 1969). Wu and Moan (1996) used high-speed strip theory and considered a Vlasov beam idealization including rotary inertia and shear deformation effects to investigate the hydroelastic responses of ships in irregular head waves. They presented linear and nonlinear hydroelastic formulations in frequency and time domains for the ship hull response analysis and concluded that nonlinearity becomes important with the high speed of the vessels.

In the cases where the hydrodynamic loading on the structure is of a non-linear character, then the time-domain analysis is more appropriate. Gu, Wu, and Xia (1989) presented a time domain hydroelastic simulation for the prediction of vertical ship motions and bending moments in the moderate regular and irregular seas. They used a Timoshenko beam model of the ship structure. Xia and Wang (1997) verified this approach with the ship model tests. They generalized the three-dimensional time domain free surface potential flow method to account for the flexibility of floating structures. This resulted in a linear time domain theory for hydroelastic analysis of ships and offshore structures. After simplifying the theory, they used Timoshenko beam idealization and slender body strip method. They numerically investigated the responses for a warship hull and a S175 containership in regular and irregular waves. The results pointed out the importance of the nonlinear effects on ship motions and

internal forces. Hence Xia et al. (1998) studied nonlinear wave loads and ship responses using a time domain strip theory. A nonlinear hydroelastic method for wave and slamming induced vertical motions and structural responses of ships is introduced. They presented numerical results for the S175 containership with two different bow flare forms and also compared the results with experiments.

2.2.2 Three-Dimensional Hydroelasticity

In order to examine the fluid-structure interaction behaviour of non-beamlike flexible floating structures (i.e. multi-hull vessels, jack-up rigs, catamarans and semi-submersibles, etc.), Wu (1984); Price and Wu (1985) and Bishop et al. (1986) presented a three-dimensional hydroelasticity theory, in which the limitations of two-dimensional theory are avoided by using three-dimensional potential theory (pulsating source distribution on the mean wetted surface of the structure) to model the fluid forces and creating a three-dimensional finite element model of the structure.

Since the three-dimensional hydroelasticity theory is well capable of modelling the non-beam like structure case, it has been used to investigate the dynamic behaviour of SWATHs in waves (Bishop et al, 1986; Bishop, Price and Temarel, 1986; Price, Temarel and Wu, 1987; Price et al. 1994) the problem of jack-up transportation (Fu, Price and Temarel, 1987), the behaviour of a dry dock (Lundgren, Price and Wu, 1989). Ergin et al. (1992) studied on a flexible cylindrical shell in air and submerged using an alternative time domain analysis to illustrate the effects of impulsive loading.

Price et al. (1994) presented a hydroelastic analysis of a SWATH (T-AGOS 19) in waves to account for the steady state responses. They presented comparisons between simplified (for preliminary design stage) and refined (for final design and the assessment of the effects of loading) stage finite element models. The main differences between the two models are the structural details and weight distribution. Stress distributions in the structure were obtained and discussed at various travelling speeds and heading angles in irregular seas in frequency domain.

Che et al. (1994) brought a new approach into the discussion of the analysis of wave induced hydroelastic response of floating, slender structures. They developed a method that combines a three dimensional structural model with fluid forces from two-dimensional potential theory (strip theory). Since a three-dimensional finite element model of the structure is used, the method allows direct computation of three-dimensional response of the structure. On the other hand, because of using a two-dimensional fluid model, the large computational effort of three-dimensional hydroelasticity (three-dimensional potential theory) is avoided. To demonstrate and to verify the method a SWATH ship is analyzed. The results of this method are compared with a full three-dimensional hydroelastic analysis. The results indicated that the 2D/3D composite method could be an alternative to three-dimensional hydroelasticity for large floating structures that can be characterized as slender.

Aksu et al. (1991) compared two and three-dimensional hydroelasticity theories including the effect of slamming. Comparisons were made in time-domain steady state and transient slamming responses for head seas. They investigated the behaviours of slender uniform and non-uniform barge structures travelling in irregular seas using both theories. In the case of uniform barge travelling in head seas, the response simulations agree in both methods. However, for a non-slender uniform barge differences occur between the two theories. Results from three-dimensional hydroelasticity theory are found to be reliable and investigation was extended to slamming.

Janardhanan, Price and Wu (1992) developed a three-dimensional time-domain hydroelastic approach, incorporating time history effect and non-linear fluid loading from wave effects. The theory is based on the fluid field representation in terms of the frequency-domain Green function.

Wu and Moan (1996) and Wu et al. (1996) reported a time-domain hydroelastic analysis for ships at high forward speed, using 2½ dimensional simplification in the fluid force prediction. The total vertical loads are decomposed into linear and nonlinear modification parts. The linear part is evaluated by use of appropriate linear

potential flow theory. The nonlinear modification part comes from the hydrodynamic force caused by slamming and nonlinear modifications in Froude-Krylov, hydrostatic restoring, radiation and diffraction forces. This non-linear hydroelastic theory to predict the wave-induced structural responses in ships with large amplitude motion in head or following seas using the decomposition approach of total response to linear and nonlinear parts, developed by Wu and Moan (1996), is applied to a catamaran model in regular head waves and theoretical results are compared with model tests in the study of Wu et al. (1996).

Cheung et al. (1998) studied the hydroelastic analysis of a SWATH structure and other methods of analysis of the primary structure of SWATH ships such as quasi-static and rigid body-dynamic are also applied together with hydroelasticity. Deflections and stresses are calculated after each method and compared. In all three methods the hydrodynamic pressure is evaluated by the source distribution method and the structural deformation and stress are modelled by the finite element method. To verify the accuracy of the hydroelastic analysis, the convergence of the solution to the number of modes is investigated. It is noted that the discrepancy between the hydroelastic prediction and the other two approaches is generally more pronounced near the stern of the ship, where the lower hulls are more flexible and hydroelastic effects are important. In addition it is reported that the first two methods generally give very close predictions of the deformation and stress. Further more, due to the elastic response, the hydroelastic approach gives consistently higher predictions of the lower hull deflection and the stress in the strut, but lower predictions of the stress in the upper hull compared with the other two methods.

The assumption in most seakeeping, two-dimensional and three-dimensional hydroelasticity theories that the advancing of the ships does not generate non-uniform steady flow around and behind the vessel is not applicable for a fast moving non-slender or thick body. This problem that the steady state disturbance cannot be omitted in high forward speeds, led Du and Wu (1998) to investigate the effect of forward speed on the hydroelastic behaviour of ship structures and to illustrate the calculations of an ellipsoid moving beneath wave surface, and a surface ship of the

semi-ellipsoid form travelling in waves. Numerical comparisons of the hydrodynamic coefficients, wave exciting forces, rigid body motions, and flexible body distortions are made for different forward speeds, different slenderness parameters, and different heading angles. The contributions from the velocity field of non-uniform steady flow to the interface boundary condition, and the generalized hydrodynamic forces are included in the three-dimensional hydroelasticity analysis.

2.3 Slamming

In rough seas where large relative amplitude ship motions occur, the bow may emerge out of the water. The impact phenomenon that follows, as the bow re-enters the incoming wave, is commonly referred to as slamming. Slamming is the main transient loading for a ship and can cause important local and global loads on a vessel. Slamming on mono-hulls is often categorized as bottom slamming and bow flare slamming.

Under certain conditions the sea imparts a severe transient loading to the hull, because of rapid and deep immersion of the bow when there is a pronounced flare or as a consequence of local emergence of the hull either near the stern or at the forefoot. After emergence, the subsequent re-entry of the forefoot may create substantial forces due to sudden pressure changes in the region as the ship strikes the water surface (bottom impact slamming). This may result in high frequency transient responses in the structure. When the relative velocity of the ship's bottom and the sea surface is large enough, the vessel will slam when its forefoot re-enters the water. An impulsive loading will be applied which will make the ship oscillate and may cause damage. There may also be local damage and equipment may suffer as result of the shock loading.

When a bow flare section of a ship enters the water, the local loads around the flare are not influenced by hydroelasticity. On the other hand hydroelasticity is important in a global analysis. When the ship is considered as elastic beam, the integrated water-entry force on a bow flare section causes transient hydroelastic response (whipping) of the beam (Faltinsen, 1997). Despite the pressure field due to impact remains

localized in space and time, slamming loads can locally create plastic deformations of the hull external structure. They are also involved in the high-frequency whipping type response of the global ship structure and lead to an increase of the vertical bending moments. In the severe cases these loads are seen responsible for the loss of ships.

Different physical effects may have an influence during slamming. When the local angle between the water surface and the body surface is very small at the impact position, an air cushion may be formed between the body surface and the water surface. Compressibility of the air influences the airflow. The airflow interacts with the water flow, which is influenced by the compressibility of the water. When the air cushion collapses, air bubbles are formed. The large loads that can occur during impact between a nearly horizontal body and a water surface can cause important local dynamic hydroelastic effects. This can lead to subsequent cavitation and ventilation (Faltinsen, 1999)

The calculation of impact load is needed in order to determine the required strength of the structure involved. A better understanding of the whole phenomenon of slamming will also give information on how to design the shape of the structure for the minimization of the impact load.

Many researchers have studied vessel impact problems since the early 1930s. The pioneering works are von Karman's (1929) impact analysis of seaplane landing and Wagner's (1932) flat plate model.

Impact forces can be obtained from the slamming pressure due to bottom impact (Ochi and Motter, 1973; Stavovy and Chuang, 1976). On the other hand, the forces applied to hull during the penetration of the waves after the initial impingement can be evaluated from the momentum slamming theory (Leibowitz, 1963). These two theories have different characteristics. Bottom impact induces a sharp peak of short duration while the penetration of the waves induces a smoother peak of relatively longer duration (Belik et al., 1980). The total slamming force may consist of the

impact and/or the momentum forces. Belik et al. (1988) reported that use of the impact forces or the momentum forces or their combination results in very small differences.

Based on the theories mentioned above, the actual magnitude of the slam can be described in two distinct ways. It is assumed that the total slamming force consists of these two distinct components.

$$F_{total}(x, t) = F_{impact}(x, t) + F_{momt}(x, t) \quad (27)$$

The first one, which is impact slamming, attempts to evaluate the forces due to sudden pressure change around bottom of the hull at the instant when the hull strikes the free surface of the waves. The characteristics of this type of slam are short duration, the compressibility of the water, the significance of the influence of air cushioning and the dependency of the impact pressure on the relative velocity at the re-entry (Bishop and Price, 1979).

Impact theory assumes that the impact pressure and hence the slamming impact force at the instant of impact is proportional to the vertical velocity (Bishop and Price, 1979). In impact theory, the transient forces are continuously distributed over a length of the hull, which was initially clear of the water near the forefoot; the distributed force must be discretised for the purposes of calculation. This can be done by assuming the transient to be stepwise distributed over some of slices into which the hull is imagined cut for the purposes of structural or hydrodynamic calculations.

The generalized two-dimensional transient excitation force at the s^{th} coordinate is

$$Z_s(t) = \int_0^l F(x, t) w_s(x) dx \quad (28)$$

where $F(x, t)$ is the transient force per unit length acting on the hull and w_s is the displacement at coordinate s .

This theory is based on the assumption that the slamming force and hence the impact pressure at the instant of impact is proportional to the n^{th} power of the impact velocity: (Belik et al., 1987)

$$\text{pressure, } p = k(\text{impact_velocity})^n$$

The constants k and n are determined experimentally by systematic drop tests on plates, sections of hulls, etc. or on ship models towed in waves.

The expression assumed for the impact force per unit length is given by

$$F_{\text{impact}}(x, t) = p_{\text{max}}(x)G(x)f(t) \quad (29)$$

In the application of impact slamming theory, the following equation for the transient loading can be used. (Bishop and Price, 1979)

$$F(x, t) = \frac{p_{\text{max}}}{T_0} G(x) t e^{(1-\frac{t}{T_0})} \quad (30)$$

where $G(x)$ is the shape factor, p_{max} is the maximum pressure and T_0 is the time that elapses between the instant at which the bottom strikes the wave surface and the instant at which the loading reaches its maximum value.

The second method, which is called momentum slamming, is associated with fluid actions describing the rate of change of momentum as the hull re-enters the water and describes the effect of pressure variations around the hull surface as it penetrates the moving fluid after the initial entry. Flare slamming can be described adequately only by the second approach.

The transient force, which is related to the rate of change of momentum of the surrounding fluid and the instantaneous buoyancy, is (Bishop and Price, 1979)

$$F(x, t) = -\left\{ \frac{D}{Dt} \left[m(x, t) \frac{D}{Dt} w_{\text{rel}}(x, t) \right] - \rho g S(x, t) \right\} \quad (31)$$

where $m(x, t)$ and $S(x, t)$ are the instantaneous added mass and submerged area of the hull section as it re-enters the water. w_{rel} is the relative displacement at a section x on the hull.

Ochi and Motter (1973) divided the slamming loads in three different problems related with the determination of the slamming pressure, the pressure distribution and the time variation of the slamming load. Subsequently several authors proposed different methods to predict these parameters. Kawakami et al. (1977) proposed a different method to predict the time variation of the slamming load, Stavovy and Chuang (1976) proposed a method to predict the maximum slamming pressure. After defining the slamming force, the structural response has been treated by several authors, for example Belik et al. (1983) and Guedes Soares (1989), who performed time simulations for irregular seas using different methods for the prediction of the slamming loads.

The main problem in slamming is the determination of the maximum slamming pressure, which is assumed by all methods in the following relation;

$$p_{\max} = \frac{1}{2} k v^2$$

where k is a non-dimensional factor that depends on the section geometry and this factor plays the main role in determining the maximum slamming pressure (Ramos and Soares, 1998). In the method of Ochi and Motter (1973) k factor is established as;

$$k = e^{(1.377 + 2.149a_1 - 0.873a_2 + 0.624a_3)}$$

Stavovy and Chuang (1976) evaluate the value of k using the local deadrise angle. It is obtained using a series of polynomials that fit experimental results. Zhao and Faltinsen (1993) compared three different methods to evaluate k in their study. The first one is based on the non-linear boundary method with a jet flow approximation. The second one was a new similarity solution for wedges with the deadrise angle varying from 4 to 81 degrees and the last one was an asymptotic solution based on the Wagner solution. The comparison of these five different empirical methods (k versus deadrise angles varying from 0 to 45^0) for the evaluation of the slamming loads based on experimental results can be found in the work by Ramos and Guedes Soares (1998) where they presented a method to predict the stresses induced on ship hull when the forward bottom impacts in water. The relative motion between the ship and waves is determined using a linear strip theory. They calculated the vibratory response of a

container ship by modelling it with finite elements and using modal superposition together with central differences for the time integration. The results obtained using different methods to calculate the slamming forces, differ very largely for the slam induced vertical moment amidships.

As well as the investigations on steady state responses, the transient responses due to slamming in regular head waves using impact and momentum slamming theories have been studied by Bishop et al. 1980 and Belik et al. 1980. The latter paper is a continuation of the previous one and the combined effects of bow slamming and steady state responses for a destroyer travelling in regular waves are investigated. In both studies transient impact and momentum loading is examined separately and using linear superposition, total responses are obtained. In order to simulate a real slam, the attention is drawn to the necessity of using both impact and momentum theories together rather than using only one. Belik and Price (1982) compared the existing slamming theories ((Ochi and Motter, 1973) and (Stavovy and Chuang, 1976) for impact slamming, (Leibowitz, 1963) for momentum slamming) in the time domain simulation of ship responses in irregular waves. The Ochi-Motter impact slamming theory is found to be contributing to the existing steady state response values much less than the Stavovy-Chuang theory. Furthermore, the latter approach was found to be more capable of predicting the localized damage on the structure (eg. plating). On the other hand the momentum slamming effect was reported as dominating both of these impact responses and providing a significant increase in the steady response. They also pointed out the dependence of magnitudes of slamming transient responses on the structural damping. In addition to impact slamming theories, bow flare slamming was incorporated into the available modal approaches to analyze transient responses due to the effects of bottom and bow flare slamming on a destroyer (Belik et al, 1988). With this paper Belik et al. clarified that the responses derived by combining impact and momentum slamming effects in the time domain are not necessarily larger than those derived from separate evaluations using the two theories because of phase differences. They concluded that a better simulation of bottom slamming is achieved by combining the two theories. In addition to the earlier

investigations of the same authors it is concluded that momentum slamming theory allows for the investigation of flare slamming and the effects of forward hull form.

The response of the hull to a transient excitation (e.g. slamming) is associated with the resonance frequencies of the distortion mode shapes of the hull (Belik, Bishop and Price, 1980, 1983). Comparisons of the predictions of hydroelasticity theory with full-scale measurements for two frigates in a severe weather trial (Bishop, Clarke and Price, 1984), a fast patrol boat travelling in rough seas (Aksu, Price, Suurbier and Temarel, 1993) include steady state and transient (slamming) responses together.

Kvalsvold and Faltinsen (1994) investigated the hydroelastic response due to the slamming against the wetdeck of a multihull vessel in head sea waves analytically and numerically. In theoretical slamming model, they used a two-dimensional, asymptotic method valid for small local angles between the undisturbed water surface and the wetdeck. Local hydroelastic effects in the local slamming area are also accounted for. Shear deformations and the rotatory inertia effects are all considered in their work. They modelled the wetdeck as a Timoshenko beam with rotatory springs at the beam ends to get the shear deformation and rotatory inertia effects properly. The hydrodynamic formulation of the problem is based on the extension of Wagner's (1932) two-dimensional theory. The main indication of the results is that the slamming loads on the wetdeck are significantly influenced by the elasticity of the wetdeck structure.

Slamming against rigid wetdecks has been studied by Kaplan and Malakhoff (1978) and Kaplan (1987, 1991). Kaplan (1992) reported that wetdeck slamming could cause a hydrodynamic loading in the order of the weight of the vessel or even larger, which may lead to severe local as well as global damages of the hull structure. Zhao and Faltinsen (1992) reported that the global heave and pitch motions of a catamaran were influenced by wetdeck slamming, however they did not account for any local or global elastic effects of the catamaran. Kvalsvold and Faltinsen (1995) improved their previous study on the wetdeck slamming of a multihull vessel in head sea waves (Kvalsvold and Faltinsen, 1994) by modelling the wetdeck as a set of three

Timoshenko beams in the transverse direction. The main difference between these two subsequent studies is reported by Kvalsøld and Faltinsen (1995); in the previous single Timoshenko beam model the lack of the inertia effects in the wetdeck outside the beam influenced the hydroelastic response when the wetted length was of the order of the beam length. In the latter study they extended the previous study to account for an arbitrary relative position between the undisturbed free surface of the waves and the wetdeck at the moment of initial water impact. As a result the resulting absolute maximum stresses are found to be slightly dependent of where the waves hit initially between two transverse stiffeners in the wet deck. In the work by Kvalsøld and Faltinsen (1995) two different approaches are used to calculate the wetted length of the beams. First one is based on the von Karman (1929) method and the other is the generalization of Wagner (1932) method. The fundamental difference between those two is that the latter method accounts for the pileup water effects.

Faltinsen (1997) studied the wetdeck slamming theoretically by a hydroelastic beam model. The analysis is simplified by introducing an initial structural inertia phase and a subsequent free vibration phase. Theoretical results are validated with drop tests of elastic plates on waves. The reported results indicate that the effect of the forward speed from the free surface conditions is not important for realistic wetdeck slamming conditions. The important effect comes from the body boundary conditions as an angle of attack effect. Another key result from the study is that both theory and experiments show that maximum bending stress is proportional to the drop velocity and is not sensitive to where the waves hit the wetdeck nor the curvature of the crest in the impact region.

Aksu et al. (1996) studied the effects of operational parameters, such as forward speed and loading condition, and seaway parameters, such as significant wave height, characteristic wave period and randomness, on the predicted steady state and slamming induced loads and stresses, using a bulk carrier and a tanker as examples. The intensity and severity of slamming are examined as a function of significant wave height and characteristic wave period used to describe the random seaways generated from ISSC wave spectra. They restricted their investigation on the symmetric bending

and shear of beamlike hulls in random head seas. In the calculation of transient slamming forces they considered the combination of the bottom impact forces (Stavovy and Chuang, 1976) and the rate of change of momentum as the forefoot penetrates the water surface (Leibowitz, 1963).

Vessel impact problems generally have been solved by two-dimensional or simplified three-dimensional model with basic assumptions of zero gravity, zero viscosity and zero compressibility. Some main examples of these two different approaches are by Cointe (1989, 1991), Zhao and Faltinsen (1993, 1996), Vorus (1996) and Zhao et al. (1997) for the two-dimensional solutions and by Troesch and Kang (1986, 1988) and Lai and Troesch (1995, 1996) for the simplified three-dimensional solutions. These are all symmetric body solutions.

On the other hand Xu et al. (1998) proposed a two-dimensional theory for asymmetric impact problems of vessels with arbitrary geometry. Based on Vorus's (1996) flat-cylinder theory, they established two types of flow models for cases of small and large asymmetry and calculated the asymmetric impact (slamming) loads due to extreme vessel motion by applying the method of discrete vortices. The difference between the two types is whether the flow is attached or separates at the keel on the first instances of impact.

Greenhow (1987) investigated the two-dimensional wedge entry into initially calm water. He considered the time dependent motions of wedges of various angles with both gravity and the nonlinearity of the boundary conditions on the wedge and free surfaces.

The water entry problem has been analyzed for studying water entry of a two-dimensional body of arbitrary cross-section by a numerical approach by Zhao and Faltinsen (1993). Through a boundary element formulation with a jet flow approximation, they simulated the flow around a wedge for different values of the deadrise angle. In view of the extension to three-dimensional problems, the model has been successively applied to asymmetric bodies (Zhao and Faltinsen, 1998).

Korobkin (1998) considered the impact of an elastic body onto a liquid, when the possibility of the liquid to escape from the impact region is highly limited. In order to solve this problem a catamaran wetdeck and its response to liquid impact is taken as example. The results mainly show that any possibility of restricting the liquid flow near the impact region has to be avoided at the design stage, since the limitation on the liquid flow leads to high level of stresses in the elastic bottom.

Faltinsen (1999) analyzed the water entry of a slender hull with wedge shaped cross sections using orthotropic plate theory. Systematic studies on the importance of hydroelasticity as a function of deadrise angle and impact velocity are also presented. The effect of structural vibrations on the fluid flow is incorporated solving the two-dimensional Laplace equation in the cross sectional fluid domain by Wagner's theory. The theory is also validated by comparison with full-scale experiments and drop tests. The effect of hydroelasticity is found to be significant in the smaller deadrise angles due to the larger impact velocity.

Campana et al. (2000) studied the impact of cylindrical bodies over the water surface in the compressible and incompressible stages. In the compressible phase the hydrodynamic analysis is carried out and a closed form expression for the maximum impact force is found for a wedge section and for a circular cylinder. For the incompressible stage they used an unsteady boundary element method to compute the free surface evaluation and the slamming force on the body. They analyzed the effect of the entry velocity reduction during the impact (e.g. the effect of the inertial force in water shock). The inertial effect leads to a characteristic maximum in the time history of the slamming force and this makes it natural to investigate the role played by the mass of the impacting body on the slamming load. In the case of a circular cylinder, a closed form relationship between the maximum slamming force and the mass of the impacting body could not be found in their investigation. They concluded that for either compressible or incompressible conditions, a similar increasing trend of the maximum slamming load acting on impacting wedges is obtained for increasing body mass.

Carcaterra and Ciappi (2000) investigated the response of simple systems (rigid and elastic) impacting on the water surface. An elastically deformable wedge and a rigid wedge coupled with an oscillator were taken as examples. The wedges were consisted of two elastically coupled bodies and the body shape is elastically deformed during the impact in the first one, while the second one is a rigid impacting body. The investigation led to the following conclusions. In both models, the hydrodynamic force evaluation was not effected by the presence of elastic coupling. The deformable wedge presented a feedback control of the impact force when the deformation tended to increase the wetted surface, a consequent velocity reduction was observed. It was noticed that when the rigid wedge is coupled with oscillator, the hydrodynamic force had an order of magnitude larger with respect the elastic reaction. Therefore in both cases the rigid wedge approximation is suggested to be used in predicting the maximum hydrodynamic slamming force.

With respect to the role of hydroelasticity on slamming, Bereznitski (2001) carried out an alternative investigation based on a large number of calculations using a two-dimensional wedge shaped body and stated that the ratio between the duration of the impact and the first period of the natural vibration of the dry structure is the key factor for defining when hydroelasticity should be taken into account or can be neglected. Bereznitski (2001) also developed a three-dimensional model for bottom slamming. He considered a steel plate with stiffeners and applied drop tests on it. The effects of hydroelasticity and compressibility are taken into account in the analysis. The factors influencing the impact interaction such as the air entrapped between the structure and the water surface, penetration of structure inclined at a specified angle, acceptability of 3-D/2-D model conversion, are discussed in this paper.

Faltinsen (2002) analyzed the water entry of a rigid wedge using matched asymptotic expansions under the assumptions of incompressible water and irrotational flow. A jet domain, inner domains at the spray and outer domain are defined. The matched asymptotic expansion solution of Armand and Cointe (1987), in which the deadrise angle is limited with very small values, is extended by assuming finite deadrise angles

when the outer and inner domain solutions are found. This new solution method is found satisfactory for gravity free water entry of a general two-dimensional body shape.

Hansen et al. (1994) investigated the wave induced high-speed vessels' hull vibrations (springing and whipping). A parametric study is also performed to determine the importance of hull flexibility and ship length on the springing and whipping response of fast mono-hull vessels. The calculations are carried out using nonlinear strip theory.

Chihua and Yousheng (1997) developed a boundary element method for calculating the two-dimensional flare ship hull slamming with a constant entry velocity. The exact nonlinear free surface boundary conditions are accounted for, and the linear element assumption is adopted. Results obtained show that the slamming on the flare section of ship hull may cause more structural damage than when using a U-shape section.

Varyani et al. (2000) presented an investigation on the slamming impact of a catamaran together with its motions in head seas including and omitting forward speed. For the ship motions they used strip theory and three-dimensional pulsating source method. On the other hand they developed a computational fluid dynamics method to predict the slamming loads acting on the catamaran.

In literature there are some fundamental experiments related with slamming. Chuang (1966, 1967) analyzed the slamming problem experimentally through a series of drop tests with a flat plate and a wedge. In the flat bottom slamming experiment the effect of the trapped air between the falling body and the water, causing the maximum impact pressure to be much lower than the pressure expected, was observed. Subsequent experiments in slamming of wedge shaped steel models with small deadrise angles were performed by the same author. The results of drop tests are used to provide charts for estimating the maximum impact pressure due to rigid body slamming of wedges.

Verhagen (1967) investigated the impact of a flat plate on a water surface theoretically and experimentally. Lewison (1970) presented a paper on the reduction of slamming pressures. He used a flat water impact theory which takes account of the air trapped between the falling body and the water surface. Two sets of experiments are introduced in the study; in the first set, pressure measurements on a flat plate were made on a large vertical drop test machine and second set of experiments were on a small scale model in head seas. As a result of the experiments it was concluded that end flanges would sharply reduce the peak pressures because of entrapping a greater volume of air. In other words, the slamming pressures under the forefoot were reduced sharply, if the air cushion was artificially reinforced. Beukelman (1978) carried out forced oscillation tests about the water surface to obtain bottom impact (slamming) pressures using two-dimensional approach.

Shibue et al. (1994) presented a transient structural response analysis for drop tests of two-dimensional cylinders on water surface to reproduce the time histories of strain under water impact pressure. They focused on the effects of maximum pressure values on the maximum strain values.

2.4 Stiffened Flat Plates

Many structures such as those used for aerospace, marine and offshore applications are, generally, made up of unstiffened/stiffened plate panels. The design of these structures involves detailed analysis for static and dynamic responses. In order to model these structures, it is necessary to identify and adopt suitable analytical/numerical methods, which will be reliable as well as economical in representing the structural behaviour of the plate panels.

Stiffened plates are encountered in bridge decks, floor slab systems, ship constructions, etc. The primary advantage of stiffening the plate lies in the structural efficiency of the system, since great savings of weight can be attained with no sacrifices in strength or serviceability of the structure. Stiffening a plate gives higher strength/weight ratio of the structure compared to a bare plate having the same

material. Hence stiffened plate construction is widely used in aerospace and marine structures, where weight is of great significance. The structural system is composed of plate elements, above which the load is applied, reinforced by stiffener (or beam, rib, stringer, girder) elements located at discrete spacings in one direction (longitudinal or transverse) and in some cases in both directions. The former stiffening system is often referred to as uniaxially or longitudinally stiffened plate and the latter as orthogonal or waffle type stiffening. If the stiffeners are symmetrical about the mid-plane of the plate they are referred to as concentric stiffening, and if they are located on one side of the plate they are referred to as eccentric stiffening (Bedair, 1997).

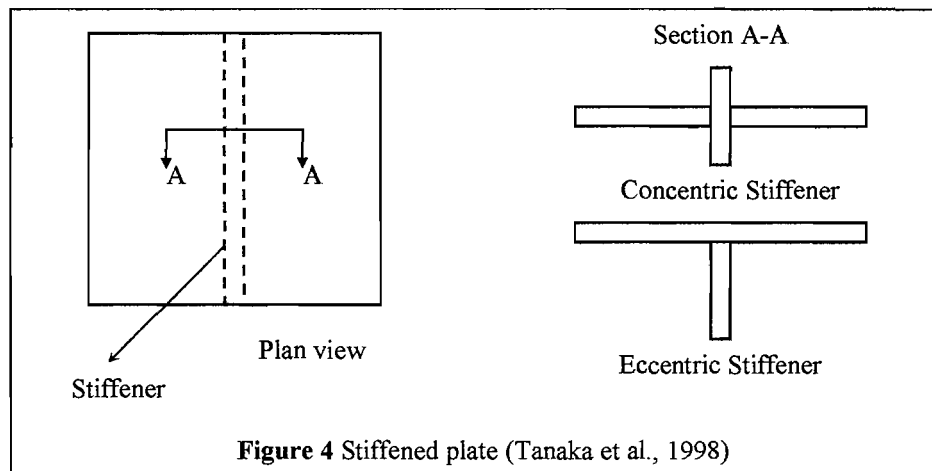


Figure 4 Stiffened plate (Tanaka et al., 1998)

The methods used for dynamic and static analyses of plates are similar. The following is a review of analytical and numerical tools for studying dynamic behaviour of stiffened plates.

The various approaches include orthotropic plate approximation, grillage approximation and plate-beam idealization. The philosophy of each depends upon the treatment of plate and stiffener elements. Research on the static and dynamic characteristics of stiffened plates can be divided into these three broad headings:

2.4.1 Orthotropic Plate Approximation

The orthotropic plate theory was first developed by Huber, in which smearing the stiffener into the plate forms a relatively simpler approach to the solution of stiffened plate problems (Satsangi et al., 1989). This approximation converts the plate from one

having stiffeners dispersed throughout, to one having orthotropic properties as seen in Figure 5 (Bedair, 1997). The resulting idealized structure is therefore composed of the original plate layer and additional layer.

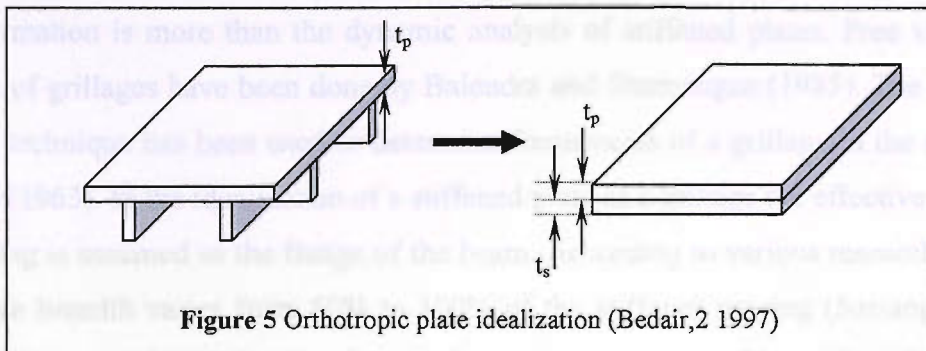


Figure 5 Orthotropic plate idealization (Bedair, 1997)

Main publications regarding orthotropic plate theory can be given as follows; Natural frequencies have been calculated according to Navier's solution by Huffington (1956) and Hoppman et al. (1956); a study of nodal patterns followed by Hoppman et al. (1957) that was modified by Thorkildsen et al. (1959) to introduce rotary inertia effects. Rotary inertia of both the plate and the stiffeners were incorporated later by Huffington et al. (1965). The response of a damped, simply supported stiffened plate subjected to sinusoidal and random excitation is determined analytically including shear and rotary inertia by Laura (1968). Smith et al. (1970) presented an experimental and analytical study of vibration of clamped stiffened and unstiffened plates subjected to inplane loading. Natural frequencies have been calculated for rectangular plates having fixed, simply supported and free boundary conditions. The influence of aspect and rigidity ratios on the plates has been examined by Grace et al. (1985). A higher order shear deformation theory was developed for investigation of free vibration characteristics of a thick, simply supported, orthotropic plate by Doong et al. (1987). The boundary element method was used for the free vibration analysis of orthotropic plates (Sun et al., 1987). This theory is used efficiently if the stiffeners are small, identical and placed uniformly at close intervals. If the stiffeners are not identical in both directions or not equally spaced then the resulting thickness becomes non-uniform (Satsangi et al., 1989). These issues impose limitations. Moreover, as the plate and the stiffeners are converted into an equivalent plate, the evaluation of the stresses in the plate and the stiffeners separately becomes difficult.

2.4.2 Grillage Approximation

The stiffened plate structure is idealized as a set of intersecting beams for the convenience of the analysis. Static analysis of stiffened plates using this approximation is more than the dynamic analysis of stiffened plates. Free vibration studies of grillages have been done by Balendra and Shanmugan (1985). The transfer matrix technique has been used to determine frequencies of a grillage in the study of Leckie (1963). In the idealization of a stiffened plate as a grillage the effective breadth of plating is assumed as the flange of the beam. According to various researchers this effective breadth varies from 50% to 100% of the stiffener spacing (Satsangi et al., 1989). There are basically two drawbacks in this approach (Satsangi et al., 1989). First the centroidal planes of the beams in different directions are assumed to be the same, which affect the accuracy of the stresses calculated. Secondly the beam properties are derived by considering the effective breadth of the plate. There is no simple method available for the calculation of effective breadth of plating. This creates difficulties in evaluating the true stresses in the plate and the stiffeners (Satsangi et al., 1989).

Hitherto two earlier methods of idealization of stiffened plates are mentioned. Both these methods fail in the case when the stiffeners are sparse and are therefore not suitable for the solution of generalized stiffened plate applications as a result of the limitations they impose (Mukherjee and Mukhopadhyay, 1988).

2.4.3 Plate and Beam Idealizations

It is more realistic to consider the plate and the stiffener as separate entities and then enforce the compatibility between the two. Various approaches exist in the literature for the analysis of stiffened plate problems by considering the plate and the stiffener as separate identities. For many plate problems of considerable practical interest, analytic solutions to the governing differential equations cannot be found. On the other hand numerical treatment of differential equations can yield approximate results, acceptable for most practical problems (Szilard, 1974). Some of these numerical

techniques are finite difference methods, energy methods, matrix method, finite strip method, finite element methods and others.

In finite difference method the derivatives in the differential equation under consideration are replaced by finite difference quantities at some selected points. These points are located at the joints of a rectangular, triangular or other reference network, called finite difference mesh (Szilard, 1974). The entire continuum is subdivided into a uniform mesh and an approximate solution is obtained (Satsangi and Mukhopadhyay, 1989). Troitsky (1976) has reviewed earlier work on the finite difference method. Finite difference method has been used to calculate natural frequencies of stiffened plates with equally spaced identical stiffeners by Wah (1964). Equations formulated from the variational principle for free vibration of stiffened plates have been solved by the finite difference method by Aksu and Ali (1976). The method has extended to include in-plane inertia and in-plane displacements by Aksu (1982). Mukhopadhyay (1989) extended his existing theory for plates using semi analytic finite difference method to the vibration and stability analysis of stiffened plates. In this method a displacement function satisfying boundary conditions along two opposite edges is assumed. This function is then substituted into the differential equations of the free vibration and stability of the stiffened plate and then by using suitable transformation, they are reduced to ordinary differential equations with constant coefficients, which are solved by the finite difference technique. The solution of the eigenvalue problem gives the natural frequencies for free vibration and the critical load for the stability analysis of the stiffened plate. Under this methodology vibration and stability analysis of concentric stiffened plates considering bending displacements of the plate and the stiffener only are studied by Mukhopadhyay (1989). The same method is extended to the vibration analysis of eccentric stiffened plates, considering bending and axial (in-plane) displacements. It is noted that the eccentricity of the stiffeners gives rise to axial and bending displacement in the middle plane of the plate resulting in three coupled partial differential equations, which have been solved by the semi analytic method (Mukhopadhyay, 1989). This method has also been applied to the static analysis of both concentric and eccentric stiffened plates. On the other hand, Mukhopadhyay and Samal (1990) have carried out

transient analysis of plates using this method. The method being semi-analytic in approach, takes much less computer time than the ordinary finite difference method (Mukhopadhyay, 1994).

As an energy method the Rayleigh-Ritz method, which involves determination of the kinetic and potential energies of the structural system using assumed shape functions that satisfy the geometrical boundary conditions and approximates the actual modes of vibrations, has been extensively used to study vibration problems of stiffened plates. The natural frequencies of the first symmetric and first antisymmetric modes of a simply supported rectangular plate with two different forms of stiffener cross section (rectangular and T) are determined using this method and the ratio (frequency of stiffened plate/frequency of unstiffened plate of equal mass) is also obtained for rectangular and T-section stiffeners (Kirk, 1970). Leissa (1973) presented comprehensive analytical results for the free vibration of rectangular plates using the Ritz method. Twenty-one cases exist involving the possible combinations of clamped, simply supported and free edge conditions in this study. Natural frequencies and mode indexes are presented for various plate aspect ratios. Madsen (1978) analyzed orthogonally stiffened panels for free vibration; he incorporated bending and warping torsion and axial deformation of the stiffener to obtain dynamic equations and applied the Rayleigh-Ritz method. Bhat (1982) studied the effect of stiffener spacing on free vibration. Wu and Liu (1988) applied this technique for the free vibration of stiffened plates having edges elastically restrained in rotation, based on plate and beam idealization. The first lower four frequencies for restrained plates with up to six stiffeners are calculated.

A transfer matrix method has been developed to predict natural frequencies and normal modes for a finite number of panels that differ in width, thickness and material properties by Mercer and Seavy (1967). Long (1971), in his formulation for free vibration, neglected in-plane displacements across the direction of stiffener in the dynamic stiffness matrix.

In finite strip method the plate is divided into a number of strips. A semi-analytical finite strip method has been developed by Cheung (1976) in order to achieve economic solution with reasonable accuracy, particularly for regular shaped structures. The method has some drawbacks like mixed boundary conditions, continuous span, internal opening and interior supports. These are mostly due to the characteristic beam functions used as displacement interpolation function along the longitudinal direction of the strip (Sheikh and Mukhopadhyay, 1993). The spline finite strip method has been subsequently proposed to eliminate most of the shortcomings of the finite strip method (Cheung et al., 1982). In this method spline functions are adopted in one direction and finite element shape functions are adopted in the other direction as interpolation functions of displacement field (Sheikh and Mukhopadhyay, 1993). In other words the spline function is used as displacement interpolation function in the longitudinal direction of the strip (along the nodal lines) (Sheikh and Mukhopadhyay, July 1993). Later this method has been generalized so that plates having any arbitrary shapes can be analyzed with a single formulation (Li et al., 1986). Sheikh and Mukhopadhyay have applied the method to static (Sheikh and Mukhopadhyay, 1992) and free vibration analysis (Sheikh and Mukhopadhyay, 1993) of stiffened plates in a linear range. The spline finite strip method has been extended to the analysis of plate structures having edges elastically restrained against translation and rotation for both unstiffened and stiffened plates (Sheikh and Mukhopadhyay, July 1993). The same authors also used this method for the linear and nonlinear transient vibration analyses of plates and stiffened plates (Sheikh and Mukhopadhyay, 2002).

Among all the numerical methods finite element method is the most realistic and versatile tool being reasonably accurate and less complex to model stiffened panels (Palani et al., 1992). Since many investigators have applied this method for the analysis of stiffened plate structures, considerable amount of literature is available in various publications. Herein only some of the main literatures on finite element analysis of plates are presented. The theory behind finite element method can be found in many textbooks (e.g. Zienkiewicz, 1977).

Olson and Hazel (1977) studied the effect of stiffness on various modes of vibration and they performed experiments using real time holography. The plate was modelled using triangular elements including bending and in-plane displacements. The stiffeners were modelled by beam bending and torsion elements. The first twenty four vibration modes were predicted and measured for four different type of stiffened plates. Experimental results were compared with those analytically obtained using the high precision triangular plate bending element. Experimental results have been compared with a finite element model consisting of a three noded plate element with three degree of freedom per node and associated with a compatible beam element by Rao et al. (1978). Different finite element models have been proposed by Mukhopadhyay and Satsangi (1984) and Deb and Booton (1988) for static analysis, and by Mukherjee and Mukhopadhyay (1988) for vibration and dynamic analysis of stiffened plates with arbitrarily located eccentric stiffeners. Similar approaches which involve plane element shape functions (eight noded Serendipity) are used in deriving the stiffness/mass properties of the stiffeners and assembled with the stiffness/mass of the plate to arrive at the stiffness/mass of the eccentric stiffened plate models in the studies above. The early studies in the literature on stiffened plates/shells with arbitrarily located stiffeners have been restricted to use eight noded isoparametric Serendipity element; however, this element locks in shear for thin plates (Palani et al., 1993). The shear strain term considered on the basis of Mindlin's theory in the isoparametric element gives rise to the shear locking problem with the decreasing thickness in the element (Barik and Mukhopadhyay, 1998). Barik and Mukhopadhyay (1998) use a new four noded plate bending element for the free vibration of arbitrary plates to overcome the drawback of isoparametric element. Two finite element models for static and vibration analysis of stiffened plates/shells with eccentric stiffeners (Palani et al., 1992) have been extended to perform the same analysis of stiffened plates/shells with arbitrarily located eccentric stiffeners in Palani et al., (1993). An isoparametric stiffened plate bending element for dynamic analysis of stiffened plates under time varying loads (distributed and point sinusoidal loading and air blast loading) has been studied by Mukherjee and Mukhopadhyay (1987).

Mukherjee and Mukhopadhyay (1988) compared the use of consistent mass matrix and lumped mass matrix in the plate formulations. In their study it is suggested that while using a coarser mesh, the lumped mass scheme produces better results, whilst those from the consistent mass scheme improve gradually as the mesh divisions are increased. Since the consistent mass matrix provides a proper discretization procedure, it involves additional computing. The tendency of the lumped mass is to render the structure more flexible. A coarser mesh gives a stiffer structure. The counter balancing effect of the lumped mass results in a softer element at a coarse mesh. However for higher mesh divisions, the consistent mass formulation gives better results than the lumped mass. The result from the consistent mass is marginally better for higher natural frequencies. They also investigated the effect of eccentricity in clamped and simply supported stiffened plates. It is concluded that for boundary conditions where the inplane motions of the supported edges are restrained (e.g. clamped), no significant change of frequencies is obtained through the consideration of inplane degrees of freedom. For plates where the inplane motions take place at the boundary (e.g. simply supported), the effect of eccentricity is significant.

Static three-dimensional finite element analysis of ship structures is studied using a superior stiffened plate element to the existing isoparametric element of (Mukhopadhyay and Satsangi, 1984) by Kumar Satish and Mukhopadhyay (2000). This element can accommodate any number of arbitrarily oriented stiffeners and eliminates the use of mesh lines along the stiffener.

Vibration of a square clamped panel with varying stiffener length is investigated by Nair and Rao (1984) using high precision triangular plate bending elements and beam elements including bending and torsion for stiffener.

Koko et al. (1992) have developed the so-called “super element”, which allows a coarser mesh to be considered, typically one or a few elements between adjacent stiffeners, to model the free vibration of stiffened plates. Only a single element per bay or span is needed to model the response.

Bardell (1988) has developed a hierarchical FEM for the vibration analysis of plates. A distinct advantage of this method is that the system matrices for a given interpolation order can be used to form the matrices for a larger interpolation order. The interpolation functions used by Bardell are based on integrated Legendre orthogonal polynomials. Beslin and Nicholas (1996) have proposed a set of trigonometric hierarchical functions in order to predict high order modes of vibration of bending plates with arbitrary boundary conditions. Barrette et al. (2000) investigate vibration analysis of stiffened plates using hierarchical finite elements with a set of trigonometric interpolation functions. The trigonometric set offers better numerical stability at higher frequency, compared to polynomial set of Bardell (1988).

Szilard (1974) and Mota Soares et al. (1980) have investigated the transient vibration analysis of bare plates subjected to sinusoidal excitation by the analytical solution and the mixed finite element model, respectively. Transient linear dynamic response of plates and shells with or without stiffeners, subjected to different kinds of load-history has been studied by the finite element method (Sinha and Mukhopadhyay, 1995).

As a conclusion finite element method is the most widely used approach. However, the method requires many elements for accurate modelling of the structure and the accuracy of the response increases with the higher mesh density. With the increasing frequency due to the shortening wavelength of structural deformation, the finite element method requires mesh refinement (Bercin, 1997). Hence the method is costly regarding computer time. Therefore the method can be seen unattractive for preliminary design where repeated calculations are inevitable.

Depending on the structural configuration, loading, boundary conditions, accuracy of the results required and the computer capabilities available, one can make a proper selection of the method for the analysis of stiffened plate problems.

3 PERIODIC RESPONSE of UNIFORM BEAMS

3.1 Modal Analysis of Beams

Modal analysis is used to determine the vibration characteristics (natural frequencies and mode shapes) of a structure or a machine component while it is being designed. The natural frequencies and mode shapes are important parameters in the design of a structure for dynamic loading conditions. It also can be a starting point for another, more detailed, dynamic analysis, such as a mode superposition harmonic, transient, or a spectrum analysis.

Here, two basic beams with different boundary conditions, free-free and pinned-pinned as shown in Figure 7 and Figure 8, respectively, are examined by a modal analysis to determine their dynamic characteristics. The Euler-Bernoulli beam theory, in which the beam deformations are assumed due to the bending moment as a result of having small cross-sectional dimensions compared to the length of the beam, is used to obtain the dynamic characteristics. The effects of rotary inertia and shear deformation are neglected in the Euler-Bernoulli beam theory. These effects are considered in the Timoshenko beam theory. These theories can be found easily in every mechanical vibration book, therefore in the following part only a brief description of the relevant basic equations related to Euler beam is presented.

An element of Euler beam subject to external force $f(x,t)$, bending moment $M(x,t)$ and shearing force $V(x,t)$ is given in Figure 6:

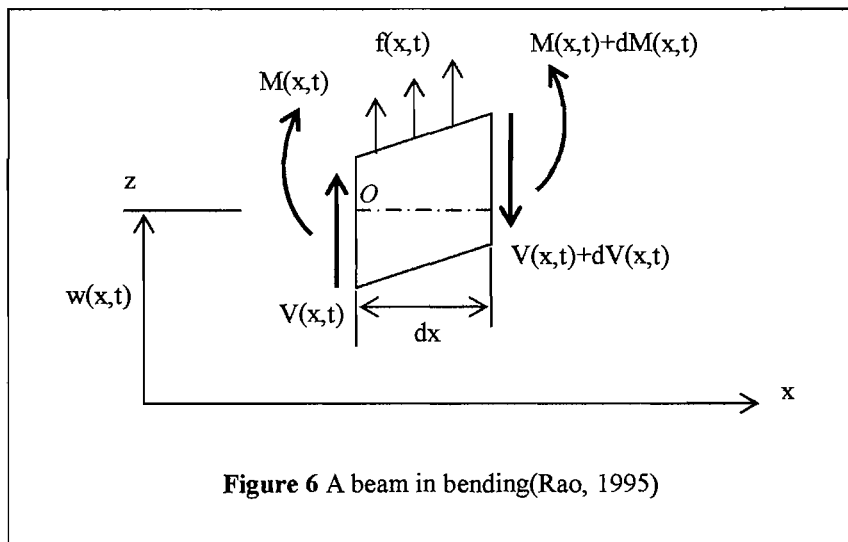


Figure 6 A beam in bending(Rao, 1995)

According to the Euler beam theory, the equation of motion for the forced lateral vibration of a uniform beam is (Rao, 1995):

$$EI \frac{\partial^4 w}{\partial x^4}(x, t) + \rho A \frac{\partial^2 w}{\partial t^2}(x, t) = f(x, t) \quad (32)$$

where $w(x, t)$ is the transverse displacement, E is Young's modulus and I is the moment of inertia of the beam cross section about the y-axis, ρ is the mass density, A is the cross-sectional area of the beam and $f(x, t)$ is the external force per unit length of the beam.

For free vibration, $f(x, t) = 0$ is substituted and after the free vibration solution:

$$W(x) = C_1 \cos \beta x + C_2 \sin \beta x + C_3 \cosh \beta x + C_4 \sinh \beta x \quad (33)$$

$$\omega = \beta^2 \sqrt{\frac{EI}{\rho A}} = (\beta l)^2 \sqrt{\frac{EI}{\rho A l^4}} \quad (34)$$

are obtained. The function $W(x)$ is the normal mode (mode shape) or characteristic function of the beam and ω is the natural frequency of vibration. For any beam there will be an infinitive number of normal modes with one natural frequency associated with each normal mode. The unknown constants C_1 to C_4 and the value of β can be determined from the boundary conditions of the beam as indicated below.

The common boundary conditions are as follows:

Free end: Bending moment = $EI \frac{\partial^2 w}{\partial x^2} = 0$

$$\text{Shear force} = \frac{\partial}{\partial x} \left(EI \frac{\partial^2 w}{\partial x^2} \right) = 0$$

Simply supported (pinned) end:

$$\text{Deflection} = w = 0$$

$$\text{Bending moment} = EI \frac{\partial^2 w}{\partial x^2} = 0$$

Fixed (clamped) end:

$$\text{Deflection} = 0$$

$$\text{Slope} = \frac{\partial w}{\partial x} = 0$$

3.1.1 Free-Free Uniform Beam

The free-free uniform beam with the dimensions shown in Figure 7 is taken as a sample:

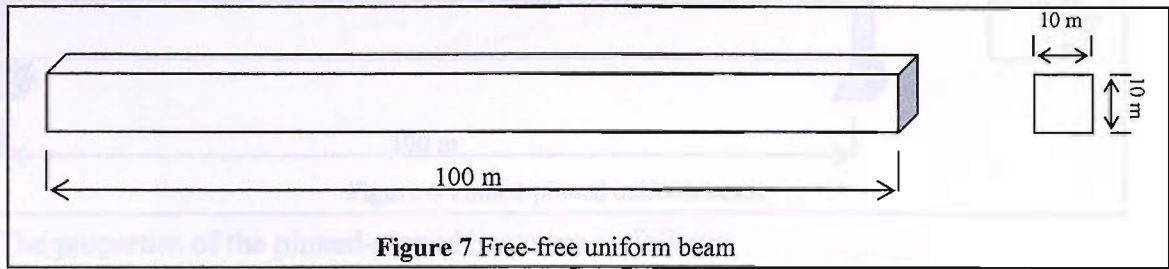


Figure 7 Free-free uniform beam

The properties of the beam are as follows:

$$\text{Young's modulus, } E = 207 \text{e}^9 \text{ N/m}^2$$

$$\text{Mass density, } \rho = 7860 \text{ kg/m}^3$$

$$\text{Moment of inertia, } I(x) = \frac{bd^3}{12} = 833.33 \text{ m}^4$$

As mentioned in the previous section, natural frequencies for each mode n can be found using the Eq.(34):

$$\omega_n = \beta^2 \sqrt{\frac{EI}{\rho A}} = (\beta_n l)^2 \sqrt{\frac{EI}{\rho A l^4}}$$

The values of $\beta_n l$ for each type of boundary condition can be found in textbooks and in this case, for the free-free uniform beam, these are:

$\beta_1 l = 4.730041$, $\beta_2 l = 7.853205$, $\beta_3 l = 10.995608$, $\beta_4 l = 14.137165$, ($\beta l = 0$ for rigid body mode) (Rao, 1995)

Using the above $\beta_n l$ values and the formula for natural frequency, the natural frequencies for the first four lateral deflected modes of free-free beam are found as follows:

$$\omega_1 = 33.144 \text{ rad/s} = 5.275 \text{ Hz} \quad \omega_2 = 91.364 \text{ rad/s} = 14.541 \text{ Hz}$$

$$\omega_3 = 179.108 \text{ rad/s} = 28.506 \text{ Hz} \quad \omega_4 = 296.079 \text{ rad/s} = 47.122 \text{ Hz}$$

The corresponding mode shapes will be:

$$W_n(x) = C_1 \left[\cosh(\beta l)_n \frac{x}{l} + \cos(\beta l)_n \frac{x}{l} \right] + C_2 \left[\sinh(\beta l)_n \frac{x}{l} + \sin(\beta l)_n \frac{x}{l} \right] \quad (33a)$$

where

$$C_1 = -C_2 \frac{\sinh(\beta l)_n - \sin(\beta l)_n}{\cosh(\beta l)_n - \cos(\beta l)_n} \quad (33aa)$$

3.1.2 Pinned-Pinned Uniform Beam

The pinned-pinned uniform beam with its dimensions is shown in Figure 8:

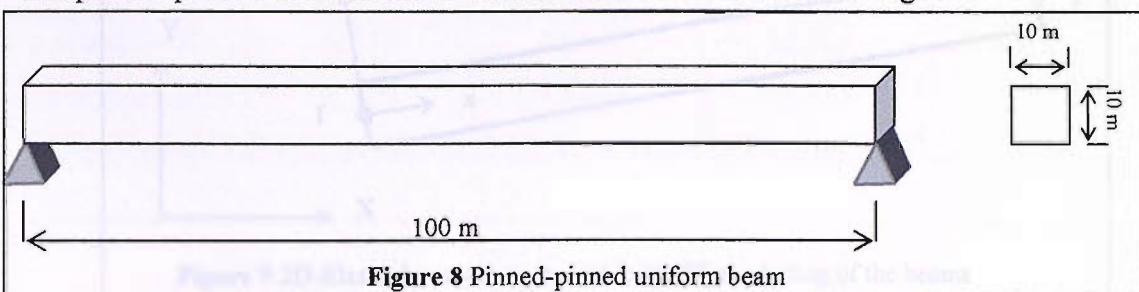


Figure 8 Pinned-pinned uniform beam

The properties of the pinned-pinned beam are as follows:

$$\text{Young's modulus, } E = 207e^9 \text{ N/m}^2$$

$$\text{Mass density, } \rho = 7860 \text{ kg/m}^3$$

$$\text{Moment of inertia, } I(x) = \frac{bd^3}{12} = 833.33m^4$$

The values of $\beta_n l$ for pinned-pinned uniform beam are:

$$\beta_1 l = \pi, \beta_3 l = 3\pi, \beta_2 l = 2\pi, \beta_4 l = 4\pi \text{ (Rao 1995)}$$

After substituting all the unknowns in Eq.(34), the natural frequencies for the first four lateral deflected modes of pinned-pinned beam are found as follows:

$$\omega_1 = 14.621 \text{ rad/s} = 2.327 \text{ Hz} \quad \omega_2 = 58.483 \text{ rad/s} = 9.308 \text{ Hz}$$

$$\omega_3 = 131.587 \text{ rad/s} = 20.943 \text{ Hz} \quad \omega_4 = 233.933 \text{ rad/s} = 37.232 \text{ Hz}$$

The corresponding mode shapes will be:

$$W_n(x) = \sqrt{\frac{2}{\rho Al}} \sin\left(\frac{n\pi x}{l}\right) \quad (33b)$$

3.2 Numerical Modal Analysis of Beams

The beams used in the previous section are modelled in the Finite Element Analysis (FEA) software called ANSYS. Beam-3 (2-D Elastic Beam) type 20 beam elements and 21 nodes are used to build the beam in the FE modelling. Beam-3 element shown in Figure 9, is a two-node uniaxial element with tension, compression, and bending capabilities. The element has three degrees of freedom at each node: translations in the nodal x and y directions and rotation about the nodal z-axis (ANSYS Elements Reference).

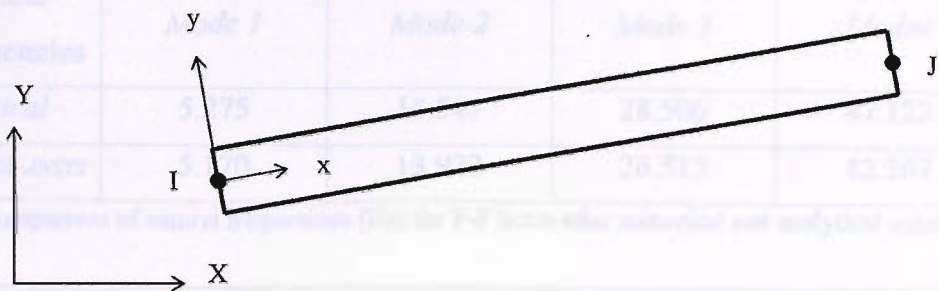


Figure 9 2D-Elastic beam element used in the FE modelling of the beams
(ANSYS Elements Reference)

The translations in the nodal x and y directions are constrained to account for the pinned-pinned boundary conditions in the FE model of the pinned-pinned beam.

Modal solution is applied after modelling the beams and 10 modes are extracted for each beam excluding the rigid body modes and the modes with longitudinal translations. The natural characteristics of these beams obtained from FEA are presented in Figure 10, Figure 12 and compared separately in the section 3.2.1 and 3.2.2.

3.2.1 Free-Free Uniform Beam

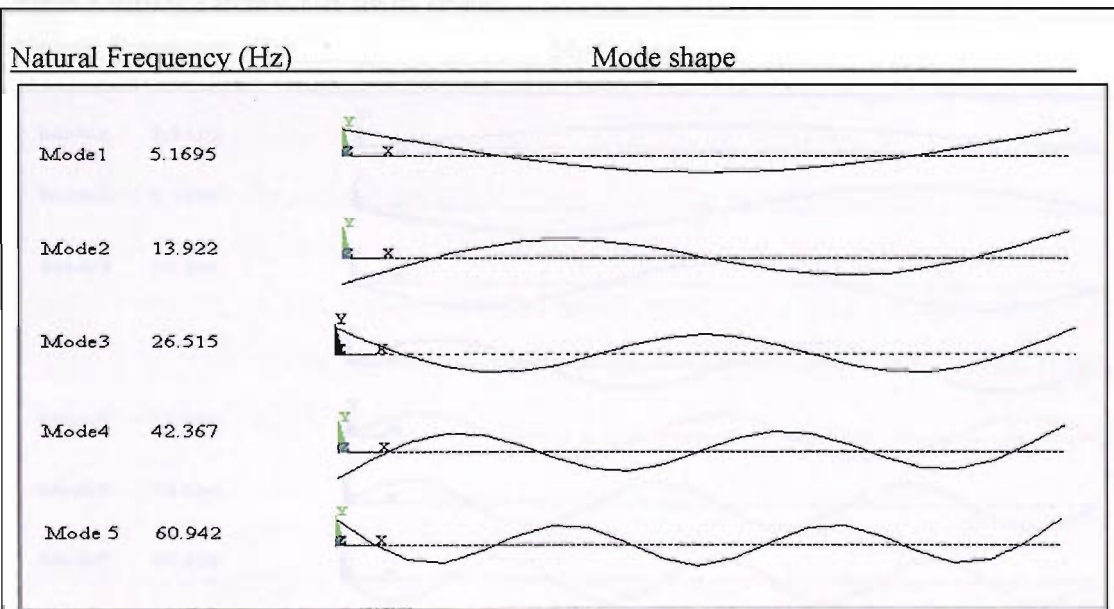


Figure 10 Mode shapes and natural frequencies of free-free uniform beam-ANSYS

| F-F beam N. Frequencies | Mode 1 | Mode 2 | Mode 3 | Mode 4 |
|----------------------------|--------|--------|--------|--------|
| Analytical | 5.275 | 14.541 | 28.506 | 47.122 |
| Numerical-ANSYS | 5.170 | 13.922 | 26.515 | 42.367 |

Table 1 Comparison of natural frequencies (Hz) for F-F beam after numerical and analytical solutions

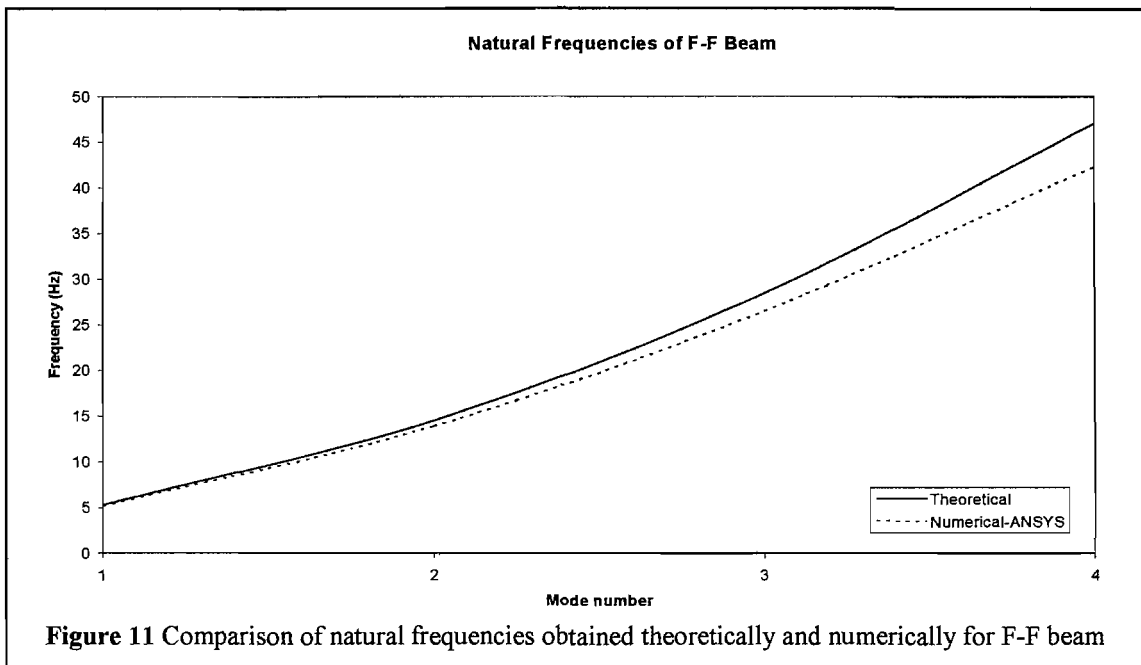


Figure 11 Comparison of natural frequencies obtained theoretically and numerically for F-F beam

3.2.2 Pinned-Pinned Uniform Beam

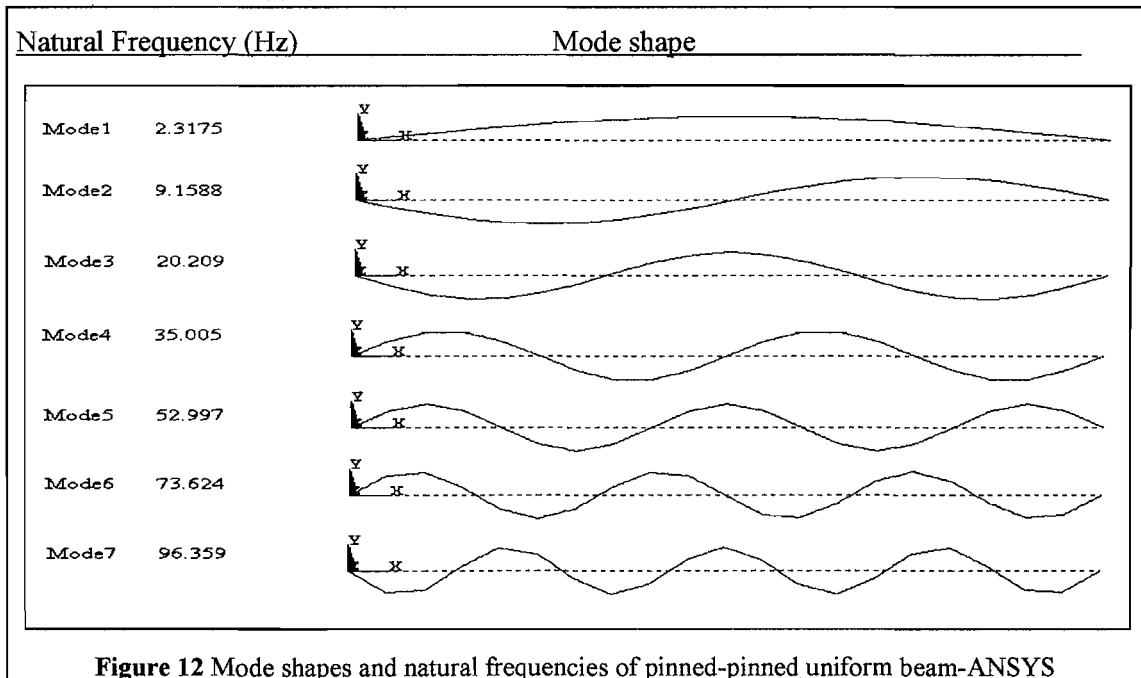


Figure 12 Mode shapes and natural frequencies of pinned-pinned uniform beam-ANSYS

| P-P beam N.Frequencies | Mode 1 | Mode 2 | Mode 3 | Mode4 |
|---------------------------|--------|--------|--------|--------|
| Analytical | 2.327 | 9.308 | 20.943 | 37.232 |
| Numerical-ANSYS | 2.318 | 9.159 | 20.209 | 35.005 |

Table 2 Comparison of natural frequencies (Hz) for P-P beam after numerical and analytical solutions

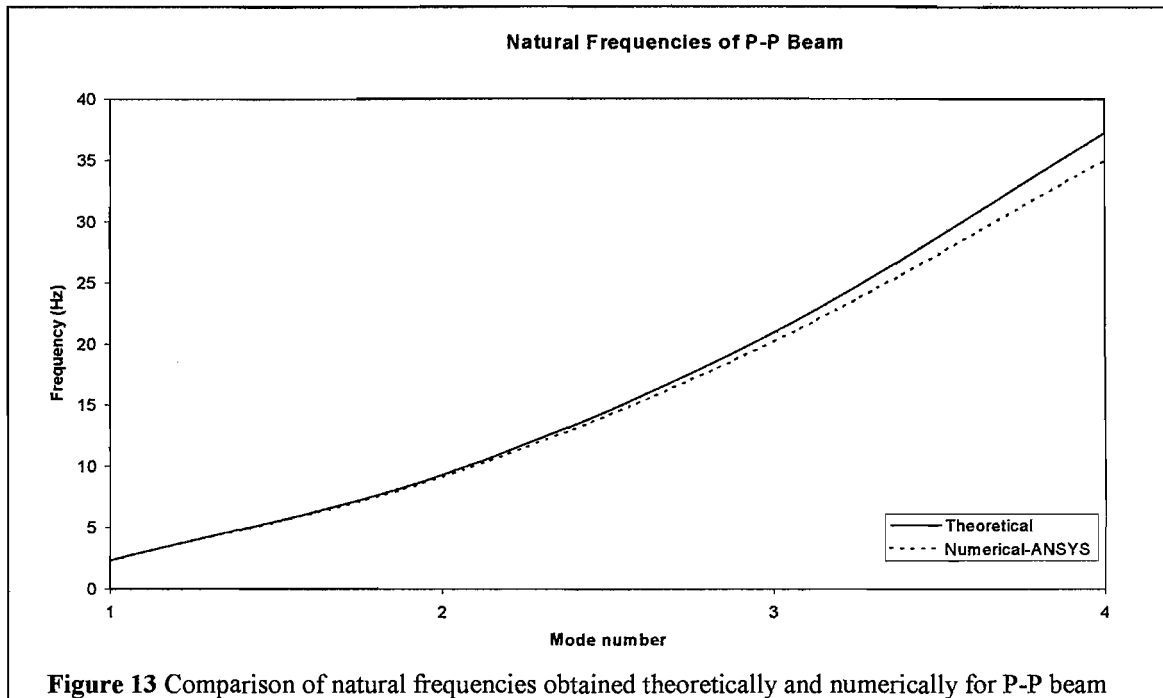


Figure 13 Comparison of natural frequencies obtained theoretically and numerically for P-P beam

The comparison of analytical and numerical modal analysis shows that the natural frequencies obtained from both methods are reasonably close (Table 1, Table 2). However, it is evident that the natural frequencies of lower modes for both beams agree better than the higher modes. In other words as the number of mode increases, the differences between the analytical and the numerical results also increase, because natural frequencies get higher with the involvement of higher modes (Figure 11, Figure 13). This effect is more dominant in F-F beam as it has higher natural frequencies than the P-P beam.

As a result the natural characteristics found through the modal analysis by FEA-ANSYS are satisfactory to use in the following mode superposition harmonic and transient analyses.

3.3 Determination of Generalized Coordinates

In the light of orthogonality relations of mode shapes (characteristic functions or principal modes), it can be shown that the mode shapes satisfy the equations (Bishop, R.E.D. and Price, W.G., 1979)

$$\int_0^l (\mu w_r w_s + I_y \theta_r \theta_s) dx = a_{rs} \delta_{rs} \quad (35)$$

$$\int_0^l (EI \theta'_r \theta'_s + kAG \gamma_r \gamma_s) dx = \omega_r^2 a_{rs} \delta_{rs} = c_{rs} \quad (36)$$

$$\int_0^l (\alpha kAG \gamma_r \gamma_s + \beta EI \theta'_r \theta'_s) dx = 2a_{rs} \omega_r \nu_r \delta_{rs} = b_{rs} \quad (37)$$

where $\mu(x)$ is the mass per unit length, $w_r(x)$ and $w_s(x)$ are two of the mode shapes, a_{rs} is the generalized mass which determines the scales of the characteristics functions, c_{rs} and b_{rs} are generalized stiffness and generalized damping respectively, $I_y(x)$ is the moment of inertia per unit length, $\theta(x,t)$ is the slope attributable to bending, $EI(x)$ is the flexural rigidity, $kAG(x)$ is the shear rigidity, k is the constant related with the shape of the cross section of the structure being examined, γ is the shear strain, α and β are damping constants relating to shearing and bending distortions respectively, ω_r is the natural frequency of the r^{th} mode, ν_r is the modal damping factor, and δ_{rs} is the Kronecker delta function defined by

$$0 \quad \text{for} \quad r \neq s$$

$$\delta_{rs} =$$

$$1 \quad \text{for} \quad r = s$$

$$\begin{aligned}
a_{ss} &= \int_0^l (\mu w_s^2 + I_y \theta_s^2) dx \\
c_{ss} &= \omega_s^2 a_{ss} = \int_0^l (EI \theta_s'^2 + kAG \gamma_s^2) dx \\
b_{ss} &= 2a_{ss} \omega_s v_s = \int_0^l (\alpha kAG \gamma_s^2 + \beta EI \theta_s'^2) dx
\end{aligned} \tag{38}$$

If no allowance is to be made for shear effect and rotatory inertia k and I_y must be taken as zero and the functions $w_r(x)$, $w_s(x)$ will be different;

$$\begin{aligned}
\int_0^l \mu(x) w_r(x) w_s(x) dx &= a_{rs} \delta_{rs} \\
\int_0^l EI(x) w_r''(x) w_s''(x) dx &= \omega_r^2 a_{rs} \delta_{rs}
\end{aligned} \tag{39}$$

In modal analysis, the equation of motion for an undamped system, expressed in matrix notation is,

$$[M]\{\ddot{w}\} + [K]\{w\} = \{0\} \tag{40}$$

For a linear system, free vibrations will be harmonic of the form:

$$\{w\} = \{w_r\} \cos \omega_r t$$

where $\{w_r\}$ is the eigenvector representing the mode shape of the r^{th} natural frequency, ω_r is the r^{th} natural circular frequency, and t is the time.

Equation (40) becomes:

$$(-\omega_r^2 [M] + [K])\{w_r\} = \{0\} \tag{41}$$

This equality is satisfied if either $\{w_r\} = \{0\}$ or if the determinant of $([K] - \omega^2 [M])$ is zero. The first option is the trivial one and, therefore, is not of interest. Thus, the second one gives the solution:

$$[K] - \omega^2 [M] = 0$$

This is an eigenvalue problem, which may be solved for up to n values of ω^2 and n eigenvectors $\{w_r\}$, which satisfy equation (41)

For mode shape normalization, the mode shapes can either be normalized to the mass matrix that each eigenvector (mode shape) $\{w_r\}$ is normalized such that:

$$\{w_r\}^T [M] \{w_r\} = 1$$

or the mode shapes can be normalized to unity instead of the mass matrix that $\{w_r\}$ is normalized such that its largest component is 1.0 (unity).

After determining the mode shapes normalized to either mass matrix or unity, it is possible to derive the generalized mass associated with the r^{th} mode shape from a comparison of (a) the mass matrix and, (b) the unit displacement normalization schemes given as:

$$(a) \{w_r\}_m^T [M] \{w_r\}_m = 1, \text{ i.e. } a_{rr} = 1$$

$$(b) \{w_r\}_u^T [M] \{w_r\}_u = a_{rr}$$

where a_{rr} is the required corresponding generalized mass.

Let s_r be a scaling factor corresponding to the r^{th} mode so that:

$$\{w_r\}_m s_r = \{w_r\}_u$$

Substituting the above expression into equation (b) gives

$$s_r \{w_r\}_m^T [M] \{w_r\}_m s_r = a_{rr}$$

which reduces to

$$\text{generalized mass} = a_{rr} = s_r^2 = \left(\frac{\{w_r\}_u}{\{w_r\}_m} \right)^2$$

Generalized masses of the beams, calculated according to the different mode shape normalization (to mass matrix and unity) in ANSYS are as follows:

Mode shapes normalized to mass matrix:

| | | | | |
|--|--|--|---|---|
| 0.960332722 Deflection term | 0.916487786 Deflection term | 0.864961161 Deflection term | 0.80781805 Deflection term | 0.747882354 Deflection term |
| 0.03967032 Rotation term | 0.083518798 Rotation term | 0.135044643 Rotation term | 0.19176211 Rotation term | 0.250268898 Rotation term |
| 1.000003042 gm(4) (kg.m²) | 1.000006584 gm(5) (kg.m²) | 1.000005805 gm(7) (kg.m²) | 0.99958016 gm(8) (kg.m²) | 0.998151252 gm(10) (kg.m²) |

Table 3 Generalized masses of the free-free beam (consisting of 20 finite elements) for modes 1-5 corresponding to actual modes 4-5-7-8-10

| | | | | | | |
|---|---|--|---|--|---|---|
| 0.99183957 <i>def. term</i> | 0.967637159 <i>def. term</i> | 0.931130446 <i>def. term</i> | 0.88749587 <i>def. term</i> | 0.8313391 <i>def. term</i> | 0.769061 <i>def. term</i> | 0.713577 <i>def. term</i> |
| 4.99705E-14 <i>rot. term</i> | 0.031851581 <i>rot. term</i> | 0.068929199 <i>rot. term</i> | 0.11634051 <i>rot. term</i> | 0.170727701 <i>rot. term</i> | 0.228925 <i>rot. term</i> | 0.28834 <i>rot. term</i> |
| 0.99183957 <i>gm(1) (kg.m²)</i> | 0.99948874 <i>gm(2) (kg.m²)</i> | 1.000059645 <i>gm(3) (kg.m²)</i> | 1.00383637 <i>gm(5) (kg.m²)</i> | 1.002066801 <i>gm(7) (kg.m²)</i> | 0.997986 <i>gm(8) (kg.m²)</i> | 1.001916 <i>gm(10)(kg.m²)</i> |

Table 4 Generalized masses of the pinned-pinned beam (consisting of 20 finite elements) for modes 1-7 corresponding to actual modes 1-2-3-5-7-8-10

Mode shapes normalized to unity:

| | | | | |
|--|--|--|--|---|
| 1.96004E+07 <i>def. term</i> | 1.97903E+07 <i>def. term</i> | 2.01884E+07 <i>def. term</i> | 2.08442E+07 <i>def. term</i> | 2.18060E+07 <i>def. term</i> |
| 8.09701E+05 <i>rot. term</i> | 1.80382E+06 <i>rot. term</i> | 3.15406E+06 <i>rot. term</i> | 4.95423E+06 <i>rot. term</i> | 7.30888E+06 <i>rot. term</i> |
| 2.04101E+07 <i>gm(4) (kg.m²)</i> | 2.15941E+07 <i>gm(5) (kg.m²)</i> | 2.33425E+07 <i>gm(7) (kg.m²)</i> | 2.57985E+07 <i>gm(8) (kg.m²)</i> | 2.91149E+07 <i>gm(10) (kg.m²)</i> |

Table 5 Generalized masses of the free-free beam (consisting of 20 finite elements) for modes 1-5 corresponding to actual modes 4-5-7-8-10

| | | | | | | |
|--|--|--|--|--|--|--|
| 3.93002E+07 <i>def. term</i> | 3.93003E+07 <i>def. term</i> | 3.92998E+07 <i>def. term</i> | 4.34487E+07 <i>def. term</i> | 3.92997E+07 <i>def. term</i> | 3.92896E+07 <i>def. term</i> | 3.92914E+07 <i>def. term</i> |
| 3.23229E+05 <i>rot. term</i> | 1.29293E+06 <i>rot. term</i> | 2.90906E+06 <i>rot. term</i> | 5.71778E+06 <i>rot. term</i> | 8.08055E+06 <i>rot. term</i> | 1.16328E+07 <i>rot. term</i> | 1.58325E+07 <i>rot. term</i> |
| 3.96235E+07 <i>gm(1) (kg.m²)</i> | 4.05932E+07 <i>gm(2) (kg.m²)</i> | 4.22088E+07 <i>gm(3) (kg.m²)</i> | 4.91665E+07 <i>gm(5) (kg.m²)</i> | 4.73802E+07 <i>gm(7) (kg.m²)</i> | 5.09224E+07 <i>gm(8) (kg.m²)</i> | 5.51239E+07 <i>gm(10)(kg.m²)</i> |

Table 6 Generalized masses of the pinned-pinned beam (consisting of 20 finite elements) for modes 1-7 corresponding to actual modes 1-2-3-5-7-8-10

The deflection and rotation values in the above tables stand for the numerical integration results of the first and the second part of the given integral respectively in Eq.(35). The sum of these two gives the generalized mass.

After mode shape normalization to mass matrix in ANSYS, generalized masses for each mode shape must be equal to 1 as explained earlier. Hence the integral in Eq.(35) giving the generalized masses is evaluated numerically for each beam and for each mode, resulting with generalized masses equal to 1 as shown in Table 3 and Table 4.

The generalized masses found after mode shape normalization to unity shown in Table 5 and Table 6 can also be used if a subsequent analysis is going to be performed based on this type of normalization.

3.4 Analytical Calculation of the Beam Deflections

The general form of the equation of motion of a multiple degrees of freedom system in matrix form is namely

$$[a]\{\ddot{p}(t)\} + [b]\{\dot{p}(t)\} + [c]\{p(t)\} = \{F(t)\} \quad (42)$$

where $[a]$ is the generalized mass matrix, $[b]$ is the generalized damping matrix, $[c]$ is the generalized stiffness matrix, $\{p(t)\}$ is the principal coordinate representing the response and $\{F(t)\}$ is the generalized force representing input loading. $[a]$, $[b]$ and $[c]$ are diagonal matrices, $\{p(t)\}$ and $\{F(t)\}$ are column vectors.

For a harmonic excitation of the form $F(t) = F \sin \omega t$ or $F(t) = F \cos \omega t$ or more conveniently in complex format $F(t) = Fe^{i\omega t}$, F indicates the amplitude and ω the frequency of the harmonic excitation.

According to the theorem due to Rayleigh, any distortion of the beam may be expressed as an aggregate of distortions in its principal modes. That is to say, for a symmetric deflection, (Bishop, R.E.D. and Price, W.G., 1979)

$$w(x, t) = \sum_{r=0}^{\infty} p_r(t) w_r(x) \quad (43)$$

where $p_r(t)$ is the r^{th} principal coordinate.

After solving principal coordinates from the equation of motion for each mode, they are substituted in Eq.(43) and then total deflection for the desired location is found using the mode shapes and principal coordinates.

For a harmonic excitation $\{F(t)\} = Fe^{i\omega t}$, the response is also harmonic and in the form $\{p(t)\} = Pe^{i\omega t}$.

$$\{\dot{p}(t)\} = Pi\omega e^{i\omega t} \quad , \quad \{\ddot{p}(t)\} = -P\omega^2 e^{i\omega t}$$

The generalized force $F_r(t)$ corresponding to $p_r(t)$ is (Rao 1995)

$$F_r(t) = \int_0^l f(x, t) w_r(x) dx \quad (44)$$

In definition, generalized force is equal to the product of the amplitude of the harmonic force with the modal displacement at the point where the force is applied.

After substituting the equations above to the equation of motion (42)

$$\{P\}(-[a]\omega^2 + i[b]\omega + [c]) = \{F\} \quad (45)$$

is obtained.

As a result of orthogonality relations

$$P_r(-a_{rr}\omega^2 + ib_{rr}\omega + c_{rr}) = F_r \quad (46)$$

can be written, where,

$a_{rr} = 1$ (Generalized mass after mode shape normalization to mass matrix)

$$b_{rr} = 2a_{rr}\omega_r v_r \text{ (Generalized damping)}$$

$$c_{rr} = \omega_r^2 a_{rr} \text{ (Generalized stiffness)}$$

For the undamped condition ($b_{rr} = 0$)

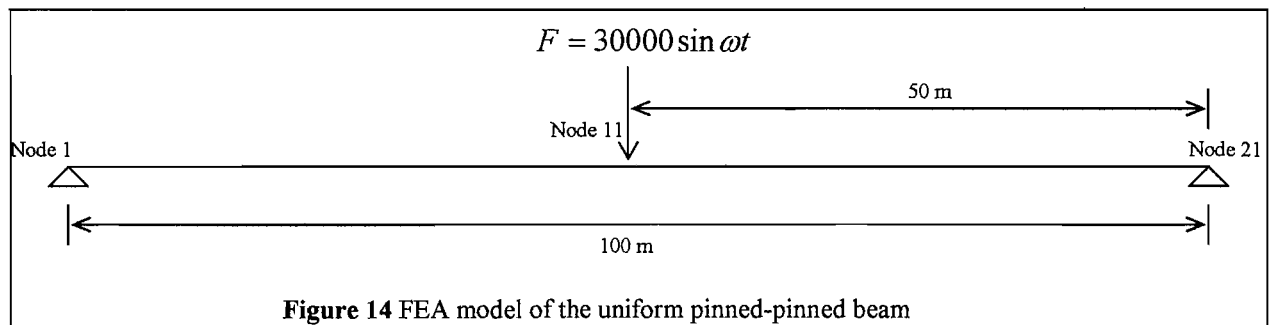
$$P_r = \frac{F_r}{(-\omega^2 + \omega_r^2)} \quad (47)$$

For the damped condition

$$P_r = \frac{F_r}{((\omega_r^2 - \omega^2) + i2\omega_r\nu_r\omega)} \quad (48)$$

Each uncoupled equation for $p_r(t)$ is solved and then substituted in the total deflection equation (43) together with modal deflections for each mode obtained from FE modal analysis.

A harmonic force is applied to the uniform pinned-pinned beam defined in Figure 8 and the FE visualization of the beam under forced vibration is illustrated in Figure 14.



3.5 Comparison of Numerical Results with Theoretical Calculations on the Frequency Domain

In this section, a comparison is made in the amplitudes of displacement between analytical calculation (Eq.43, Eq.47 & Eq.48) and ANSYS after applying mode superposition harmonic analysis on the pinned-pinned uniform beam considering both undamped and damped conditions. Following the presentation of the key results, discussion is made in section 3.6.

3.5.1 Undamped Condition

Forcing frequency range is taken between 0-100 Hz and the comparisons are made at nodes 5, 11, and 14 with the harmonic force applied at node 11. Only the responses at node 5 are presented here in Table 7 and Figure 15. In the analytical solution, totally 5, 10 and 17 principal modes are used for harmonic mode superposition.

| forcing freq.(Hz) | 2 | 10 | 30 | 50 | 80 | 100 |
|-------------------|-------------|-------------|-------------|-------------|-------------|-------------|
| ANSYS | 8.18150E-06 | 1.73590E-07 | 2.34200E-08 | 5.19140E-09 | 5.13480E-09 | 1.84260E-08 |
| 17 mode | 8.18195E-06 | 1.73610E-07 | 2.33978E-08 | 5.16994E-09 | 5.11214E-09 | 1.84486E-08 |
| 10 mode | 8.18202E-06 | 1.73541E-07 | 2.34685E-08 | 5.24441E-09 | 5.19753E-09 | 1.83500E-08 |
| 5 mode | 8.18092E-06 | 1.74650E-07 | 2.22350E-08 | 3.66922E-09 | 1.09529E-09 | 6.57520E-10 |

Table 7 The values of undamped case amplitudes (in meters) at node 5 (F applied at node 11) on the frequency domain between ANSYS and theory (superposition of first 5,10, and 17 modes)

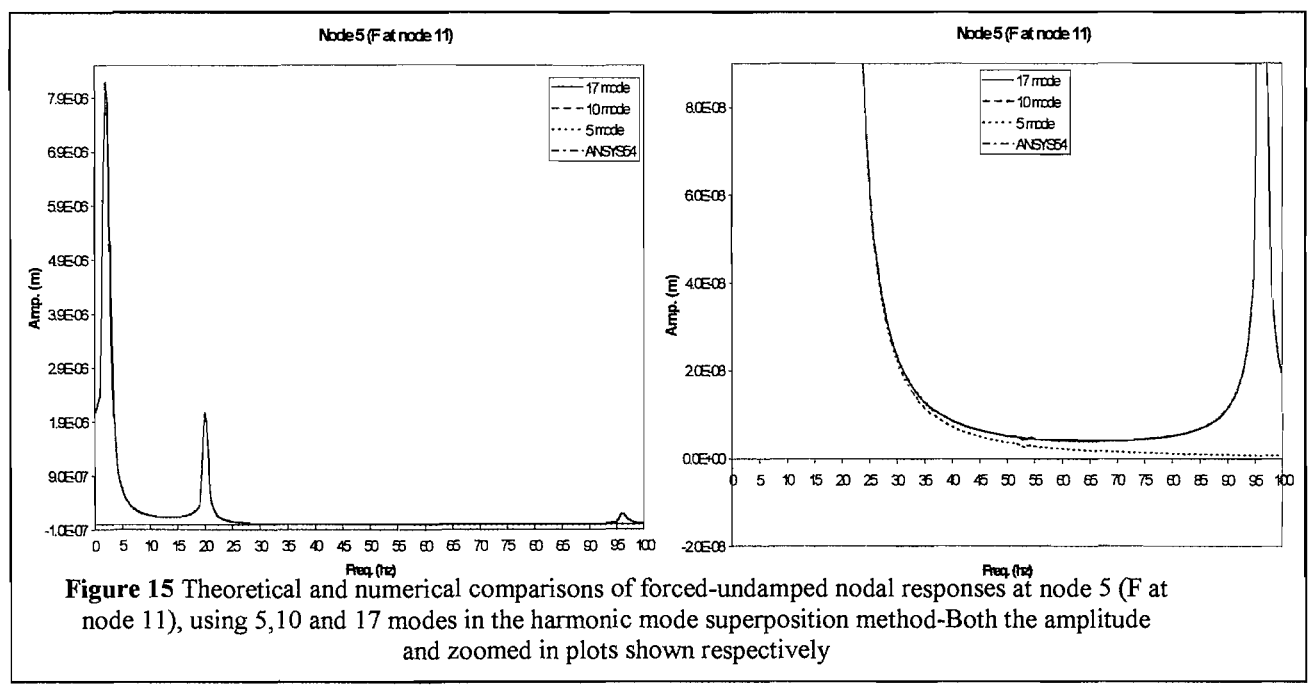


Figure 15 Theoretical and numerical comparisons of forced-undamped nodal responses at node 5 (F at node 11), using 5,10 and 17 modes in the harmonic mode superposition method-Both the amplitude and zoomed in plots shown respectively

3.5.2 Damped Condition

Three different modal damping ratios 0.01, 0.1 and 0.5 are considered in the system. The amplitudes are found at nodes 5, 11, and 14, for the damping ratio 0.01. Only the results found at node 5 with harmonic force applied at node 11 and node 12 are presented here in Figure 16 and Figure 17 separately. To see the overall effect of using different damping ratios, Figure 20 and Figure 21 are also added to the end of this section.

Damping Ratio = 0.01

| forcing freq.(Hz) | 2 | 10 | 30 | 50 | 80 | 100 |
|-------------------|-------------|-------------|-------------|-------------|-------------|-------------|
| ANSYS | 8.16279E-06 | 1.73597E-07 | 2.33918E-08 | 5.16859E-09 | 5.10420E-09 | 1.78065E-08 |
| 17 mode | 8.16330E-06 | 1.73597E-07 | 2.33913E-08 | 5.16905E-09 | 5.10396E-09 | 1.78062E-08 |
| 10 mode | 8.16337E-06 | 1.73528E-07 | 2.34620E-08 | 5.24350E-09 | 5.18930E-09 | 1.77114E-08 |
| 5 mode | 8.16228E-06 | 1.74638E-07 | 2.22297E-08 | 3.66921E-09 | 1.09530E-09 | 6.57525E-10 |

Table 8 The values of damped case (dmp.r.=0.01) amplitudes (in meters) at node 5 (F applied at node 11) on the frequency domain between ANSYS and theory (superposition of first 5,10, and 17 modes)

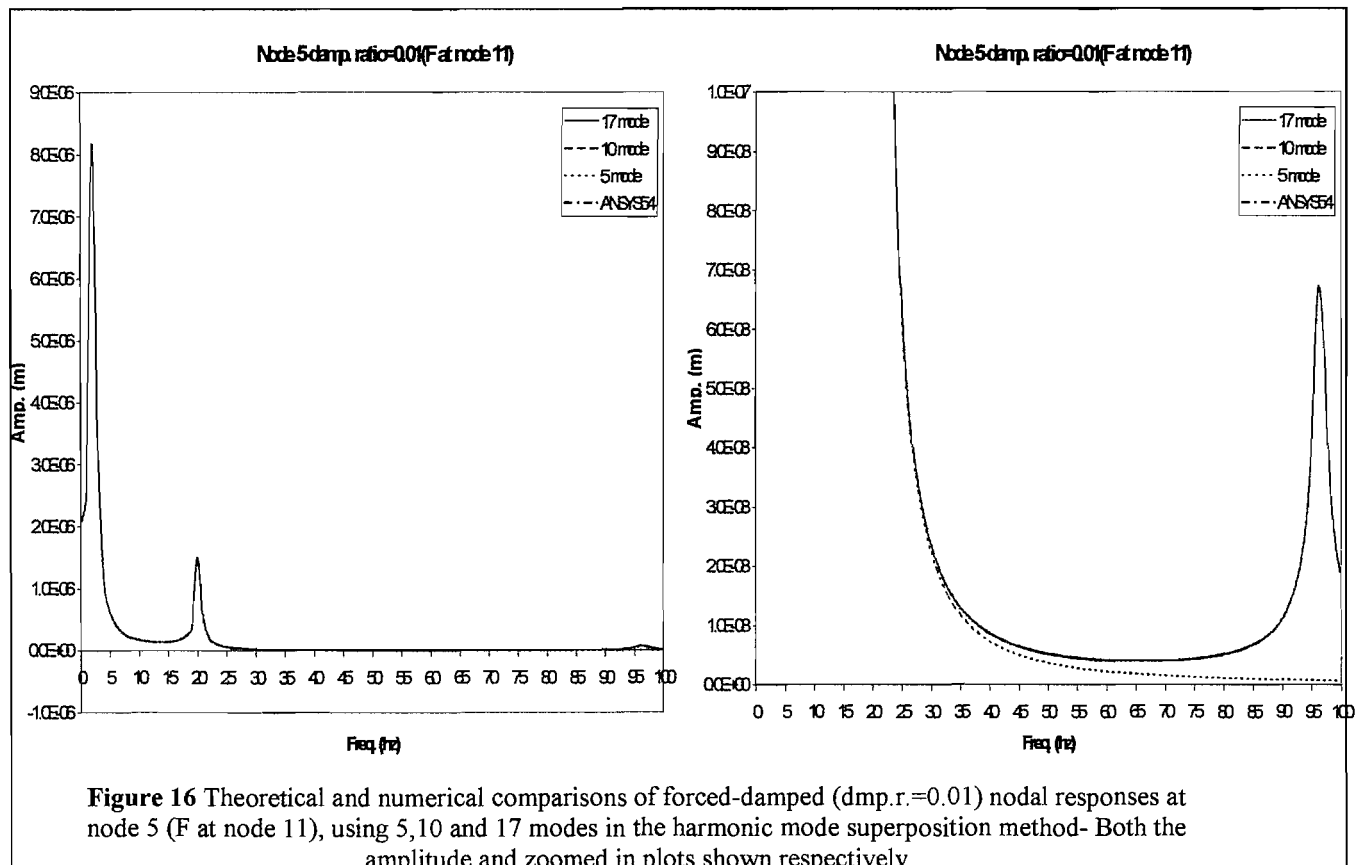


Figure 16 Theoretical and numerical comparisons of forced-damped (dmp.r.=0.01) nodal responses at node 5 (F at node 11), using 5,10 and 17 modes in the harmonic mode superposition method- Both the amplitude and zoomed in plots shown respectively

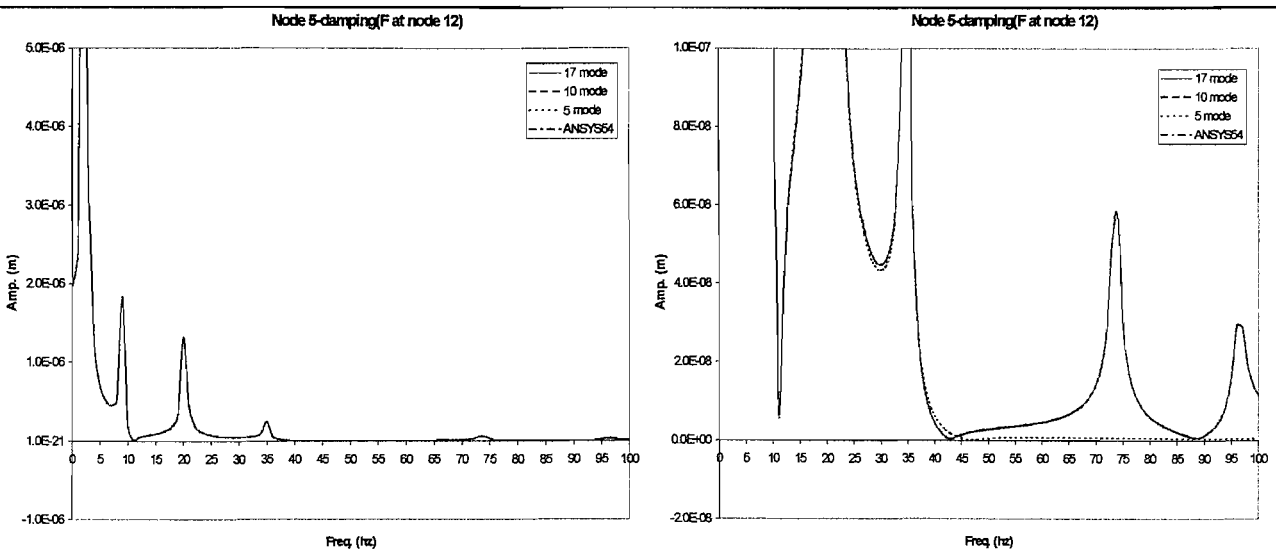


Figure 17 Theoretical and numerical comparisons of forced-damped ($dmp.r.=0.01$) nodal responses at node 5 (F at node 12), using 5, 10 and 17 modes in the harmonic mode superposition method-Both the amplitude and zoomed in plots shown respectively

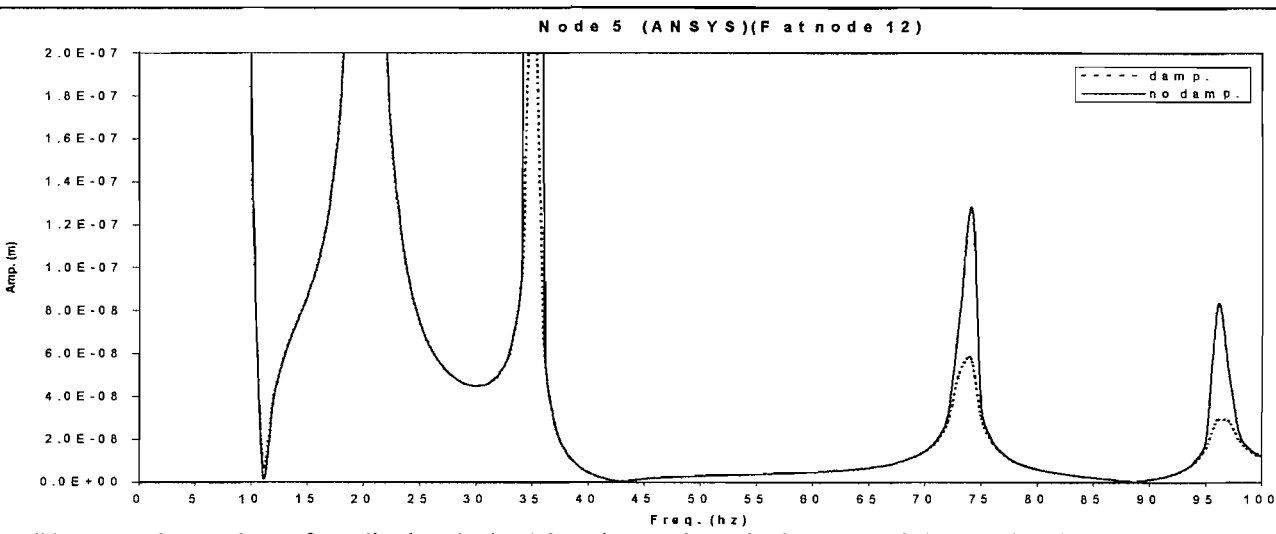


Figure 18 Comparison of amplitudes obtained from harmonic excitation-ANSYS (F at node 12) with and without damping ($dmp.r.=0.01$)

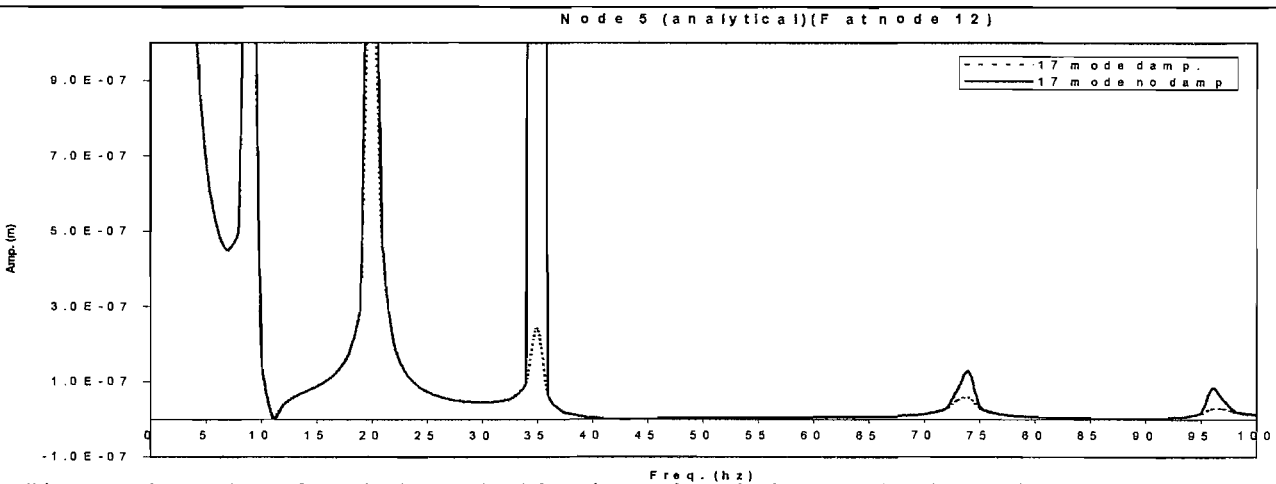
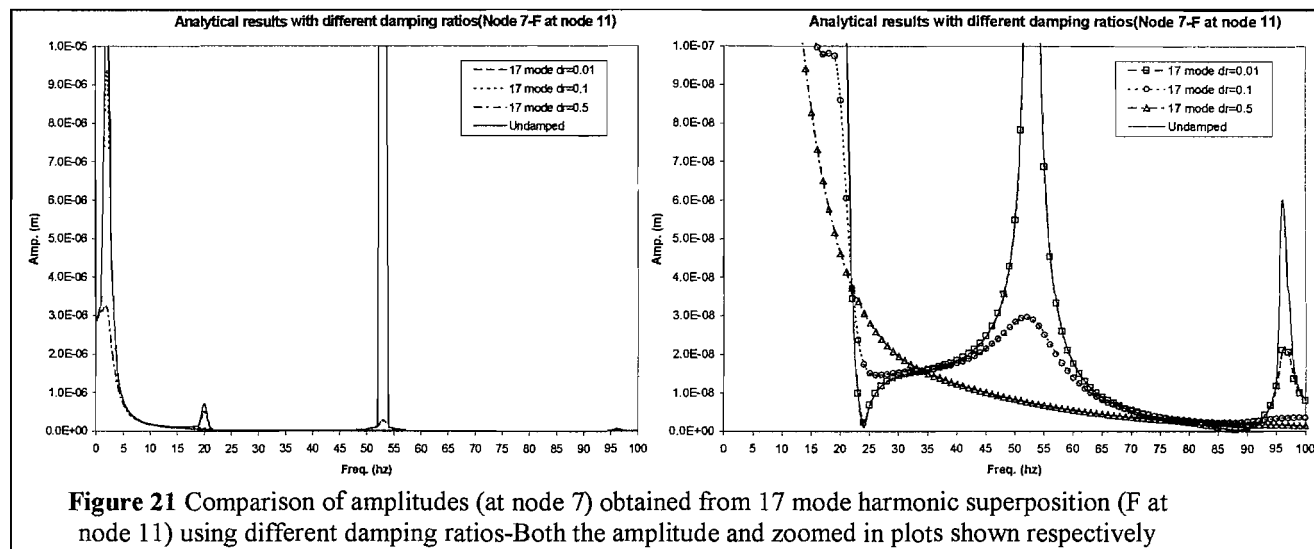
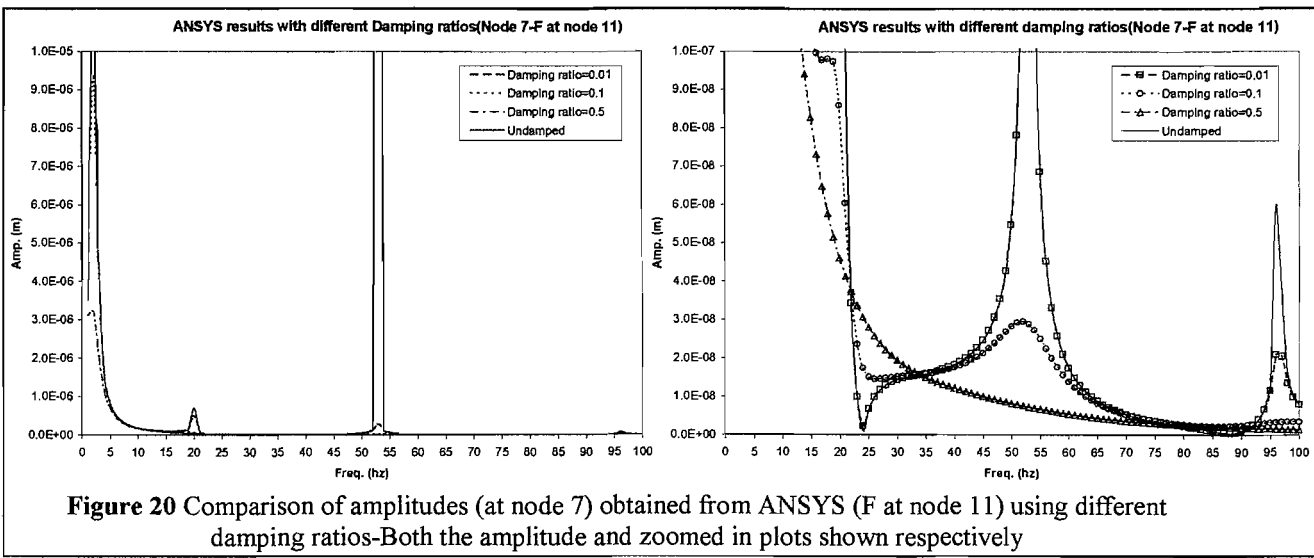


Figure 19 Comparison of amplitudes obtained from harmonic excitation-analytical (F at node 12) with and without damping ($dmp.r.=0.01$)



3.6 Discussion

At the beginning of Chapter 3, theoretical and numerical-ANSYS modal analyses are applied to a uniform beam with two different boundary conditions, free-free and pinned-pinned, as the basis of following harmonic and transient mode superposition analyses. Good agreements are obtained after comparing both theoretical and numerical methods.

Generalized components in the generalized equation of motion are determined depending on the normalization of mode shapes according to mass matrix and unity.

Expected generalized mass values are obtained and confirmed after mode shape normalization to mass matrix.

After obtaining the principal modes, natural frequencies and the generalized components, a harmonic mode superposition method is used to calculate the amplitudes of the total deflections in different nodes for a frequency range of 0-100 Hz.

In the mode superposition method 5,10 and 17 principal modes are used to see the difference when different numbers of modes are superposed.

When the figures showing amplitudes versus frequencies are examined in both undamped and damped harmonic responses, it's seen that there are significant peaks in the amplitudes. These peaks occur at different frequencies with different magnitudes for each node location due to resonance. However the natural frequencies of the pinned-pinned beam in Figure 12 do not coincide with all the frequencies where peaks in the amplitudes occur. Because, $p_r(t)$ in Eq. (43) is equal to zero for particular modes as a result of zero value generalized force which is equal to the product of the amplitude of the harmonic force with the modal displacement at the point where the force is applied. In other words, there are peaks at 2.318Hz, 20.209Hz, 52.997Hz and 96.359Hz, except 9.159Hz, 35.005Hz and 73.624Hz in Figure 15. By simply looking at Figure 12, it is easy to notice that at node 11, where force is applied, the modal deflections for natural frequencies 9.159Hz (mode2), 35.005Hz (mode4) and 73.624Hz (mode6) are all zero. To make this point clearer, Figure 17, representing forced-damped ($damp.r. = 0.01$) nodal responses at node 5 when harmonic force is applied at node 12, is also a good example. There are six peaks in this graph and all coincide with the natural frequencies of the pinned-pinned beam in Figure 12 except 52.997Hz. Because in this case, modal deflection required at the force application node 12 for generalized force calculation is not zero at 52.997Hz(mode5-Figure 12), but the modal deflection at node 5 itself is zero. This results with a zero value contribution of mode 5, which has a natural frequency of

52.997Hz, in the mode superposition method and erases the resonance effect from Figure 17 for this particular natural frequency.

Another conclusion that must be given here is the effect of using 5, 10 and 17 number of modes in harmonic mode superposition. As the forcing frequency increases, convergence of 5 modes is not sufficient. On the other hand, using 10 and 17 modes brings the contribution of higher modes to the overall response and makes the mode superposition converge successfully (Figure 16). The ANSYS results agree with the analytical mode superposition method results using 10 and 17 modes as seen in Figure 16.

Same analysis is repeated for damped condition and results are compared analytically and numerically. As expected, the amplitudes decreased with the existence of damping which can be seen in Figure 18 and Figure 19. To see the effect of different damping ratios in ANSYS and theory, and to be sure about modelling the damping correctly in two methods, harmonic responses of pinned-pinned beam with damping, at node 7 is presented in Figure 20 and Figure 21 respectively. In these figures it is evident that as the damping ratio increases from 0.01 to 0.1 and 0.5, the amplitudes decreases accordingly.

Both ANSYS and analytical calculations give the same responses. Thus, the modelling of harmonic response with damping also verifies each other in these methods.

4 DRY ANALYSIS of a SWATH

Dry analysis of a multi-hulled vessel is presented in this chapter. Multi-hulled vessels have a great importance in naval architecture because of their advantages. A SWATH-like uniform ship is taken as an example. The concept of the Small Waterplane Area Twin Hull ship (SWATH) evolved through many years and is still quite attractive. Since the early 70s, a lot of research has been carried out concerning the structural design of these vessels. A SWATH ship's key advantages are:

- Ability to sustain a high proportion of its normal cruising speed in rough seas, in other words it has overall seakeeping quality,
- Steadiness and ride quality ending up with the decrease in the possibility of becoming seasick,
- Its broad loading deck compared to a single hull ship of equivalent displacement.

The dry analysis of an idealised SWATH ship is carried out, as a preamble to a future deck analysis.

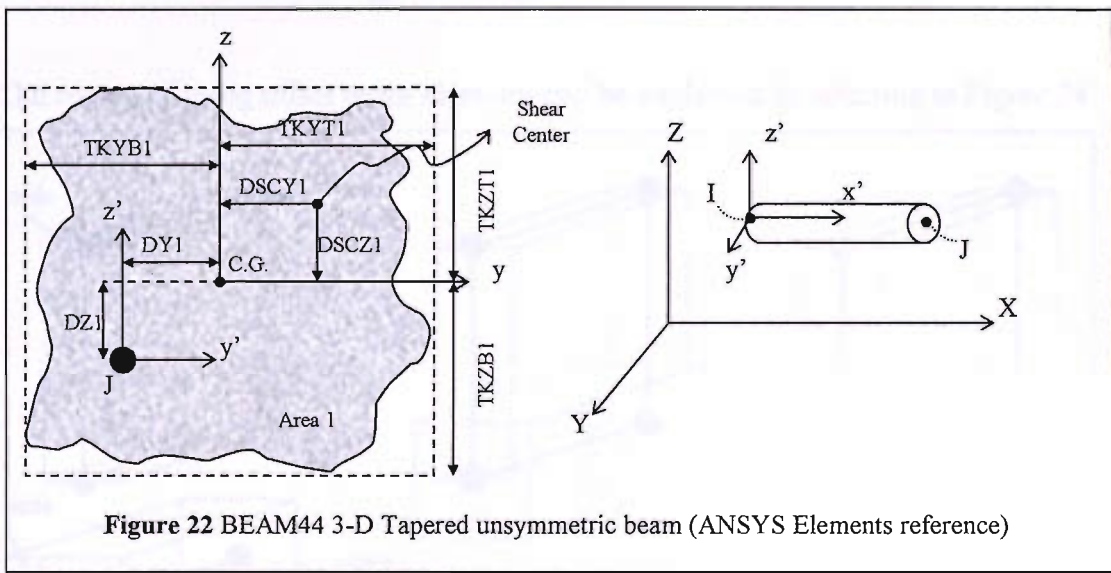
4.1 Modelling of a Uniform Idealised SWATH Ship by ANSYS

The dynamic characteristics of the SWATH ship in vacuo are determined using the FEA program ANSYS (modal analysis) after modelling it with the same dimensions used by Wu (1984).

To create the FE model of the ship, Beam44 (3-D tapered unsymmetrical beam) and Shell 63 type of elements are used in ANSYS. Beam44 in Figure 22, is a two-node uniaxial element with tension, compression, torsion, and bending capabilities. The element has six degrees of freedom at each node: translations in the nodal x, y, and z directions and rotations about the nodal x, y, and z axes. This element allows a different unsymmetrical geometry at each end and permits the end nodes to be offset from the centroidal axis of the beam axes (ANSYS Elements reference). Beam 44 can also be used with any cross section type such as rectangular, I, L, T, Z, including any user defined cross section.

The geometry, node locations, and coordinate system for this element are shown in Figure 22. The element is located by a reference coordinate system (x' , y' , z') and offsets. The reference system is defined by nodes I, J. The principal axes of the beam are in the element coordinate system (x , y , z) with along the cross-section centroid (C.G.).

DX , DY and DZ are offset constants and they define the centroid location of the section relative to the node location. $TKZT1$ and $TKYT1$ are top thicknesses at end 1 where $TKZB1$ and $TKYB1$ are bottom thicknesses (ANSYS Elements reference).



Element Shell63 in Figure 23 has both bending and membrane capabilities. Both in-plane and normal loads are permitted. The element has six degrees of freedom at each node: translations in the nodal x , y , and z directions and rotations about the nodal x , y , and z axes (ANSYS Elements reference).

The geometry, node locations, and coordinate system for this four-node element are as shown in Figure 23.

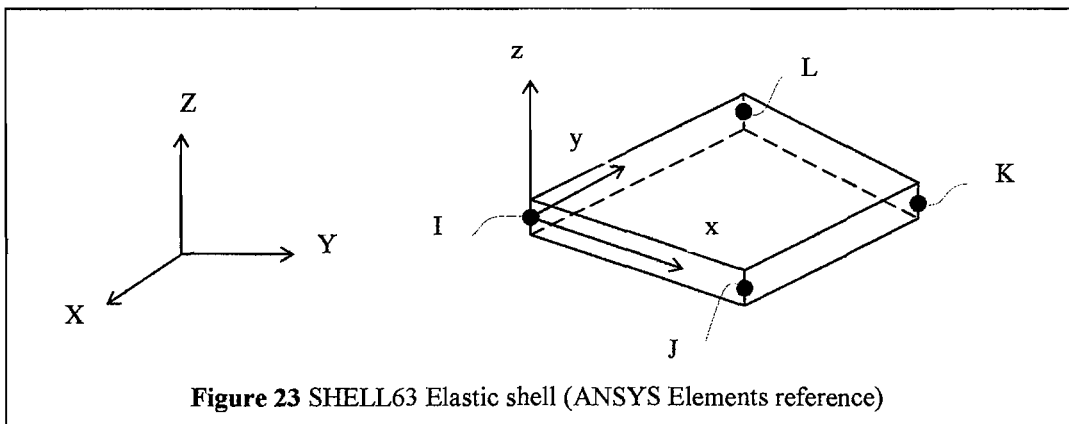


Figure 23 SHELL63 Elastic shell (ANSYS Elements reference)

Beam44 elements are used to model lower hulls and Shell63 elements are used to model struts and the deck as given in Figure 26.

The reason of using offset beam elements can be explained by referring to Figure 24.

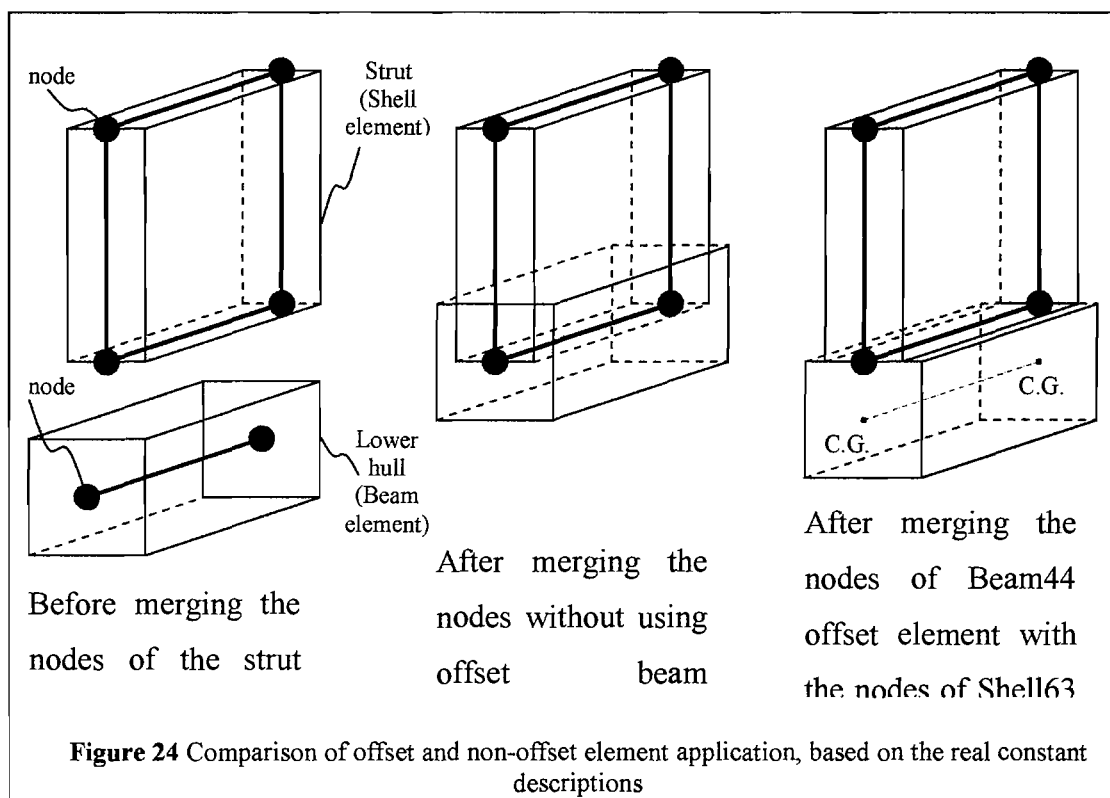


Figure 24 Comparison of offset and non-offset element application, based on the real constant descriptions

While modelling the SWATH-like ship, the main dimensions are taken same as the main dimensions of the model SWATH in Wu's thesis (1984). In the following section, modal analysis results will be compared with each other. The only difference from Wu's model is, mass and stiffness distributions used in his model are taken as uniform in this current model.

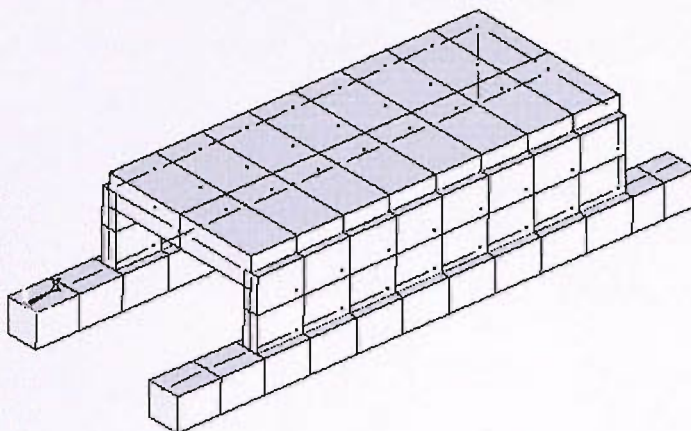


Figure 25 Visualization of elements in the model, based on the real constant descriptions

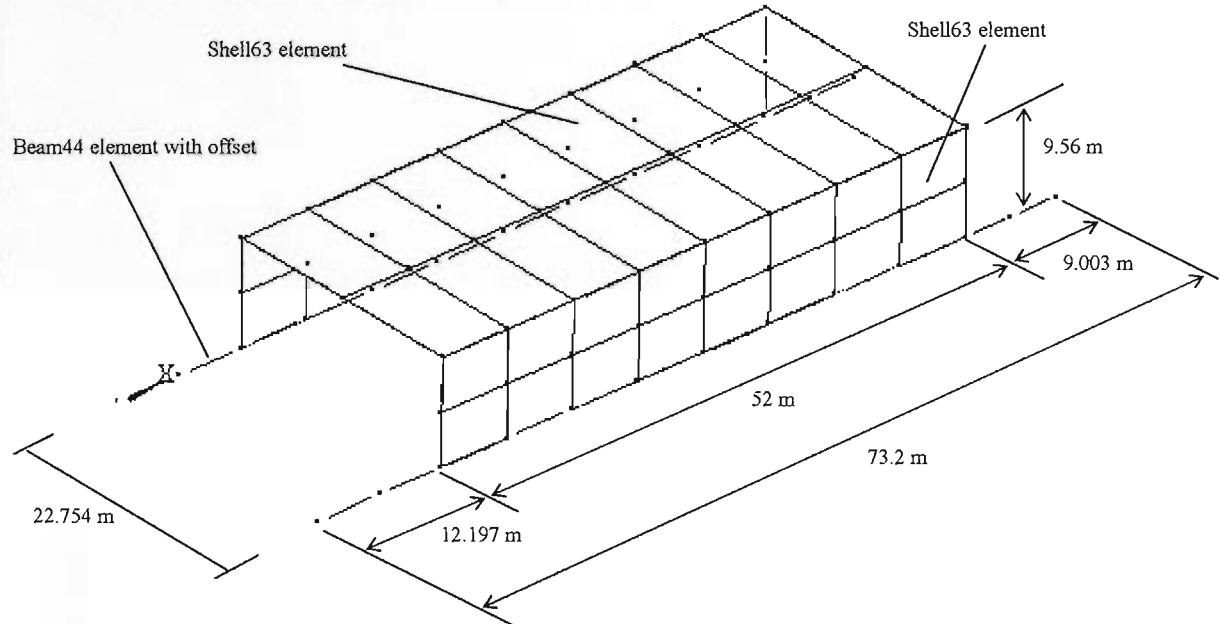


Figure 26 Finite element idealization of the SWATH model

$\Delta = 2788\text{ton}$, (10.66 ton less than the model of Wu)

Dimension of lower hulls with square cross section = $4.541 \times 4.541\text{m}$ (Beam 44 element thickness for lower hulls is also 4.541m)

Width of struts with rectangular cross section = 2.189m (Shell 63 element thickness for struts)

Height of bridging structure = 4.225m (Shell 63 element thickness for bridge)

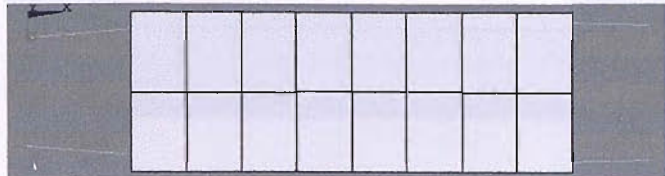
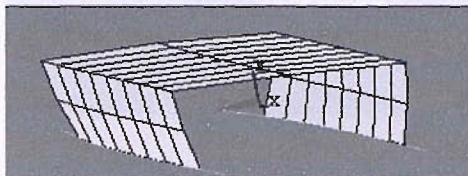
Young's modulus, E for the lower hulls, $E_h = 1411074110\text{ N/m}^2$

for the struts and the bridge, $E_s = E_b = 0.6E_h = 846644466\text{ N/m}^2$

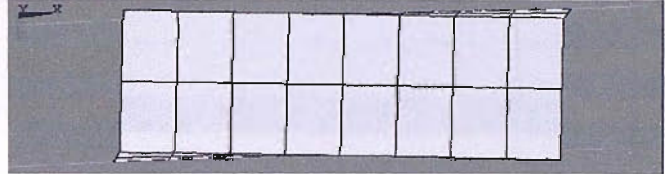
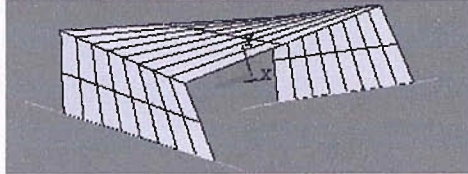
4.1.1 Modal Analysis of the Idealised SWATH Ship by ANSYS

The following natural frequencies and mode shapes were obtained:

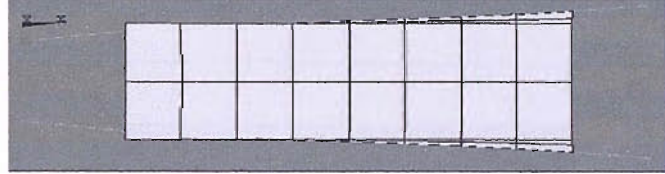
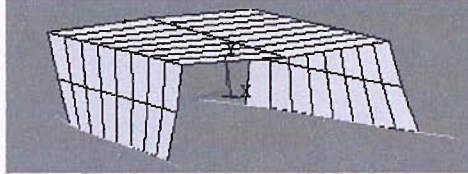
Mode 7, Natural Freq.=1.433 Hz



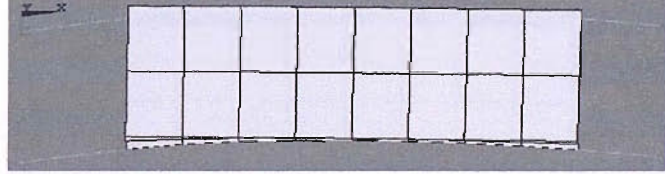
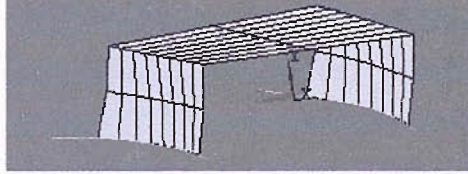
Mode 8, Natural Freq.=1.439 Hz



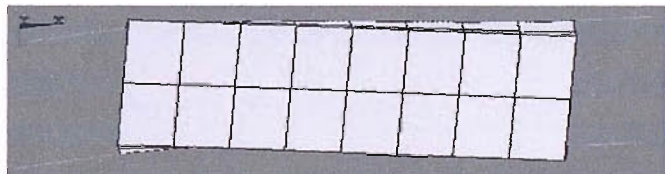
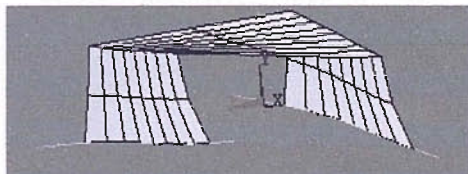
Mode 9, Natural Freq.=1.813 Hz



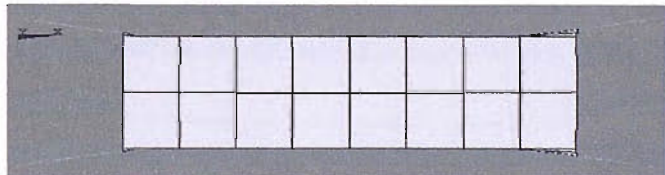
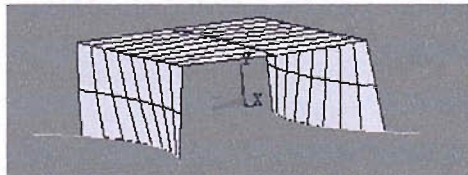
Mode 10, Natural Freq.=2.297 Hz



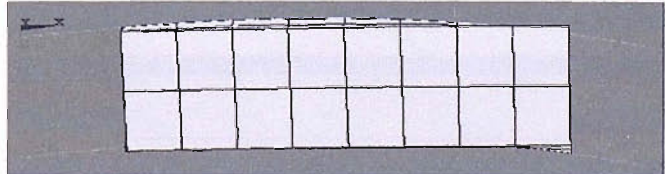
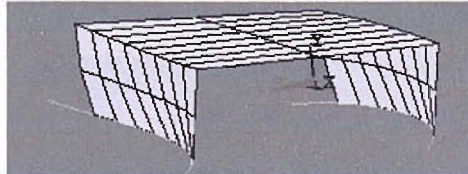
Mode 11, Natural Freq.=2.909 Hz



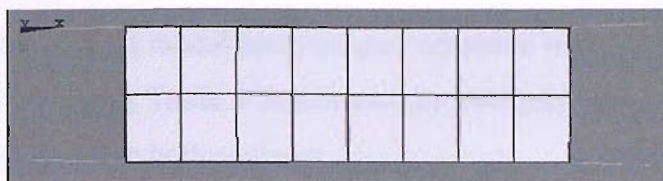
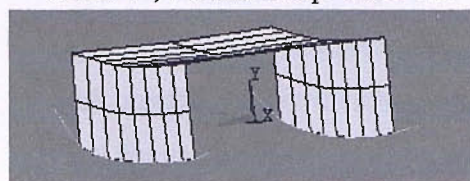
Mode 12, Natural Freq.=2.980 Hz



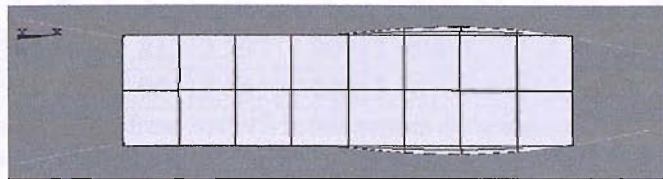
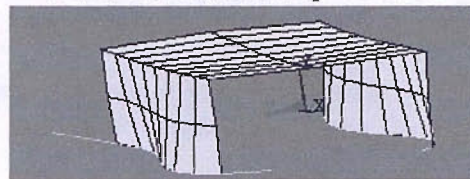
Mode 13, Natural Freq.=3.161 Hz



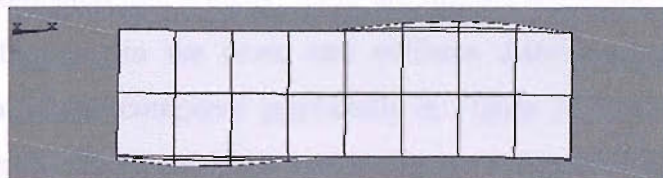
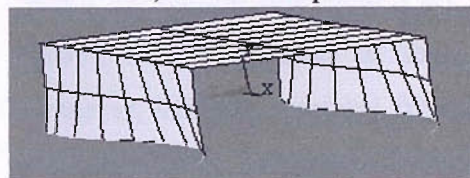
Mode 14, Natural Freq.=5.355 Hz



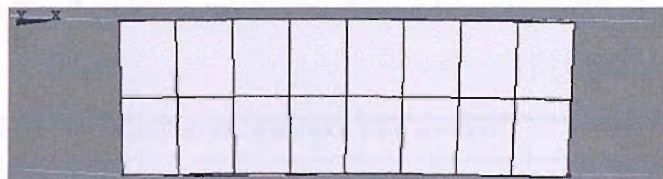
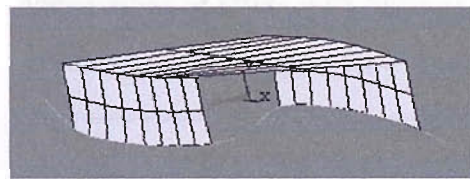
Mode 15, Natural Freq.=5.511 Hz



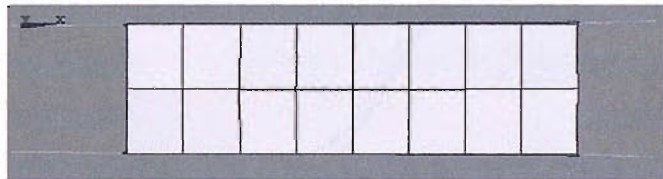
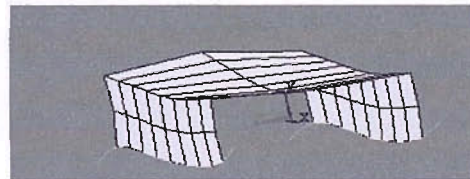
Mode 16, Natural Freq.=5.591 Hz



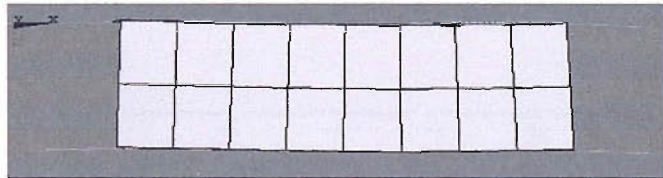
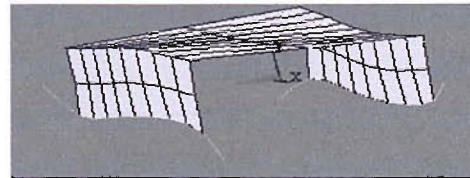
Mode 17, Natural Freq.=5.738 Hz



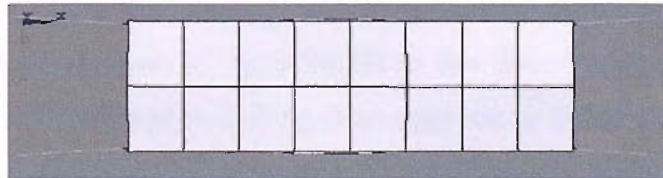
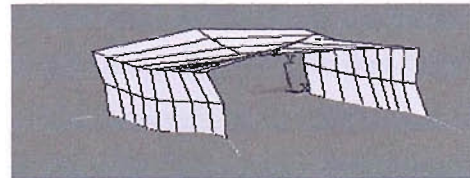
Mode 18, Natural Freq.=7.505 Hz



Mode 19, Natural Freq.=8.736 Hz



Mode 20, Natural Freq.=9.004 Hz



4.2 Comparison of FEA results with an Existing Study on the Similar Model

SWATH and Discussion

The preliminary results obtained from current modal analysis are compared with the model created by Wu (1984). The following Table 9 represents the comparison of natural frequencies of non-rigid body modes in both analyses.

| Mode index | 7 | 8 | 9 | 10 | 11 | 12 | 13 | 14 | 15 |
|---------------------------------------|-------|-------|-------|-------|-------|-------|-------|-------|-------|
| Natural Freq. (Hz)(ANSYS) | 1.433 | 1.439 | 1.813 | 2.297 | 2.909 | 2.980 | 3.161 | 5.355 | 5.511 |
| Natural Freq. (Hz)(Wu's model) | 1.515 | 1.539 | 1.954 | 2.661 | 3.126 | 3.143 | 3.413 | 5.612 | 5.738 |

Table 9 Comparison of natural frequencies obtained from ANSYS in this current document and the modal analysis done by Wu (1984).

When the natural frequencies are compared numerically, there are differences in the values, mainly because of the difference in the mass and stiffness distribution. However, when the natural frequencies are compared graphically in Figure 27, it is seen that they both have similar characteristics. On the other hand, if this model SWATH ship was going to be build, an intense attention has to be paid on the connections of struts with hulls as a result of the local modal deflections especially in higher frequencies (sec. 4.1.1).

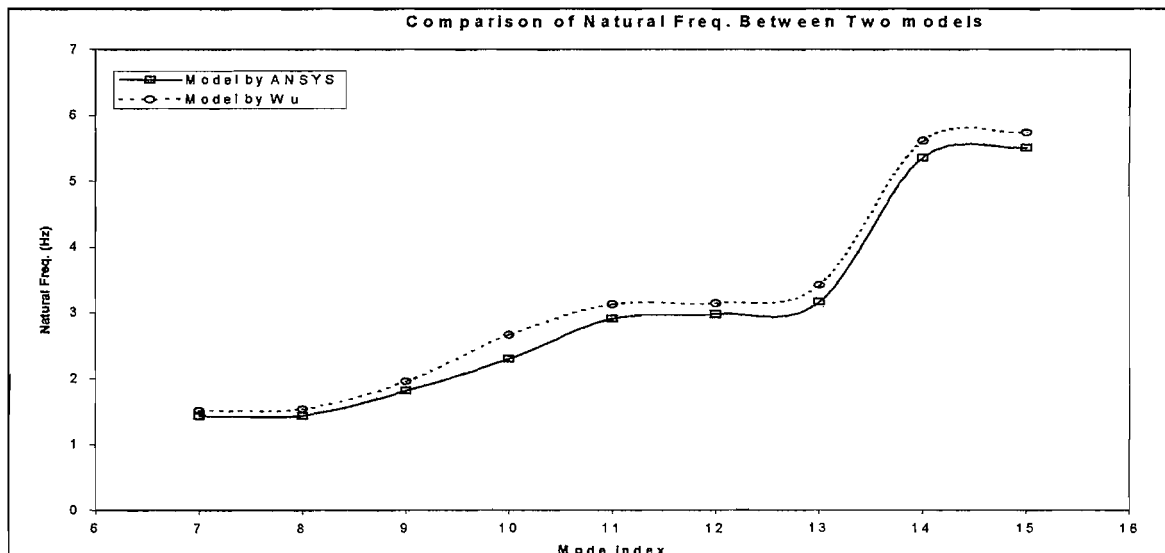


Figure 27 Comparison of the natural frequencies of the SWATH-like vessel modeled by Wu and the similar one modeled in this document

The results above show that the 3D-dry analysis of the SWATH in this document is done successfully. At the same time an advanced modelling in comparison to beam is performed and especially useful knowledge is gained regarding offset node application. These all can form the basis of a more complicated dry analysis.

5 THEORETICAL and NUMERICAL MODELLING of TRANSIENT ANALYSIS

If a structure is excited by a suddenly applied non-periodic excitation, the response is transient since steady state oscillations are not produced. When the forces are applied for a short interval of time, the term ‘transient’ should be applied to the situation. Subsequent motion of the structure is free vibration, which will decay due to the damping present.

If the forces are applied for a short time, the maximum response will occur during the first oscillations. If the damping is small, its effect on the maximum response will be small (Thomson, 1981).

5.1 Impulse Excitation

The simplest form of a transient force is the impulsive force. An impulsive force is one that has a large magnitude F and acts for a very short period of time Δt . By designating the magnitude of the impulse $F\Delta t$ by \hat{F} , it can be written that (Rao, 1995),

$$\hat{F} = \int_t^{t+\Delta t} F dt \quad (49)$$

When \hat{F} is equal to unity, such force is called the unit impulse and defined as;

$$\hat{f} = \lim_{\Delta t \rightarrow 0} \int_t^{t+\Delta t} F dt = F dt = 1 \quad (50)$$

5.1.1 Response to an Impulse

Considering the response of a single degree of freedom system to an impulse excitation as an example is important in studying the response under more general excitations.

If a viscously damped spring-mass system is subjected to a unit impulse at $t = 0$, as shown in Figure 28, the equation of motion of this underdamped system and its solution is given by;

$$m\ddot{x} + c\dot{x} + kx = 0$$

$$x(t) = e^{-\zeta\omega_n t} \left\{ x_0 \cos \omega_d t + \frac{\dot{x}_0 + \zeta\omega_n x_0}{\omega_d} \sin \omega_d t \right\} \quad (51)$$

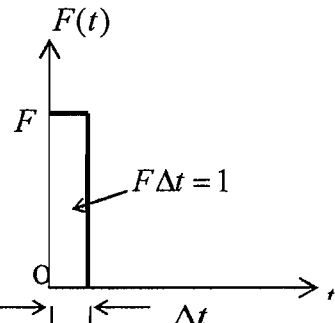


Figure 28 Unit impulse (Rao, 1995)

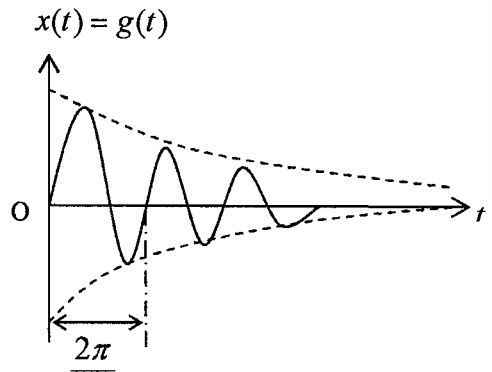


Figure 29 Impulse response function (Rao, 1995)

where $\zeta = \frac{c}{2m\omega_n}$ damping ratio,

$$\omega_d = \omega_n \sqrt{1 - \zeta^2}$$
 frequency of damped vibration,

$$\omega_n = \sqrt{\frac{k}{m}}$$
 natural frequency of the system.

If the mass is at rest before the unit impulse is applied ($x = \dot{x} = 0$ for $t < 0$), from the impulse-momentum relation (Rao, 1995);

$$\text{Impulse} = \hat{f} = 1 = m\dot{x}(t = 0) - m\dot{x}(t < 0) = m\dot{x}_0 \quad (52)$$

Thus the initial conditions are given by;

$$\begin{aligned} x(t = 0) &= x_0 = 0 \\ \dot{x}(t = 0) &= \dot{x}_0 = \frac{1}{m} \end{aligned} \quad (53)$$

In view of Eqs.(53), Eq.(51) reduces to

$$x(t) = g(t) = \frac{e^{-\zeta\omega_n t}}{m\omega_d} \sin \omega_d t \quad (54)$$

Equation (54) is the response of a single degree of freedom underdamped system to a unit impulse, which is also known as the impulse response function, denoted by $g(t)$ in Figure 29.

If the magnitude of the impulse is \hat{F} instead of unity, the initial velocity \dot{x}_0 is \hat{F}/m and the response of the system becomes

$$x(t) = \hat{F} \frac{e^{-\zeta \omega_n t}}{m \omega_d} \sin \omega_d t = \hat{F} g(t) \quad (55)$$

If the impulse \hat{F} is applied at an arbitrary time $t = \tau$ as shown in Figure 31(a), it will change the velocity at $t = \tau$ by an amount \hat{F}/m . Assuming that $x = 0$ until the impulse is applied, the displacement x at any subsequent time t , caused by a change in the velocity at time τ , is given by Eq.(55) with t replaced by the time elapsed after the application of the impulse, that is, $t - \tau$;

$$x(t) = \hat{F} g(t - \tau), \quad \text{shown in Figure 31(b)} \quad (56)$$

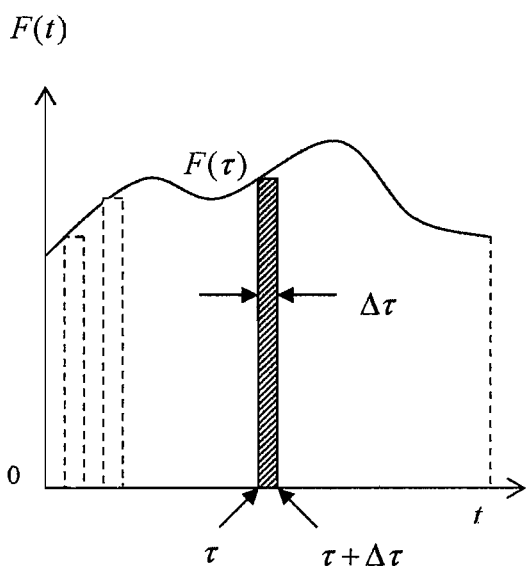


Figure 30 Arbitrary forcing function (Rao, 1995)

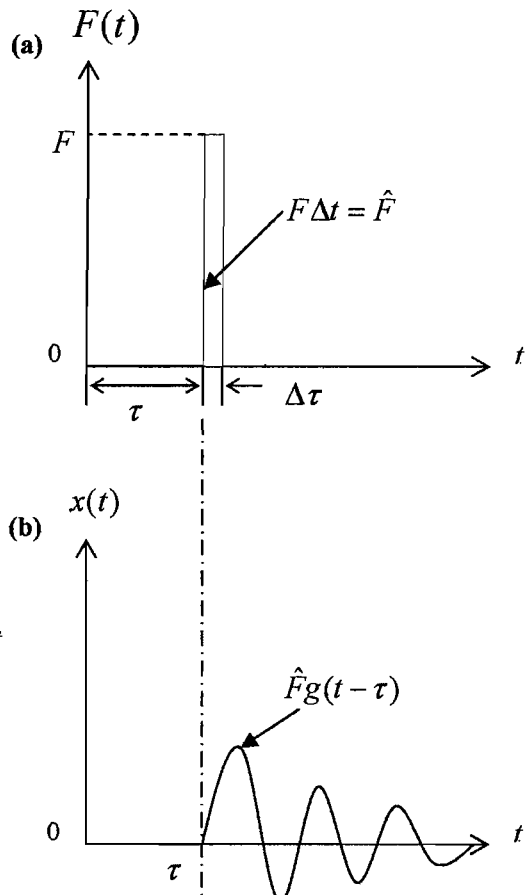


Figure 31 Impulse at arbitrary time (Rao, 1995)

5.1.2 Response to a General Forcing Condition-Arbitrary Excitation

An arbitrary external force $F(t)$, shown in Figure 30, may be assumed to be made up of a series of impulses of varying magnitude. Assuming that at time τ , the force $F(\tau)$ acts on the system for a short period of time $\Delta\tau$, the impulse acting at $t = \tau$ is given by $F(\tau)\Delta\tau$ and its contribution to the response at time t is dependent upon the elapsed time $(t - \tau)$. So the response of the system at t due to this impulse alone is given by Eq.(56) with $\hat{F} = F(\tau)\Delta\tau g(t - \tau)$;

$$\Delta x(t) = F(\tau)\Delta\tau g(t - \tau) \quad (57)$$

The total response at time t can be found by summing all the responses due to the elementary impulses acting at all times τ (Rao, 1995);

$$x(t) \cong \sum F(\tau)g(t - \tau)d\tau \quad (58)$$

If $\Delta\tau \rightarrow 0$ and summation is replaced by integration;

$$x(t) = \int_0^t F(\tau)g(t - \tau)d\tau \quad (59)$$

The integral in Eq.(59) is called the Convolution Integral (Rao, 1995). By substituting the impulse response function $g(t)$ in Eq.(54) into Eq.(59),

$$x(t) = \frac{1}{m\omega_d} \int_0^t F(\tau) e^{-\zeta\omega_n(t-\tau)} \sin \omega_d(t-\tau)d\tau \quad (60)$$

which represents the response of an under-damped single degree of freedom system to the arbitrary excitation $F(t)$, is obtained (Rao, 1995).

For the undamped case of single degree of freedom system to the arbitrary excitation,

$$\zeta = 0 \quad \text{and} \quad \omega_d = \omega_n \Rightarrow x(t) = \frac{1}{m\omega_n} \int_0^t F(\tau) \sin \omega_n(t-\tau)d\tau \quad (61)$$

5.2 Transient Response of the Beams

Transient analysis is the basis for modelling the excitation and the response induced by slamming. Because of the nature of the slamming forces, transient excitations will be studied in the following parts.

Any arbitrary excitation can be regarded as a superposition of impulses of varying amplitude and time of application as explained earlier.

To be able to build the basic idea of modelling the excitation and the response for any arbitrary excitation, triangular and sinusoidal impulses are applied to a pinned-pinned and free-free beam as examples. The responses to these impulses are obtained by using numerical evaluation (convolution sum) of convolution integral. The results are then compared with ANSYS (transient analysis using both mode superposition and full methods). The method for numerical evaluation of convolution integral used in the extraction of principal coordinates is also compared with the analytical solution of convolution integral.

The symmetric responses (i.e. vertical displacement $w(x,t)$, bending moment $M(x,t)$, and shear force $V(x,t)$) at any point along the structure can be expressed by summations in the form;

$$w(x,t) = \sum_{r=0}^{\infty} p_r(t) w_r(x) \quad (62)$$

$$M(x,t) = \sum_{r=0}^{\infty} p_r(t) M_r(x) \quad (63)$$

$$V(x,t) = \sum_{r=0}^{\infty} p_r(t) V_r(x) \quad (64)$$

where $p_r(t)$ is the r^{th} principal coordinate.

Together with the orthogonality, system can be regarded as consisting of n single degree of freedom uncoupled equations of motion. After solving each uncoupled equation for $p_r(t)$ using generalized components, different number of mode shapes from FE analysis are used together in the total deflection equations similar to the method in section 3.4.

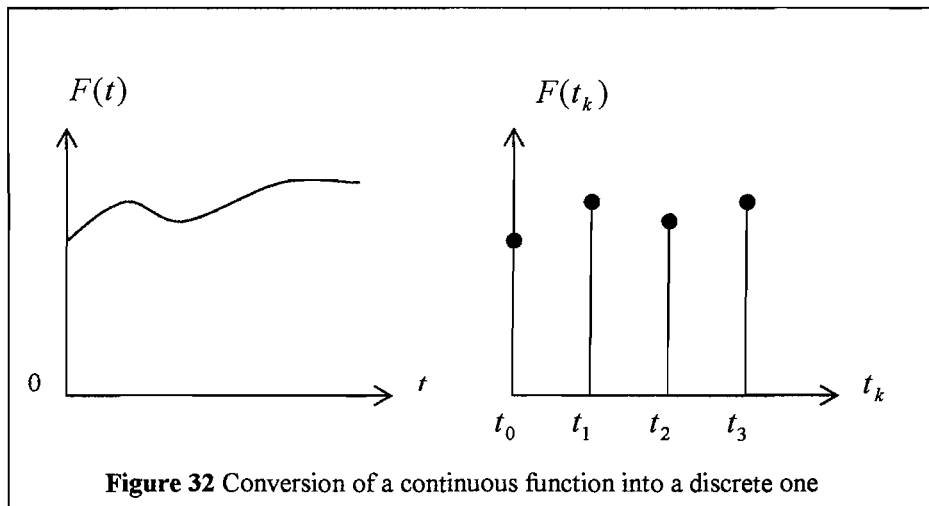
The response of an underdamped single degree of freedom system given by Eq.(60) can be taken as the principal coordinate of r^{th} mode;

$$p_r(t) = \frac{1}{a_r \omega_d} \int_0^t F_r(\tau) e^{-\zeta \omega_{n_r} (t-\tau)} \sin \omega_d (t-\tau) d\tau \quad (65)$$

5.2.1 Methodology

For the forcing functions that can not be easily modelled analytically, a discrete time method may be used to obtain the solution of convolution integral. According to this method excitation and response are going to be treated as discrete functions of time.

The continuous forcing function $F(t)$ will be defined for discrete values of time t_k ($k = 0, 1, 2, \dots$) as seen in Figure 32. The discrete time values are taken ordinarily at equal time interval, so that $t_k = kT$, where T is the sampling period. As an illustration, assuming that the continuous-time function $F(t)$ shown in Figure 32 is sampled every T seconds beginning at $t = 0$, the discrete-time function $F(t_k) = F(k)$ consists of the sequence $F(0), F(1), F(2), \dots$, where for simplicity the sampling period T is omitted from the argument (Meirovitch, 1986).



Under this methodology the response of the system can be denoted as the discrete-time response by $p(n)$:

$$p(n) = \sum_{k=0}^{\infty} F(k)g(n-k) = \sum_{k=0}^n F(k)g(n-k), \quad t_n = nT \Rightarrow n \quad (66)$$

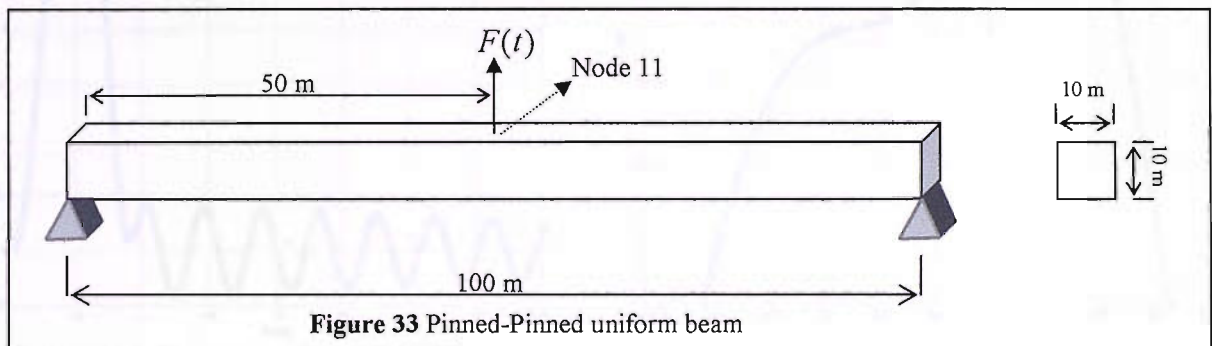
Equation (66) is the response of a linear discrete-time system in the form of a convolution sum and it represents the discrete-time counterpart of the convolution integral given by Eq.(59) where p is the principal coordinate representing the response, F is the generalized force and g is the impulse response as issued in section 5.1.1.

The rectangular and triangular pulses in Figure 34 are applied to the pinned-pinned

While using this method it is important that the sampling interval T is small enough that the angular frequency ω_0 exceeds the highest natural frequency of the system being analyzed. If it does not, higher frequency components present in $x(n)$ or $p_r(n)$ will lead to errors. ω_0 is called the Nyquist frequency and given by $\omega_0 = \pi/T$ (Newland, 1989).

5.2.2 Pinned-Pinned Uniform Beam

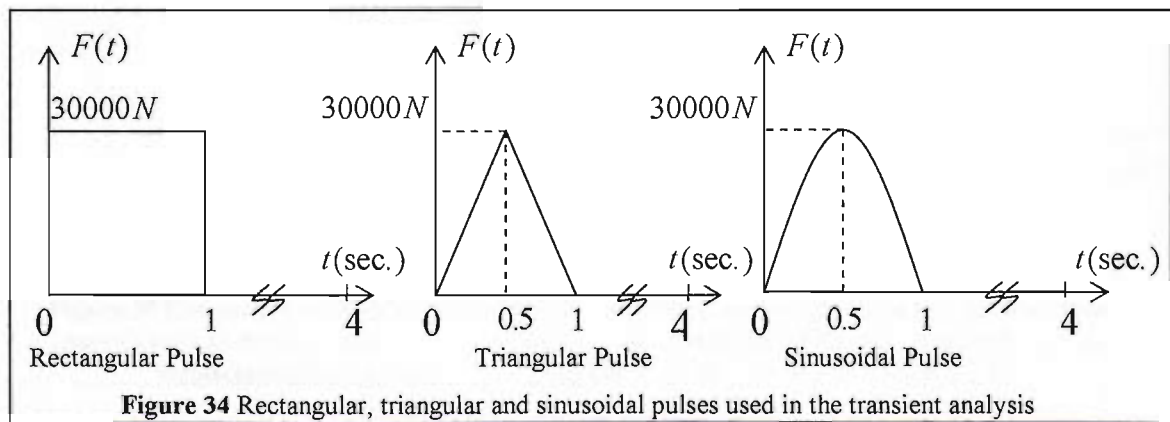
The same pinned-pinned uniform beam, which is studied in chapter 3 with the same properties, shown in Figure 33 is under transient excitation.



| Mode | 1 | 2 | 3 | 4 | 5 | 6 | 7 | 8 | 9 | 10 | 11 | 12 | 13 | 14 | 15 | 16 | 17 |
|--------------|-----|-----|------|------|------|------|------|-------|-------|-------|-------|-------|-------|-------|-------|-------|-------|
| N.Freq. (Hz) | 2.3 | 9.2 | 20.2 | 35.0 | 53.0 | 73.6 | 96.4 | 120.7 | 146.4 | 173.0 | 200.4 | 228.5 | 257.0 | 286.0 | 315.4 | 345.3 | 375.5 |

Table 10 Natural Frequencies of the pinned-pinned beam (Hz)

Rectangular and triangular pulses illustrated in Figure 34 are applied to the pinned-pinned beam. ANSYS results are compared with the results in which principal coordinates are evaluated from the numerical solution of the convolution integral by using the method explained in section 5.2.1.



The rectangular and triangular pulses in Figure 34 are applied to the pinned-pinned beam. Here only the responses to the triangular impulse are given in Figure 35. Rectangular impulse responses show the same characteristics with a different overall response as shown in Figure 89 in Appendix. To compare the accuracy in evaluating the principal coordinates by convolution sum, two different discrete time intervals are used, $T = 0.01$ s and $T = 0.002$ s.

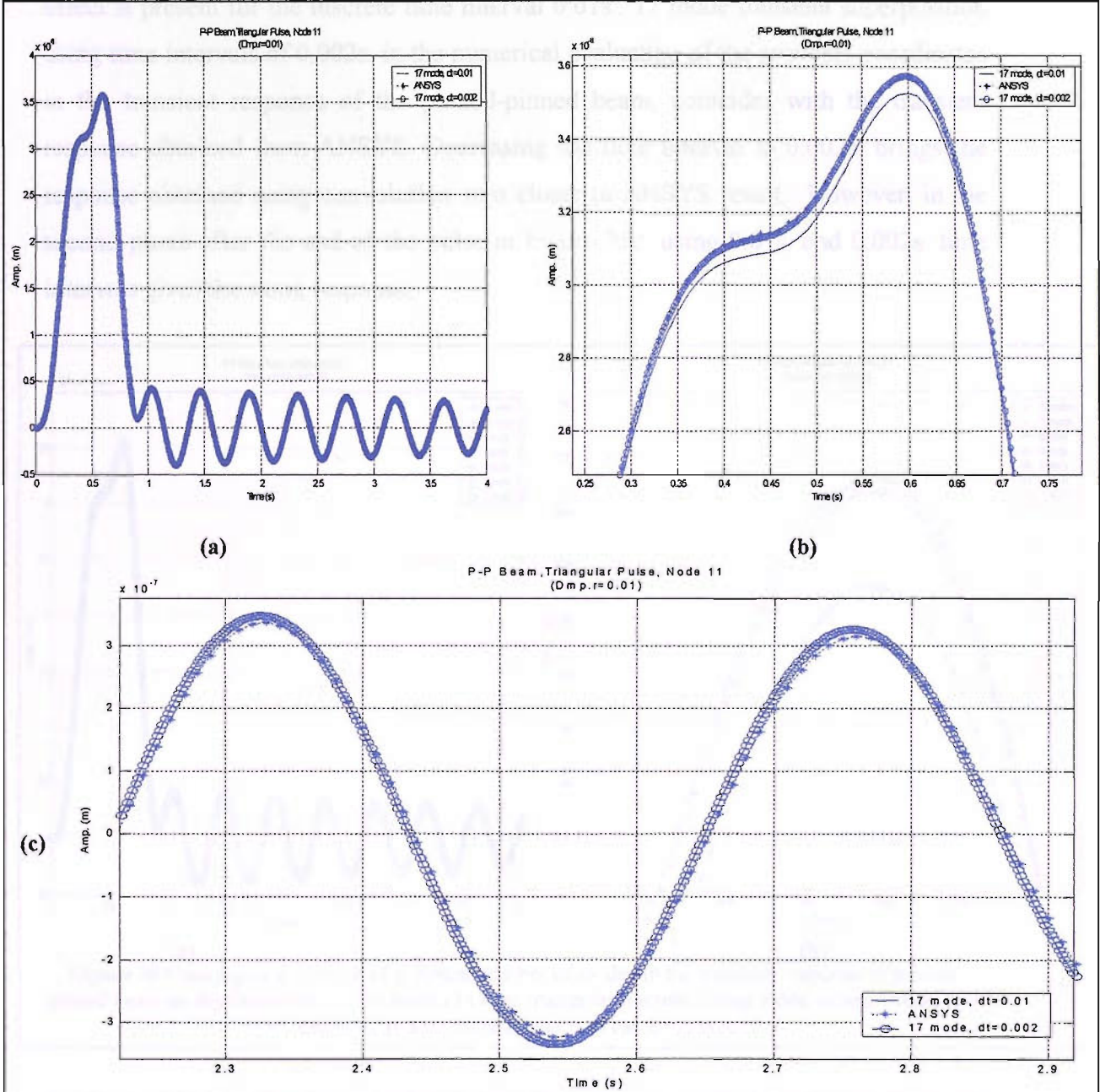


Figure 35 Comparison of ANSYS results against convolution sum results using two different time intervals such as $dt=0.01$ s. and $dt=0.002$ s. for the transient response of the pinned-pinned beam as displacements(uz) at node 11 to a triangular impulse as shown in section 5.2.2

When the damped transient response in Figure 35a is examined, two phases are significant. The first phase which takes place during the pulse between 0-1sec. and the second phase which is after the end of the pulse between 1-4sec decaying due to the damping ratio 0.01.

Figure 35b shows the zoom-in view of the first phase and here the Nyquist frequency effect is present for the discrete time interval 0.01s.. 17 mode transient superposition using time intervals of 0.002s. in the numerical evaluation of the principal coordinates in the transient response of the pinned-pinned beam, coincides with the transient response obtained from ANSYS. Decreasing the time interval to 0.002s. brings the response obtained using convolution sum closer to ANSYS result. However, in the second phase after the end of the pulse in Figure 35c, using 0.01s. and 0.002s. time intervals gives the same response.

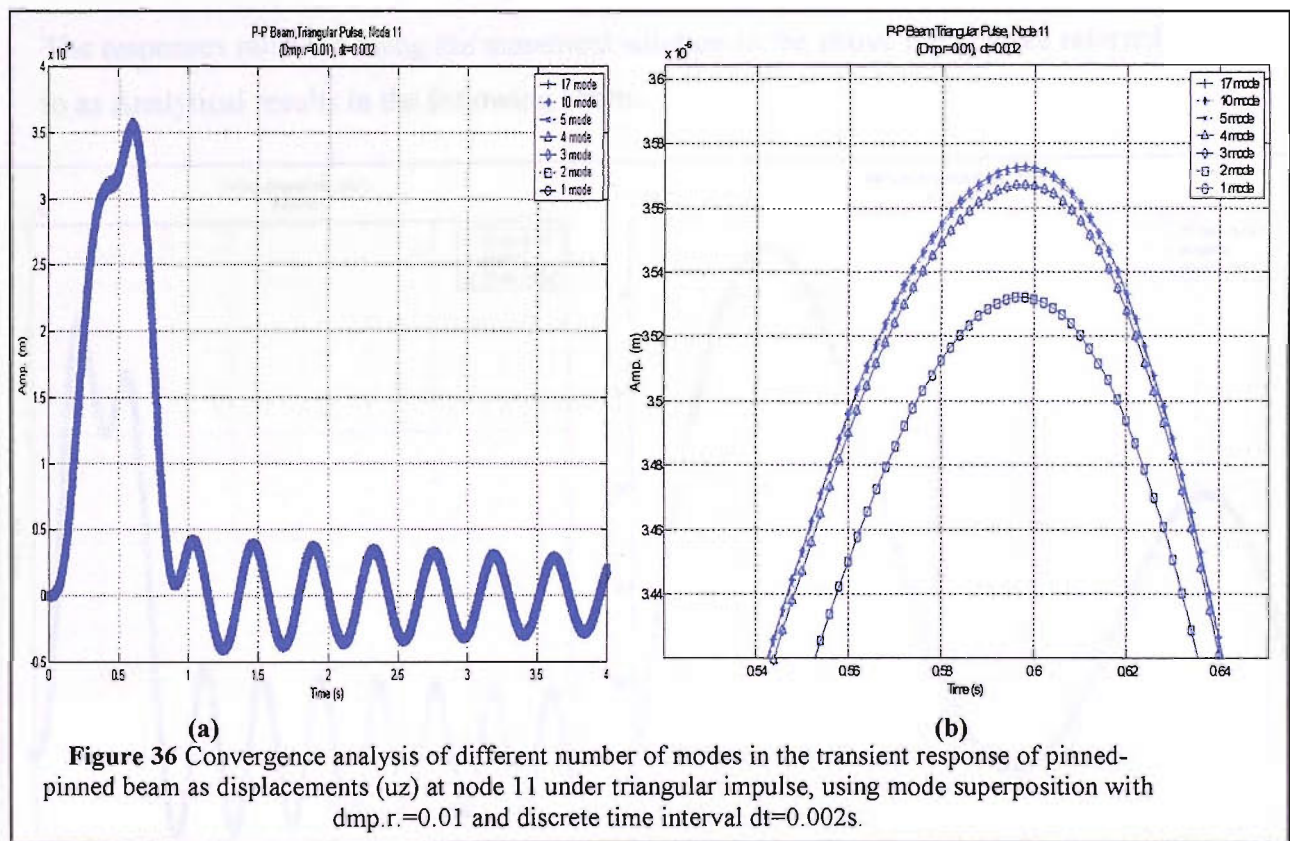


Figure 36 Convergence analysis of different number of modes in the transient response of pinned-pinned beam as displacements (uz) at node 11 under triangular impulse, using mode superposition with $dmp.r=0.01$ and discrete time interval $dt=0.002s$.

Another issue, which is illustrated in Figure 36, is the convergence of the modes in the mode superposition method used in the transient analysis. Convergence occurs after superposing 5 modes as seen in Figure 36b. In other words, the superposition of first 4 modes does not converge.

The sinusoidal pulse shown in Figure 34 is also applied to the pinned-pinned beam and displacements and bending moments in the middle of the beam are calculated for two different discrete time intervals same as before. Results are then compared with using analytical solution of the convolution integral in the extraction of principal coordinates. The procedure followed in this stage is as follows;

$$F(t) = \begin{cases} 30000 \sin \pi t & 0 \leq t \leq 1 \\ 0 & t < 0 \text{ and } t > 1 \end{cases} \quad (67)$$

The response during the pulse is given by:

$$p_r(t) = \frac{1}{a_{nr}\omega_d} \int_0^t F_r(\tau) e^{-\zeta\omega_{nr}(t-\tau)} \sin \omega_d(t-\tau) d\tau \quad (68)$$

and the response any time subsequent to the termination of pulse is given the same as Eq.(60) with only difference in the upper limit of the integral,

$$p_r(t) = \frac{1}{a_{nr}\omega_d} \int_0^1 F_r(\tau) e^{-\zeta\omega_{nr}(t-\tau)} \sin \omega_d(t-\tau) d\tau \quad (69)$$

The responses obtained using the numerical solution to the above integral are referred to as Analytical results in the following charts.

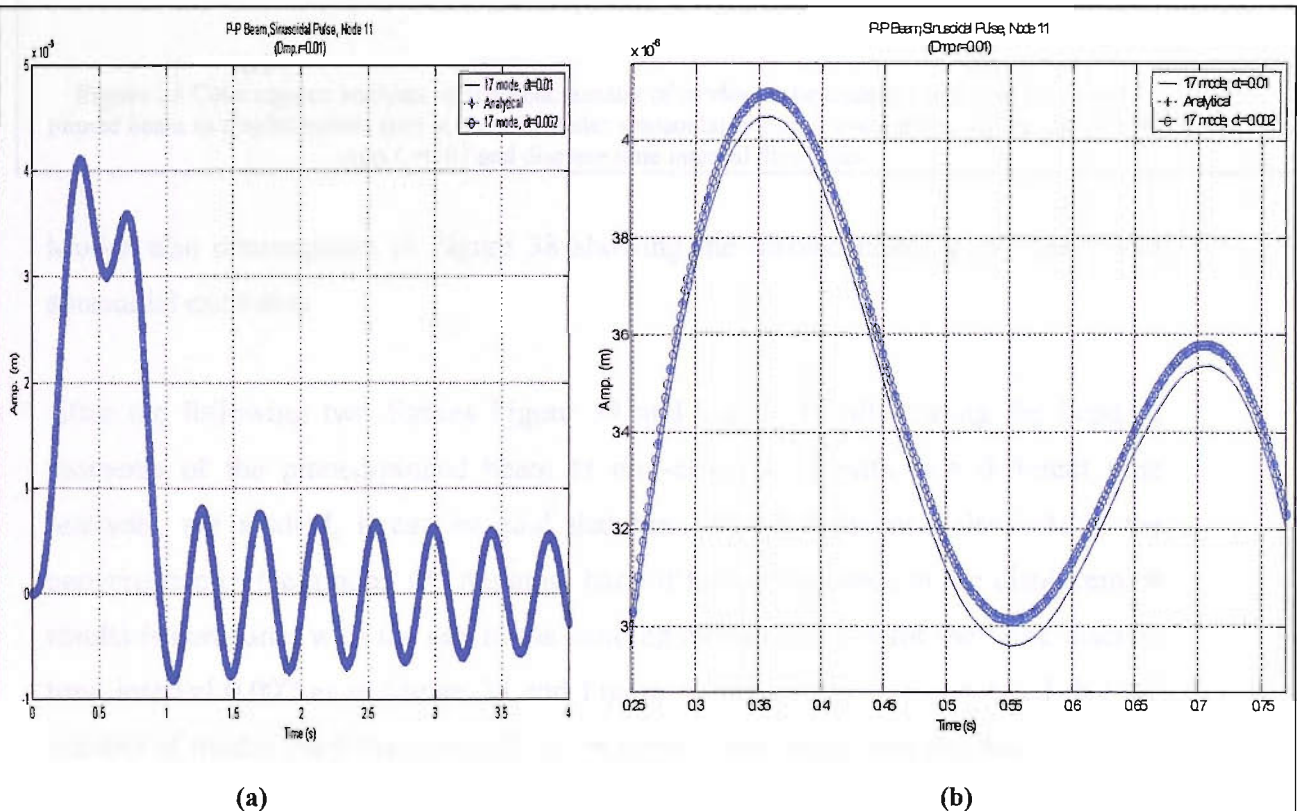


Figure 37 Comparison of analytical results against convolution sum results using two different time intervals such as $dt=0.01s$. and $dt=0.002s$. for the transient response of the pinned-pinned beam as displacements (uz) at node 11 to a sinusoidal impulse as shown in section 5.2.2

In Figure 37, the response belonging to convolution sum method with 0.01s. time interval differs from the other two. Convolution sum method with 0.002s. time interval gives the same response as analytical solution method.

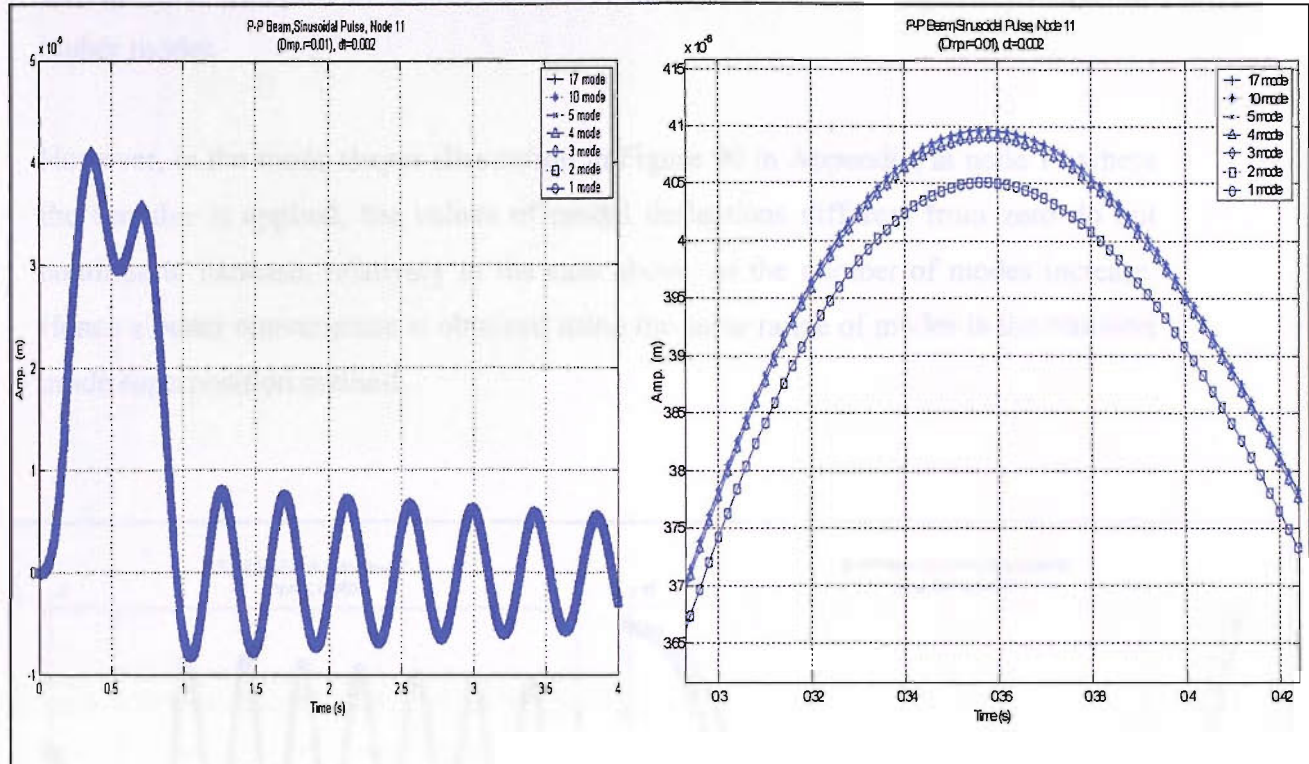


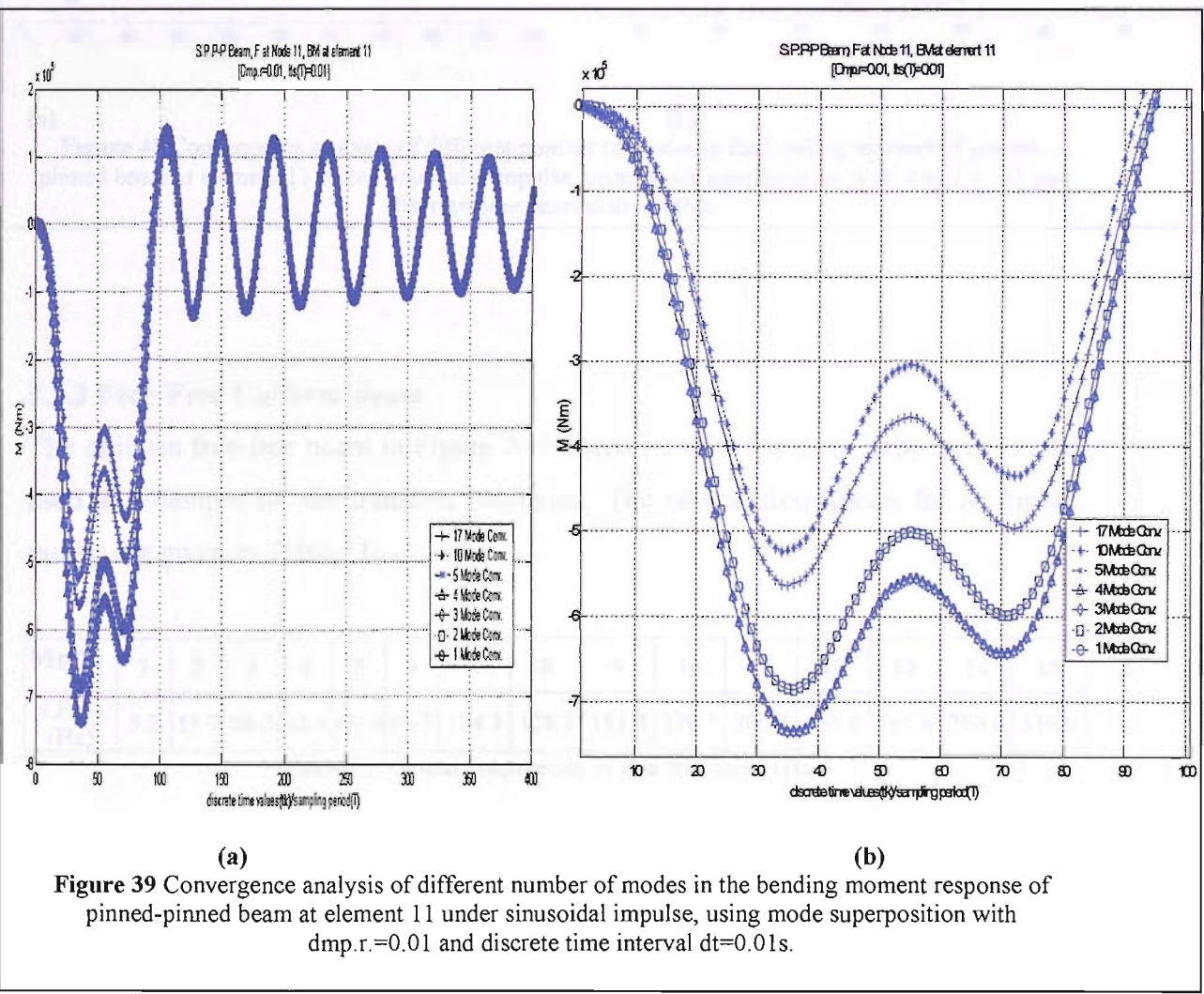
Figure 38 Convergence analysis of different number of modes in the transient response of pinned-pinned beam as displacements (uz) at node 11 under sinusoidal impulse, using mode superposition with $dmp.r.=0.01$ and discrete time interval $dt=0.002s$.

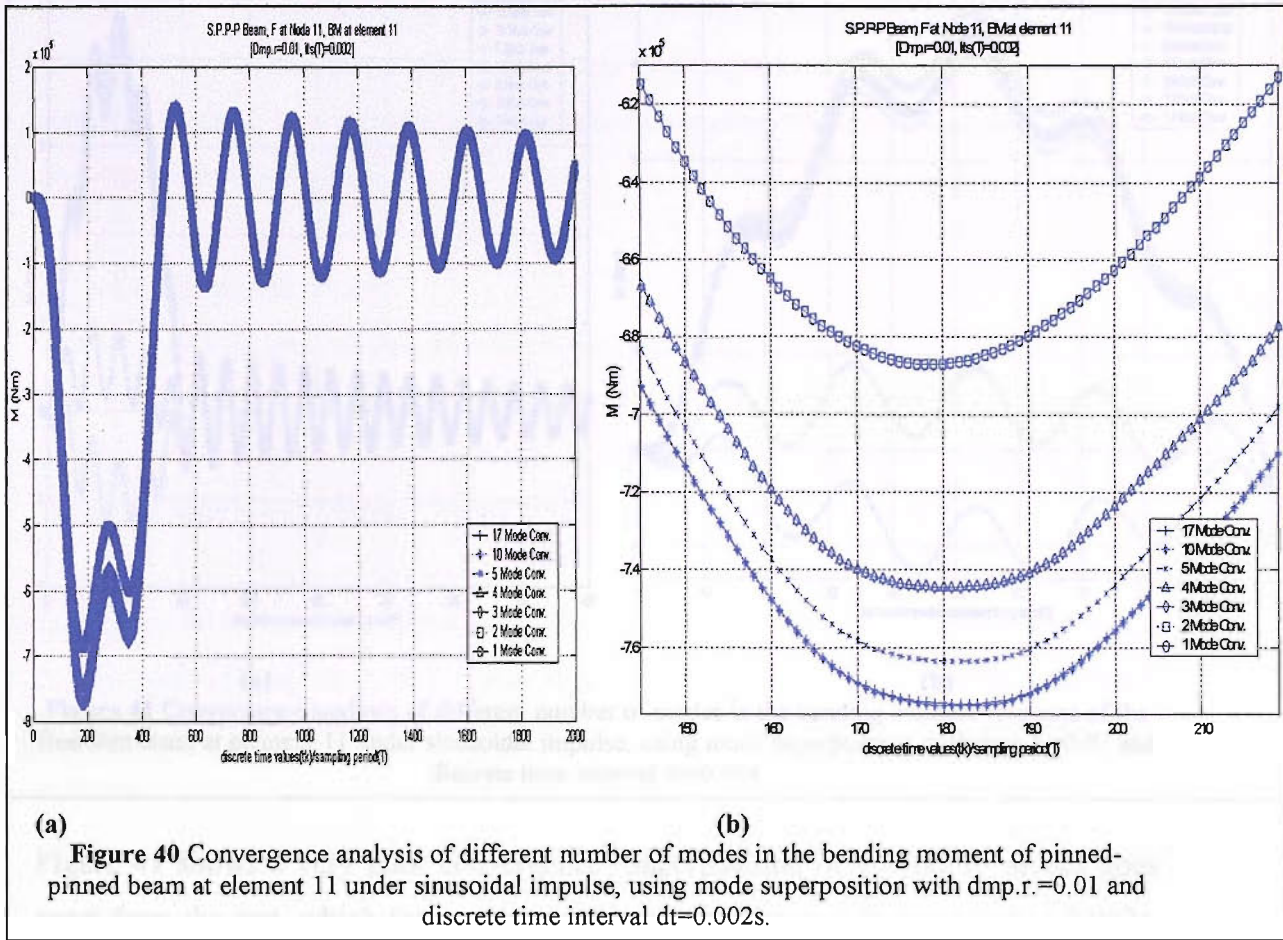
Modes also converge in Figure 38 showing the displacements over time under sinusoidal excitation.

After the following two figures Figure 39 and Figure 40, illustrating the bending moments of the pinned-pinned beam at mid-element 11 with two different time intervals, are studied, it can be said that the Nyquist frequency also effects the convergence of the modes. On the other hand if the convergence in the displacement results is compared with the one in the bending moment results for the same discrete time interval 0.002 as in Figure 38 and Figure 40 respectively, it is noticed that the number of modes used has more effects on bending moments than the displacements. This can be explained by the similar logic given in the discussion 3.6 related with modal bending and modal- uz deflections.

Referring to the mode shapes and modal bending moments of pinned-pinned beam in Appendix is necessary at this stage. In the modal bending illustrations at mid-element 11 in Figure 91, the values of bending moments different from zero continue to increase as the number of modes increase resulting with the convergence pushed into higher modes.

However, in the mode shapes illustration in Figure 90 in Appendix, at node 11 where the impulse is applied, the values of modal deflections different from zero do not continue to increase, relatively to the case above, as the number of modes increase. Hence a better convergence is obtained using the same range of modes in the transient mode superposition method.





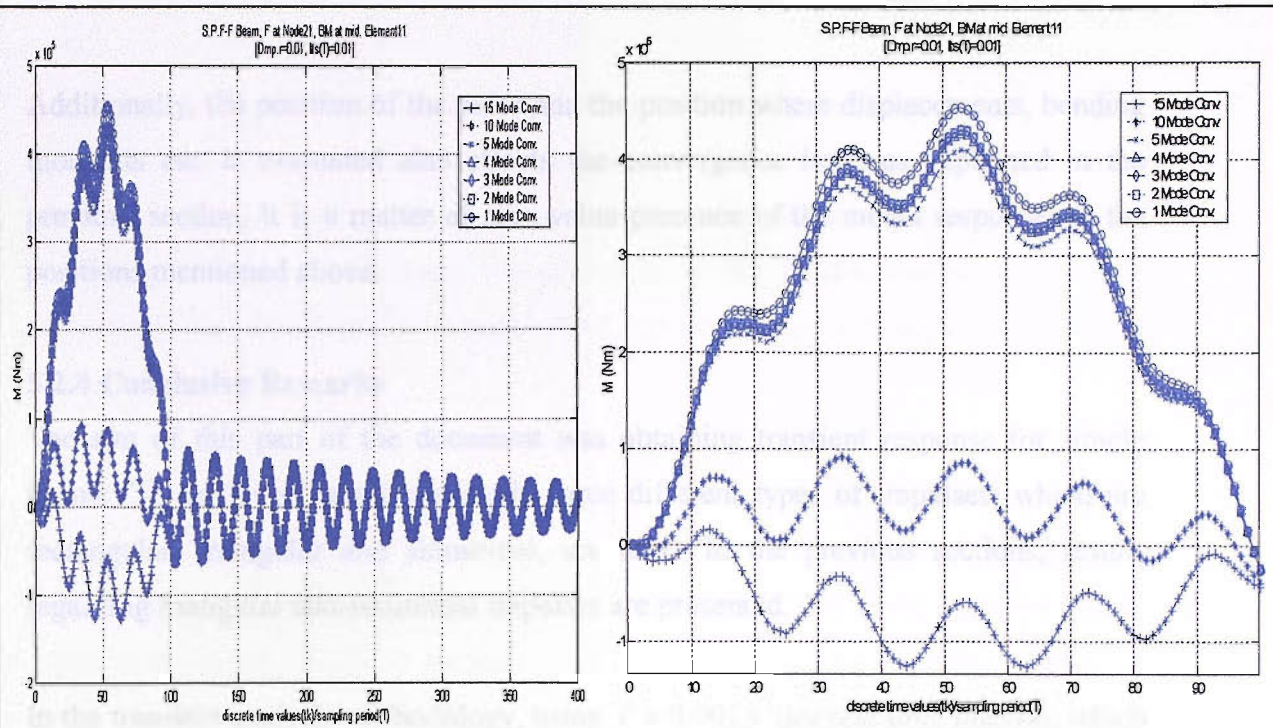
5.2.3 Free-Free Uniform Beam

The uniform free-free beam in Figure 7 in chapter 3 with the same properties is also used as a sample for the transient excitation. The natural frequencies for its higher modes are given in Table 11:

| Mode | 1 | 2 | 3 | 4 | 5 | 6 | 7 | 8 | 9 | 10 | 11 | 12 | 13 | 14 | 15 |
|--------------|-----|------|------|------|------|------|-------|-------|-------|-------|-------|-------|-------|-------|-------|
| N.Freq. (Hz) | 5.2 | 13.9 | 26.5 | 42.4 | 60.9 | 81.7 | 104.3 | 128.3 | 153.4 | 179.5 | 206.2 | 233.6 | 261.6 | 290.0 | 319.0 |

Table 11 Natural Frequencies of free-free beam (Hz)

This time the same sinusoidal impulse is applied on the free-free beam at node 21. Following figures illustrate the bending moments at element 11 with two different discrete time intervals used as before.

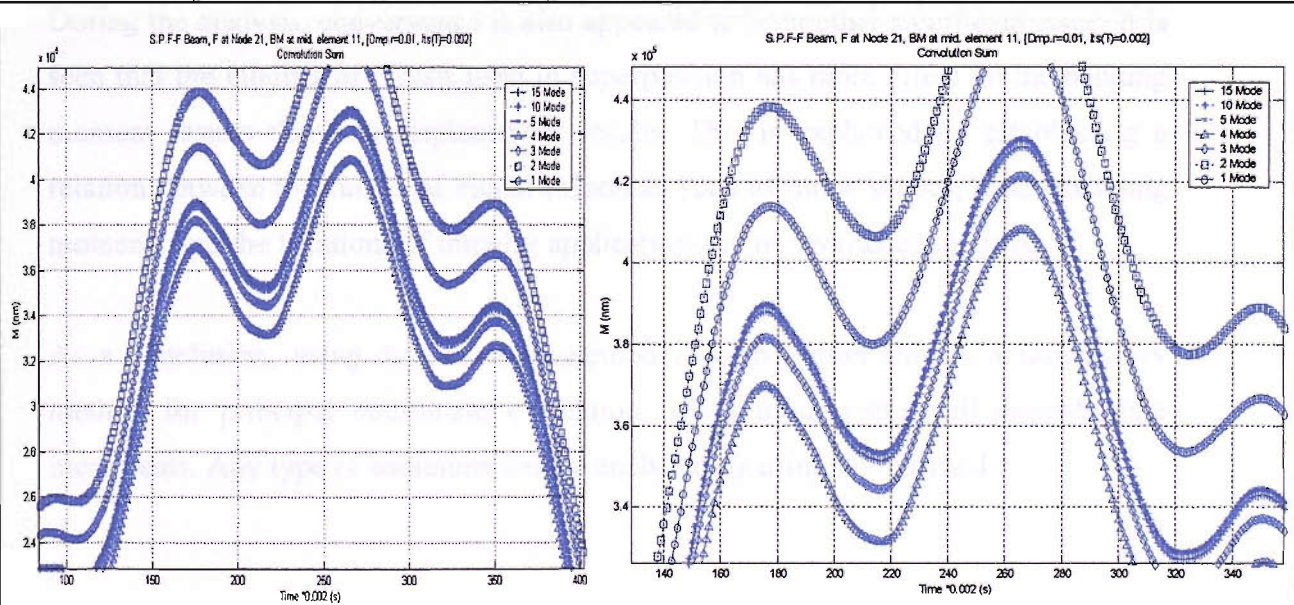


(a)

(b)

Figure 41 Convergence analysis of different number of modes in the bending moment response of the free-free beam at element 11 under sinusoidal impulse, using mode superposition with $dmp.r.=0.01$ and discrete time interval $dt=0.01s$.

Figure 41 shows a very poor convergence. Superposition of 10 and 15 modes goes apart from the rest, which form a cluster. As the time interval is decreased to 0.002s, the same illustration turns into Figure 42, in which now a relatively better convergence is observed. This suggests that if a smaller time interval than 0.002s is used the expected convergence is going to be the best of all.



(a)

(b)

Figure 42 Convergence analysis of different number of modes in the bending moment response of the free-free beam at element 11 under sinusoidal impulse, using mode superposition with $dmp.r.=0.01$ and discrete time interval $dt=0.002s$.

Additionally, the position of the pulse and the position where displacements, bending moments etc. is evaluated also effects the convergence issue as explained in the previous section. It is a matter of zero value presence of the modal responses at the positions mentioned above.

5.2.4 Conclusive Remarks

The aim of this part of the document was obtaining transient response for simple beams. To do the comparisons easily three different types of impulses, which are rectangular, triangular and sinusoidal, are used. In the previous sections, results regarding triangular and sinusoidal impulses are presented.

In the transient analysis methodology, using $T = 0.002$ s. discrete time interval, which is small enough, particularly for pinned-pinned beam gives closer results to ANSYS and analytical calculations. Apart from being required by the nature of discrete systems, smaller time intervals are needed because of the high natural frequencies of the beams which can be seen in Table 10 and Table 11. The beams taken as examples have rigid characteristics and especially free-free beam has quite high natural frequencies. Hence, a smaller time interval than 0.002s. in the transient analysis of free-free beam must be used.

During the analysis, convergence is also appeared to be another significant issue. It is seen that the number of modes used in superposition has more effect on the bending moment results than the displacement results. This is explained by establishing a relation between the values of modal responses such as mode shapes, modal bending moments and the locations of impulse application and the evaluated response.

As a conclusion, using discrete-time method in convolution sum is a satisfactory method for principal coordinate evaluation, when used with small enough time increments. Any type of excitation can be analyzed by using this method.

5.3 Transient Response of the Flat Unstiffened and Stiffened Plates

The aim of this section is to analyze the transient response of a local structure on a vessel, consisting of stiffened (in various directions) flat plates. This report is a part of modelling of the excitation and response induced by impact slamming on more realistically visualized structural parts which can potentially be studied as a part of a further study.

The following work begins with a brief theory on plates and continues with the transient response formulation of the plates. Various stiffened plates are modelled next and these are compared with other stiffened plates studied in the literature. In the subsequent section, a modal analysis is applied on four main models of plates by using ANSYS-FEA software. These are unstiffened, longitudinally, transversely and orthogonal stiffened plates. Later on, modal characteristics of these models are used in the transient mode superposition to get transient response and then compared with the ANSYS results (both mode superposition and full methods are used). The penultimate section is all about carrying the experience gained in the previous section to an analysis of a realistic plate taken from a tanker bottom forward end. Discussions can be found throughout the sections. This part of document ends up with the general conclusive remarks given in section 5.3.6. Complementary figures regarding the discussions are presented in the Appendix (Figure 104 - Figure 127).

5.3.1 Theory of Plates

It is important to have a brief idea about the theory beyond the plates before starting to model their behaviour under excitation.

The governing equation for a rectangular plate subjected to lateral loads is given by (Vinson, 1974);

$$\nabla^4 W = \frac{\partial^4 W}{\partial x^4} + 2 \frac{\partial^4 W}{\partial x^2 \partial y^2} + \frac{\partial^4 W}{\partial y^4} = \frac{f(x, y)}{D} \quad (70)$$

$$D = \frac{Eh^3}{12(1-\nu^2)} \quad (71)$$

$W(x, y)$ is the lateral deflection, $f(x, y)$ is the lateral load per unit area, ν is the Poisson's ratio and D represents the bending of flexural rigidity of the plate.

After solving the homogenous part of the equation (70) by using particular boundary conditions for the corresponding type of plate, and natural frequencies can be obtained. For the case of a simply supported flat plate (all edges) natural frequencies are (Szilard, 1974):

$$\omega_{mn} = \pi^2 \left[\left(\frac{m}{a} \right)^2 + \left(\frac{n}{b} \right)^2 \right] \sqrt{\frac{D}{\rho t_p}} \quad m, n = 1, 2, 3, \dots \quad (72)$$

and corresponding natural modes are (Meirovitch, 1967)

$$W_{mn}(x, y) = A_{mn} \sin \frac{m\pi x}{a} \sin \frac{n\pi y}{b} \quad m, n = 1, 2, 3, \dots \quad (73)$$

where ρ and t_p are the density and thickness of the plate respectively, a and b are the length and the width of the plate respectively and A_{mn} is the vibration amplitude for each value of m and n .

5.3.2 Transient Response

To be able to examine the response of a flat plate to an arbitrary excitation, a triangular impulse is applied to a fixed ended (all edges) flat plate with 3 different types of stiffening. These include longitudinal, transverse and orthogonal stiffening. The responses to these impulses are obtained by using numerical evaluation (convolution sum) of convolution integral. The results are then compared with ANSYS.

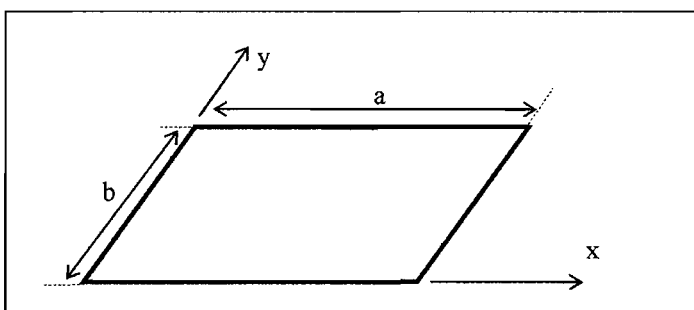


Figure 43 Uniform rectangular plate (Meirovitch, 1967)

Using the same theorem given in the part “transient response of the beams”, the displacement of a uniform rectangular plate defined over the domain $0 < x < a$ and $0 < y < b$ as in Figure 43 is (Meirovitch, 1967);

$$w(x, y, t) = \sum_{m=1}^{\infty} \sum_{n=1}^{\infty} W_{mn}(x, y) p_{mn}(t) \quad m, n = 1, 2, 3, \dots \quad (74)$$

where the normal modes $W_{mn}(x, y)$ depend on the boundary conditions and $p_{mn}(t)$ are the corresponding principal coordinates which are solved from the equation of motion for each mode and substituted in the equation above to obtain the total deflections for the desired location. Principal coordinates can be calculated from the following equation for the undamped case (Meirovitch, 1967);

$$p_{mn}(t) = \frac{1}{\omega_{mn}} \int_0^t F_{mn}(\tau) \sin \omega_{mn}(t - \tau) d\tau \quad (75)$$

for an under damped case;

$$p_{mn}(t) = \frac{1}{\alpha_r \omega d_{mn}} \int_0^t F_{mn}(\tau) e^{-\zeta \omega_{mn}(t-\tau)} \sin \omega d_{mn}(t - \tau) d\tau, \quad \omega d_{mn} = \omega_{mn} \sqrt{1 - \zeta^2} \quad (76)$$

The generalized force $F_{mn}(t)$, corresponding to $p_{mn}(t)$ is (Meirovitch, 1967);

$$F_{mn}(t) = \int_0^a \int_0^b W_{mn}(x, y) f(x, y, t) dx dy \quad (77)$$

All the variables in the formulations above are the same as the ones in previous section. The same methodology used in the transient response of beams is also applied on the plates. The mode shapes for clamped stiffened and unstiffened plates are obtained from ANSYS, and these modal responses are then used in the subsequent numerical transient analysis as well as transient analysis in ANSYS using mode superposition method.

5.3.3 Verification of Modal Analysis

The position, physical properties and orientation of stiffeners create considerable variations in the modal properties as compared with the bare plates of similar construction. This makes each of the stiffened plate identification problem rather unique (Mukhopadhyay, 2000).

As the unique behaviour of modelling and analyzing of stiffened plates mentioned above, before moving on to particular interest of stiffened plates, herein a verification on modelling and modal analysis issues is presented using plates with different stiffening conditions taken as examples from literature.

The single stiffened rectangular plate in Figure 44 is studied and used for comparisons in literature by many researchers (Olson-1977, Koko-1992, Mukhopadhyay-2000 and

Rikards-2001). Hence the same stiffened plate with the same parameters as follows is modelled and analyzed by ANSYS in two different ways. Both models consist of flat plates created by Shell-63 finite elements, however the first model has Beam-44 stiffeners (designated as beam model) and the second model has Shell-63 stiffeners (designated as shell model) as the plate itself.

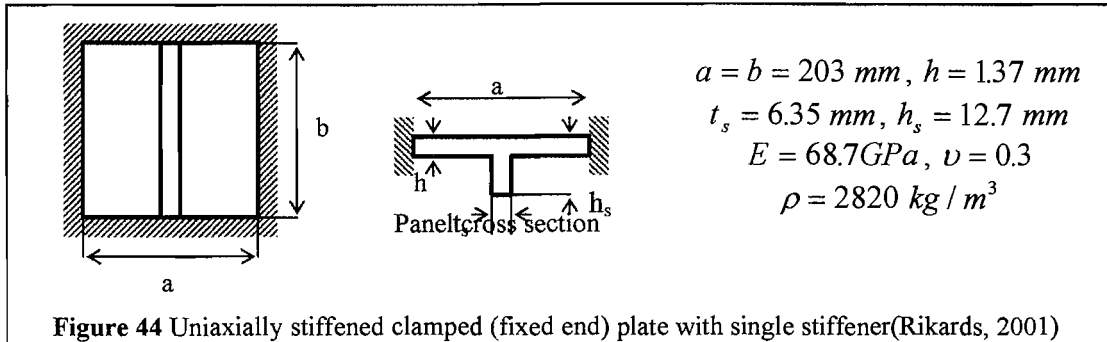


Figure 44 Uniaxially stiffened clamped (fixed end) plate with single stiffener(Rikards, 2001)

Here a and b are the side lengths of the plate, h the plate thickness, t_s the stiffener thickness, h_s the stiffener depth from the base of the plate, E the Young's modulus, ν the Poisson's ratio and ρ is the density.

The natural frequencies of the plate above, obtained currently from ANSYS for beam and shell models, are compared with the studies in literature in the following Table 12:

| Mode | Olson, 1977 | | ANSYS (Rikards, 2001) | ANSYS-Present | |
|------|-------------|------------|-----------------------|---------------|-------------|
| | Theory | Experiment | Shell model | Beam model | Shell model |
| 1 | 718.1 | 689 | 712.6 | 726.3 | 726.6 |
| 2 | 751.4 | 725 | 742.9 | 737.8 | 735.3 |
| 3 | 997.4 | 961 | 983.8 | 988.8 | 988.7 |
| 4 | 1007.1 | 986 | 993.6 | 994.7 | 993.8 |
| 5 | 1419.8 | 1376 | 1398.5 | 1402.0 | 1401.9 |
| 6 | 1424.3 | 1413 | 1402.5 | 1403.2 | 1402.5 |
| 7 | 1631.5 | 1512 | 1599.5 | 1529.5 | 1503.8 |
| 8 | 1853.9 | 1770 | 1831 | 1876.3 | 1879 |
| 9 | 2022.8 | 1995 | 1983.6 | 1986.7 | 1986.5 |
| 10 | 2025.0 | 2069 | 1985.8 | 1987.7 | 1987.3 |
| 11 | 2224.9 | 2158 | 2175.6 | 2181.7 | 2174.2 |
| 12 | 2234.9 | 2200 | 2185 | 2192.6 | 2192.6 |

Table 12 Experimental and numerical frequencies of single stiffened clamped plate

Mode shapes found after the modal analysis using ANSYS in this study match the mode shapes presented in the literature (Rikards-2001 and Mukhopadhyay-2000). 12 mode shapes are illustrated in Figure 92 and Figure 93 in Appendix for both beam and shell models. Mode shapes for beam and shell models match as well. Additionally, for most of the modes in both figures, the plate motions dominate the stiffener motions.

When the natural frequencies are compared in Table 12, natural frequencies obtained from experiment are obviously different from the others, basically because of their complex nature due to the presence of damping which is difficult to reflect, besides the boundary conditions are never perfectly achieved. There may also be manufacturing variances between parts of the structure in the experiment.

On the other hand, when present ANSYS results (natural frequencies) with shell model is compared with the corresponding ANSYS results in literature, it is seen that they are reasonably close to each other. The main reason for the differences in these two is because of not being modelled with exactly the same type of finite elements.

In the present analysis, both beam and shell models give very close natural frequencies as seen in the last two columns of Table 12.

Selected vibration mode shapes of the present analysis are presented in Figure 45. Mode 1 is an overall (global) vibration mode, modes 12 and 24 are local plate-only vibration modes and mode 20 is a coupled vibration mode with stiffener-plate interaction.

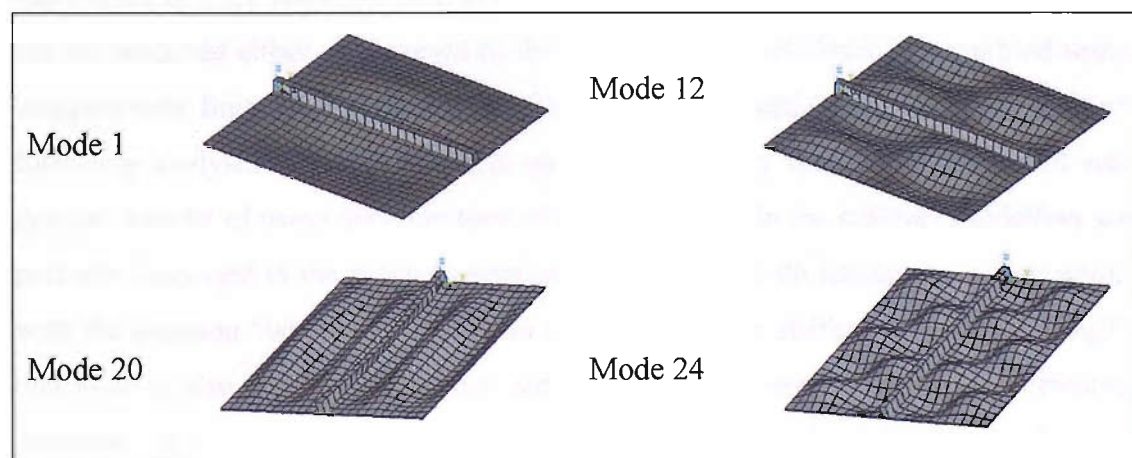


Figure 45 Selected vibration modes of shell stiffened plate

The biggest differences in the natural frequencies are at mode 7 and mode 11. Coupled vibration modes with stiffener plate interactions are more significant at these modes in Figure 92 and Figure 93 in Appendix. In other words, stiffener involved modes have different natural frequencies, because stiffener type is the only difference between two models.

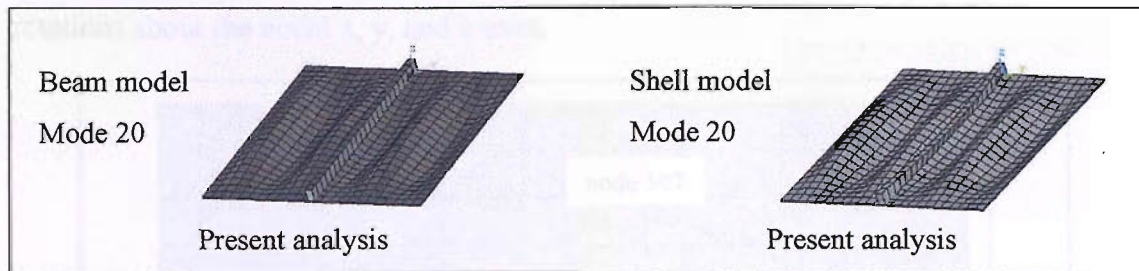


Figure 46 Comparison of vibration mode 20 for beam and shell models (Stiffened clamped plate)

In the present study another difference between two models is, as seen in Figure 46, shell model has a coupled vibration mode with stiffener-plate interaction at mode 20, where for the same mode, beam model doesn't have a coupled vibration mode due to its stiffener's high rigidity.

5.3.4 Analysis of Plates (6m x 12m)

A rectangular plate as shown in Figure 47, 12m length, 6m width with 0.03m thickness is taken as an example and modelled to analyze with fixed end boundary conditions at all sides.

The choice of right finite element to use in stiffener modelling is important. Stiffeners can be modelled either using beam or shell elements. If a stiffener is assembled using inappropriate finite element, then the physical representation of the system and all following analyses (modal, transient, etc) will not carry the characteristics of real system. Results of using different type of finite elements in the stiffener modelling are partially discussed in the previous section incorporating with literature. In connection with the question “whether to use beam or shell model in stiffened plate modelling?” this plate is also modelled and analyzed with stiffeners depending on the stiffening direction, in three different ways, longitudinally, transversely and orthogonal, as in Figure 48. In each way of stiffening, Beam44 and Shell99 elements are used

separately to model stiffeners. While modelling the plates, Shell-99, 8 nodded quadrilateral elements are used in ANSYS, which enable changing the locations of nodes in order to be able to connect with stiffeners. For the beam type stiffeners, because of the same reason explained, Beam-44 elements with offset nodes are used. For stiffeners modeled as plates, Shell-99 finite elements are used. Both elements have six degrees of freedom at each node: translations in the nodal x, y, and z and rotations about the nodal x, y, and z-axes.

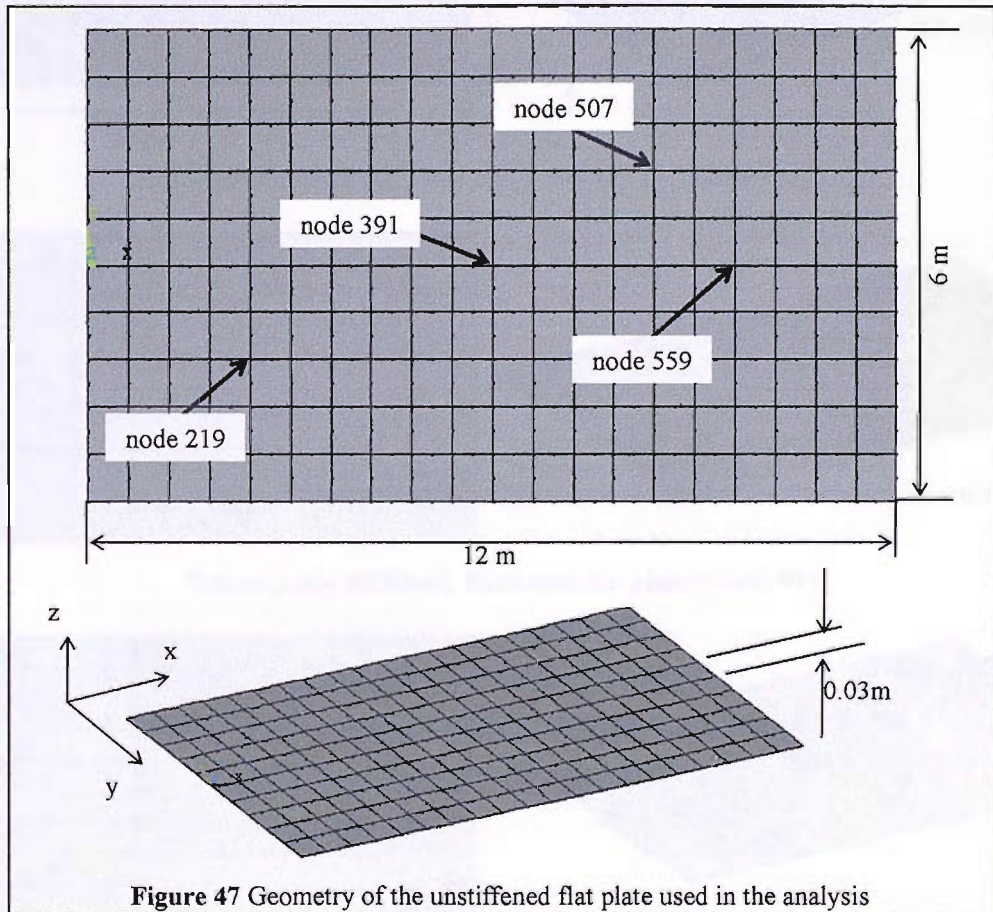


Figure 47 Geometry of the unstiffened flat plate used in the analysis

The material properties of the stiffeners and the plates are as follows:

Young's modulus, $E = 207e^9 \text{ N/m}^2$, Poisson's ratio, $\nu = 0.3$, Mass = 16977.6 kg

Mass density for: Longitudinally stiffened plate, $\rho = 7218.37 \text{ kg/m}^3$

Transversely stiffened plate, $\rho = 7525.53 \text{ kg/m}^3$

Orthogonal stiffened plate, $\rho = 6935.29 \text{ kg/m}^3$

All stiffeners used have rectangular cross-sections with the dimensions as:

Longitudinal stiffeners, length 12m, depth 0.2m and thickness 0.02m

Transverse stiffeners, length 6m, depth 0.2m and thickness 0.02m

In order to ease the comparison, all models have the same mass, but different mass densities as given above.

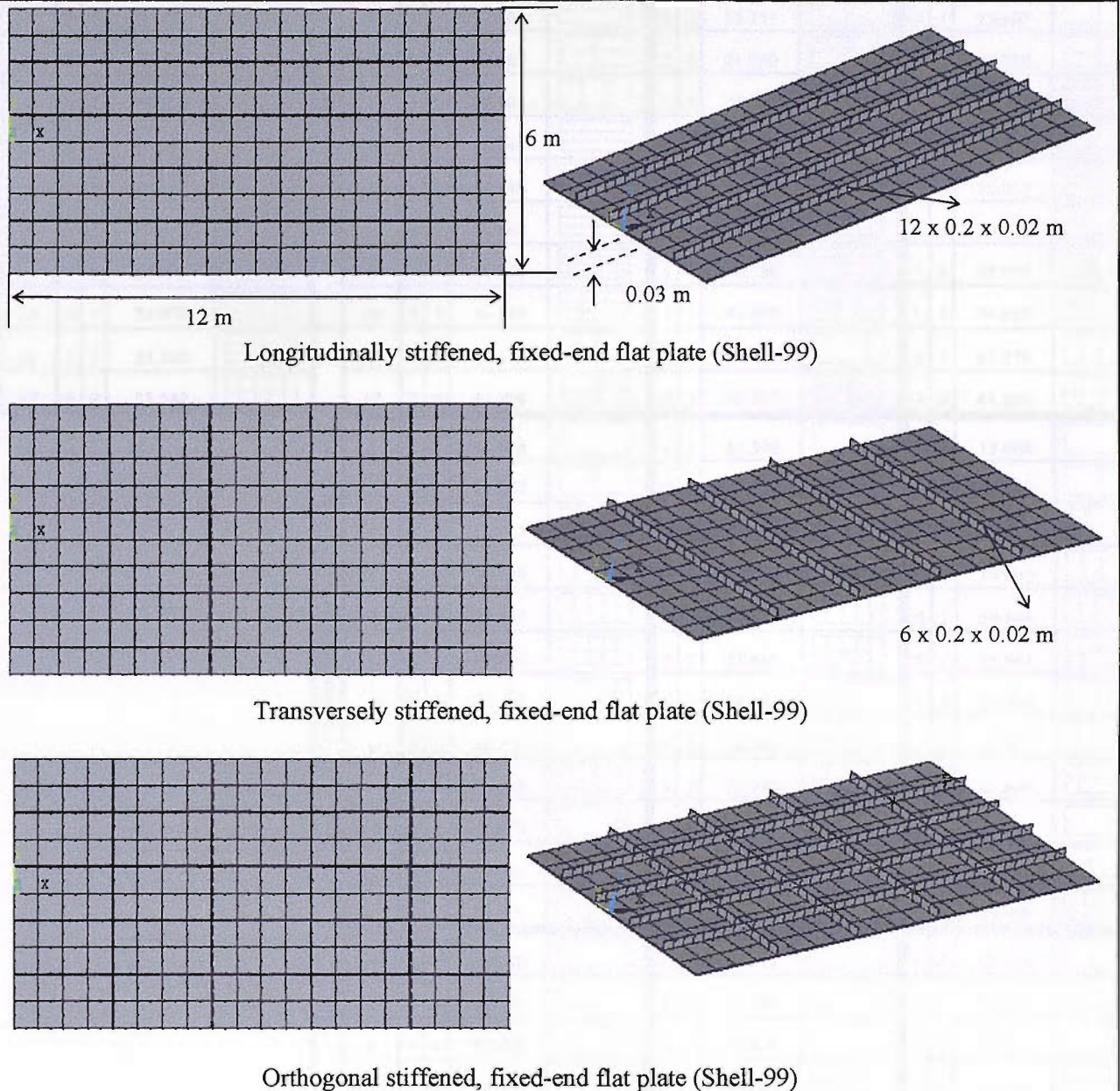


Figure 48 Stiffened plate models in three directions

When the modal analysis is done for each model, it is noted that stiffeners with Shell99 elements buckle by twisting about their line of attachment to the plating due to their low torsional rigidity. This is known as tripping (Hughes, 1983). In reality this phenomenon is overcome by using tripping brackets. However in this study it would just increase the modelling time and its complexity. Instead, to prevent tripping, the rotations about x and y-axes at the free ends of the shell stiffeners are constrained.

| Boundary Condition: Fixed end | | | | | | | | | | | | | | | | | | | |
|-------------------------------|---|---|----------------|------------------------------|-------------------------|----|---|----------------|------------|---|-----------------|----------------|------------|--------|---|----------------|------------|--------|--|
| Flat plate-no stiffeners | | | | Shell stiffened(no tripping) | | | | Beam stiffened | | | Shell stiffened | | | | | | | | |
| mode no | m | n | Frequency (Hz) | Node lines | mode no | m | n | Frequency (Hz) | Node lines | m | n | Frequency (Hz) | Node lines | m | n | Frequency (Hz) | Node lines | | |
| 1 | 1 | 1 | 5.059 | | Longitudinal Stiffening | 1 | 1 | 8.865 | | 1 | 1 | 7.384 | | 1 | 1 | 7.153 | | | |
| 2 | 2 | 1 | 6.553 | | | 2 | 2 | 15.935 | | 1 | 2 | 14.362 | | 1 | 2 | 14.034 | | | |
| 3 | 3 | 1 | 9.220 | | | 3 | 1 | 17.104 | | 2 | 1 | 15.751 | | 2 | 1 | 15.003 | | | |
| 4 | 4 | 1 | 13.045 | | | 4 | 2 | 22.367 | | 2 | 2 | 21.059 | | 2 | 2 | 19.950 | | | |
| 5 | 1 | 2 | 13.164 | | | 5 | 3 | 1 | 27.501 | 1 | 3 | 25.852 | | 1 | 3 | 25.545 | | | |
| 6 | 2 | 2 | 14.628 | | | 6 | 1 | 3 | 28.546 | 3 | 1 | 28.665 | | 3 | 1 | 26.879 | | | |
| 7 | 3 | 2 | 17.152 | | | 7 | 3 | 2 | 32.548 | 2 | 3 | 31.189 | | 2 | 3 | 30.015 | | | |
| 8 | 5 | 1 | 17.975 | | | 8 | 2 | 3 | 32.868 | 3 | 2 | 32.958 | | 3 | 2 | 30.596 | | | |
| 9 | 4 | 2 | 20.785 | | | 9 | 1 | 4 | 41.705 | 1 | 4 | 40.736 | | 3 | 3 | 38.937 | | | |
| 10 | 6 | 1 | 23.972 | | | 10 | 3 | 3 | 41.834 | 3 | 3 | 41.698 | | 1 | 4 | 40.615 | | | |
| 11 | 1 | 3 | 25.343 | | | 11 | 4 | 1 | 41.924 | 4 | 1 | 44.873 | | 4 | 1 | 41.370 | | | |
| 12 | 5 | 2 | 25.542 | | | 12 | 2 | 4 | 45.888 | 2 | 4 | 45.335 | | 4 | 2 | 44.251 | | | |
| Transversely Stiffening | | | | | | | | | | | | 1 | 1 | 13.836 | | 1 | 1 | 13.608 | |
| | | | | | Transversely Stiffening | 2 | 2 | 1 | 14.827 | 2 | 1 | 14.815 | | 2 | 1 | 13.979 | | | |
| | | | | | | 3 | 3 | 1 | 16.743 | 3 | 1 | 15.990 | | 3 | 1 | 14.928 | | | |
| | | | | | | 4 | 4 | 1 | 20.139 | 4 | 1 | 19.847 | | 4 | 1 | 19.061 | | | |
| | | | | | | 5 | 5 | 1 | 22.387 | 5 | 1 | 20.537 | | 5 | 1 | 19.646 | | | |
| | | | | | | 6 | 5 | 2 | 27.671 | 5 | 2 | 27.613 | | 5 | 2 | 24.861 | | | |
| | | | | | | 7 | 5 | 2 | 28.097 | 6 | 1 | 28.286 | | 5 | 2 | 26.304 | | | |
| | | | | | | 8 | 3 | 2 | 28.477 | 5 | 2 | 28.503 | | 6 | 1 | 27.367 | | | |
| | | | | | | 9 | 6 | 1 | 28.945 | 3 | 2 | 29.432 | | 3 | 2 | 27.869 | | | |
| | | | | | | 10 | 2 | 2 | 31.578 | 3 | 2 | 32.138 | | 2 | 2 | 30.789 | | | |
| | | | | | | 11 | 2 | 2 | 31.724 | 3 | 2 | 32.142 | | 2 | 2 | 31.021 | | | |
| | | | | | | 12 | 7 | 1 | 35.367 | 7 | 1 | 34.428 | | 7 | 1 | 33.536 | | | |
| Orthogonal Stiffening | | | | | | | | | | | | 1 | 1 | 18.080 | | 1 | 1 | 15.185 | |
| | | | | | Orthogonal Stiffening | 2 | 2 | 1 | 22.774 | 2 | 1 | 21.326 | | 2 | 1 | 20.168 | | | |
| | | | | | | 3 | 3 | 1 | 32.390 | 3 | 1 | 32.300 | | 3 | 1 | 30.261 | | | |
| | | | | | | 4 | 1 | 2 | 38.870 | 1 | 2 | 38.636 | | 1 | 2 | 35.032 | | | |
| | | | | | | 5 | 2 | 2 | 41.451 | 2 | 2 | 41.528 | | 2 | 2 | 37.607 | | | |
| | | | | | | 6 | 4 | 1 | 45.979 | 4 | 1 | 48.122 | | 3 | 2 | 44.041 | | | |
| | | | | | | 7 | 3 | 2 | 47.769 | 3 | 2 | 48.667 | | 4 | 1 | 44.372 | | | |
| | | | | | | 8 | 4 | 2 | 60.240 | 4 | 2 | 63.239 | | 1 | 3 | 56.808 | | | |
| | | | | | | 9 | 5 | 1 | 61.008 | 3 | 3 | 64.668 | | 5 | 2 | 56.851 | | | |
| | | | | | | 10 | 3 | 3 | 61.035 | 5 | 3 | 64.792 | | 5 | 3 | 57.226 | | | |
| | | | | | | 11 | 5 | 3 | 61.760 | 5 | 3 | 65.475 | | 5 | 1 | 58.782 | | | |
| | | | | | | 12 | 3 | 3 | 63.981 | 5 | 3 | 67.745 | | 5 | 3 | 58.880 | | | |

Table 13 Table of the natural frequencies and the node lines for all the plate models

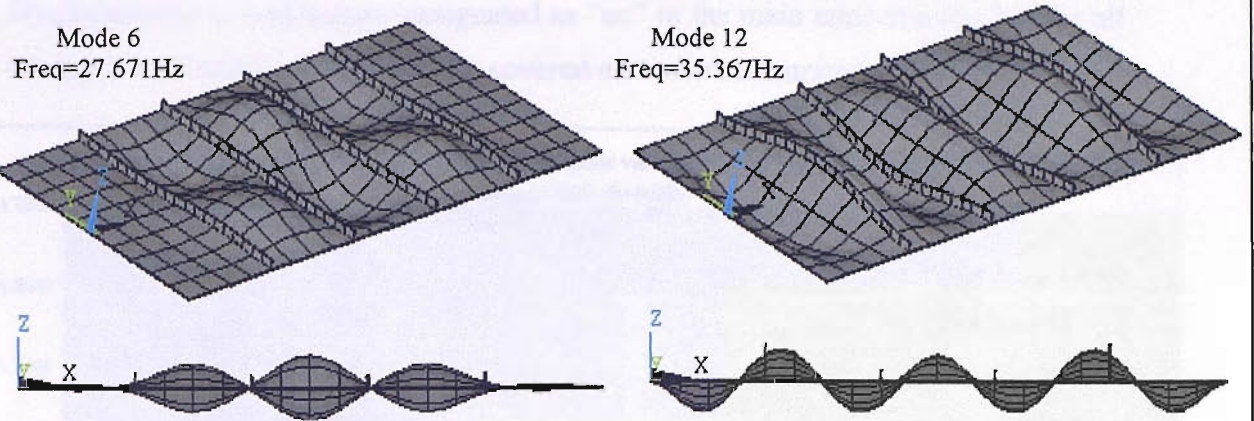
The mode shapes of the unstiffened and stiffened plates whose natural frequencies given in Table 13 can be found in the Appendix for further interest. In most of these mode shapes, because of the dimensions given to the stiffeners, flat plate's vibration modes are dominant over the vibration modes of stiffeners.

When the natural frequencies of various stiffened models in Table 13 are compared with the unstiffened model, the increase in the natural frequencies due to stiffening is the first significant observation as expected. Between the stiffened plates, shell stiffened model with tripping effects has the lowest frequencies for all stiffening directions.

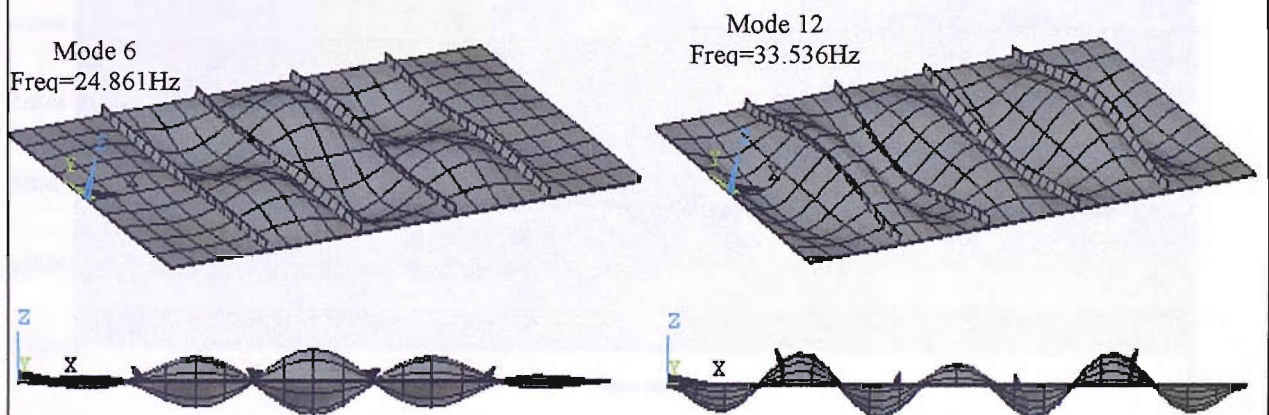
In the cases of shell model without tripping and beam model, it is not possible to clarify the trend of natural frequencies. For these models, each natural frequency and mode shape for a particular mode number must be compared individually depending on the stiffening direction. At the same time, there are shifts in some of the mode shapes/node lines, which can be noted while comparisons are being made between stiffened models.

The first eight mode shapes and their node lines match one to one for longitudinal beam stiffened and shell stiffened plates as seen in Table 13. In transversely stiffening, first five modes match one to one for all three types of models where this matching number is six between shell (no tripping) and beam models. On the other hand first five modes match for all three types and eight modes match for shell (no tripping) and beam models in orthogonal stiffening. Using these statements, it can be said that the beam model and its corresponding shell model are closer to each other in modal responses.

The effect of tripping on the plates is illustrated at mode 6 and 12 in Figure 49 for transversely shell stiffened plates with and without constraints to prevent tripping. Orthogonal shell stiffened plates without rotational constraints have considerably less amount of tripping because of having the support affect on the connections of perpendicular stiffeners which can be seen in Figure 103 in the Appendix.



Transversely stiffened (Shell99-no tripping), fixed end flat plate

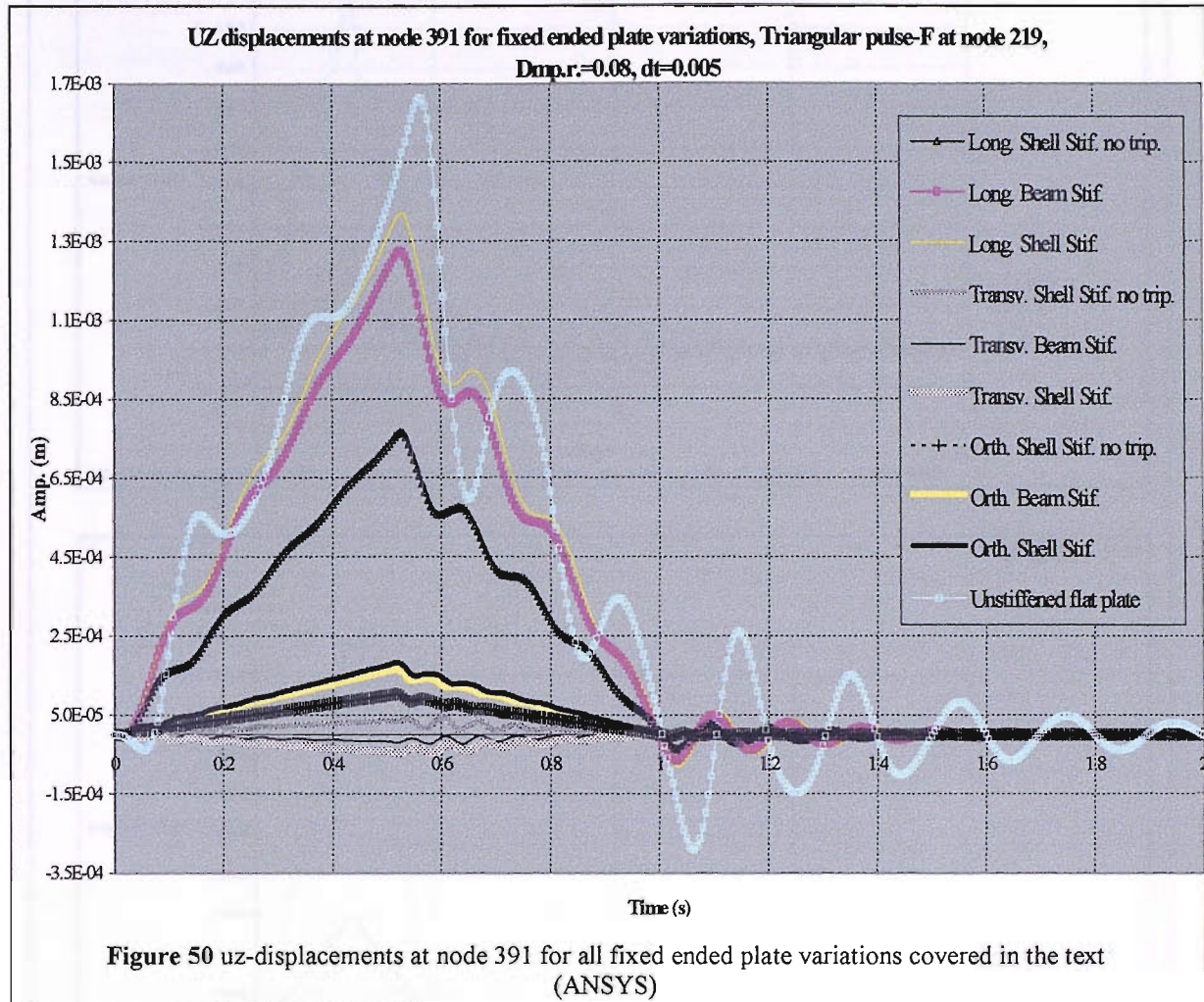


Transversely stiffened (Shell99), fixed end flat plate

Figure 49 Plates with and without tripping

After obtaining the modal characteristics for the plates, herein the transient response of the plates is presented. The triangular pulse in Figure 34 is applied to the stiffened variations of the clamped flat plate in Figure 48, on their 219-numbered node as shown in Figure 47. The responses regarding the translations in z-direction (perpendicular to undeflected plate surface) are obtained from ANSYS for three nodal points, which are node 391, 507 and 559 shown in Figure 47, and then compared with the results using the mode superposition method in which principal coordinates are evaluated from convolution integral using Eq.(65) together with discrete time method.

Displacements in z-direction (designated as “uz” in the main text) at node 391 for all the types and variations of stiffening covered earlier are illustrated in Figure 50.



From Figure 50 it's seen that at node 391, which is in the middle of the plate, unstiffened flat plate has the biggest amplitude of all, as expected. Then the sequence continues with longitudinal, orthogonal and transverse stiffened plates. Transversely stiffened plates have smaller amplitudes at node 391 than the orthogonal stiffened ones, because orthogonal stiffened plate has the lowest material density.

It also can be noticed that in Figure 50, beam and shell stiffened plates have closer responses than the shell stiffened plates with no tripping. Figure 104 in Appendix, which shows the responses separately according to the stiffening direction, can be referred for further interest.

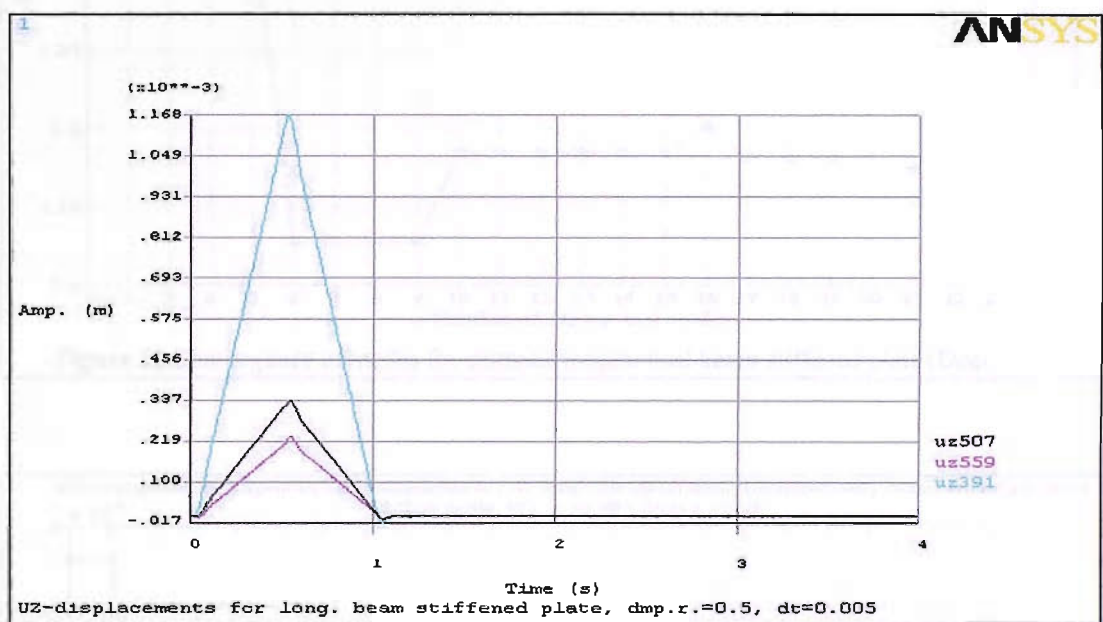
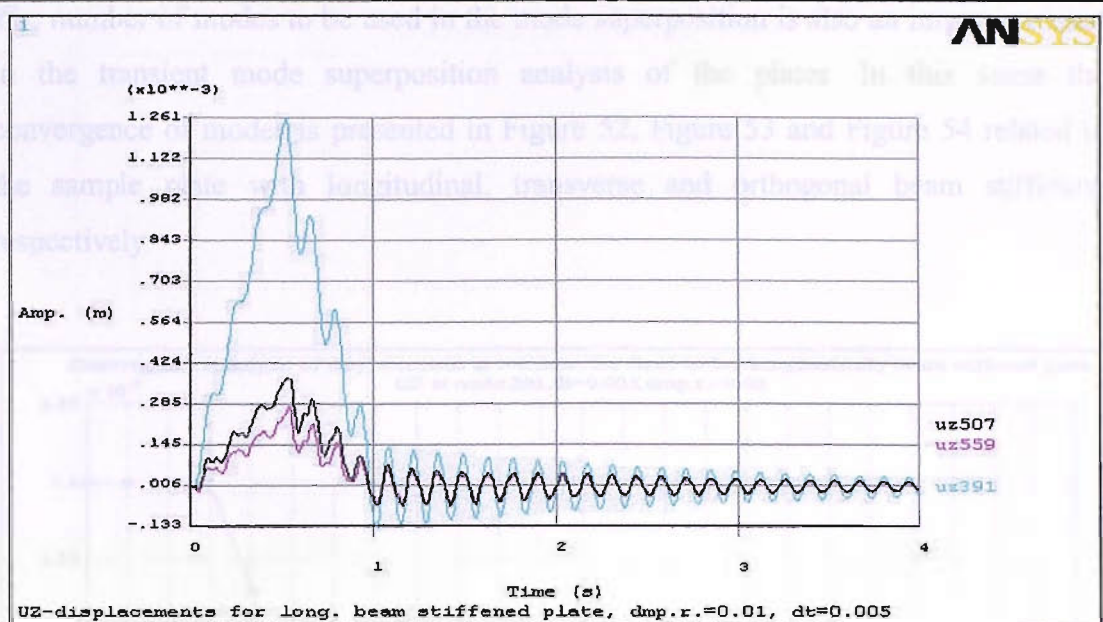
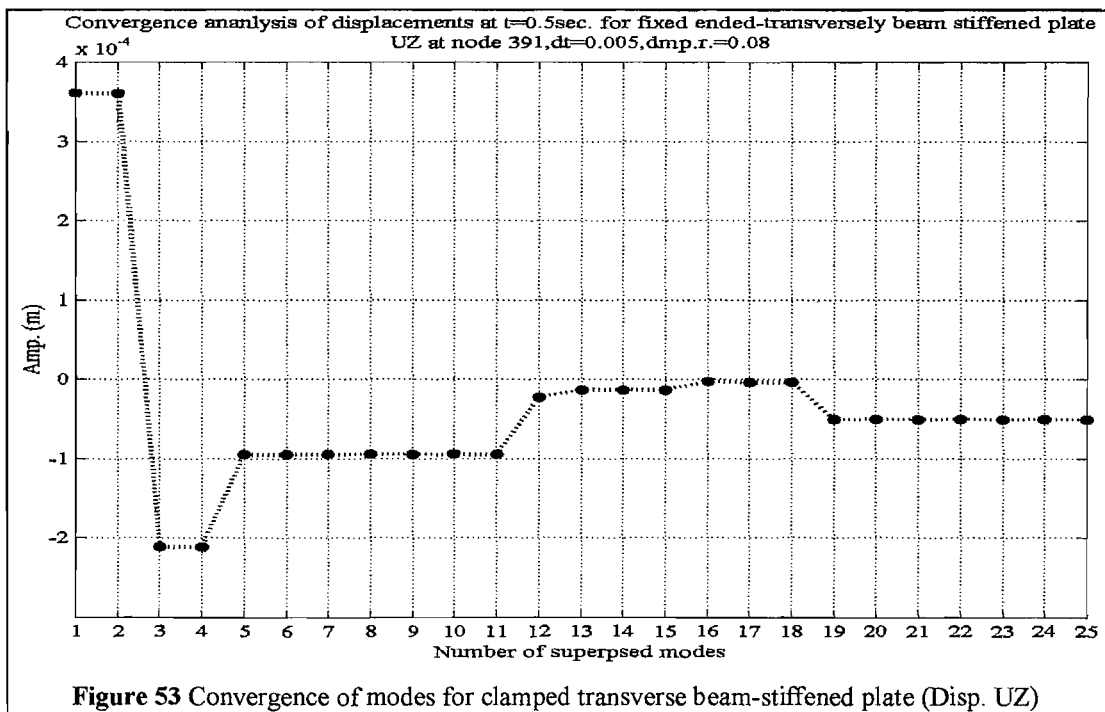
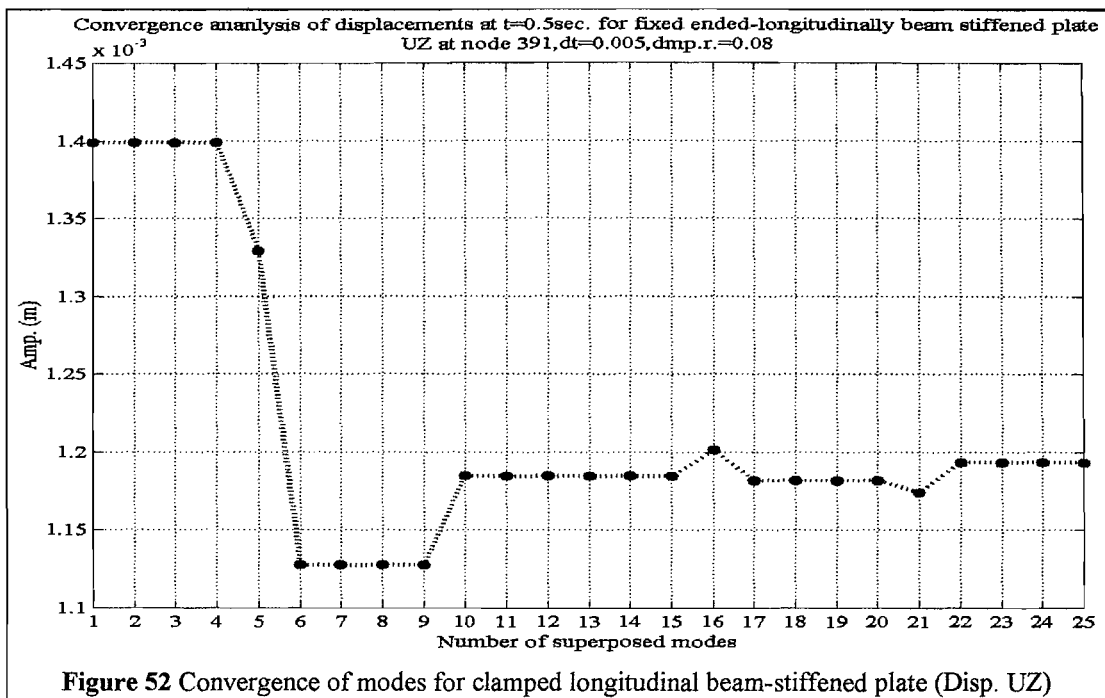


Figure 51 Nodal responses (uz-displacements) for longitudinally stiffened beam under triangular impulse with damping ratio 0.01 and 0.5, discrete time interval $dt=0.005$

The effect of different damping ratios is presented in Figure 51 by using ratios 0.01 and 0.5. However both ratios stand for the underdamped vibration case, it can be seen that ratio 0.5 gives a very limited view on the response and dies out as soon as the excitation is over. On the other hand damping ratio 0.01 increases the chance of having beating effect. Because for this ratio the difference between damping frequency and the natural frequency of the system becomes very small. As a result for both reasons mentioned above damping ratio 0.08 is used in all analyses regarding these plates.

The number of modes to be used in the mode superposition is also an important issue in the transient mode superposition analysis of the plates. In this sense the convergence of modes is presented in Figure 52, Figure 53 and Figure 54 related to the sample plate with longitudinal, transverse and orthogonal beam stiffening respectively.



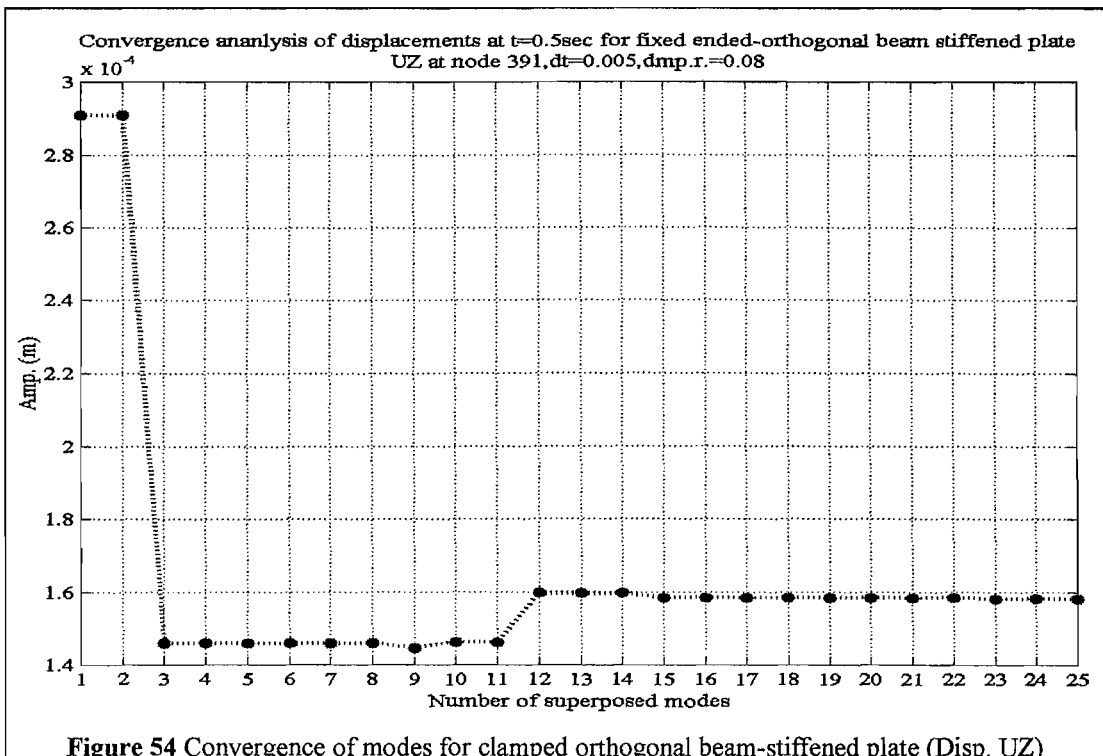
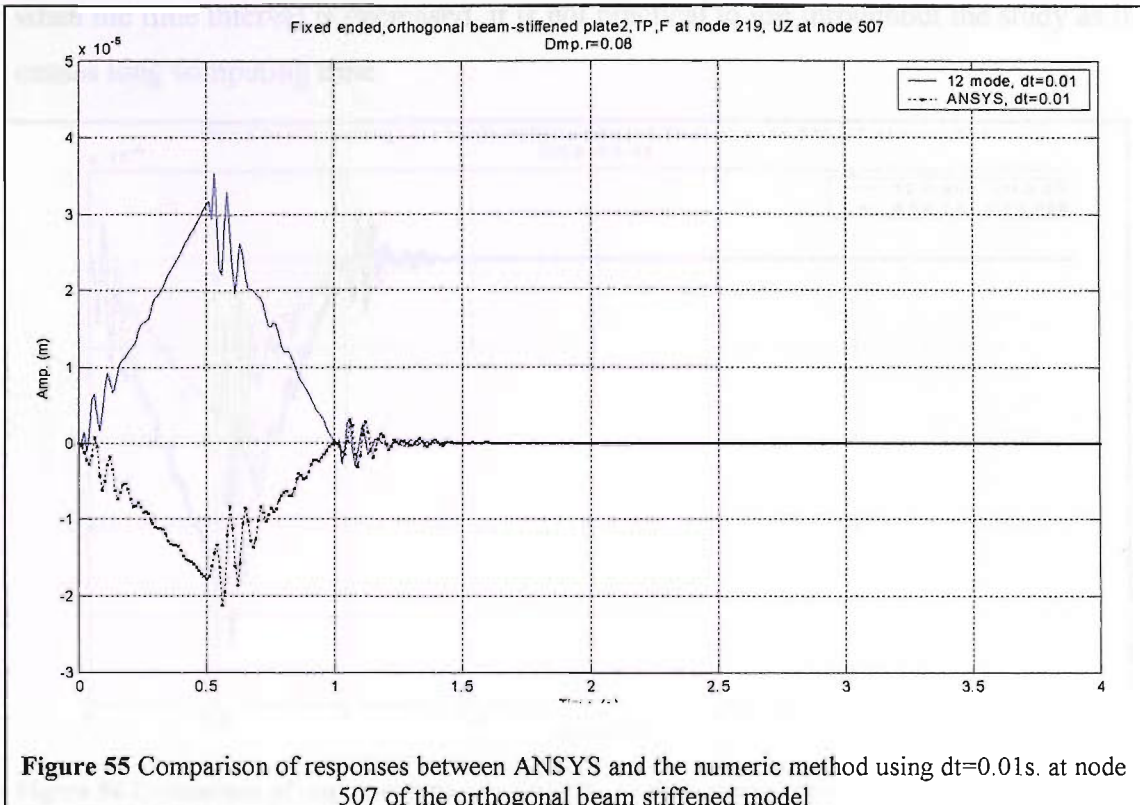


Figure 54 Convergence of modes for clamped orthogonal beam-stiffened plate (Disp. UZ)

All the convergence figures given above are evaluated for the amplitudes at time $t=0.5\text{sec}$. When Figure 52 for the longitudinally beam stiffened model is examined it is seen that there are groups of convergence. In the first mode shape of longitudinal beam stiffened plate, there is a non-zero modal uz -deflection at the node 391, which is the mid-point of the plate, as can be seen in Figure 98 in Appendix, illustrating the mode shapes of this stiffened plate. The following 3 modes until mode 5 don't contribute to the displacement at node 391 for this reason. Modal uz -deflection in mode 5 lowers the amplitude and the decrease in the amplitude continues with mode 6 as well and the total amplitude in mode 6 goes on constant until mode 9, because of the same reason explained for modes 1 to 4. Contribution of mode 10 brings the total amplitude into a new value and a convergence can be said to be achieved after mode 10.

For the transversely beam stiffened model however the convergence is not stable until mode 19 as seen in Figure 53, superposition of 12 modes can be assumed as the start of convergence, since after 12 modes the difference in the amplitudes is not big and superposing modes after 12 costs more computing time. On the other hand orthogonal beam stiffened model shows a good convergence after 12 modes (Figure 54).

Figure 105, Figure 106 and Figure 107 in Appendix illustrating the amplitudes on the time domain for the longitudinally, transversely and orthogonal beam stiffened models respectively, show that the convergence after the end of triangular impulse, occur in the lower modes than the period of excitation.



In the following analyses 12 mode shapes are used in the transient mode superposition and results compared with ANSYS. All the major differences in the responses between the method used in this document and the ANSYS are mainly because of the size of time interval (Nyquist frequency effect). This conclusion can be noticed when the orthogonal beam stiffened plates are analyzed with both $dt=0.005s$. and $dt=0.001s$. here in the figures below as well as the rest in Appendix. To have an idea of the affect of discrete time interval, illustrations in Figure 55, Figure 56 and Figure 57 represent the amplitudes calculated by using discrete time interval $dt=0.01s$, $dt=0.005s$. and $dt=0.001s$. at node 507. The reason for choosing particularly this node is, between the 3 nodes of the orthogonal beam stiffened model being examined, node 507 has the biggest differences in the amplitudes between three intervals which makes it easy to present.

During the analyses it is noticed that the responses from ANSYS and the numeric method do not match well especially during the impulse phase when $dt=0.01s$. is used (Figure 55). Hence $dt=0.005s$. is used in the rest of the analysis. However $dt=0.001s$ is also used for the orthogonal beam stiffened beam to show how closer responses get when the time interval is decreased, it is not practical to use throughout the study as it causes long computing time.

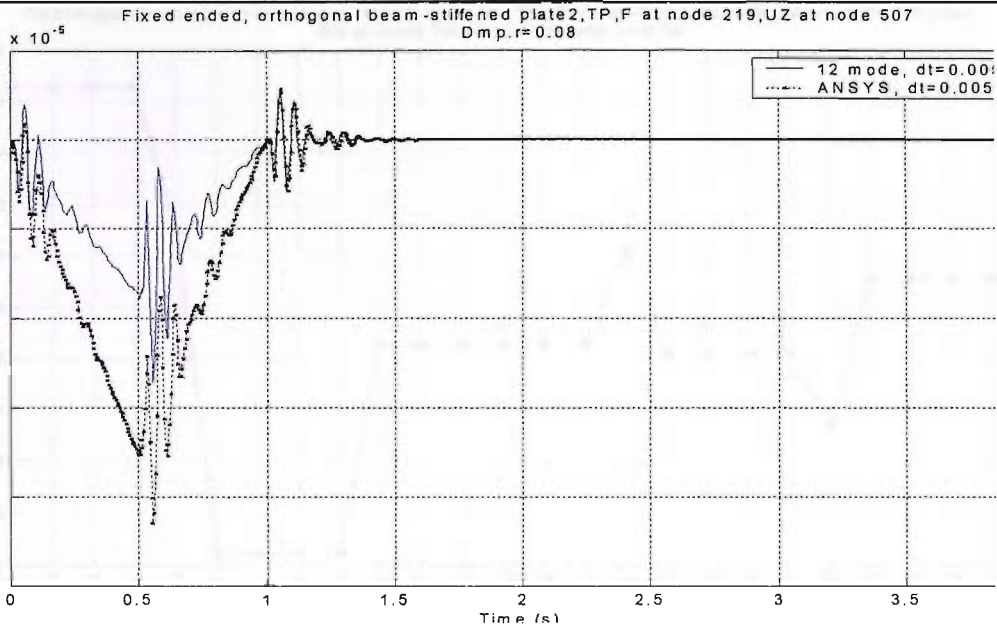


Figure 56 Comparison of responses between ANSYS and the numeric method using $dt=0.005s$. at node 507 of the orthogonal beam stiffened model

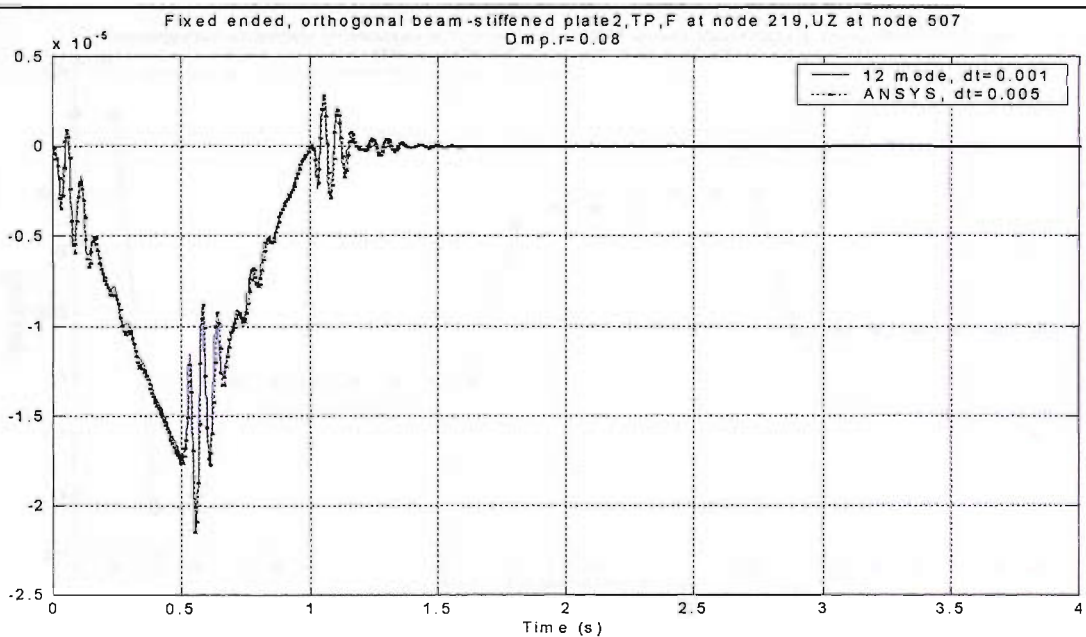
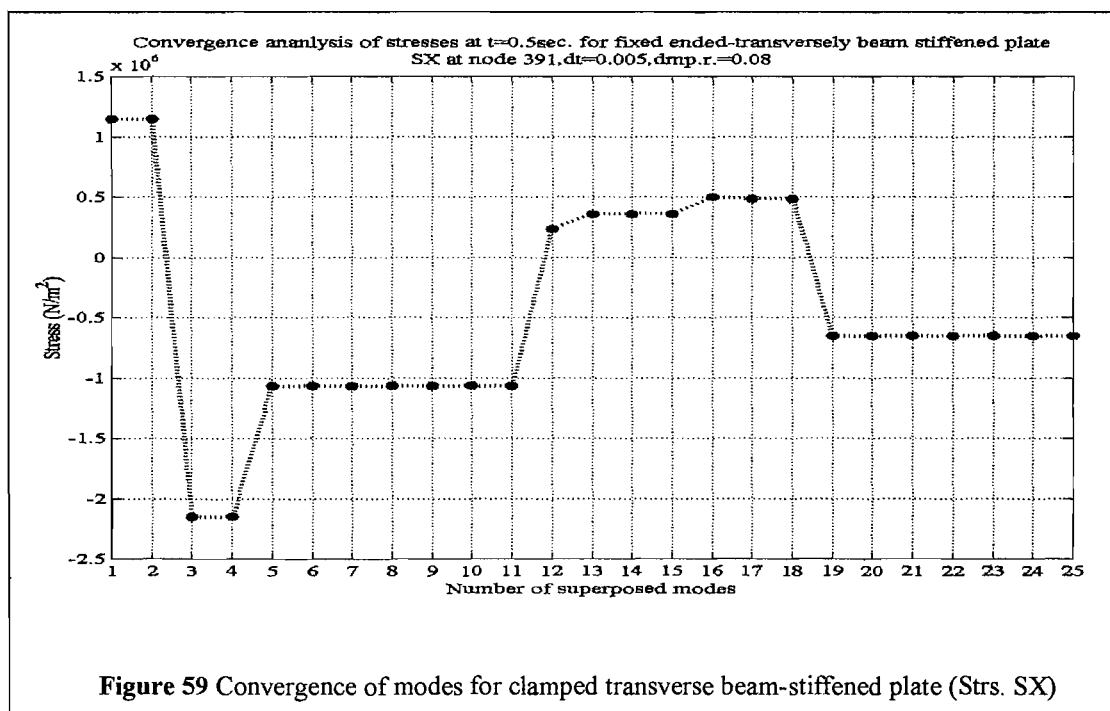
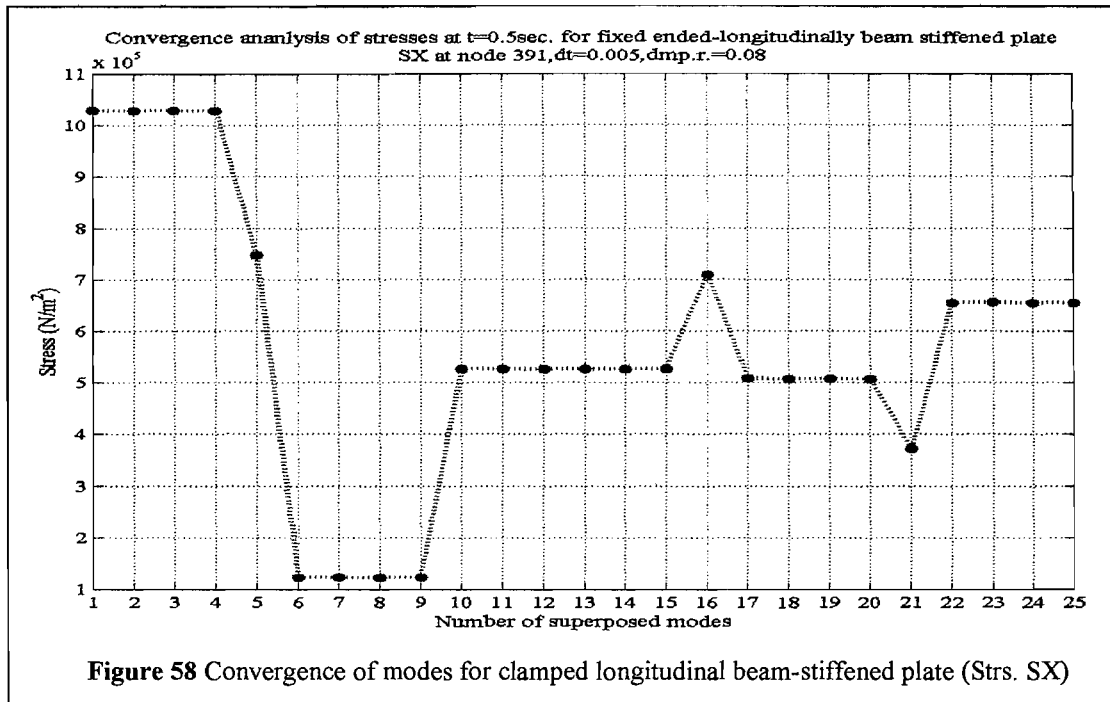
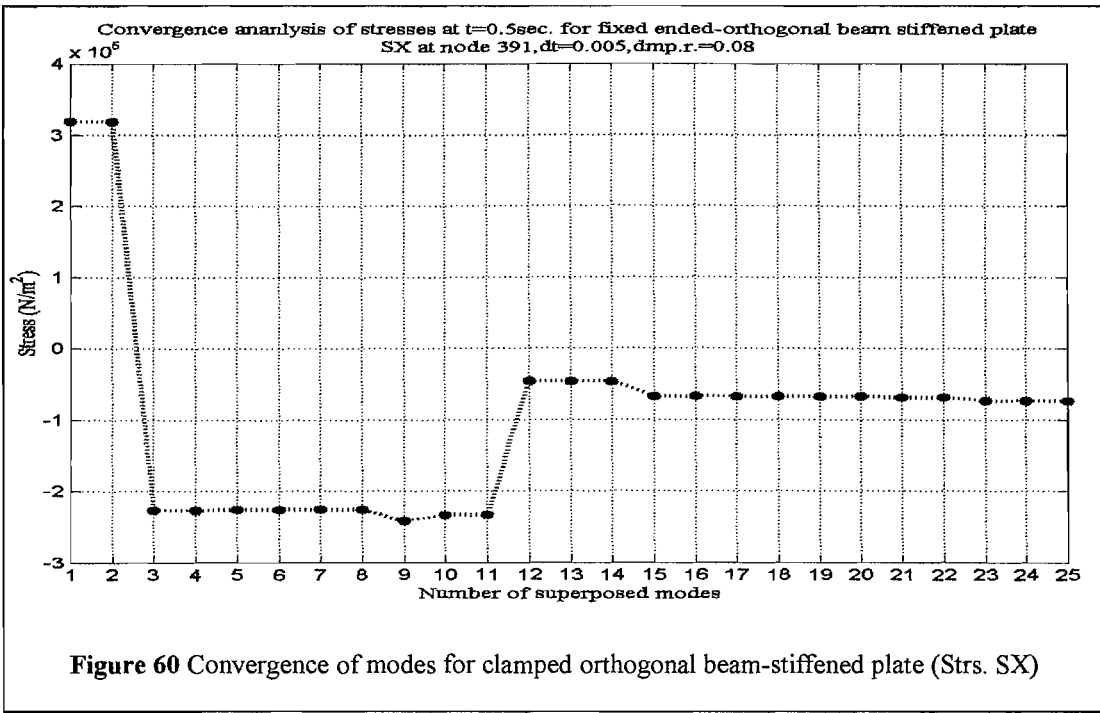


Figure 57 Comparison of responses between ANSYS and the numeric method using $dt=0.005s$. and $dt=0.001s$. respectively at node 507 of the orthogonal beam stiffened model

Triangular impulse responses (displacement-uz and stress-sx illustrations) for all the models in Table 13 at node 559 are attached to the Appendix for further details. Here Figure 58, Figure 59 and Figure 60 represent the convergence of modes in the stress values at node391 for longitudinally, transversely and orthogonal beam stiffened models.





When the convergence illustrations in Figure 58 to Figure 60 for the sx-direct stresses are compared with the convergence illustrations in Figure 52 to Figure 54 for uz-displacements, it's clear that two groups of figures have the same nature in terms of the trends of the plots. Modal sx-stress values are much bigger than the modal uz-translation values, which can be seen in Figure 119 in Appendix. These value groups both contribute to the total responses; hence the differences after superposing 12 modes are bigger in stress convergence illustrations than the corresponding illustrations of displacement convergence.

As a result it can be said that 12-mode superposition is satisfactory for the convergence of stress responses regarding especially orthogonal and longitudinal beam stiffened plate. However for the transverse stiffening case, contribution of higher modes is required for a better convergence.

5.3.5 Analysis of a Realistic Plate (Tanker bottom forward end)

Hitherto only flat plates of 6m width 12m length and 0.03m thickness with details given in Figure 47 are used to model the stiffened plates with rectangular cross-sectioned stiffeners as in Figure 48. In this part, stiffened plating between bulkheads (station 82 and fore perpendicular) of a single bottomed 36,000 DWT oil tanker is taken as the example. It is clear from the node lines and natural frequencies of different type of stiffened plates with different finite elements in Table 13 that, there is not a direct agreement in the characteristics between the variations of stiffened plates. The modal characteristics are all unique. Thus the question of whether to model the system with shell element stiffeners or beam element stiffeners still exists. Up to this point various stiffened plates are created using shell and beam finite elements and their characteristics studied. At this stage, there is a stiffened forward bottom plate of a tanker with the dimensions and details given in Figure 61a. This stiffened plate can be modelled and analyzed in different ways in FEA mainly using different finite elements to model the stiffeners. Stiffeners can be modelled either using beam or shell elements.

In this document, the stiffeners are modelled using Beam-44 finite elements and Shell-63 elements separately. Modal analysis is applied on both models and results are presented. Transient response of stiffened plate model having stiffeners constructed with Beam44 elements is also investigated.

The plate shown in Figure 61 is modelled with fixed end boundary conditions. The flat plate with dimensions of 12.2m x 7.85m is modelled using Shell-63, 4 nodded finite elements. The stiffeners are modelled using offset Beam-44 (and Shell-63 for the following model) finite elements. Both elements have six degree of freedom at each node: translations in the nodal x, y, and z and rotations about the nodal x, y, and z axes.

Centre girder and transverse stiffeners both have T-cross sections. On the other hand bottom longitudinals have L-cross sections. Figure 61 also represents the FE model of the plate.

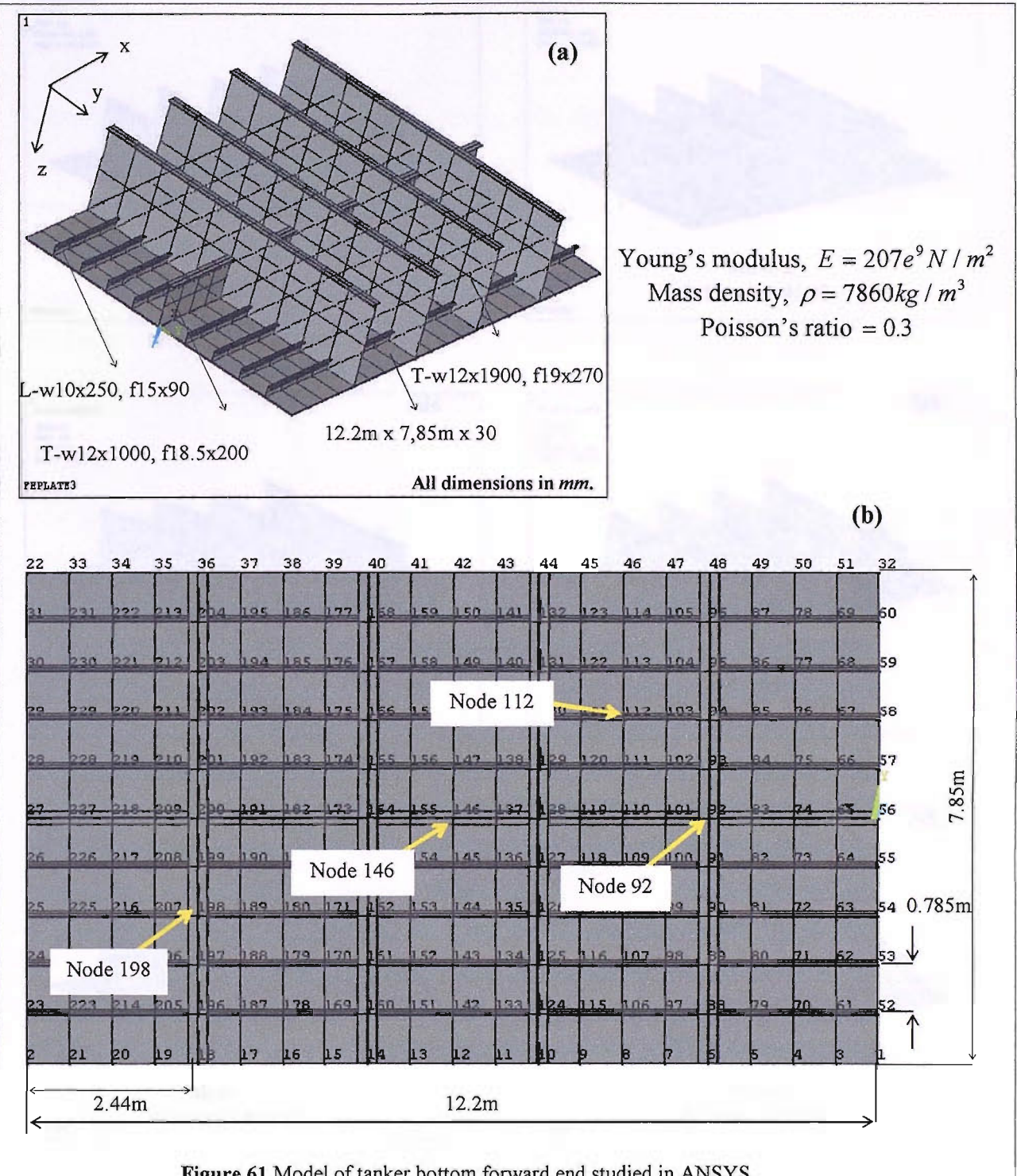


Figure 61 Model of tanker bottom forward end studied in ANSYS

A modal analysis is performed for the plate illustrated above and 12 modes are extracted from ANSYS and the first six of these modes are given in Figure 62. The rest of the mode shapes are attached to the Appendix (Figure 120-Figure 122).

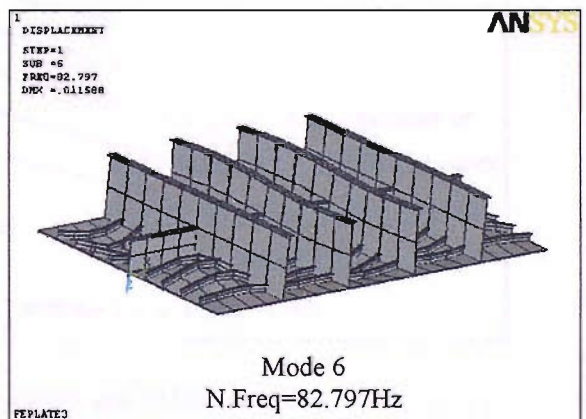
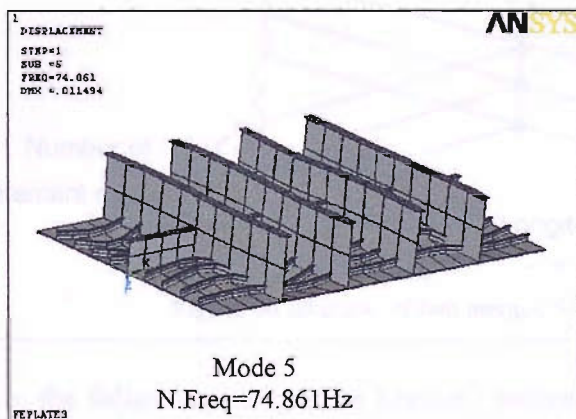
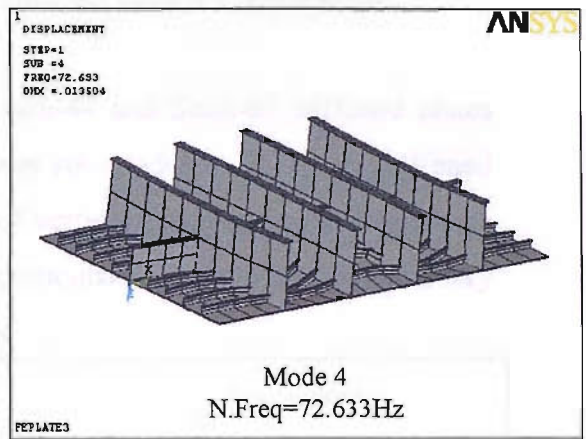
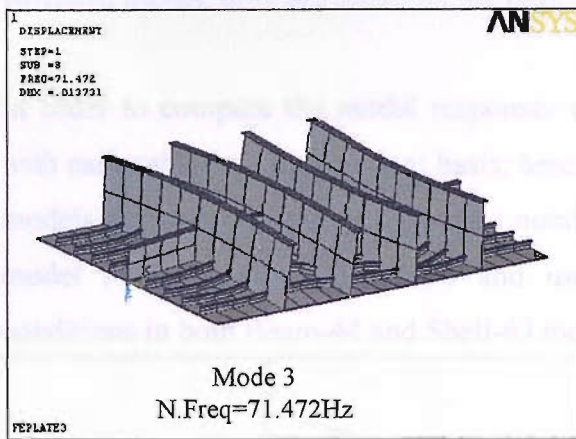
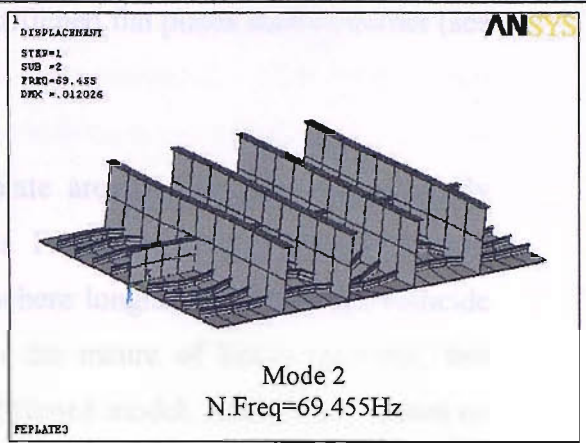
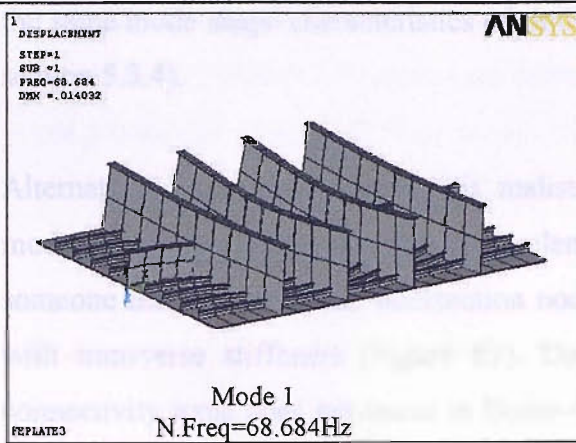


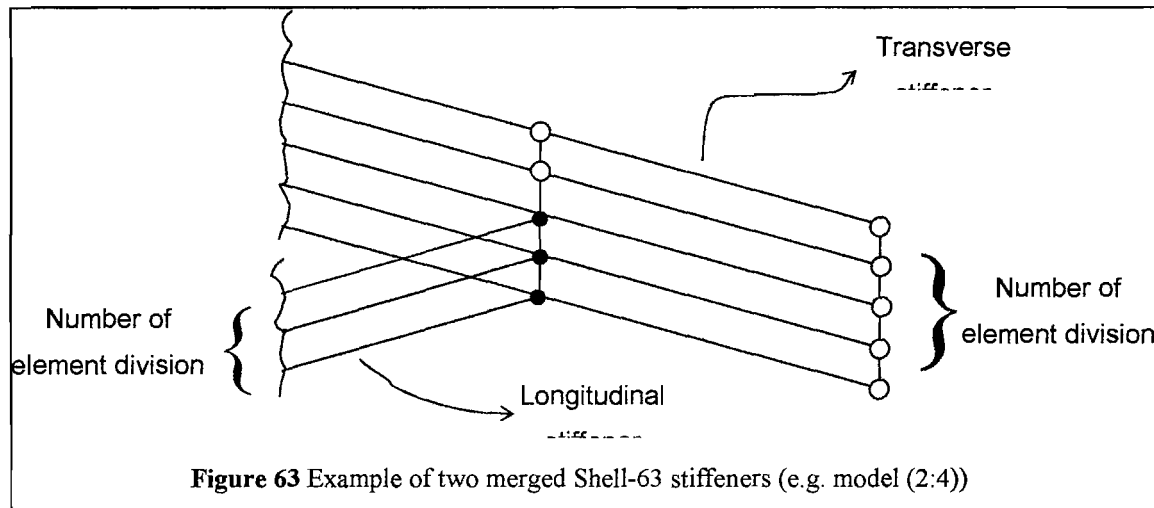
Figure 62 First six mode shapes of the stiffened (Beam-44) tanker plate

When all the mode shapes are examined it is significant that there are coupled vibration modes in which stiffeners and the flat plate interact within 12 mode shapes. Vibration of the flat plate is dominant over the stiffeners. Local deflections are noticeable for the flat plate. The coupled vibration modes of this model simply show

the same mode shape characteristics of similar stiffened flat plates studied earlier (see section 5.3.4).

Alternatively, the stiffeners of this realistic plate are modelled and subsequently modally analyzed using Shell-63 finite elements. From the modelling point of view, someone must consider the intersection nodes where longitudinal stiffeners coincide with transverse stiffeners (Figure 63). Due to the nature of beam elements, this connectivity issue does not occur in Beam-44 stiffened model. Additionally based on the same reason, when fixed end boundary conditions are applied to Beam-44 stiffened model, only the nodes on the edges of main flat plate are constrained.

In order to compare the modal responses of Beam-44 and Shell-63 stiffened plates with each other on an equivalent basis; herein three sub-models (all Shell-63 stiffened models) are created depending on the number of vertical element division. A fourth model (1:1)^{*} is also established and used particularly to match the boundary conditions in both Beam-44 and Shell-63 models.



In the following paragraphs Shell-63 stiffened models are called as (4:8), (4:7), (1:1) and (1:1)^{*} models, depending on their number of vertical element division.

When the preliminary modal analysis is applied on the models above, it is noticed that due to the low stiffness of Shell-63 stiffeners in comparison to Beam-44 stiffeners, there are no coupled vibration and flat plate deflected modes in the first 12 modes until higher modes are reached (e.g. for model (4:8), mode 87-72.172hz; for model (4:7), mode 111-70.682hz; for model (1:1), mode 59-68.141; for model (1:1)^{*}, mode

63-50.238, are the first modes where significant plate deflections can be seen). For this very reason around 200 modes are extracted in the analyses for each model, and it is not possible to present all these modes in this document. Here follows some of the mode shapes of the mentioned models:

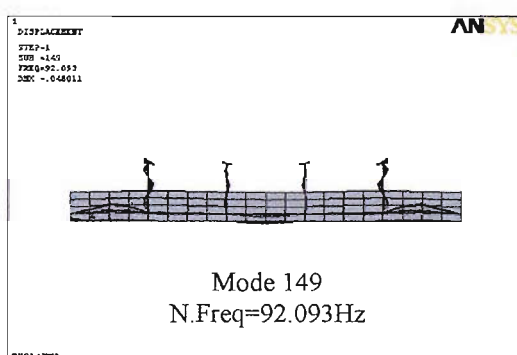
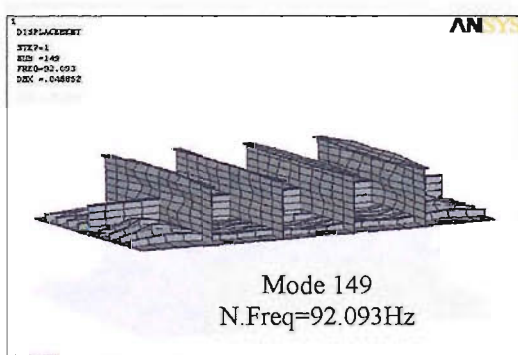
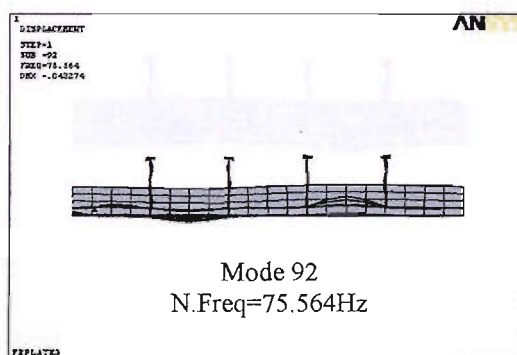
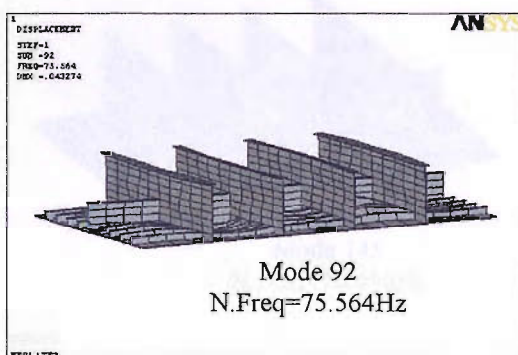
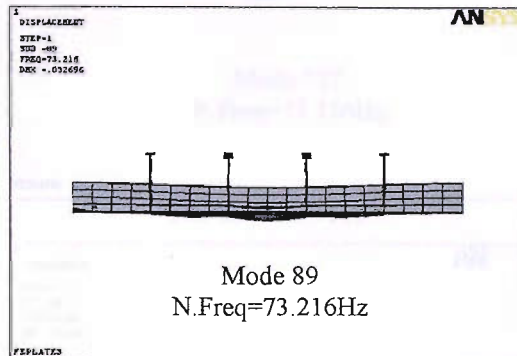
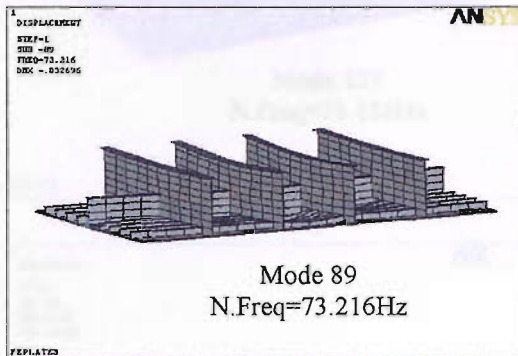


Figure 64 Some of the coupled vibration mode shapes and natural frequencies of model (4:8)

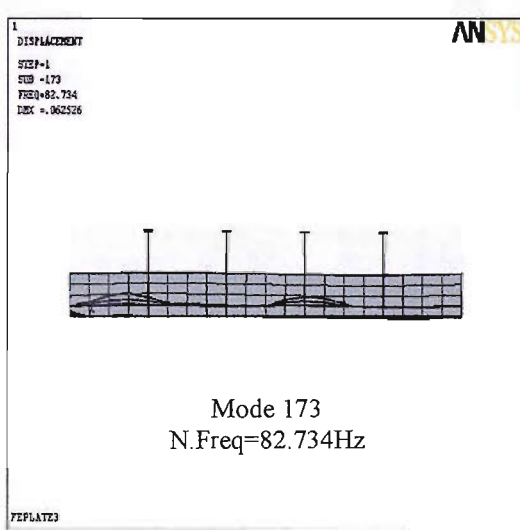
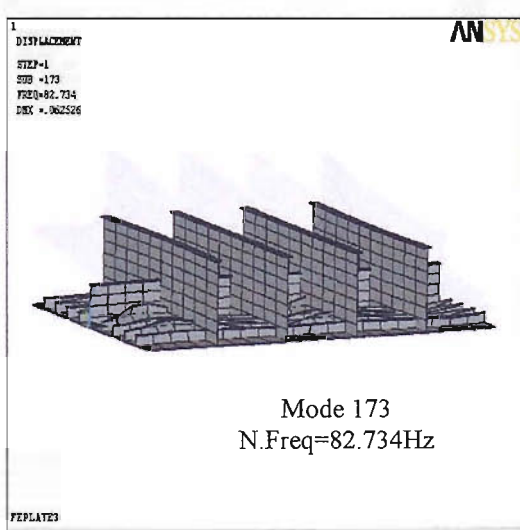
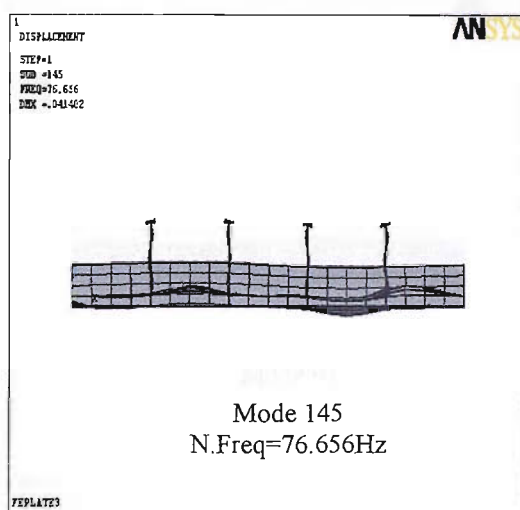
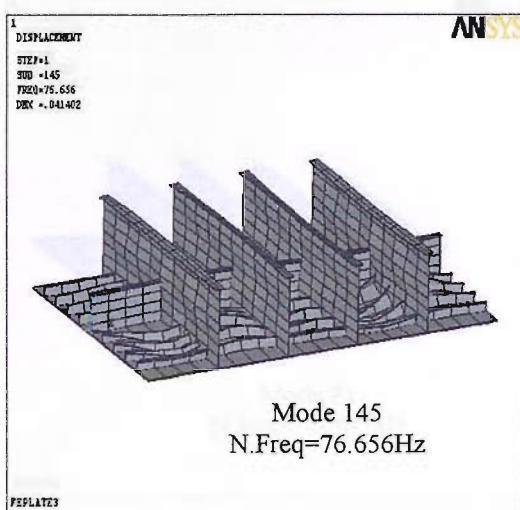
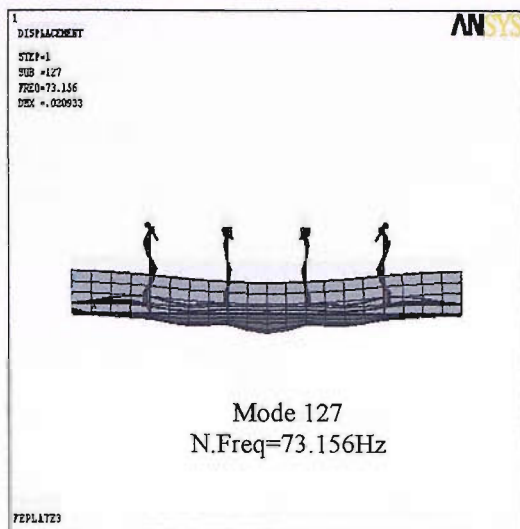
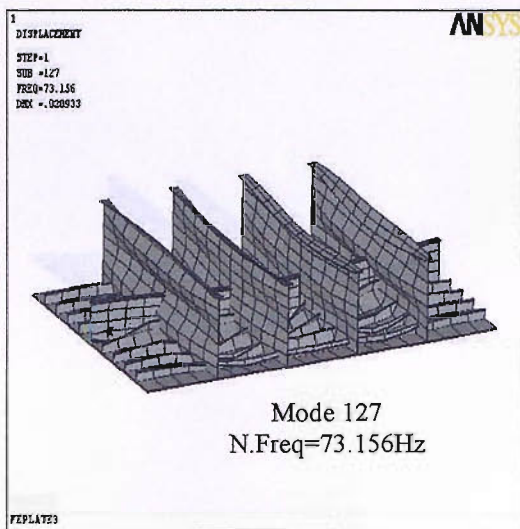


Figure 65 Some of the coupled vibration mode shapes and natural frequencies of model (4:7)

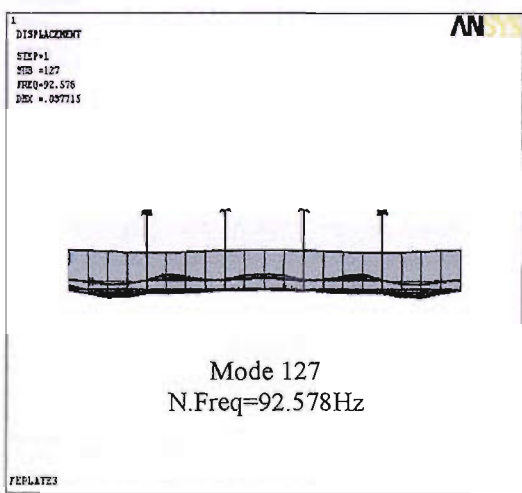
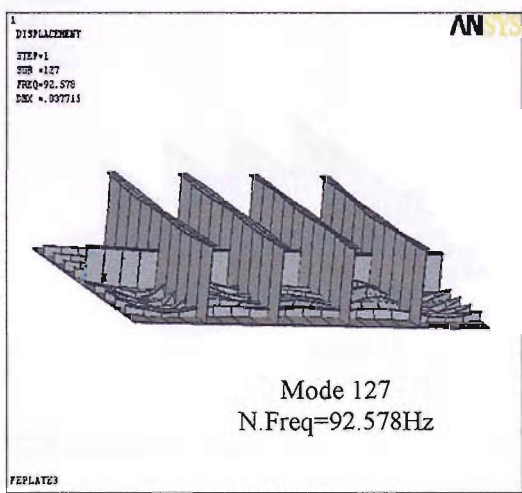
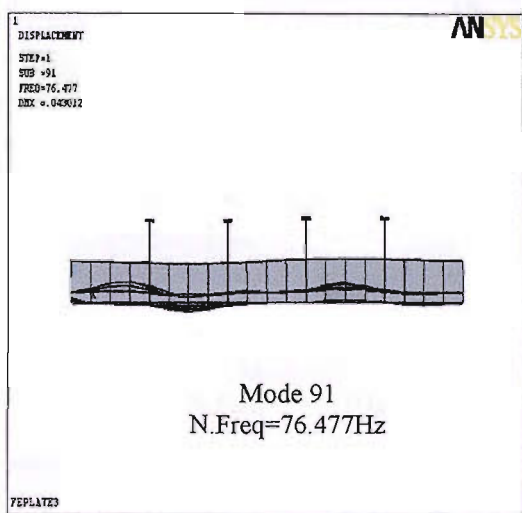
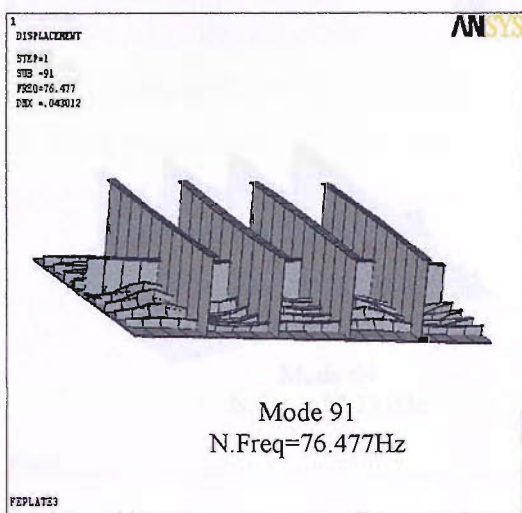
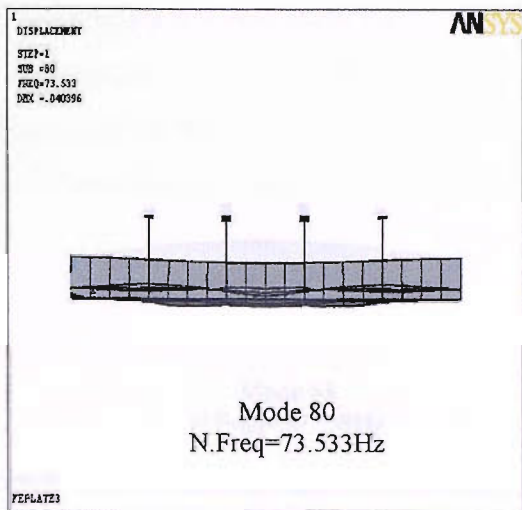
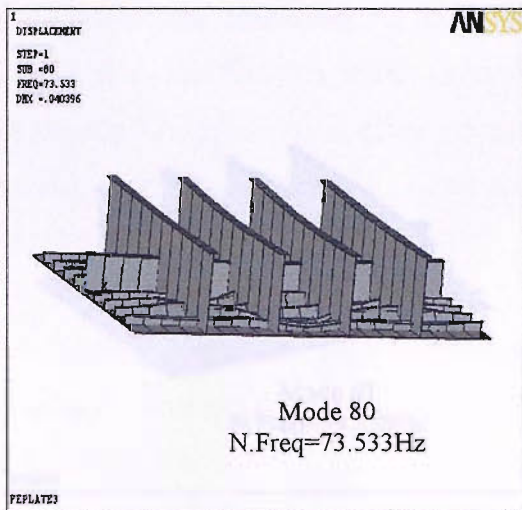


Figure 66 Some of the coupled vibration mode shapes and natural frequencies of model (1:1)

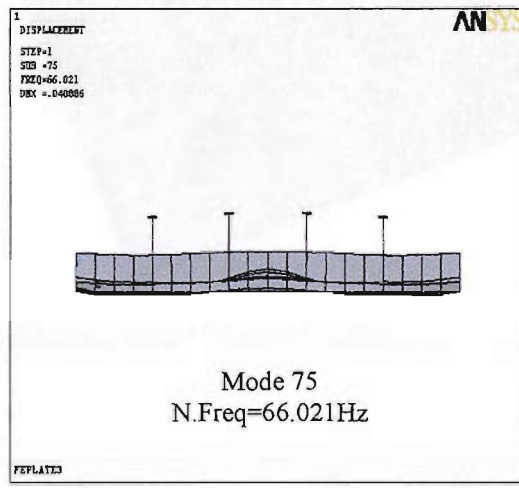
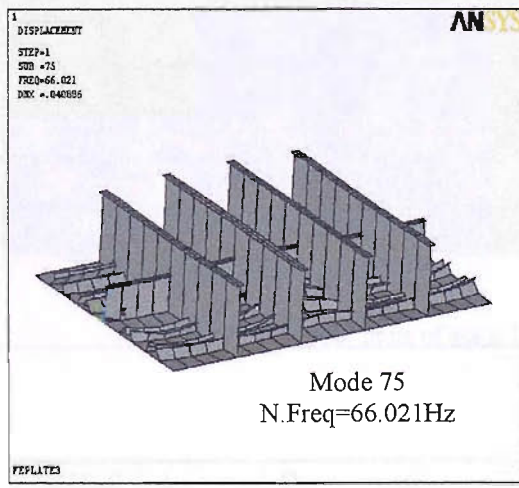
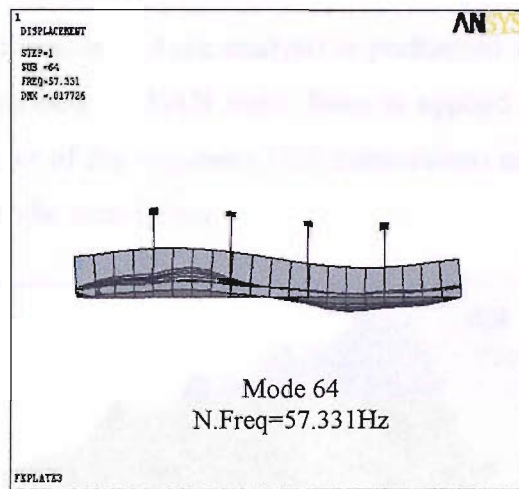
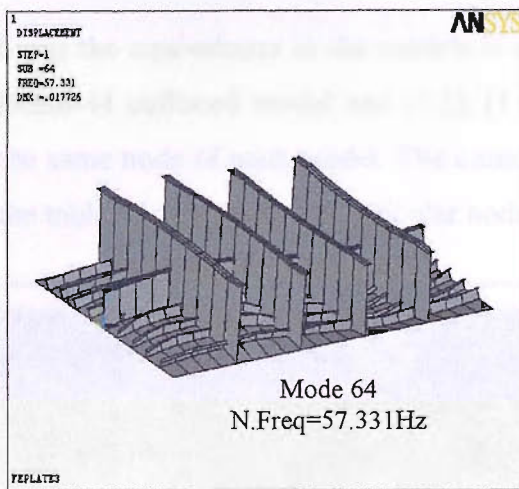
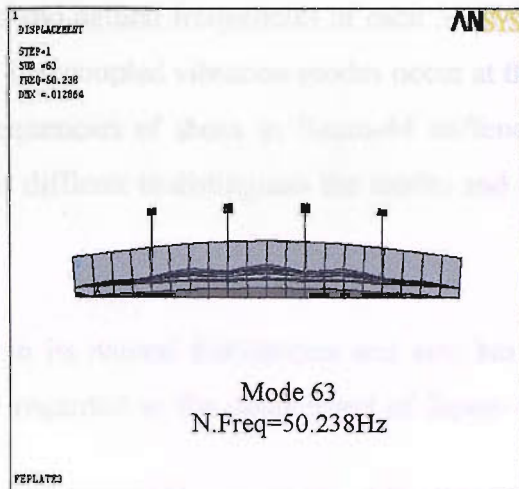
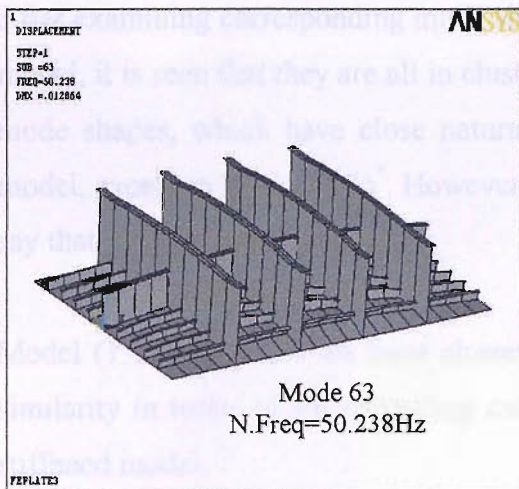


Figure 67 Some of the coupled vibration mode shapes and natural frequencies of model (1:1)*

After examining corresponding mode shapes and natural frequencies of each Shell-63 model, it is seen that they are all in clusters. The coupled vibration modes occur at the mode shapes, which have close natural frequencies of those in Beam-44 stiffened model, except in model (1:1)^{*}. However, it is difficult to distinguish the modes and to say that they have a similar trend.

Model (1:1) which has the least clustering in its natural frequencies and also has a similarity in terms of FE modelling can be regarded as the counterpart of Beam-44 stiffened model.

Since the equivalence in the models is questionable, a static analysis is performed on Beam-44 stiffened model and (1:1), (1:1)^{*} models. A 30kN static force is applied at the same node of each model. The contour plot of the responses (UZ translations) and the table of deflections at particular nodes can be seen below.

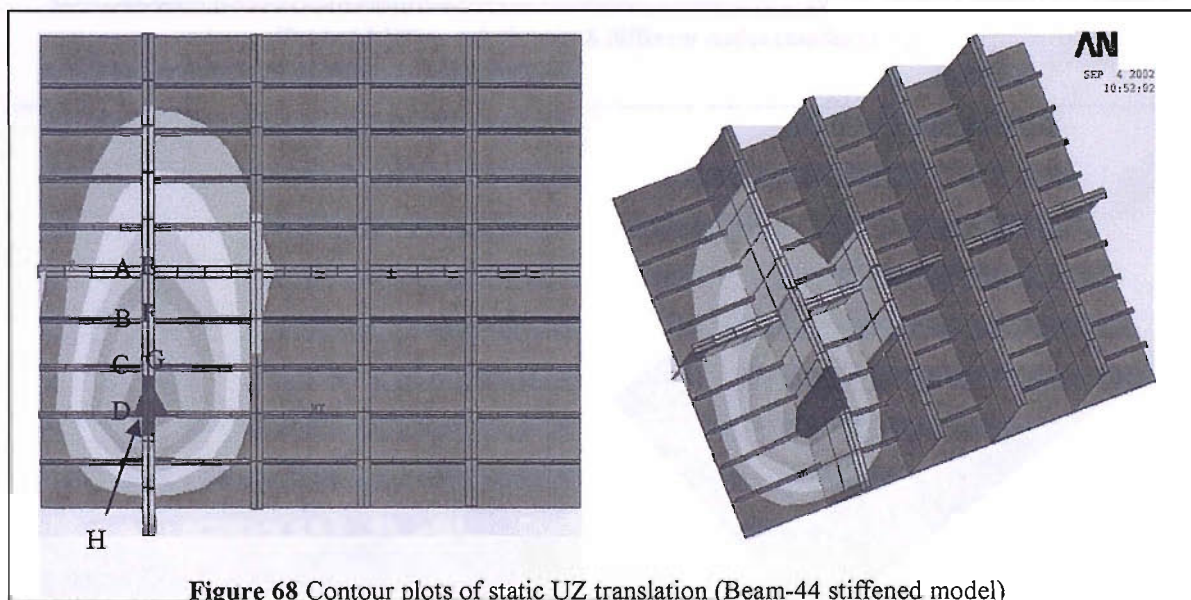


Figure 68 Contour plots of static UZ translation (Beam-44 stiffened model)

| NODE | A | B | C | D | E | F | G | H |
|--------------|----------|----------|----------|----------|----------|----------|----------|----------|
| UZ(m) | 0.77e-5 | 0.12e-5 | 0.15e-4 | 0.17e-4 | 0.10e-4 | 0.14e-4 | 0.19e-4 | 0.22e-4 |

Table 14 UZ-translations at 8 different nodes (Beam-44 stiffened model)

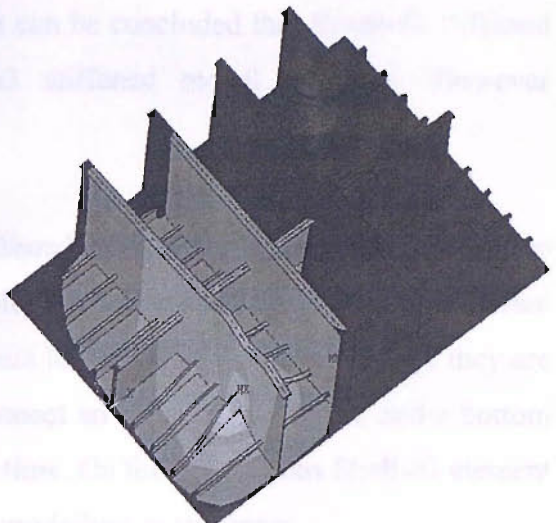
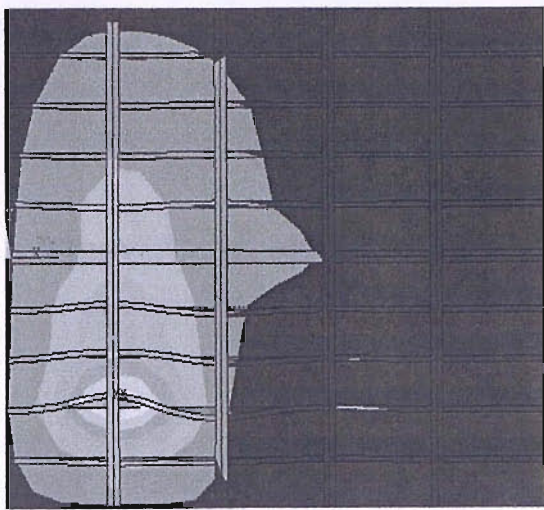


Figure 69 Contour plots of static UZ translation (model (1:1))

| NODE | A | B | C | D | E | F | G | H |
|-------|---------|---------|---------|---------|---------|---------|---------|---------|
| UZ(m) | 0.57e-5 | 0.11e-4 | 0.12e-4 | 0.25e-4 | 0.85e-5 | 0.15e-4 | 0.14e-4 | 0.33e-4 |

Table 15 UZ-translations at 8 different nodes (model (1:1))

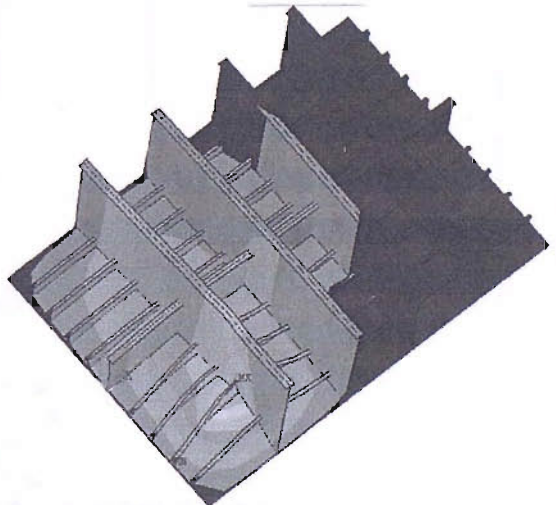
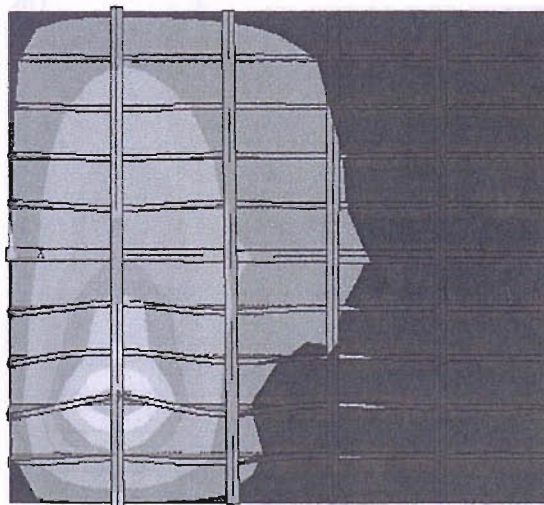


Figure 70 Contour plots of static UZ translation (model (1:1))

| NODE | A | B | C | D | E | F | G | H |
|-------|---------|---------|---------|---------|---------|---------|---------|---------|
| UZ(m) | 0.17e-4 | 0.27e-4 | 0.29e-4 | 0.44e-4 | 0.22e-4 | 0.31e-4 | 0.32e-4 | 0.50e-4 |

Table 16 UZ-translations at 8 different nodes (model (1:1))

When the UZ translations are statically examined, it can be seen that all three responses have similar nature. As a result it can be concluded that Beam-44 stiffened plate model behaves similar to Shell-63 stiffened model statically. However difficulties exist in the dynamic responses.

In terms of FE modelling and analyzing stiffened plates with alternative elements, one must also consider the case where a double bottom panel is to be analyzed. Beam elements representing stiffeners have a certain limitation in this matter. Since they are two node elements, it is not possible to connect an upper bottom plate and a bottom plate to the same beam element at the same time. On these occasions Shell-63 element is the only alternative to be used for the FE modelling of stiffeners.

A double bottom stiffened panel taken from a tanker (between bulkheads at station 110 and 130) is also modelled and modally analyzed. The details of the panel are given in Figure 71.

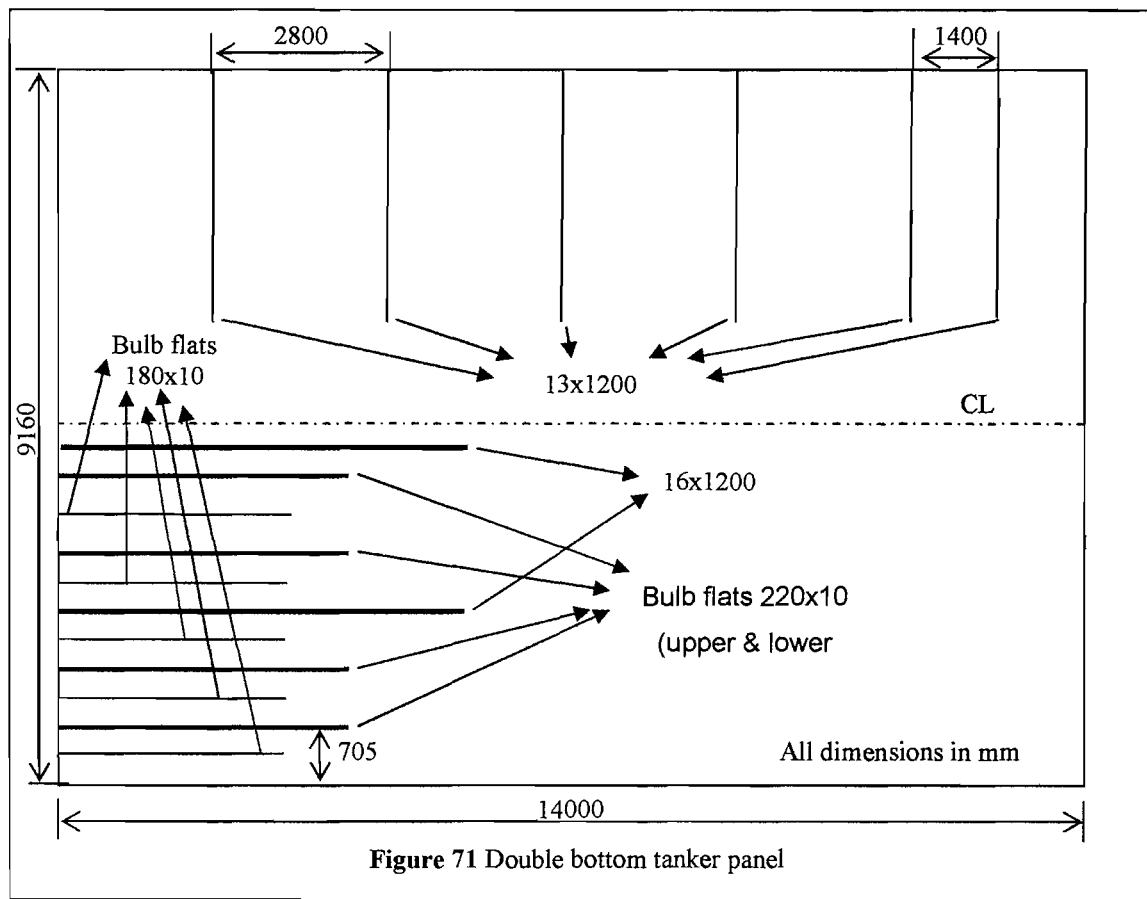


Figure 71 Double bottom tanker panel

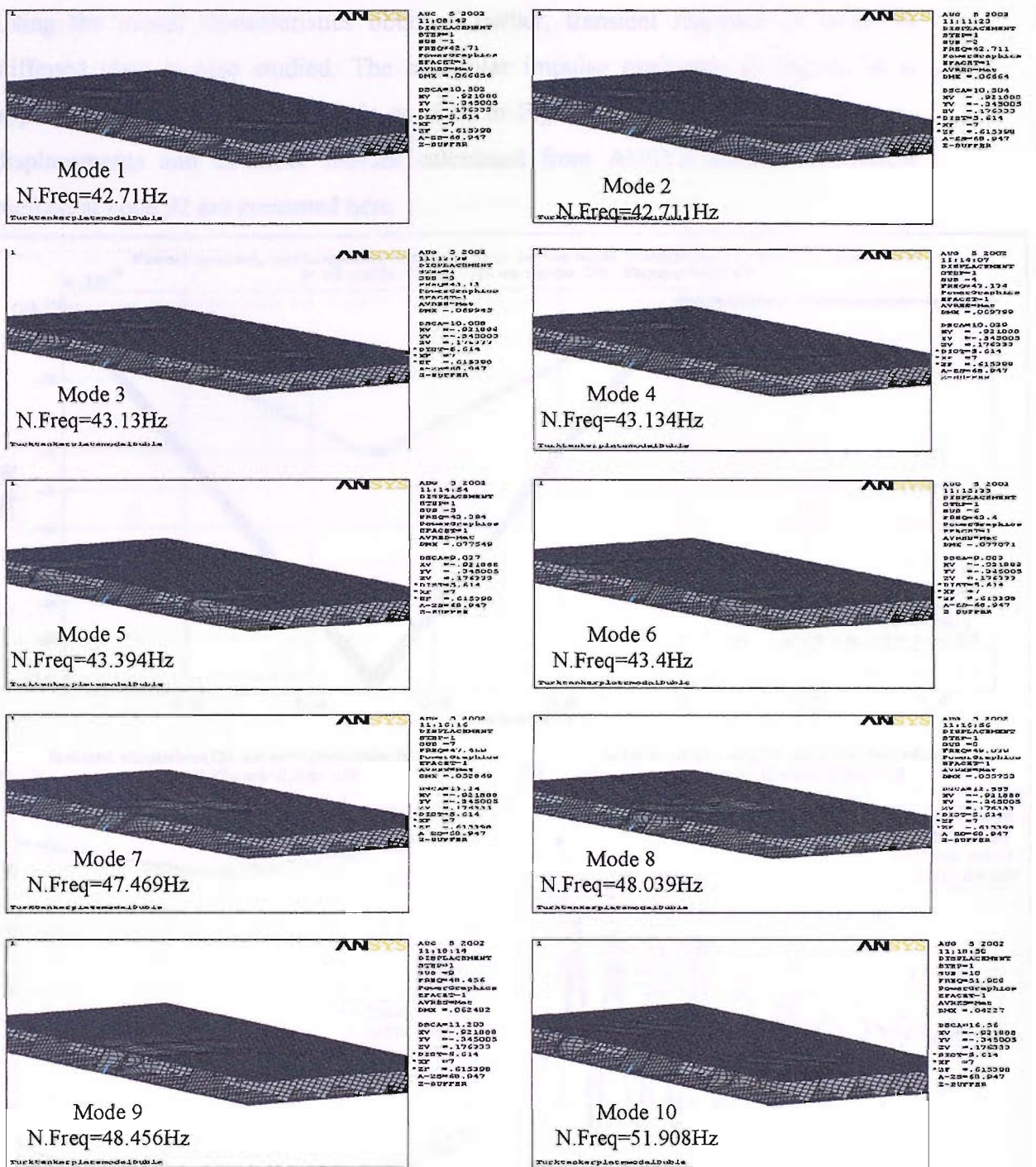


Figure 72 Mode characteristics of double bottom panel

After the modal responses of the double bottom panel are studied, it is seen that there are local deflections on the upper and lower plates due to the horizontal bending of the stiffeners. There are no global vibration modes. Basically the deflections on the stiffeners are dominant. Additionally the same model is constructed using the same elements as a single bottom plate. In this case no plate deflection is observed and all deflections occurred on the stiffeners. Expectedly natural frequencies significantly decreased.

Using the modal characteristics obtained earlier, transient response of Beam-44 stiffened plate is also studied. The triangular impulse excitation in Figure 34 is applied on its 198-numbered node as seen in Figure 61. Responses including uz-displacements and sx-direct stresses calculated from ANSYS and the numerical method at node 92 are presented here.

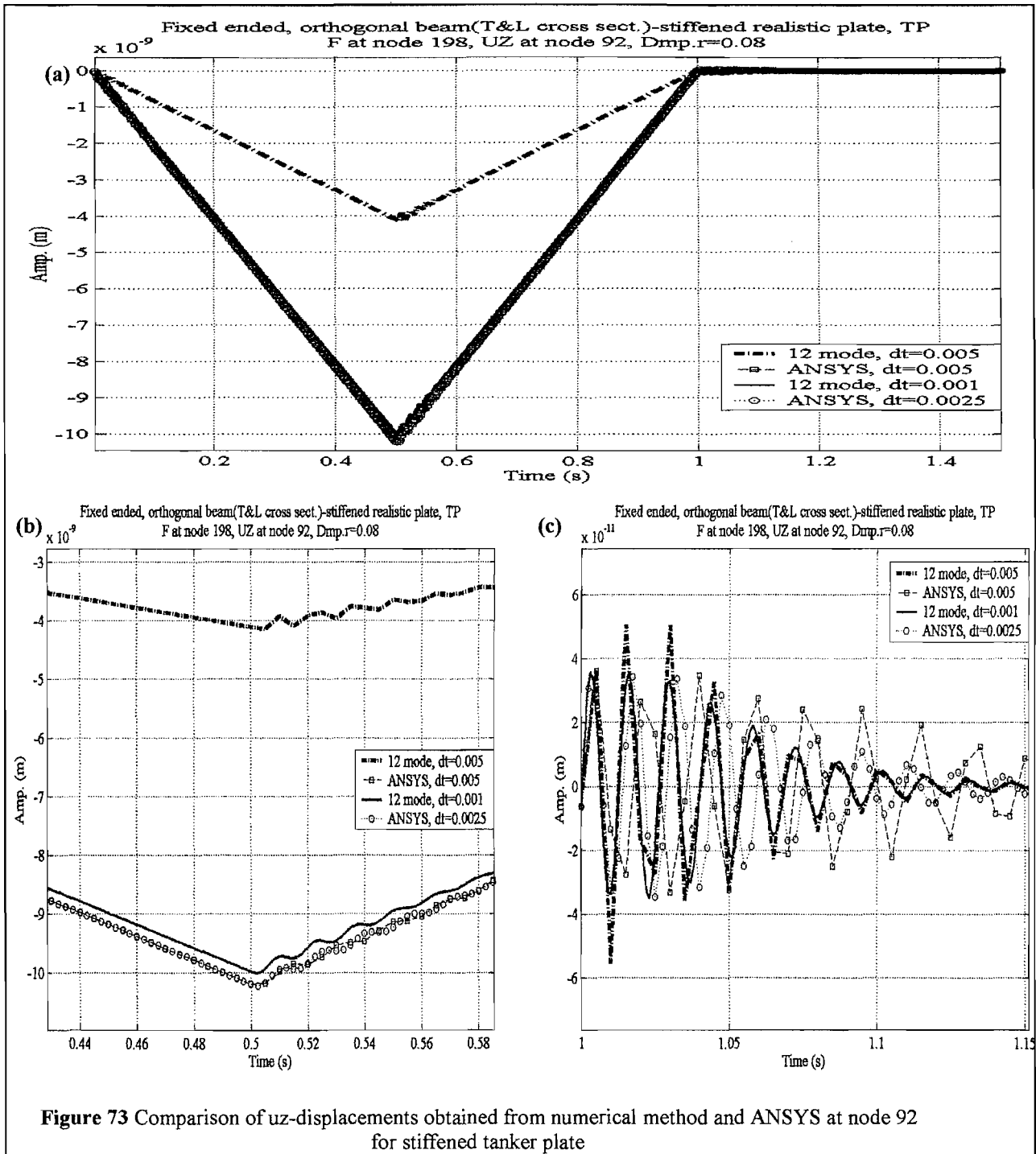


Figure 73 Comparison of uz-displacements obtained from numerical method and ANSYS at node 92 for stiffened tanker plate

Responses at nodes at 146 and 112 are given in the Appendix (Figure 123-Figure 125). Numerical calculations are done using 12-mode superposition. Initially discrete

time interval is taken as 0.005s. for both ANSYS and numerical method in the uz -displacement calculations. When the responses are plotted for both methods in Figure 73, it's seen that the differences are big. Since the natural frequencies of this stiffened plate are high, the discrete time intervals are required to be smaller than 0.005s. (Nyquist frequency effect). Hence smaller time intervals such as $dt=0.001$ s. in numerical method and $dt=0.0025$ s. in ANSYS are used additionally. Time interval $dt=0.001$ s. is not applied in ANSYS for the computational simplicity. New time intervals gave closer agreements than the previous time intervals and in the following sx-direct stress calculations, only latter intervals are used as seen in Figure 74.

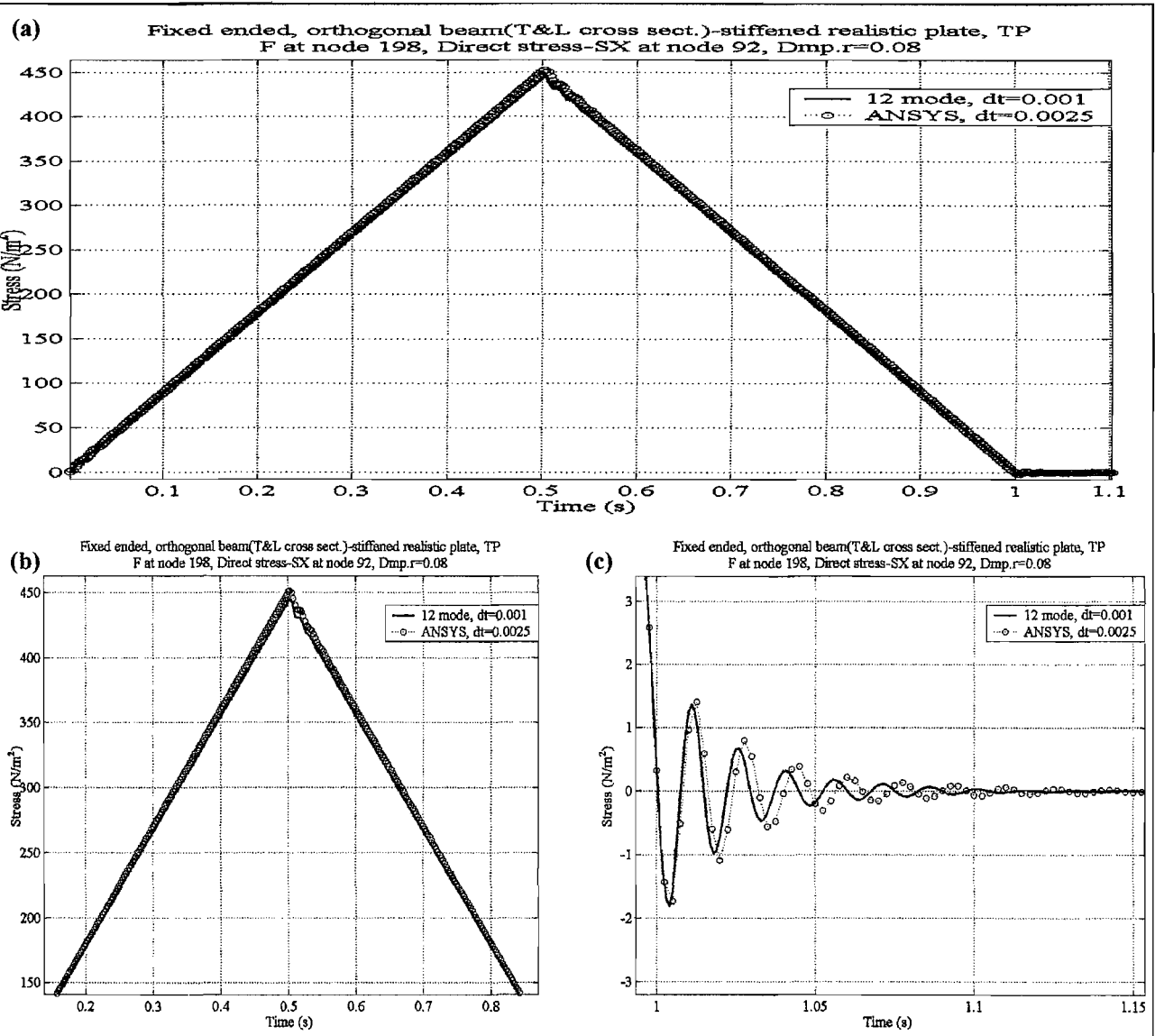


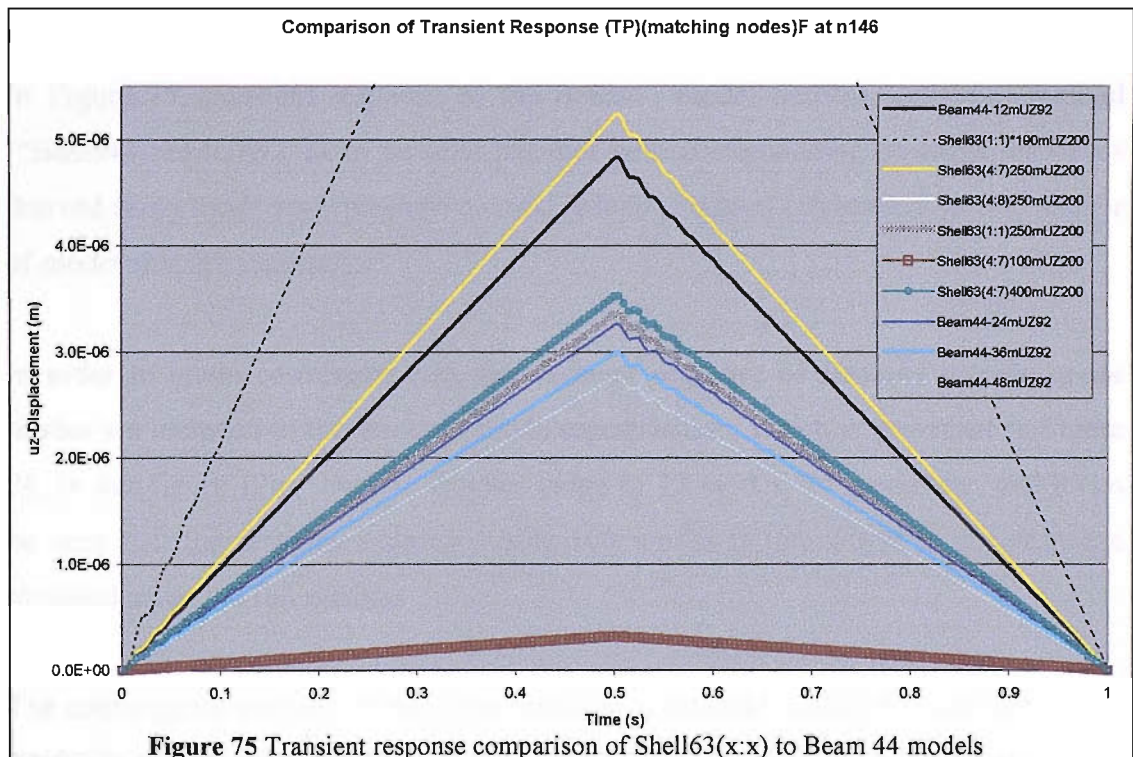
Figure 74 Comparison of sx-direct stresses obtained from numerical method and ANSYS at node 92 for stiffened tanker plate

The graphs in Figure 73 prove that 0.005s. time interval is not small enough to get the right deflections especially for the numeric method. At the same time it can be

clarified from the same figure that the transient mode superposition method that ANSYS uses is also dependent on the so-called time integration steps. Because significantly in the second phase of the response, there is a considerable amount of amplitude difference between two ANSYS responses obtained using $dt=0.005s$. and $dt=0.0025s$. which can also be seen in Figure 73c.

Subsequent stress results from ANSYS and numerical method are reasonably close when $dt=0.0025s$. and $dt=0.001s$. are used respectively. When two solution methods using these time intervals are compared between displacements and stresses, their agreement is parallel to each other. In other words using intervals $dt=0.001s$. and $dt=0.0025s$. for each corresponding method results in the same closeness for both displacement and stress calculations.

Additionally comparison of Shell63 (x:x)-shell stiffened- models to Beam44(i.e. Beam stiffened) models in transient response using mode superposition method is carried out at some corresponding nodes of each model (Figure 75).



The preliminary results showed that each Shell63 (x:x) model has a different response to transient excitation. It is difficult to determine the most suitable Shell63 (x:x) model to represent this particular tanker panel. On the other hand, when examining the Beam44 model and its response, it does not show an early convergence when

using the mode superposition method; however modelling dilemmas, like those occurring in Shell63 model, do not occur.

In order to assess whether the use of different mode extraction methods changes the modal deflections, Block Lanczos and Subspace mode extraction methods are also used in ANSYS. It is found that both methods give the same results. This also can be seen in Figure 76, where “Beam44-12mUZ92” legend represents the transient mode superposition response using Subspace mode extraction method (12 modes, UZ at node 92) and “Beam44-12mUZ92LM” legend represents the transient mode superposition response using Block Lanczos mode extraction method.

Full method, which uses the full system matrices to calculate the transient response (no matrix reduction), is used as an alternative FE transient response solution method to the mode superposition method in ANSYS. Due to its nature, full method does not require the mode shapes or number of modes to be superimposed to be specified in order to obtain the transient response.

In Figure 76, transient response of the Beam44 model derived using full method (“Beam44-FuMUZ92”) can be seen together with corresponding transient responses derived using mode superposition method, which is directly depended on the number of modes that are superposed.

In order to attain convergence in the transient response of Beam44 models, more modes are included in the transient mode superposition, which is presented in Figure 76. In this figure 12m, 24m etc denotes usage of 12 modes, 24 modes etc. and it can be seen that the response obtained using 100 modes is the closest to the response obtained using the full method.

The convergence analyses of transient response of Beam44 model obtained both using ANSYS and numerical method (Convolution) can also be seen in the following figures (Figure 77). For simplicity, constant damping ratio is used in the numerical method, which is equivalent to the stiffness damping ratio (B), used in ANSYS. In this figure the transient force is applied at the node 198 and the vertical displacements calculated at the point of application and three other nodes, shown in Figure 61.

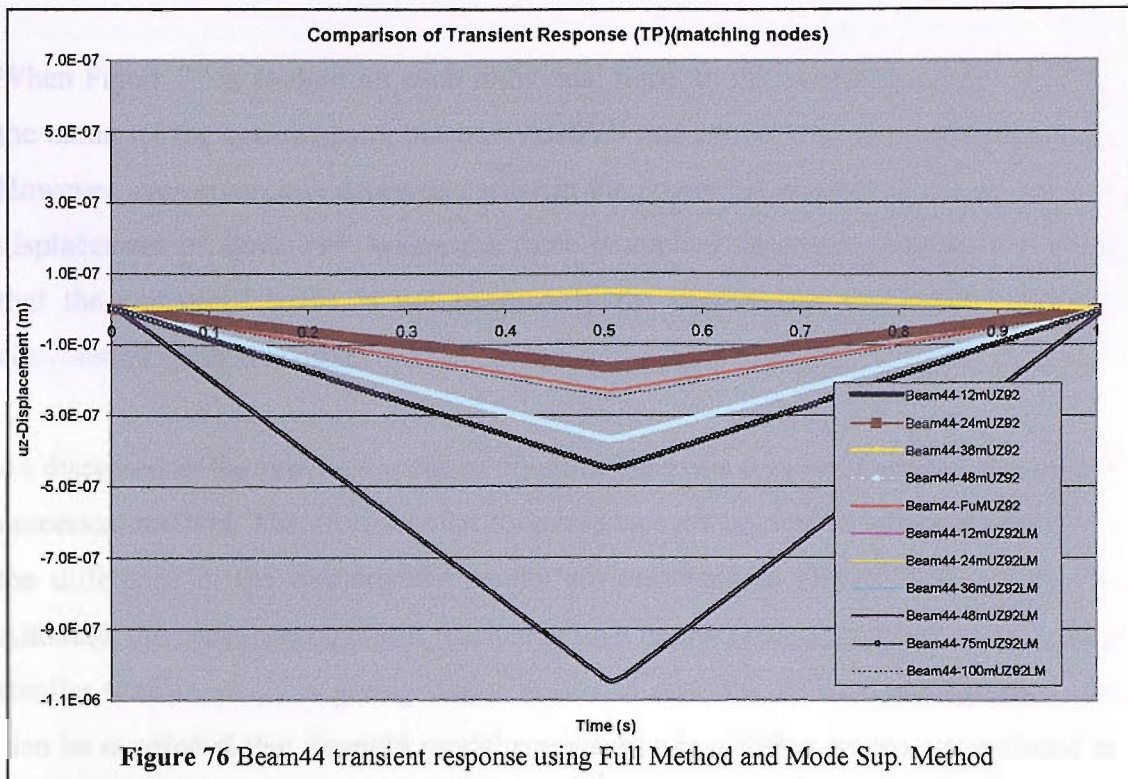


Figure 76 Beam44 transient response using Full Method and Mode Sup. Method

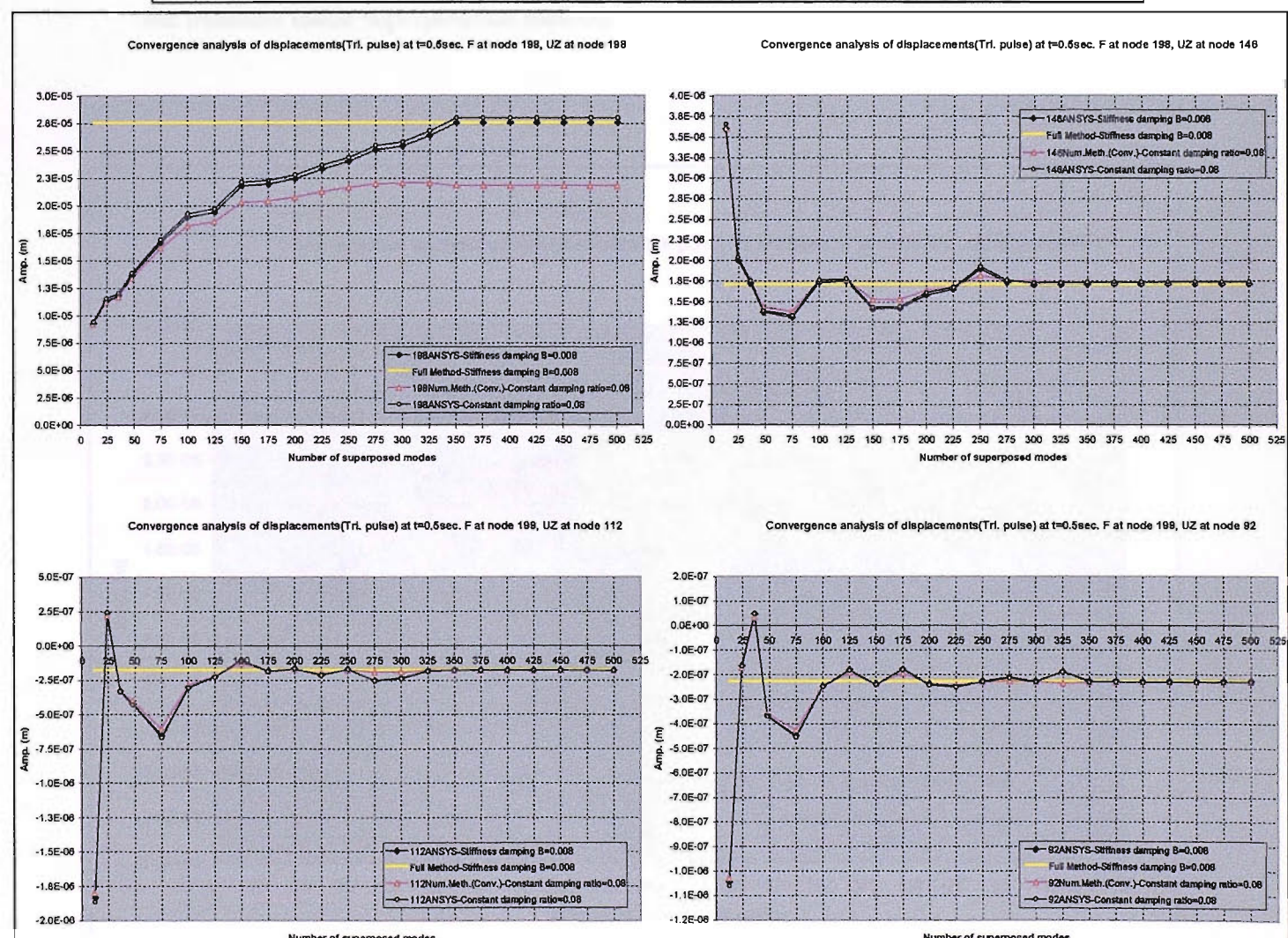


Figure 77 Convergence plots of displacements obtained by ANSYS & Numerical Method

When Figure 77 is studied for each individual node, in the overall it can be said that the nature of the convergence, between ANSYS and convolution methods, is similar. However, convergence is achieved earlier in the numerical method especially, for the displacement of, node 198, where the force is applied; however, it should be noted that the converged value is not necessarily the correct one when the numerical convolution method is used.

As discussed in the previous sections, the time intervals play an important role in the numerical method. Therefore smaller time intervals are applied to the same nodes and the difference in the convergence results are presented in Figure 78 & Figure 79. Although the convergence is still reached at high numbers of superposed modes, using smaller time intervals is giving closer results to ANSYS. From these figures it can also be concluded that Beam44 model converges when higher modes are included in the transient mode superposition method.

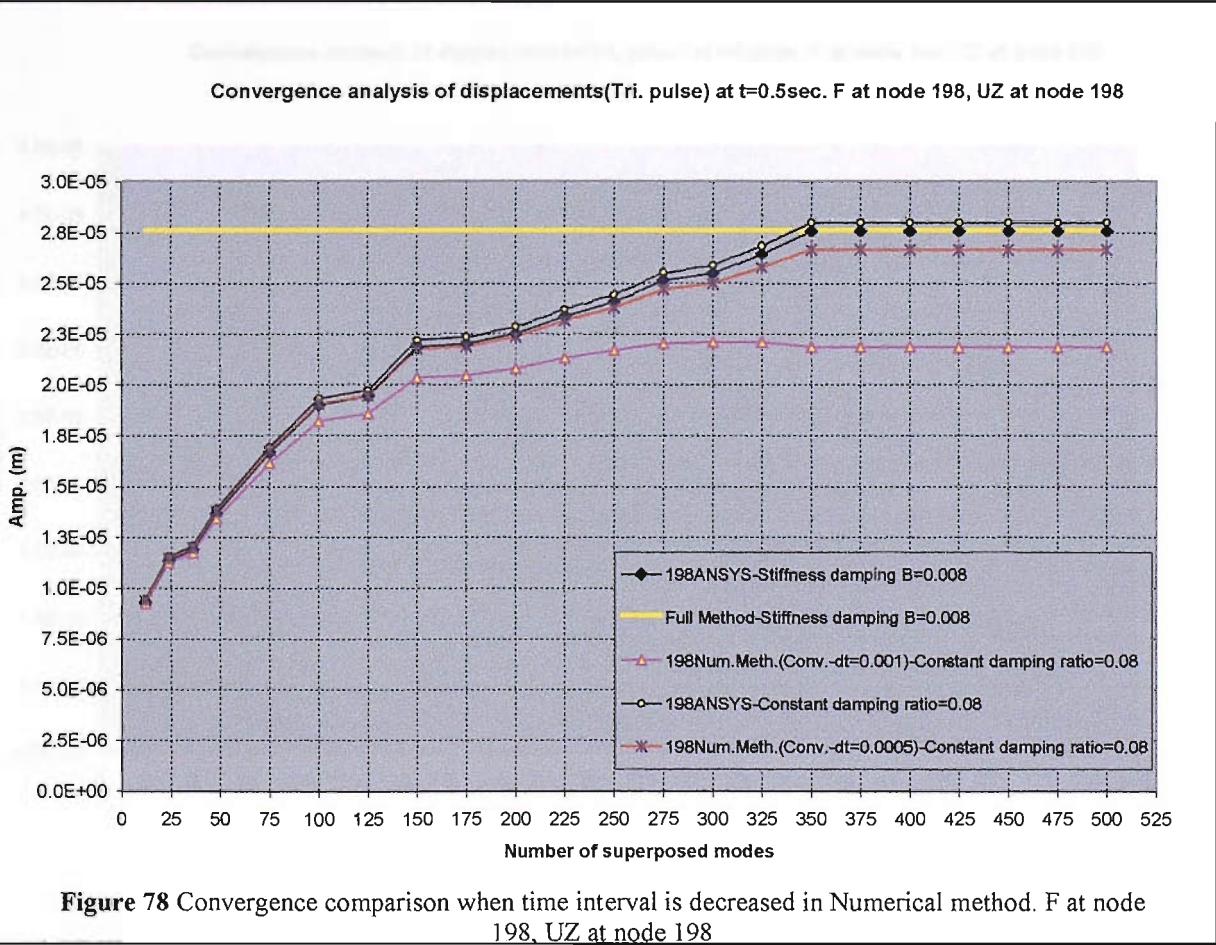
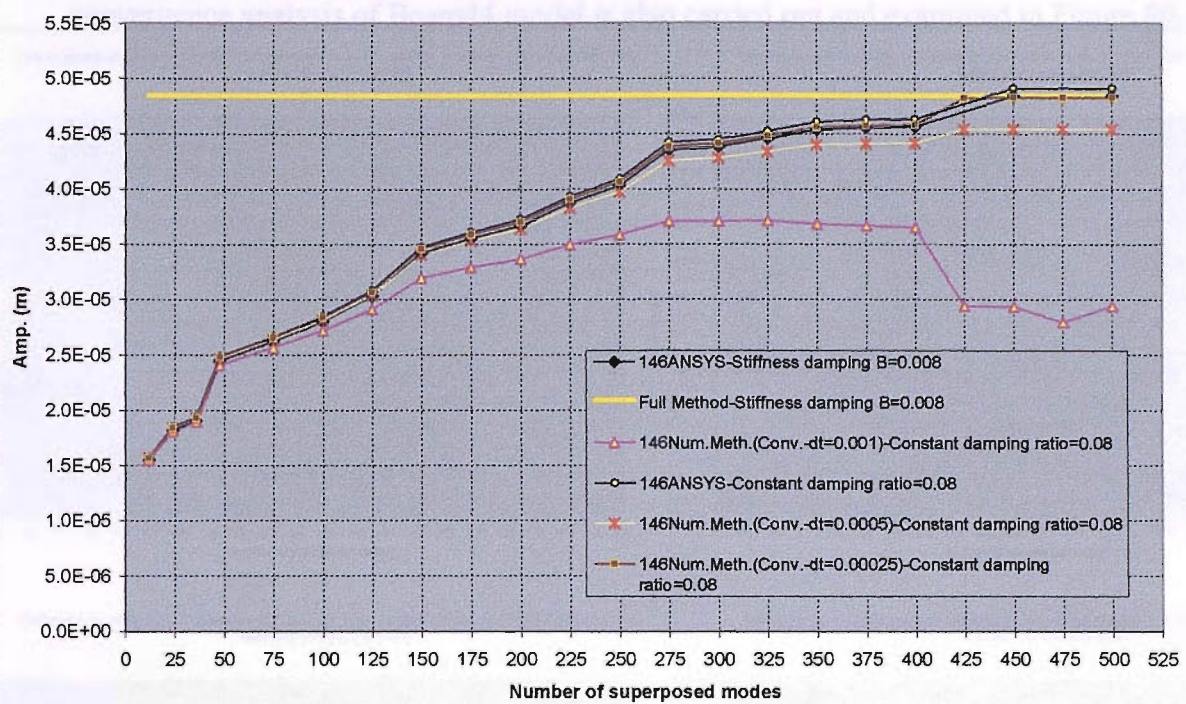


Figure 78 Convergence comparison when time interval is decreased in Numerical method. F at node 198, UZ at node 198

Convergence analysis of displacements(Tri. pulse) at t=0.5sec. F at node 146, UZ at node 146



Convergence analysis of displacements(Tri. pulse) at t=0.5sec. F at node 146, UZ at node 137

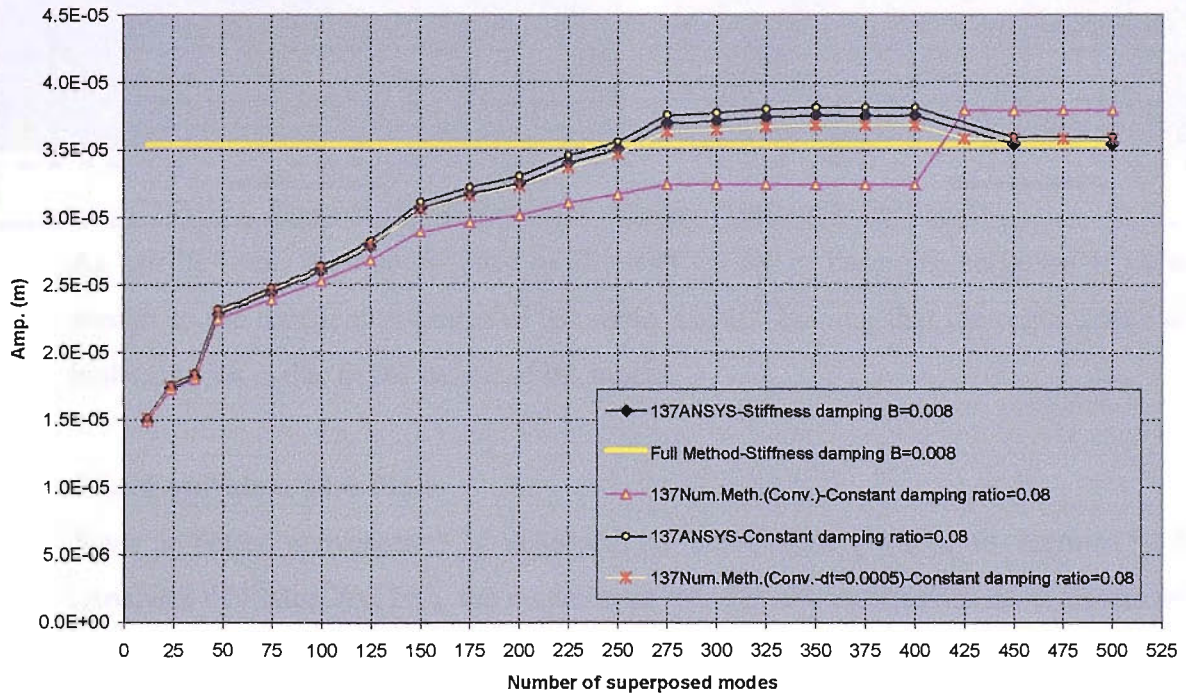


Figure 79 Convergence comparison when time interval is decreased in Numerical method. F at node 146, UZ at node 146 & 137

To verify whether the Beam44 model would respond to harmonic excitation with a better rate of convergence than the transient excitation, harmonic response convergence analysis of Beam44 model is also carried out and examined in Figure 80.

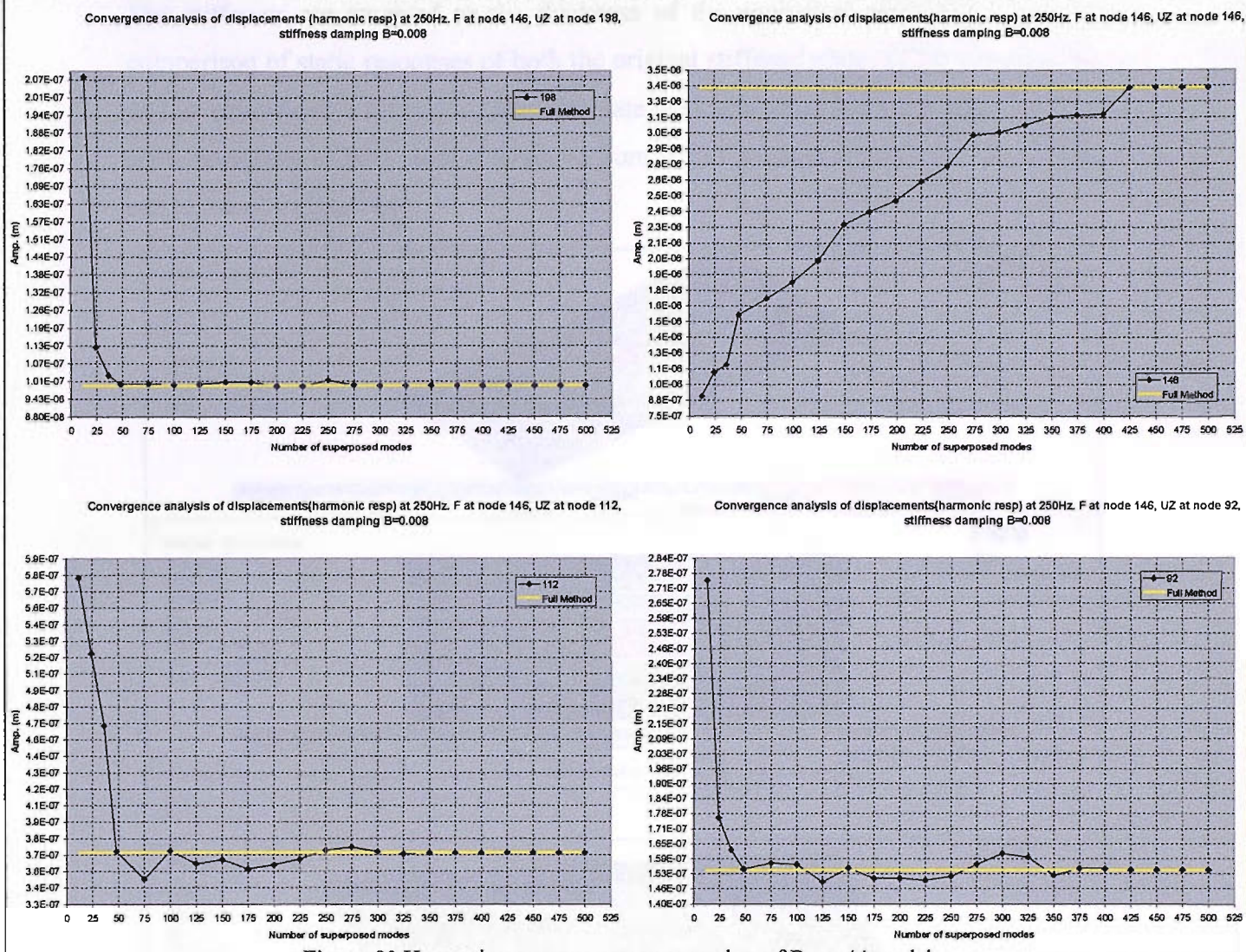


Figure 80 Harmonic response convergence plots of Beam44 model

As can be seen, the convergence of Beam44 model in harmonic response is quite similar to the transient response of the same model, showing that the requirement of higher modes is due to the nature of the model.

5.3.6 Equivalent Flat Plate

Since a better convergence is achieved on the stiffened plates in section 5.3.4 (Analysis of Plates, 6x12m), the question of whether the dimensions of stiffeners on realistic plate or their modelling is causing the difficulty in convergence, has arisen. Therefore for further investigations on the equivalent plate concept the clamped

horizontally beam stiffened plate model in section 5.3.4 is taken and an equivalent flat plate representing the corresponding stiffened plate is modelled.

The stiffeners are smeared to the thickness of the equivalent plate and using the comparison of static responses of both the original stiffened plate (FEHbeamstifplate) and its equivalent, a new equivalent flat plate thickness of $0.04013m$ is obtained. The static responses of both models obtained from ANSYS (force is applied at the centre) can be seen in Figure 81:

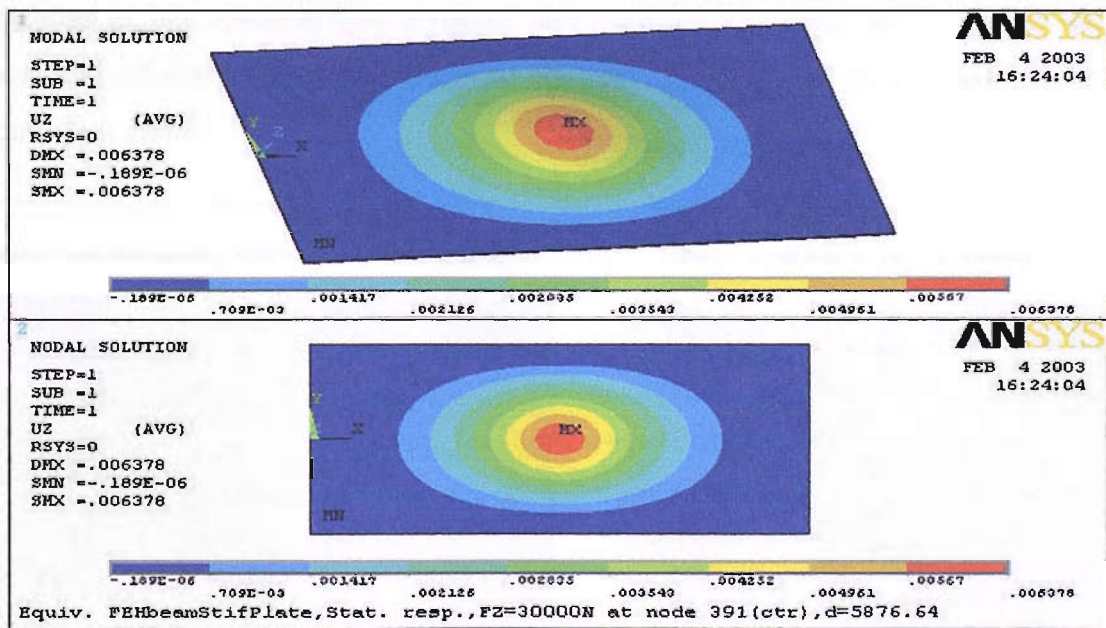
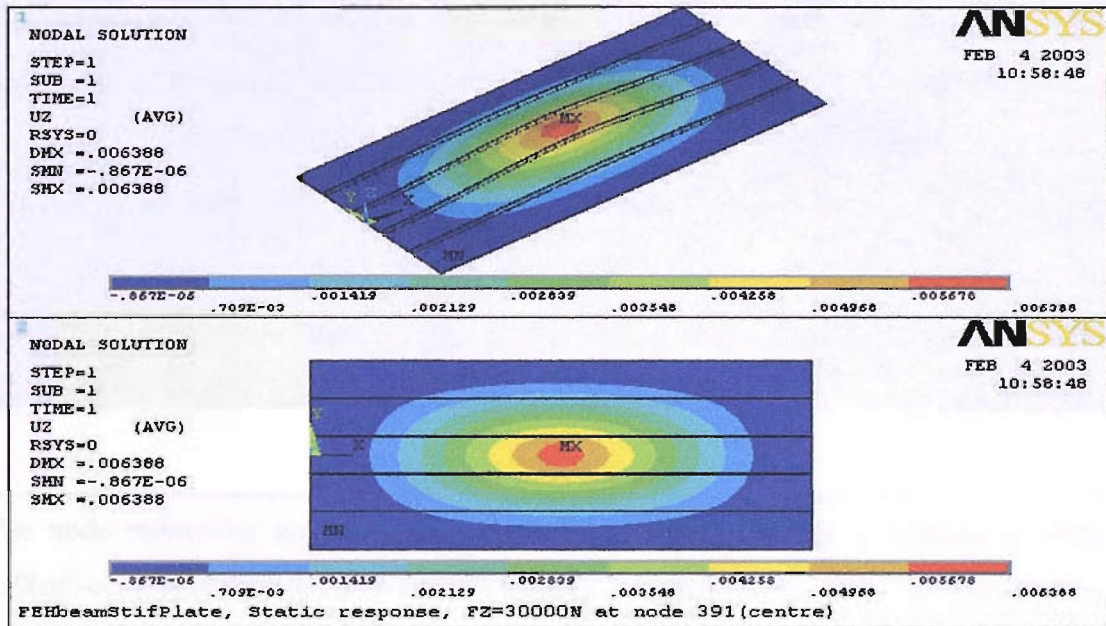


Figure 81 Static response results obtained both for original (first 2 graphs) and equivalent (last 2 graphs) plate from ANSYS

When both static responses are compared the contour plots have very similar nature and maximum deflections, which are in the centre of the plates, have the same value of 0.00637m.

| 62 | 101 | 100 | 99 | 98 | 97 | 96 | 95 | 94 | 93 | 92 | 91 | 90 | 89 | 88 | 87 | 86 | 85 | 84 | 83 | 82 | 81 | 80 | 79 | 78 | 77 | 76 | 75 | 74 | 73 | 72 | 71 | 70 | 69 | 68 | 67 | 66 | 65 | 64 | 63 | 42 |
|-----|-----|-----|-----|-----|-----|-----|-----|-----|-----|-----|-----|-----|-----|-----|-----|-----|-----|-----|-----|-----|-----|-----|-----|-----|-----|-----|-----|-----|-----|-----|-----|-----|-----|-----|-----|-----|-----|-----|-----|----|
| 120 | 148 | 176 | 204 | 232 | 260 | 288 | 316 | 344 | 372 | 400 | 428 | 456 | 484 | 512 | 540 | 568 | 596 | 624 | 652 | 681 | | | | | | | | | | | | | | | | | | | | |
| 119 | 129 | 147 | 157 | 175 | 185 | 203 | 213 | 231 | 241 | 259 | 269 | 287 | 297 | 315 | 325 | 343 | 353 | 371 | 381 | 399 | 409 | 427 | 437 | 455 | 465 | 483 | 493 | 511 | 521 | 539 | 549 | 567 | 577 | 595 | 605 | 623 | 633 | 651 | 661 | 50 |
| 118 | 146 | 174 | 202 | 230 | 258 | 286 | 314 | 342 | 370 | 398 | 426 | 454 | 482 | 510 | 538 | 566 | 594 | 622 | 650 | 679 | | | | | | | | | | | | | | | | | | | | 59 |
| 117 | 128 | 145 | 156 | 173 | 184 | 201 | 212 | 229 | 240 | 257 | 268 | 285 | 296 | 313 | 324 | 341 | 352 | 369 | 380 | 397 | 408 | 425 | 436 | 453 | 464 | 481 | 492 | 509 | 520 | 537 | 548 | 565 | 576 | 593 | 604 | 621 | 632 | 649 | 660 | 58 |
| 116 | 144 | 172 | 200 | 228 | 256 | 284 | 312 | 340 | 368 | 396 | 424 | 452 | 480 | 508 | 536 | 564 | 592 | 620 | 648 | 677 | | | | | | | | | | | | | | | | | | | | 57 |
| 115 | 127 | 143 | 155 | 171 | 183 | 199 | 211 | 227 | 239 | 255 | 267 | 283 | 295 | 311 | 323 | 339 | 351 | 367 | 379 | 395 | 407 | 423 | 435 | 451 | 463 | 479 | 491 | 507 | 519 | 535 | 547 | 563 | 575 | 591 | 603 | 619 | 631 | 647 | 659 | 56 |
| 114 | 142 | 170 | 198 | 226 | 254 | 282 | 310 | 338 | 366 | 394 | 422 | 450 | 478 | 506 | 534 | 562 | 590 | 618 | 646 | 675 | | | | | | | | | | | | | | | | | | | | 55 |
| 113 | 126 | 141 | 154 | 169 | 182 | 197 | 210 | 225 | 238 | 253 | 266 | 281 | 294 | 309 | 322 | 337 | 350 | 365 | 378 | 393 | 406 | 421 | 434 | 449 | 462 | 477 | 490 | 505 | 518 | 533 | 546 | 561 | 574 | 589 | 602 | 617 | 630 | 645 | 658 | 54 |
| 112 | 140 | 168 | 196 | 224 | 252 | 280 | 308 | 336 | 364 | 392 | 420 | 448 | 476 | 504 | 532 | 560 | 588 | 616 | 644 | 673 | | | | | | | | | | | | | | | | | | | | 53 |
| 111 | 125 | 139 | 153 | 167 | 181 | 195 | 209 | 223 | 237 | 251 | 265 | 279 | 293 | 307 | 321 | 335 | 349 | 363 | 377 | 391 | 405 | 419 | 433 | 447 | 461 | 475 | 489 | 503 | 517 | 531 | 545 | 559 | 573 | 587 | 601 | 615 | 629 | 643 | 657 | 52 |
| 110 | 138 | 166 | 194 | 222 | 250 | 278 | 306 | 334 | 362 | 390 | 418 | 446 | 474 | 502 | 530 | 558 | 586 | 614 | 642 | 669 | | | | | | | | | | | | | | | | | | | | 51 |
| 109 | 124 | 137 | 152 | 165 | 180 | 193 | 208 | 221 | 236 | 249 | 264 | 277 | 292 | 305 | 320 | 333 | 348 | 361 | 376 | 389 | 404 | 417 | 432 | 445 | 460 | 473 | 488 | 501 | 516 | 529 | 544 | 557 | 572 | 585 | 600 | 613 | 628 | 641 | 656 | 50 |
| 108 | 136 | 164 | 192 | 220 | 248 | 276 | 304 | 332 | 360 | 388 | 416 | 444 | 472 | 500 | 528 | 556 | 584 | 612 | 640 | 668 | | | | | | | | | | | | | | | | | | | | 49 |
| 107 | 123 | 135 | 151 | 163 | 179 | 191 | 207 | 219 | 235 | 247 | 263 | 275 | 291 | 303 | 319 | 331 | 347 | 359 | 375 | 387 | 403 | 415 | 431 | 443 | 459 | 471 | 487 | 499 | 515 | 527 | 543 | 555 | 571 | 583 | 599 | 611 | 627 | 639 | 655 | 48 |
| 106 | 134 | 162 | 190 | 218 | 246 | 274 | 302 | 330 | 358 | 386 | 414 | 442 | 470 | 498 | 526 | 554 | 582 | 610 | 638 | 666 | | | | | | | | | | | | | | | | | | | | 47 |
| 105 | 122 | 133 | 150 | 161 | 178 | 189 | 206 | 217 | 234 | 245 | 262 | 273 | 290 | 301 | 318 | 329 | 346 | 357 | 374 | 385 | 402 | 413 | 430 | 441 | 458 | 469 | 486 | 497 | 514 | 525 | 542 | 553 | 570 | 581 | 598 | 609 | 626 | 637 | 654 | 46 |
| 104 | 132 | 160 | 188 | 216 | 244 | 272 | 300 | 328 | 356 | 384 | 412 | 440 | 468 | 496 | 524 | 552 | 580 | 608 | 636 | 664 | | | | | | | | | | | | | | | | | | | | 45 |
| 103 | 121 | 131 | 149 | 159 | 177 | 187 | 205 | 215 | 233 | 243 | 261 | 271 | 289 | 299 | 317 | 327 | 345 | 355 | 373 | 383 | 401 | 411 | 429 | 439 | 457 | 467 | 485 | 495 | 513 | 523 | 541 | 551 | 569 | 579 | 597 | 607 | 625 | 635 | 653 | 44 |
| 102 | 130 | 158 | 186 | 214 | 242 | 270 | 298 | 326 | 354 | 382 | 410 | 438 | 466 | 494 | 522 | 550 | 578 | 606 | 634 | 662 | | | | | | | | | | | | | | | | | | | | 43 |
| 1 | 3 | 4 | 5 | 6 | 7 | 8 | 9 | 10 | 11 | 12 | 13 | 14 | 15 | 16 | 17 | 18 | 19 | 20 | 21 | 22 | 23 | 24 | 25 | 26 | 27 | 28 | 29 | 30 | 31 | 32 | 33 | 34 | 35 | 36 | 37 | 38 | 39 | 40 | 41 | 2 |

Figure 82 Node references

The node references are shown in Figure 82. When the force is applied at node 219(off-centre) and node 391(centre of plate), the static nodal response distribution for each node is shown in Figure 83. As can be seen, reasonably good agreement is achieved in the displacements obtained; nevertheless, off-centre application of the force and off-centre responses lead to larger differences between the original and the equivalent plates.

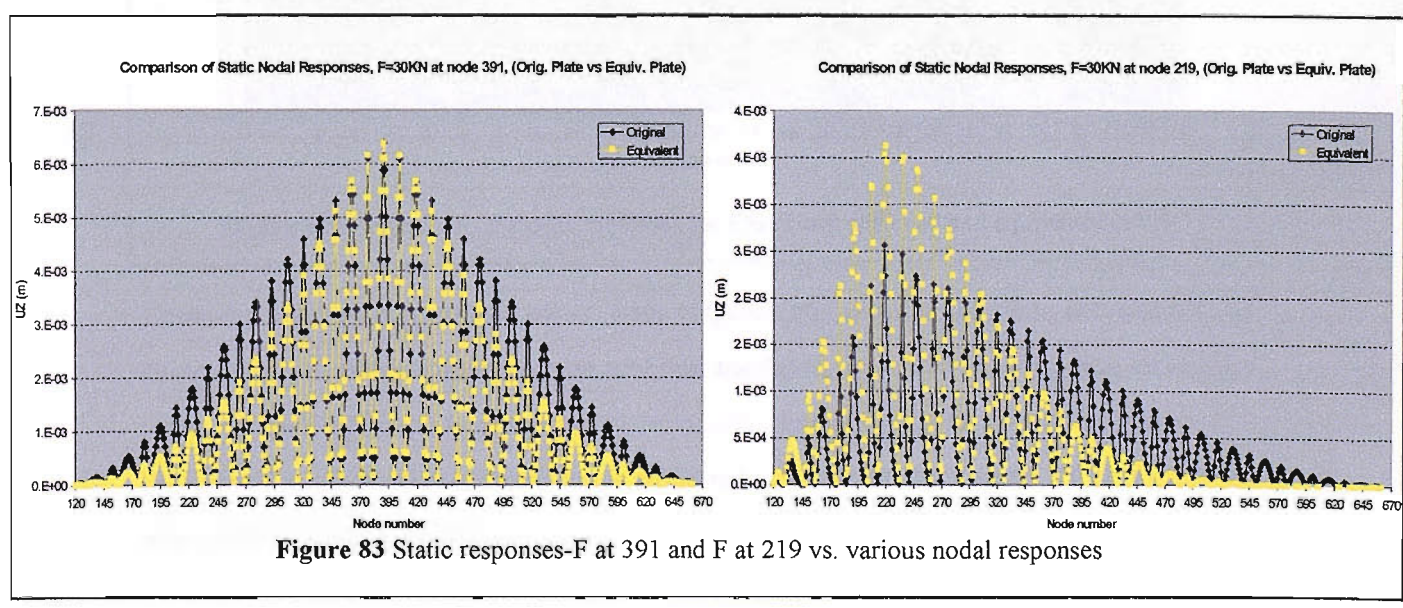


Figure 83 Static responses-F at 391 and F at 219 vs. various nodal responses

For the dynamic case the natural frequencies of the original and equivalent plate, shown in Table 17 and Figure 84, show a reasonably good agreement, especially for the lowest mode shapes. It has also been ascertained that the mode shapes of the equivalent plate are similar to those of the original one, shown in Table 13.

| Natural freq.(Hz) | Mode index | 1 | 2 | 3 | 4 | 5 | 6 | 7 | 8 | 9 | 10 | 11 | 12 |
|--------------------------------|------------------|------|------|------|------|------|------|------|------|------|------|------|------|
| | FEHBeamStifPlate | 7.4 | 14.4 | 15.8 | 21.1 | 25.9 | 28.7 | 31.3 | 33.0 | 41.0 | 41.9 | 44.9 | 45.7 |
| Equivalent FEHBeamStifPlate | 7.8 | 10.1 | 14.3 | 20.2 | 20.4 | 22.6 | 26.5 | 27.8 | 32.2 | 37.1 | 39.3 | 39.5 | |
| | | | | | | | | | | | | | |

| Natural freq.(Hz) | Mode index | 13 | 14 | 15 | 16 | 17 | 18 | 19 | 20 | 21 | 22 | 23 | 24 | 25 |
|--------------------------------|------------------|------|------|------|------|------|------|------|------|------|------|------|------|------|
| | FEHBeamStifPlate | 48.7 | 55.9 | 56.6 | 63.1 | 65.0 | 66.3 | 68.9 | 71.2 | 72.6 | 75.5 | 81.5 | 83.0 | 83.8 |
| Equivalent FEHBeamStifPlate | 41.6 | 45.5 | 48.1 | 48.7 | 51.0 | 58.4 | 59.6 | 60.8 | 64.7 | 67.1 | 67.6 | 71.0 | 72.3 | |
| | | | | | | | | | | | | | | |

Table 17 Natural frequencies

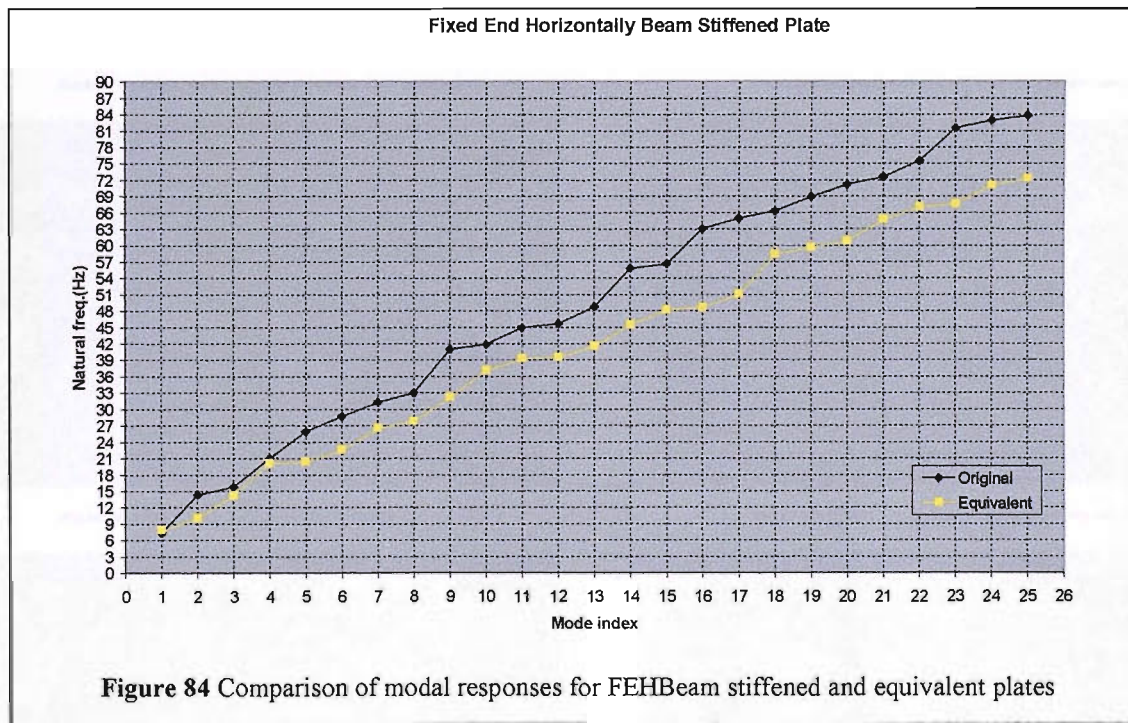


Figure 84 Comparison of modal responses for FEHBeam stiffened and equivalent plates

Transient response comparisons of both original and equivalent plate are carried out using transient mode superposition and full methods, in ANSYS. Applying triangular pulse on two different nodes, namely at centre (node 391) and off-centre (node 219), the transient displacement responses obtained are shown in Figure 85 & Figure 86 when using mode superposition analysis and Figure 126 & Figure 127(Appendix-B).

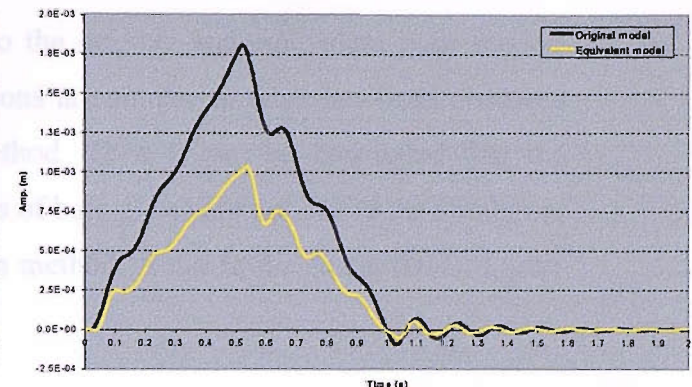
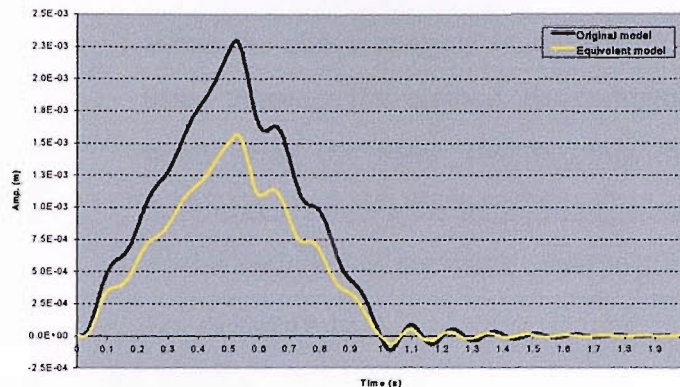
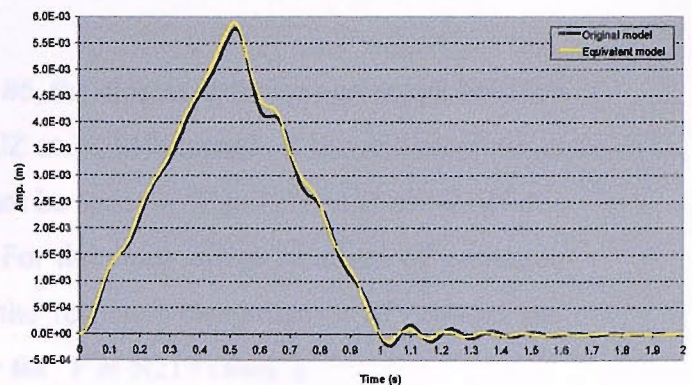
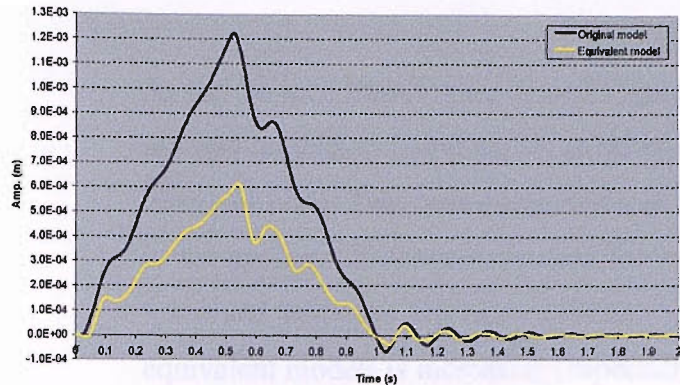


Figure 85 Original vs equivalent plate transient responses F at node 391, UZ at nodes 219,391,507,559

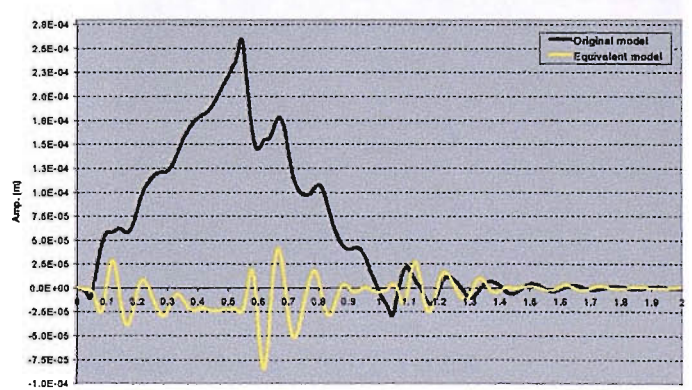
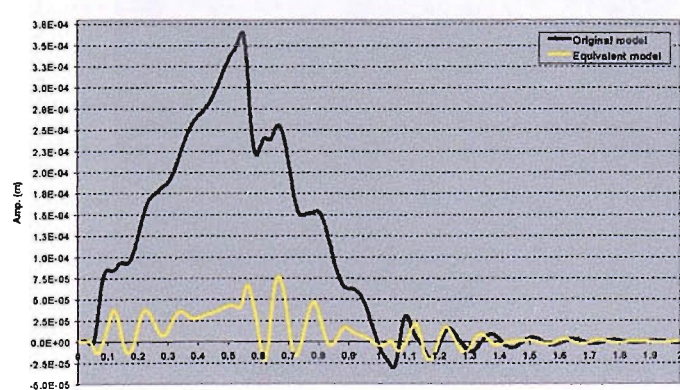
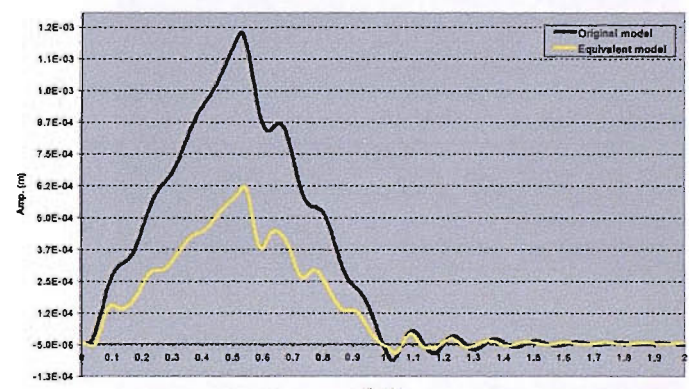
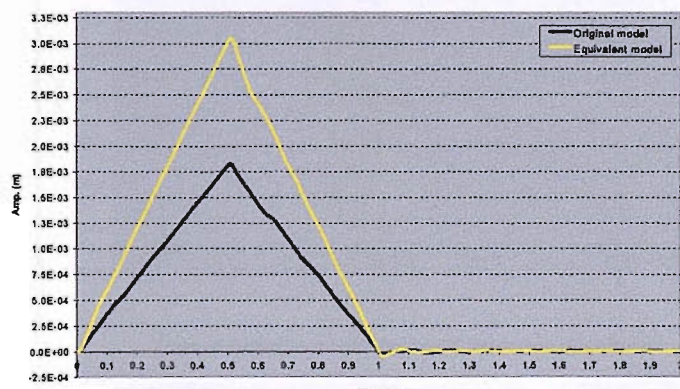


Figure 86 Original vs equivalent plate transient responses F at node 219, UZ at nodes 219,391,507,559

As can be seen from Figure 85 and Figure 86, the closest response agreement between the two models is found on “F at N391-UZ at N391”, namely force and response at centre of plate. The same agreement can not be seen on “F at N219-UZ at N219” due to the applied off-centre excitation force. For the cases where locations of excitation force and response are more off-centre, the response disagreement of original and equivalent models is increasing (especially for “F at N219 cases”).

When the above analysis is applied on to the original and equivalent plate models using transient full method, the comparisons are similar to what has been observed when using the mode superposition method. Thus it can be concluded that the differences between the transient responses of both plates are not due to the number of modes included in the mode superposition method (Refer to the Appendix-B, Figure 126 & Figure 127).

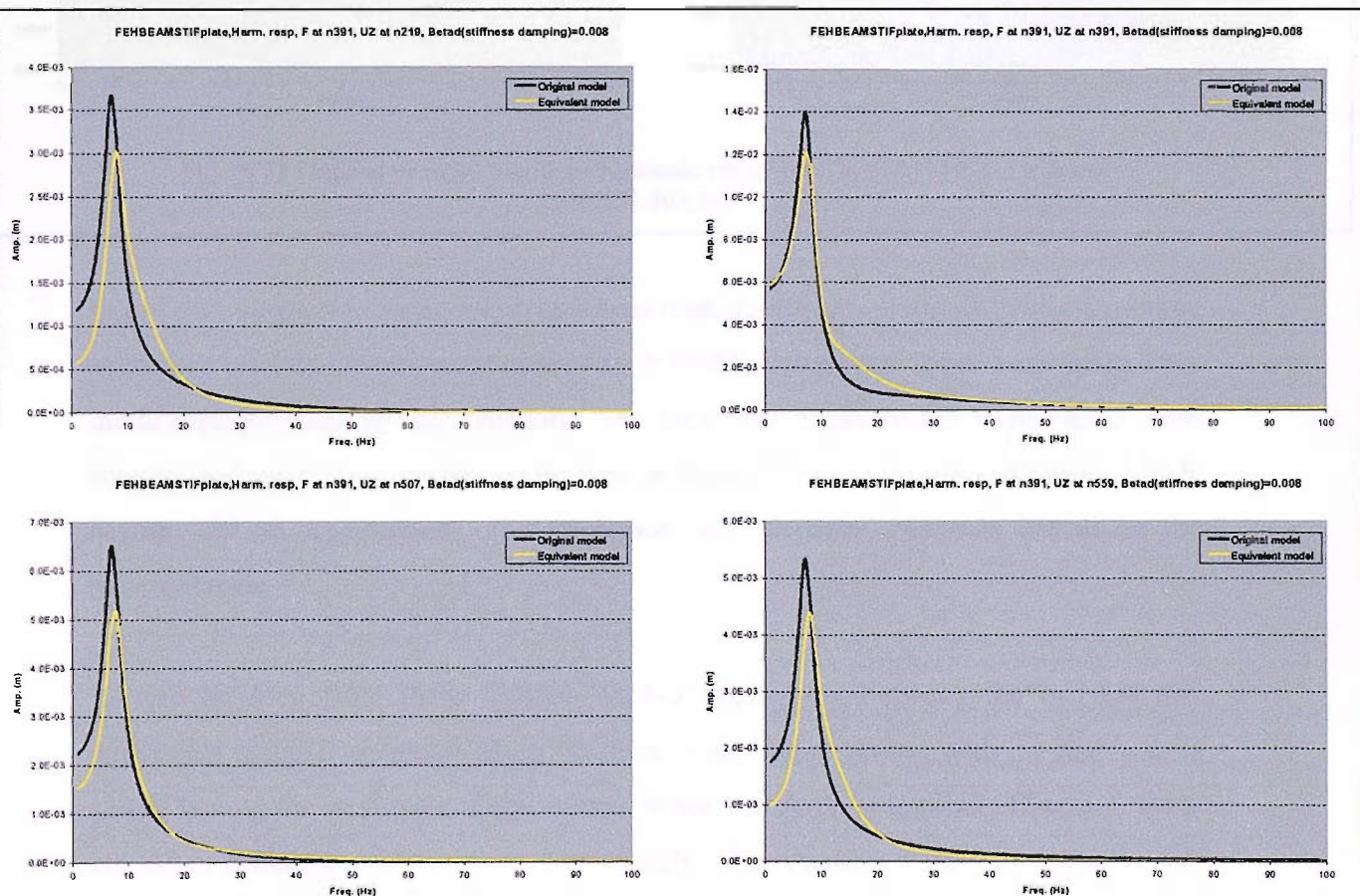


Figure 87 Original vs. equivalent plate harmonic responses F at node 391, UZ at nodes 219,391,507,559

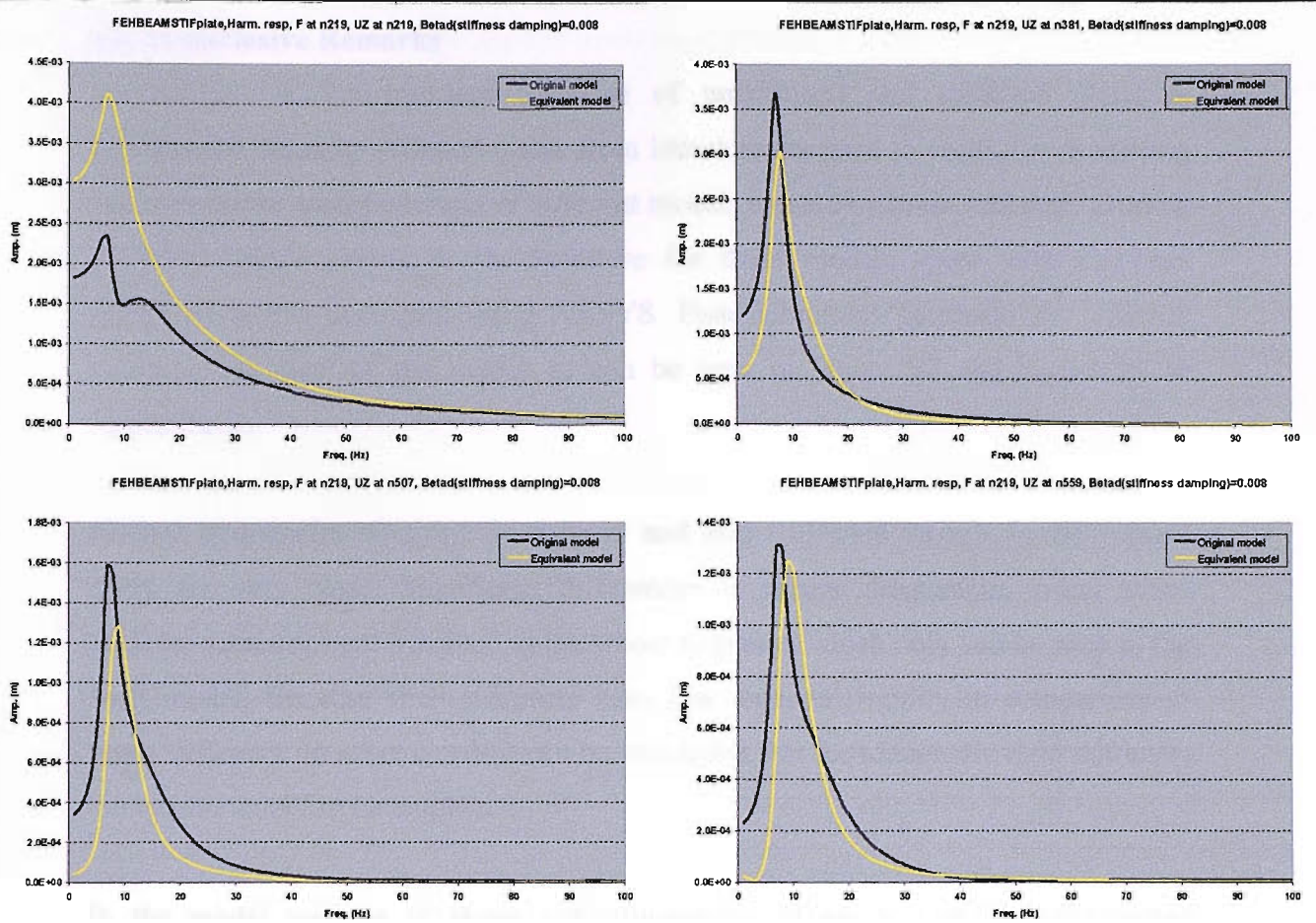


Figure 88 Original vs equivalent plate harmonic responses F at node 219, UZ at nodes 219, 391, 507, 559

In order to verify this, tentative, conclusion both models are analysed under harmonic excitation of 30000N in amplitude with 0-100Hz frequency range and using both mode superposition and full methods. The harmonic displacement responses of both original and equivalent model can be seen in Figure 87 & Figure 88 and Figure 128 & Figure 129 of Appendix-B. The excitation and response positions are as in the transient case.

As can be seen from these figures the best agreement between the original and equivalent plates is obtained when the force is applied at centre; with the response at centre having the best overall agreement. When the force is applied off-centre, there are larger differences between the two models. The situation is the same whether the full or mode superposition is used. This confirms that the differences between the responses of the two models are due to the concept used for equivalence, rather than the method used for calculating the response.

5.3.7 Conclusive Remarks

In section 5.3, the transient response of unstiffened and stiffened plates is investigated. Initially stiffened plates from literature are used to verify the modelling and subsequent modal analysis of different models created by beam and shell element stiffeners. Mode shapes in the literature for these models agree with the ones presented in this document using ANSYS. Plate vibrations dominate the stiffener vibrations in most of the modes as can be seen in Figure 92 and Figure 93 in Appendix-B.

Natural frequencies obtained from beam and shell stiffened models in the present study are very close. Significant differences in natural frequencies occur when stiffener vibrations get involved in the whole response, which only can be seen in the shell model. Because shell stiffeners have low torsional rigidity in comparison to beam stiffeners. In other words it can be concluded that for torsionally rigid stiffeners the beam model can be employed.

In the modal analysis of plates with dimensions of 6m x 12m, coupled global deflections of stiffeners and the flat plates can be seen for each variation of stiffening presented in Figure 95-Figure 103 in Appendix-B. When the various stiffened models in Table 13 are examined, it can be said that the beam model and its corresponding shell model give closer modal characteristics. Shell model with no tripping has distinct modal characteristics, which in general can be assumed to be close to beam model rather than the shell model with tripping due to its increased rigidity by constraining the stiffeners at their free edges.

Transient responses of these stiffened plates are investigated using ANSYS and the numerical method. For a particular location (node 391) their uz -displacements are compared (Figure 50). It is noticed that for each directional stiffening, beam and shell models give similar responses. Since it is known from previous chapters as an important issue, different discrete time intervals are used in the evaluation of the responses. Different damping ratios such as 0.01, 0.08 and 0.5 are considered in the stiffened plates. Responses are obtained for these ratios in Figure 51 and as a matter of illustrating the response phases in the main text properly, damping ratio 0.08 is used in all calculations. In this section numerical method is found to be sensitive to

the time intervals as well. The closest results to ANSYS are achieved using $dt=0.005s$. for the stiffened plates.

On the other hand convergence analyses done for the displacement and stress responses show that there is a need of at least 12 modes or more for the convergence of the transient mode superposition.

In the realistic plate analysis, beam and shell element stiffeners are used to model the stiffened single bottomed tanker plate. Certain amount of agreement achieved in the modal responses of both models. As a result there are coupled vibration modes in the model characteristics of the both type of stiffened tanker plate.

In the transient response analysis of the tanker plate, smaller time intervals are required to use due to higher natural frequencies. Hence $dt=0.001s$. and $dt=0.0025s$. work out well for the numerical method and ANSYS respectively in terms of agreement in the displacements and stresses.

Additionally, transient and harmonic response analyses are carried out on Shell(x:x) and Beam 44 models using both ANSYS and numerical methods. Different methods and discrete time intervals are compared and convergence results are studied. It has been shown that inclusion of a large number of modes is required to achieve convergence. Furthermore the convolution integral method developed in this thesis requires a small time interval in order to converge to the correct value.

Finally, an equivalent flat plate is created for dynamic response comparisons to the stiffened plate similar to the one in section 5.3.4. Static, transient and harmonic results are presented using different methods in ANSYS and numerical method described in this document. It can be concluded that the concept of static equivalence used may lead to some discrepancies in responses, depending on the position of applied force and calculated response.

6 CONCLUSIONS

The following conclusions can be:

- Theoretical and numerical modal analysis of uniform beams.
 - Natural frequencies obtained from two methods are reasonably close for both free-free and pinned-pinned boundary conditions. As the number of modes increases, the differences between the analytical and the numerical results also increase with the involvement of higher modes. This effect is more dominant in the Free-Free beam as it has higher natural frequencies than the Pinned-Pinned beam. As a conclusion the natural characteristics found through the modal analysis by FEA-ANSYS are satisfactory to use in the following mode superposition harmonic and transient analysis.
- Comparison of numerically and theoretically derived harmonic responses in the frequency domain.
 - There are peaks occurring at different frequencies with different magnitudes for each node location due to resonance, as illustrated for the displacements.
 - As the forcing frequency increases, convergence of 5 modes is not sufficient. On the other hand using 10 and 17 modes brings the contribution of higher modes to the overall response and makes the mode superposition method converges successfully.
 - Same analysis is repeated for damped condition and results are compared analytically and numerically. The amplitudes decrease with increasing of damping, as expected.
 - ANSYS results agree with the analytical mode superposition method results using 10 and 17 modes and as a conclusion it can be said that both ANSYS and analytical calculations give the same responses. Thus, the modelling of harmonic response with damping also verifies each other in these methods.
- Dry analysis of a SWATH
 - The preliminary results obtained from current modal analysis are compared with the model created by Wu (1984). When the present modal characteristics are compared numerically with Wu's results, there are

differences in the values, mainly because of the difference in the mass and stiffness distribution. However, when the natural frequencies are compared graphically it is seen that they both have similar characteristics. Thus it can be seen that a more complex dry analysis was conducted successfully, which can be used in a future load analysis involving wet deck slamming.

- Transient response of the beams.
 - Modelling of transient excitation and response for beams is achieved satisfactorily. Attention is withdrawn to the size of time intervals. In the transient analysis methodology, using $dt = 0.002$ s. discrete time interval, which is small enough, particularly for pinned-pinned beam gives closer results to ANSYS and analytical calculations. Smaller time intervals are needed because of the high natural frequencies of the beam.
 - It is seen that the number of modes used in superposition has more effect on the bending moment results than the displacement results. This is explained by establishing a relation between the values of modal responses such as mode shapes, modal bending moments and the locations of impulse application and the evaluated response.
 - As a conclusion, using discrete-time method in convolution sum is a satisfactory method for principal coordinate evaluation, when used with small enough time increments.
- Transient response of the flat unstiffened and stiffened plates.
 - Stiffened plates from literature are used to verify the modelling and subsequent modal analysis of different models created by beam and shell element stiffeners. Mode shapes in the literature for these models agree in general with the ones presented in this document using ANSYS. Plate vibrations dominate the stiffener vibrations in most of the modes.
 - Natural frequencies obtained from beam and shell stiffened models in the present study are very close. Significant differences in natural frequencies occur when stiffener vibrations get involved in the whole response, which only can be seen in the shell model. It can be concluded that for torsionally rigid stiffeners the beam model can be employed.

- In the modal analysis of plates with dimensions of 6m x 12m, coupled global deflections of stiffeners and the flat plates can be seen for each variation of stiffening.
- Shell model with no tripping has distinct modal characteristics, which in general can be assumed to be close to beam model rather than the shell model with tripping due to its increased rigidity by constraining the stiffeners at their free edges.
- Transient responses of these stiffened plates are investigated using ANSYS and the numerical method. It is noted that for both unidirectional and orthogonal stiffening, beam and shell models give similar responses.
- Convergence analyses done for the displacement and stress responses show that there is a need of at least 12 modes or more for the convergence of the transient mode superposition.
- It is shown that similar modal responses can be obtained by using beam and shell stiffened models. However it is difficult to establish which mode shapes to use in a subsequent transient analysis. Furthermore beam stiffeners bring limitations in modelling double bottom structures.
- In the transient response analysis of the tanker plate, smaller time intervals are required due to high natural frequencies, as a conclusion $dt=0.001s$. and $dt=0.0025s$. worked out well for the numerical method and ANSYS respectively in terms of agreement in the displacements and stresses.
 - Beam and shell stiffened models are analysed further for transient and harmonic responses. Although drawing firm conclusions is proved to be difficult. Beam stiffened model proved to be more well-behaved.
 - Numerical method and ANSYS results compared well with each other in terms of convergence. Discrete time interval again played an important role in mode superposition method.
- The basic analysis of the stiffened plate and its equivalent (unstiffened) both statically and dynamically, showed that more thought is required in this respect than just using static equivalence. Overall nodal responses can not be said to agree well, especially when the excitation and/or the response are off-centre.

7 RECOMMENDATIONS FOR FURTHER WORK

The points mentioned in the conclusions are the foundations of modelling a wedge-like bow of a mono or multi-hulled vessel and conducting transient response analysis as a result of impact slamming. The findings presented in this document can be used as the basis for the next stages of a further study.

Before moving into next step, more refinement is needed in modelling of plates. First of all the type of finite element to be used in stiffener modelling must be chosen carefully since it has been found that this plays a key role in the analysis. Transient analysis of stiffened plates taken from a real vessel (e.g. a tanker panel) can be studied in further detail using different finite elements for the stiffeners. When these points are addressed the issue of modelling a flat unstiffened plate successfully as an equivalent of a stiffened plate in terms of dynamic characteristics can be tackled. This would decrease the modelling and computing time of any stiffened plate which already proved to be an issue during this study. Similar simplification can be extended to modelling of double bottom structures with or without the use of solid elements.

When the modified flat plate is created then a wedge can be modelled using two modified plates with various deadrise angles. Moreover modal and transient analyses can be applied on this wedge.

Finally, the analysis can be concluded by examining these aspects in a real ship's forward section and incorporating it within complete fluid-structure interaction problem.

REFERENCES

- Aksu, G., 1982, "Free vibration of stiffened plates including in-plane inertia", *J. Appl. Mech., Trans. ASME*, 49, pp. 206-226
- Aksu, G., and Ali R., 1976, "Free vibration analysis of stiffened plates using finite difference method", *J. Sound Vib.*, 44, pp. 147-158
- Aksu, S., Price, W.G. and Temarel, P., 1991, "A comparison of two dimensional and three dimensional hydroelasticity theories including the effects of slamming", *Proc. ImechE*, 205, pp. 3-15
- Aksu, S., Price, W.G., Suhrbier, K.R., Temarel, P., 1993, "A comparative study of the dynamic behaviour of a fast patrol boat travelling in rough seas", *Marine structures*, 6, pp.421-441.
- Aksu, S., Price, W.G. and Temarel, P., 1996, "Steady state and transient responses of bulk carriers and tankers in random seas", *Trans. RINA*, 138, pp.72-102
- ANSYS Elements Reference. 000853. Ninth Edition. SAS IP, Inc.
- Ba. M. and Guilbaud, M., 1994, "A fast method evaluation for the translating and pulsating Green's function", *Shiffstechnik*, 42, pp.68-80
- Balendra, T. and Shanmugan, N.E., 1985, "Free vibration of plated structures by grillage method", *J. Sound Vib.*, 99, 3, pp. 333-350
- Bardell, N., Mead, D. and Zhu, D., 1988, "Free vibration of an orthogonally stiffened plate", *J. Sound Vib.*, 127, pp. 19-48
- Barik, M. and Mukhopadhyay, M., 1998, "Finite element free flexural vibration analysis of arbitrary plates", *Finite Element in Analysis and Design*, 29, pp. 137-151
- Barrette, M., Berry, A. and Beslin, O., 2000, "Vibration of stiffened plates using hierarchical trigonometric functions", *J. Sound Vib.*, 235, 5 , pp. 727-747
- Bedair, O.K., 1997, "Analysis of stiffened plates under lateral loading using sequential quadratic programming (SQP)", *Computers & Structures*, 62, 1, pp.63-80
- Bedair, O.K., 1997, "The application of mathematical programming techniques to the stability analysis of plate/stiffener assemblies", *Computer Methods in Applied Mechanics and Engineering*, 148, pp. 353-365

- Belik, O. and Price, W.G., 1982, “Comparison of slamming theories in the time simulation of ship responses in irregular waves”, Int. Shipbuild. Progress, 29, 335, pp. 173-187
- Belik, O., Bishop, R.E.D. and Price, W.G., 1980, “On the slamming response of ships to regular head waves”, Trans. RINA, 122, pp. 325-337
- Belik, O., Bishop, R.E.D. and Price, W.G., 1983, “A simulation of ship responses due to slamming in irregular head waves”, Trans. RINA, 125, pp. 237-253
- Belik, O., Bishop, R.E.D. and Price, W.G., 1987, “Influence of bottom and flare slamming on structural responses”, Trans. RINA, Vol.130, pp.261-275
- Bercin, A.N., 1997, “Eigenfrequencies of rectangular plate assemblies”, Computers & Structures, 65, 5, pp. 703-711
- Bereznitski, A., 2001, “3D model for bottom slamming”, Proc. OMAE’01, Brazil, pp.1-8
- Bereznitski, A., 2001, “Slamming the role of hydroelasticity”, Int. Shipbuild. Prog., 48, 4, pp.333-351
- Beslin, O. and Nicholas, J., 1996, “A hierarchical functions set of predicting very high order plate bending modes with any boundary conditions”, J. Acoust. Soc. America
- Beukelman, W., 1978, “Bottom impact pressures due to forced oscillation”, pp.107-126
- Bhat, R.B., 1982, “Vibrations of panels with nonuniformly spaced stiffeners”, J. Sound Vib., 84, pp. 449-452
- Bingham, H., Korsmeyer, F. and Newman, J., 1994, “Prediction of the seakeeping characteristics of ships”, Proc. 20th Symposium on Naval Hydrodynamics, Calif.
- Bishop, R.E.D. and Price, W.G., 1979, “**Hydroelasticity of ships**”, Cambridge University Press.
- Bishop, R.E.D. and Price, W.G., 1991, “Some comments on present day ship dynamics”, The Dynamics of Ships, Phil. Trans. R. Soc. Lond., A334, pp.187-197
- Bishop, R.E.D., Chalmers, D.W., Price, W.G. and Temarel, P., 1986, “The dynamic characteristics of unsymmetrical ship structures”, Trans RINA, 128, pp. 205-215
- Bishop, R.E.D., Price, W.G. and Tam, P.K.Y., 1977, “A unified dynamic analysis of a ship response to waves, Trans. RINA, 119, pp. 363-390

- Bishop, R.E.D., Price, W.G. and Tam, P.K.Y., 1980, “On the dynamics of slamming”, Trans. RINA, 120, pp. 259-280
- Bishop, R.E.D., Price, W.G. and Temarel, P., 1980, “Antisymmetric vibration of ship hulls”, Trans RINA, 122, pp. 197-208
- Bishop, R.E.D., Price, W.G. and Temarel, P., 1986, “On the hydroelastic response of a SWATH to regular oblique waves”, Advances in Marine Structures, pp.89-110
- Bishop, R.E.D., Price, W.G. and Wu, Y., 1986, “A general linear hydroelasticity theory of floating structures moving in a seaway”, Phil. Trans. Royal Soc. London, A316, pp. 375-426
- Bishop, R.E.D., Clarke, J.D. and Price, W.G., 1984, “Comparison of full scale and predicted responses of two frigates in severe weather trial”, Trans. RINA, 128, pp.205-215
- Blok, J.J. and Beukelman, W., 1984, “The high speed displacement ship systematic series hull forms-Seakeeping characteristics”, Trans SNAME, 92, pp.125-150
- Campana, E.F., Carcaterra, A., Ciappi, E. and Iafrati, A., 2000, “Some insights into slamming forces: compressible and incompressible phases”, Proc. Instn. Mech. Engnrs., 214, pp. 881-888
- Carcaterra, A and Ciappi, E., 2000, “Prediction of the compressible tage slamming force on rigid and elastic systems impacting on the water surface”, Nonlinear Dynamics, 21, pp.193-220
- Chang, M.S., 1977, “Computations of three-dimensional ship motions with forward speed”, Proc. Int. Numer. Ship Hydrodyn., second, pp.124-135, Uni. of, California, Berkeley
- Chapman, R.B., 1975, “Numerical solution for hydrodynamic forces on a surface piercing plate oscillating in yaw and sway”, Proc. 1st Int.Symp. Numer. Hydrodyn., pp.333-350
- Che, Xiling, Riggs, R. H. and Ertekin, C.R., 1994, “Composite 2D/3D hydroelastic- analysis method for floating structures”, J. Engineer. Mech., 120, 7, pp. 1499-1520
- Cheung, K.F., Seidl, L.H and Wang, S., 1998, “Analysis of SWATH ship structures”, Marine Technology, 35, 2, April, pp. 85-97

- Cheung, Y.K., 1976, “Finite strip method in structural analysis”, Pergamon Press, Oxford
- Cheung, Y.K., Fan, S.C. and Wu, C.Q., 1982, “Spline finite strip in structural analysis”, Proceedings of the Int. Con. on Finite Element Methods, Shanghai, pp. 704-709
- Chihua, L. and Yousheng H., “Ship hull slamming analysis with nonlinear boundary element method”, China Ocean Engineering, 11, 4, pp.411-418
- Chuang, S., 1966, “Experiments on flat bottom slamming”, J. Ship Res., March, pp.10-17
- Chuang, S., 1967, “Experiments on slamming of wedge shaped bodies”, J. Ship Res., 11, 3, pp.190-198
- Cointe, R. and Armand, J.L., 1987, “Hydrodynamic impact analysis of a cylinder”, J. Offshore Mechanics and Arctic Engineering, 109, pp. 237-243
- Cointe, R., 1989, “Two-dimensional water-solid impact”, ASME, Journal of offshore Mechanics and Arctic Engineering, 111, pp. 109-114
- Cointe, R., 1991, “Free surface flows close to a surface piercing body”, Mathematical Approaches in Hydrodynamics, Society for Industrial and Applied Mathematics, pp.319-334
- Cummins, W.E., 1962, “The impulse response function and ship motions”, Schiffstechnik, 9, pp.101-109
- De Kat, J.O. and Paulling, J.R., 1989, “The simulation of ship motions and capsizing in severe seas, Trans. SNAME, 97, pp.139-168
- Deb, A. and Booton, M., 1988, “Finite element models for stiffened plates under transverse loading”, Computers & Structures, 28, pp. 361-372
- Doong, J.L. and Chen, T.J., 1987, “Vibration and stability of an orthotropic plate”, Appl. Acoust., 22, pp. 1-13
- Du, S.X. and Wu, Y.S., 1998, “The effect of forward speed on the hydroelastic behaviours of ship structures”, PRADS’98, pp.597-603
- Ergin, A., 1992, “**A hydroelasticity study of submerged cylinders in finite and infinite depths of water**”, Ph.D. Thesis, University of Southampton.
- Ergin, A., Price, W.G., Randall, R and Temarel, P., 1992, “Dynamic characteristics of a submerged, flexible cylinder vibrating in finite water depths”, J. Ship Res., 36. Pp. 154-167

- Faltinsen, O. and Zhao, R., 1991a, "Flow predictions around high speed ships in waves" Proc. Math. Appr. Hydrodyn. Soc. Ind. Appl. Math. Philadelphia, Pa., pp. 265-288
- Faltinsen, O. and Zhao, R., 1991b, "Numerical prediction of ship motions at high forward speed", Phil. Trans. R. Soc. London, A334, pp. 241-257
- Faltinsen, O. M., 1993, "On the seakeeping of conventional and high speed vessels", J. Ship Res., 37, 2, pp.87-101
- Faltinsen, O.M., 1997, "The effect of hydroelasticity on ship slamming", Phil. Trans. R. Soc. Lond. A, 355, pp.575-591
- Faltinsen, O.M., 1999, "Water entry of a wedge by hydroelastic orthotropic plate theory", Journal of Ship Research, Vol. 43, No. 3, pp.180-193.
- Faltinsen, O.M., 2002, "Water entry of a wedge with finite deadrise angle", J. Ship Res., 46, 1, pp. 39-51
- Finkelstein, A.B., 1957, "The initial value problem for transient water waves", Comm. on Pure and Appl. Math., 10, pp.511-522
- Fonseca, N. and Guedes Soares, C., 1998, "Time domain analysis of large amplitude vertical motions and wave loads", J. Ship Res., 42, 2, pp.139-153
- Froude. W., 1861, "On the rolling of ships", Inst. Nav. Archit., Trans.2, pp.180-229
- Fu, Y., Price, W.G. and Temarel, P., 1987, "The dry and wet towage of a jack-up in regular and irregular waves", Trans. RINA, 129, pp.147-159
- Gerritsma, J. and Beukelman., W., 1964, "The distribution of the hydrodynamic forces on a heaving and pitching ship model in still water", Proc. 5th Symposium on Naval Hydrodynamics, pp.219-251
- Grace, N.F. and Kennedy, J.B., 1985, "Dynamic analysis of orthotropic plate structures", ASCE J. Engrg. Mech., 111, pp. 1027-1037
- Greenhow, M., 1987, "Wedge entry into initially calm water", Appl. Ocean Res., 9, 4, pp.214-223
- Grim. O. and Schenzle, P., 1969, "Berechnung der Torsionsbelastung eines schiffes in seegang", Institut fur Schiffbau der Universitat Hamburg, Bericht Nr.236 and Nr.237
- Gu, M. Wu, Y. and Xia, J., 1989, "Time domain analysis of nonlinear hydroelastic response of ships, 4th PRADS, Bulgaria

- Guedes Soares, C., 1989, “Transient response of ship hulls to wave impact “, Int. Shipbuild. Prog., 36, pp.137-156
- Guevel, P. and Boguis, R., 1982, “Ship motions with forward speed in infinite depth”, Int. Shipbuild. Prog., 29
- Hansen, P.F., Jensen, J.J. and Pedersen, P.T., 1994, “Wave induced springing and whipping of high speed vessels”, Hydroelasticity in Marine Technology, Balkema, pp.191-204
- Haskind, M.D., 1946a, “The hydrodynamic theory of ship oscillations in rolling and pitching”, Transl., Tech. Res. Bull., No.1-12, pp.3-43, SNAME, 1953
- Haskind, M.D., 1946b, “The oscillation of a ship in still water”, Transl. Tech. Res. Bull., No.1-12, pp.45-60, SNAME, 1953
- Hermundstad, O.A., Aarsnes J.V. and Moan T., 1999, “Linear hydroelastic analysis of high speed catamarans and monohulls”, J. Ship Res., 43, 1, pp. 48-63
- Hermundstad, O.A., Wu, M.K. and Moan, T., 1994, “Hydroelastic response analysis of a high speed monohull”, Proced. Int. Conf. on Hydroelasticity in Marine Tech., Trondheim, Norway, pp. 245-259
- Hermundstad, O.A., 1995, “Theoretical and experimental hydroelastic analysis of high speed vessels”, Ph.D. thesis, Dept. of Marine Structures, The Norwegian Institute of Technology
- Hoppman, W.H. 2nd and Magness, L.S., 1957, “Nodal patterns and free flexural vibration of stiffened plates”, J. Appl. Mech., Trans. ASME, 79, pp. 526-530
- Hoppman, W.H. 2nd, Huffington, Huffington, J.J. Jr. and Magnewss, L.S., 1956, “A study of orthogonally stiffened plates”, J. Appl. Mech., Trans. ASME, 78, pp. 343-350
- Huffington, J.J. Jr. and Schumacher, R.N., 1965, “Flexure of panel stiffened plates”, Res. Dept. RR-59, Martin Co., Baltimore, MD, pp. 1-61
- Huffington, J.J. Jr., 1956, “Theoretical determination of rigidity properties of orthogonally stiffened plates”, J. Appl. Mech., Trans. ASME, 23, pp. 15-23
- Hughes, O., 1983, **“Ship Structural Design”**, John Wiley & Sons.
- Inglis, R.B., and Price, W.G., 1980, “Comparison of calculated responses for arbitrary shaped bodies using two and three-dimensional theories”, Int. Shipbuild. Prog., 27, pp.86-95

- Janardhanan, K., Price, W.G. and Wu, Y., 1992, "Generalized fluid impulse response function for oscillating marine structures", *J. Fluids and Structures*, 6, pp.207-222
- Jensen, J.J. and Pedersen, P.T., 1979, "Wave induced bending moments in ships- a quadratic theory", *Trans. RINA*, 121, pp.151-165
- Jensen, J.J. and Pedersen, P.T., 1981, "Bending moments and shear forces in ships sailing in irregular waves", *J. Ship Res.*, 24, 4, pp.243-251
- Kaplan, P. and Malakhoff, A., 1978, "Surface effect ship loads: Lessons learned and their implications for other advanced marine vehicles", *Proc. SNAME spring meeting/STAR Symp.*, Pittsburg, PA:SNAME
- Kaplan, P., 1987, "Analysis and prediction of flat bottom slamming impact of advanced marine vehicles in waves", *Int. Shipbuild. Prog.*, 34, pp.44-53
- Kaplan, P., 1991, "Structural loads on advanced marine vehicles, including effects of slamming", *FAST'91*, pp.781-795
- Kaplan, P., 1992, "Advanced marine vehicles structural loads-present state of the art", *Proc. HPMV'92 Conference and exhibit*: USA
- Kawakami, M., Michimoto, J. and Kobayashi, K., 1977, "Prediction of long term whipping vibration stress due to slamming of large full ships in rough seas", *Int. Shipbuild. Prog.*, 24, pp.83-110
- King, B.K., Beck, A.R. and Magee, A.R., 1988, "Seakeeping calculations with forward speed using time-domain analysis", *Proc. 18th Symposium on Naval Hydrodynamics*, Michigan
- Kirk, C.L., 1970, "Natural frequencies of stiffened rectangular plates", *J. Sound Vib.*, 13, 4, pp. 375-388
- Koko T. S., Olson M.D., 1992, "Vibration analysis of stiffened plates by super elements", *Journal of Sound and Vibration*, 158(1), 149-167.
- Koko, T.S. and Olson, M.D., 1992, "Vibration analysis of stiffened plates by super elements", *J. Sound Vib.*, 158, 1, pp. 149-167
- Korobkin, A., 1998, "Elastic response of catamaran wetdeck to liquid impact", *Ocean Engng.*, 25, 8, pp.687-714
- Korvin-Kroukovsky, B.V. and Jacobs, W.R., 1957, "Pitching and heaving motions of a ship in regular waves", *Trans. SNAME*, 65

- Korvin-Kroukovsky, B.V., 1955, "Investigation of ship motions in regular waves", Trans. SNAME, 63
- Kriloff, A., 1896, "A new theory of the pitching motion of ships on waves and of the stresses produced by this motion", Inst. Nav. Archit., Trans.37, pp.326-368
- Kumar Satish, Y.V. and Mukhopadhyay, M., 2000, "Finite element analysis of ship structures using a new stiffened plate element", Appl. Ocean Res., 22, pp. 361-374
- Kvalsvold, J. and Faltinsen, O.M., 1994, "Slamming loads on wetdecks of multihull vessels", Hydroelasticity in Marine Technology, Balkema, Norway
- Kvalsvold, J. and Faltinsen, O.M., 1995, "Hydroelastic modelling of wetdeck slamming on multihull vessels", J. Ship Res., 39, 3, Sept., pp.225-239
- Lai, C. and Troesch, A.W., 1995, "Modelling issues related to the hydrodynamics of three dimensional steady planing", J. Ship Res., 39,1
- Lai, C. and Troesch, A.W., 1996, "A vortex lattice method for high speed planing", Int. J. Numerical Meth. Fluids, 22, pp.495-513
- Laura, P.A., 1968, "Effect of shear rotatory inertia on flexural vibrations of rib-stiffened plates", J. Acoust. Soc. America, 44, 1, pp. 283-284
- Leckie, F.A., 1963, "Application of transfer matrices to plate vibration", Ing. Arch., 32, pp. 100-111
- Leibowitz, R.C., 1963, "A method of predicting slamming pressure forces and the responses of a ship hull", DTMB report no:1961
- Leissa, A.W., 1973, "The free vibration of rectangular plates", J. Sound Vib., 31, 3, pp. 257-293
- Lewis, F.M., 1929, "The inertia of water surrounding a vibrating ship, Trans. SNAME, 37, pp.1-20
- Lewison, G.R.G.,1970, "On the reduction of slamming pressures", Trans. RINA, 112, pp.285-306
- Li, W.Y., Cheung, Y.K. and Tham, L.G., 1986, "Spline finite strip analysis of general plates", Proc. ASCE J. Eng. Mech. Div., 112, pp. 43-54
- Liapis, S.J. and Beck, R.F., 1985, "Seakeeping computations using time-domain analysis", Proc. Int. 4th Symposium on Naval Hydrodynamics, National Academy of Sciences, Washington DC, pp.34-54

- Long, B.R., 1971, “A stiffness-type analysis of vibration of a class of stiffened plates”, *J. Sound Vib.*, 19, pp. 463-472
- Lundgren, J., Price, W.G and Wu, Y., 1989, “A hydroelastic investigation into the behaviour of a floating dry dock in waves”, *Trans. RINA*, 131, pp.213-231
- Madsen, N.F., 1978, “Vibration of orthogonally stiffened panels”, *J. Ship Res.*, 22, 2, pp. 100-109
- Mayerhoff, W.K. and Schlachter, G., 1980, “An approach for the determination of hull girder loads in a seaway including hydrodynamic impacts”, *Ocean Engng.*, 7, pp.305-326
- Meirovitch, L., 1967, “**Analytical Methods in Vibrations**”, The MacMillan Company.
- Meirovitch, L., 1986, “**Elements of Vibration Analysis**”, McGraw-Hill Book Company.
- Mercer, C.A. and Seavy, C., 1967, “Prediction of natural frequencies and normal modes of skin stringer panel rows”, *J. Sound Vib.*, 6, pp. 149-162
- Mota Soares, C.A., Trabucho Compos, L.M. and Viegas Gago, A.F., (1980), “Dynamic analysis of plates by mixed elements”, *Proc. Recent Advances in Structural Dynamics Conf.*, Southampton, pp. 51-60
- Mukherjee, A and Mukhopadhyay, M., 1988, “Finite element free vibration of eccentrically stiffened plates”, *Computers & Structures*, 30, pp. 1303-1317
- Mukherjee, A. and Mukhopadhyay, M., 1987, “Finite element analysis of stiffened plates under time varying load”, *Proc. 20th Midwestern Mechanics Conf.*, Purdue Univ., In., USA, pp. 666-672
- Mukhopadhyay M., Chakraborty S., 2000, “Estimation of in-plane elastic parameters and stiffener geometry of stiffened plates”, *Journal of Sound and Vibration*, 231(1), 99-124.
- Mukhopadhyay, M and Satsangi, S.K., 1984, “Isoparametric stiffened plate bending element for the analysis of ship structures”, *Trans. RINA*, 126, pp. 141-151
- Mukhopadhyay, M., 1989, “Vibration and stability analysis of stiffened plates by semi-analytic finite difference method, Part 1: Consideration of bending displacements only”, *J. Sound Vib.*, 130, 1, pp. 27-39

- Mukhopadhyay, M., 1989, “Vibration and stability analysis of stiffened plates by semi-analytic finite difference method, Part 2: Consideration of bending and axial displacements only”, *J. Sound Vib.*, 130, 1, pp. 41-53
- Mukhopadhyay, M., 1994, “Stiffened plates in bending”, *Computers & Structures*, 50, 4, pp. 541-548
- Nair , P.S. and Rao, M.S., 1984, “On vibration of plates with varying stiffener length”, *J. Sound Vib.*, 95, 1, pp. 19-29
- Newland, D.E., 1989, “**Mechanical Vibration Analysis and Computation**”, Longman.
- Newman, J.N., 1964, “A slender body theory for ship oscillations in waves”, *J Fluid Mech.*, 18, pp.602-618
- Newman, J.N., 1977, “**Marine hydrodynamics**” MIT press, Massachusetts
- Newman, J.N., 1978, “The theory of ship motions” *Advances in Appl. Mech.*, 18, pp.221-283
- Ochi, M.K. and Motter, L.E., 1973, “Prediction of slamming characteristics and hull responses for ship design”, *Trans. SNAME*, 81, pp.144-190
- Ogilvie, T.F. and Tuck, E.O., 1969, “A rational strip theory for ship motions, part 1”, Rep. No. 013, Uni. of Michigan
- Ogilvie, T.F., 1964, Recent progress toward the understanding and prediction of ship motions”, 5th Symposium on Naval Hydrodynamics, pp.3-80
- Olson M.D., Hazell C.R., 1977, “Vibration studies on some integral rib-stiffened plates”, *Journal of Sound and Vibration*, 50(1), 43-61.
- Olson, M.D. and Hazel, C.R., 1977, “Vibration studies on some integral rib-stiffened plates”, *J. Sound Vib.*, 50, 1, pp. 43-61
- Palani G.S., Iyer, N.R. and T.V.S.R. Appa Rao, 1992, “An efficient finite element model for static and vibration analysis of eccentrically stiffened plates/shells”, *Computers & Structures*, 43, 4, pp. 651-661
- Palani, G.S., Iyer, N.R. and T.V.S.R. Appa Rao, 1993, “An efficient finite element model for static and vibration analysis of plates with arbitrarily located eccentric stiffeners”, *J. Sound Vib.*, 166, 3, pp. 409-427
- Petyt, M., 1990, “**Introduction to finite element vibration analysis**”, Cambridge University Press.

- Price, W.G. and Wu, Y.S., 1985, "Hydroelasticity of marine structures", *Theoretical and Appl. Mech.*, pp. 311-317
- Price, W.G., Temarel, P. and Keane, A.J., 1994, "Hydroelastic analysis of a SWATH in waves", *Int. Conf. of Hydroelasticity in Marine Technology*, Balkema, pp. 1994
- Price, W.G., Temarel, P. and Wu, Y., 1987, "Responses of a SWATH travelling in irregular seas", *J. Underwater Technn*, 13, pp.2-10
- Ramos, J. and Soares Guedes C., 1998, "Vibratory response of ship hulls to wave impact loads", *Int. Shipbuild. Prog.*, 45, 441, pp.71-87
- Rao Bapu, M.N., Guruswamy, P., Venkateswara Rao M. and Pavitran, S., 1978, "Studies of vibration of some rib-stiffened cantilever plates", *J. Sound Vib.*, 57, pp. 389-402
- Rao, S.S., 1995, "**Mechanical vibrations**", Addison-Wesley Publishing Company.
- Rikards R., Chate A., Ozolins O., 2001, "Analysis for buckling and vibrations of composite stiffened shells and plates", *Composite Structures*, 51, 361-370.
- Salvesen, N., Tuck, E.O. and Faltinsen, O.M., 1970, "Ship motions and sea loads", *Trans. SNAME*, 78, pp.250-287
- Satsangi, S.K., Mukhopadhyay, M., 1989, "A review of static analysis of stiffened plates", *Journal of Structural Engineering*, 15, 4, pp. 117-126
- Sheikh, A.H. and Mukhopadhyay, M., 1992, "Analysis of stiffened plate with arbitrary planform by the general spline finite strip method", *Computers & Structures*, 42, pp. 57-63
- Sheikh, A.H. and Mukhopadhyay, M., 1993, "Transverse vibration of plate structures with elastically restrained edges by the spline/finite strip method", *J. Vib. Acoustics*, 115, pp. 295-302, July
- Sheikh, A.H. and Mukhopadhyay, M., 2002, "Linear and nonlinear transient vibration analysis of stiffened plate structures", *Finite Elements in Analysis and Design*, 38, pp. 477-502
- Sheikh, A.H. and Mukhopadhyay, M., 1993, "Free vibration analysis of stiffened plates with arbitrary planform by the general spline finite strip method", *J. Sound Vib.*, 162, 1, pp. 147-164

- Shibue, T., Ito, A. and Nakayama, E., 1994, "Structural response analysis of cylinders under water impact", *Hydroelasticity in Marine Technology*, Balkema, pp.221-228
- Sinha, G. and Mukhopadhyay, M., 1995, "Transient dynamic response of arbitrary stiffened shells by the finite element method", *J Vib Acoust.*, 117, pp. 11-16
- Smith G.A., Laura, P.A. and Matis, M., 1970, "Experimental and analytical study of vibrating stiffened rectangular plates subjected to in plane loading", *J. Acoust. Soc. America*, 48, 3, 2, pp. 707-713
- Stavovy, A.B. and Chuang, S.L., 1976, "Analytical determination of slamming pressures for high speed vehicles in waves", *J. Ship Res.*, 20, pp.190-198
- Sun, W. and Zhu, J., 1987, "Boundary element method for the dynamic problem of orthotropic plates", *Adv. Topics in Vibs.*, ASME, DE-Vol 8, Bk. No. 400408-NY
- Szilard, R., 1974, "**Theory and Analysis of Plates, Classical and Numerical Methods**", Prentice-Hall, Inc.
- Szilard, R., 1974, "**Theory and analysis of plates, classical and numerical methods**", Prentice Hall, New Jersey
- Tanaka, M., Bercin, A.N., 1998, "Static bending analysis of stiffened plates using the boundary element method", *Engineering Analysis with Boundary Elements*, 21, pp. 147-154
- Tasai, F. and Takaki, M., 1969, "Theory and Calculation of ship responses in regular waves", *J. Soc. Nav. Arch. Japan*
- Thomson, T., William, 1981, "**Theory of vibration with applications**", Prentice-Hall, Inc.
- Thorkildsen, R.L. and Hoppman, W.H. 2nd, 1959, "Effect of rotary inertia on frequencies of vibration of stiffened plates", *J. Appl. Mech., Trans. ASME*, 26, pp. 298-300
- Troesch, A.W. and Kang, C.G., 1986, "Hydrodynamic impact loads on three dimensional bodies", 16th Symposium on Naval Hydrodynamics, Uni. California, Berkeley, July
- Troesch, A.W. and Kang, C.G., 1988, "Evaluation of impact loads associated with flare slamming", SNAME 13th STAR Symposium, Pittsburg, June

- Troitsky, M.S., 1976, “Stiffened plates bending stability and vibration”, Elsevier Scientific Publishing Co., Amsterdam
- Varyani, K.S., Gatiganti, R.M. and Gerigk, M., 2000, “Motions and slamming impact on catamaran”, Ocean Engng., 27, pp.729-747
- Verhagen, J.H.G., 1967, “The impact of a flat plate on a water surface”, J. Ship Res., 9, pp.211-223
- Vinson, J.R., 1974, **“Structural Mechanics: The Behaviour of Plates and Shells”**, John Wiley & Sons.
- von Karman, 1929, “The impact of seaplane floats during landing”, NACA, Technical note 321, Washington DC
- von Kerczek, C. and Tuck, E.O., 1969, “The representation of ship hulls by conformal mapping functions”, J. Ship Res., 13, pp.284-298
- Vorus, W.S., 1996, “A flat cylinder theory for vessel impact and steady planing resistance”, J. Ship Res., 40, pp.89-106
- Wagner, H., 1932, “Über stoss und gleitvergange an der oberflache von flussigkeiten”, Zeitschr.f. Angewandte Mathematik und Mechanik, 12, pp. 192-235
- Wah, T., 1964, “Vibration of stiffened plates”, Aeronaut. Quart., 15, p. 285-298
- Watanabe, I and Soares Guedes,C., 1999, “Comparative study on the time-domain analysis of nonlinear ship motions and loads”, Marine Structures, 12, pp.153-170
- Wenyang, D. and Yishan, D., 1999, “Time-domain calculation of hydrodynamic forces on ships with large flare: Three-dimensional case”, Int. Shipbuild. Prog., 46, 446, pp.209-221
- Westlake, P.C. and Wilson, P.A., 2000, “A new conformal; mapping technique for ship sections”, Int. Shipbuild. Prog., 47, 5-22
- Wu, J.R. and Liu, W.H., 1988, “Vibration of rectangular plates with edge restraints and intermediate stiffeners”, J. Sound Vib., 123, 1, pp. 103-113
- Wu, M., Aarsnes, J.V., Hermunstad, O.A. and Moan, T., 1996, “A practical prediction of wave induced structural responses in ships with large amplitude motion”, Proc. 21st Symp. On Naval Hydrodynamics
- Wu, M.K. and Moan, T., 1996, “Linear and nonlinear hydroelastic analysis of high speed vessels”, J. Ship Res., 40, pp. 149-163

- Wu, Y., 1984, “**Hydroelasticity of Floating Bodies**”, Ph.D. Thesis, Brunel University.
- Wu, Y., Xia, J. and Du, S., 1991, “Two engineering approaches to hydroelastic analysis of slender ships”, Dynamics of Marine Vehicles and Structures in Waves, Elsevier Science Publishers, pp.157-165
- Wu, Y., 1984, “**Hydroelasticity of Floating Bodies**”, Ph.D. Thesis, Brunel University, UK
- Wu, G.X. and Taylor, R.E., 1987, “A Green’s function form for ship motions at forward speed”, Int. Shipbuild. Prog., 34
- Xia, J. and Wang, Z., 1997, “Time domain hydroelasticity theory of ships responding to waves”, J. Ship Res., 41, 4, pp. 286-300
- Xia, J., 1996, “AQ hydroelastic body boundary condition of floating structures”, Ship Technology Res., 43, pp.172-174
- Xia, J., Wang, Z and Jensen, J.J., 1998, “Nonlinear wave loads and ship responses by a time domain strip theory”, Marine Structures, 11, pp. 101-123
- Xu, L., Troesch, A.W. and Vorus, W.S., 1998, “Asymmetric vessel impact and planing hydrodynamics”, J. Ship Res., 42, 3, Sept., pp.187-198
- Yamamoto, Y., Fijino, M. and Fukasawa, T., 1980, “Motion and longitudinal strength of a ship in head sea and the effects of nonlinearities, Naval Architecture and Ocean Engng., JSNAJ, 18
- Ye, H.K. and Hsiung, C.C., 1999, “Time domain motion computations of twin- and mono-hull ships in head seas”, Int. Shipbuild. Prog., 46, 445, pp.91-123
- Yeung, R.W. and Kim, S.H., 1984, “A new development in the theory of oscillating and translating slender ships”, 15th Symposium on Naval Hydrodynamics
- Zhao, R. and Aarsnes, J.V., 1995, “Numerical and experimental studies of nonlinear motions and loads of a high speed catamaran”, Proc. 3rd Int. Conf. Fast Sea Transportation
- Zhao, R. and Faltinsen, O., 1992, “Slamming loads on high-speed vessels”, Proc. 19th ONR Conference, Korea, Washington DC: National Academy Press
- Zhao, R. and Faltinsen, O., 1993, “Water entry of two-dimensional bodies”, J. Fluid Mech., 246, pp. 593-612

- Zhao, R. and Faltinsen, O.M., 1998, “Water entry to axisymmetric bodies with and without flow separation”, 22nd Symposium on Naval Hydrodynamics, Washington DC, USA
- Zhao, R., Faltinsen, O.M. and Aarsnes, J.V., 1996, “Water entry of arbitrary two-dimensional sections with and without flow separation”, 21st Symposium on Naval Hydrodynamics, Trondheim, Norway
- Zhao, R., Faltinsen, O.M. and Haslum, H.A., 1997, “A simplified nonlinear analysis of a high-speed planing craft in calm water”, FAST’97
- Zienkiewicz, O.C., 1977, **“The finite element method”**, McGraw-Hill, New York

APPENDIX – A – Complementary figures relating to beam analysis

Transient Response of the Beams

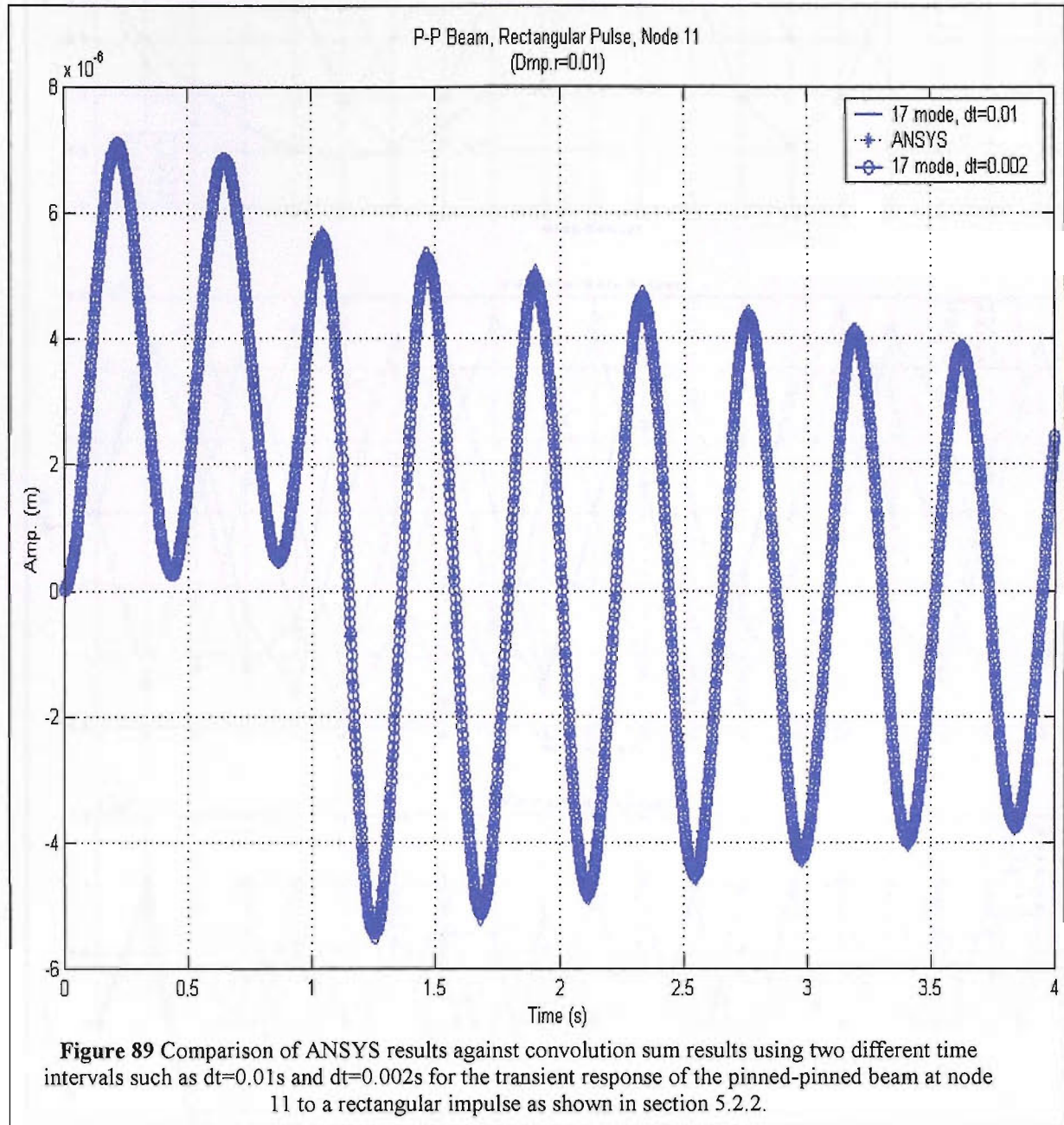


Figure 89 Comparison of ANSYS results against convolution sum results using two different time intervals such as $dt=0.01$ s and $dt=0.002$ s for the transient response of the pinned-pinned beam at node 11 to a rectangular impulse as shown in section 5.2.2.

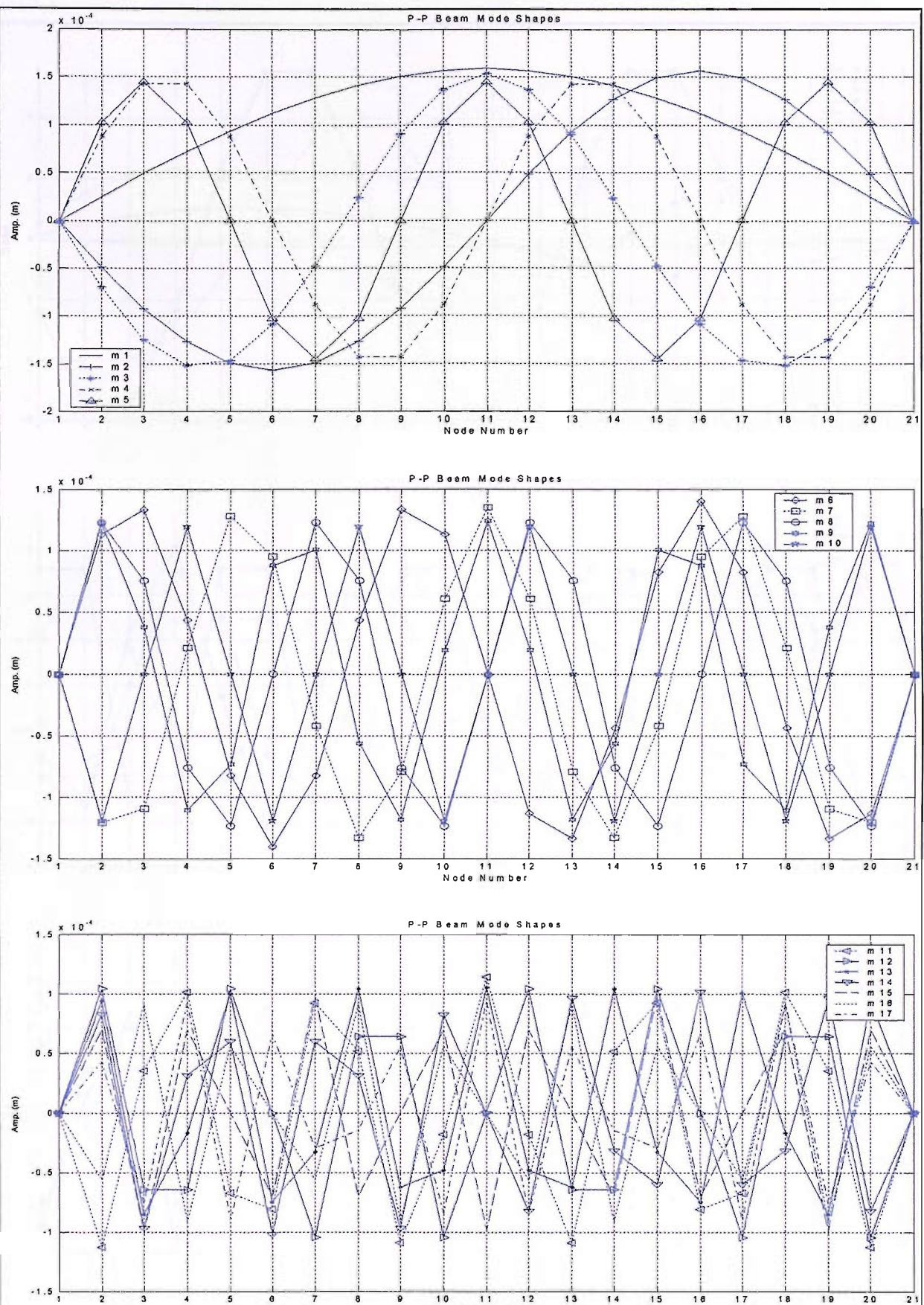


Figure 90 Mode shapes of the pinned-pinned beam

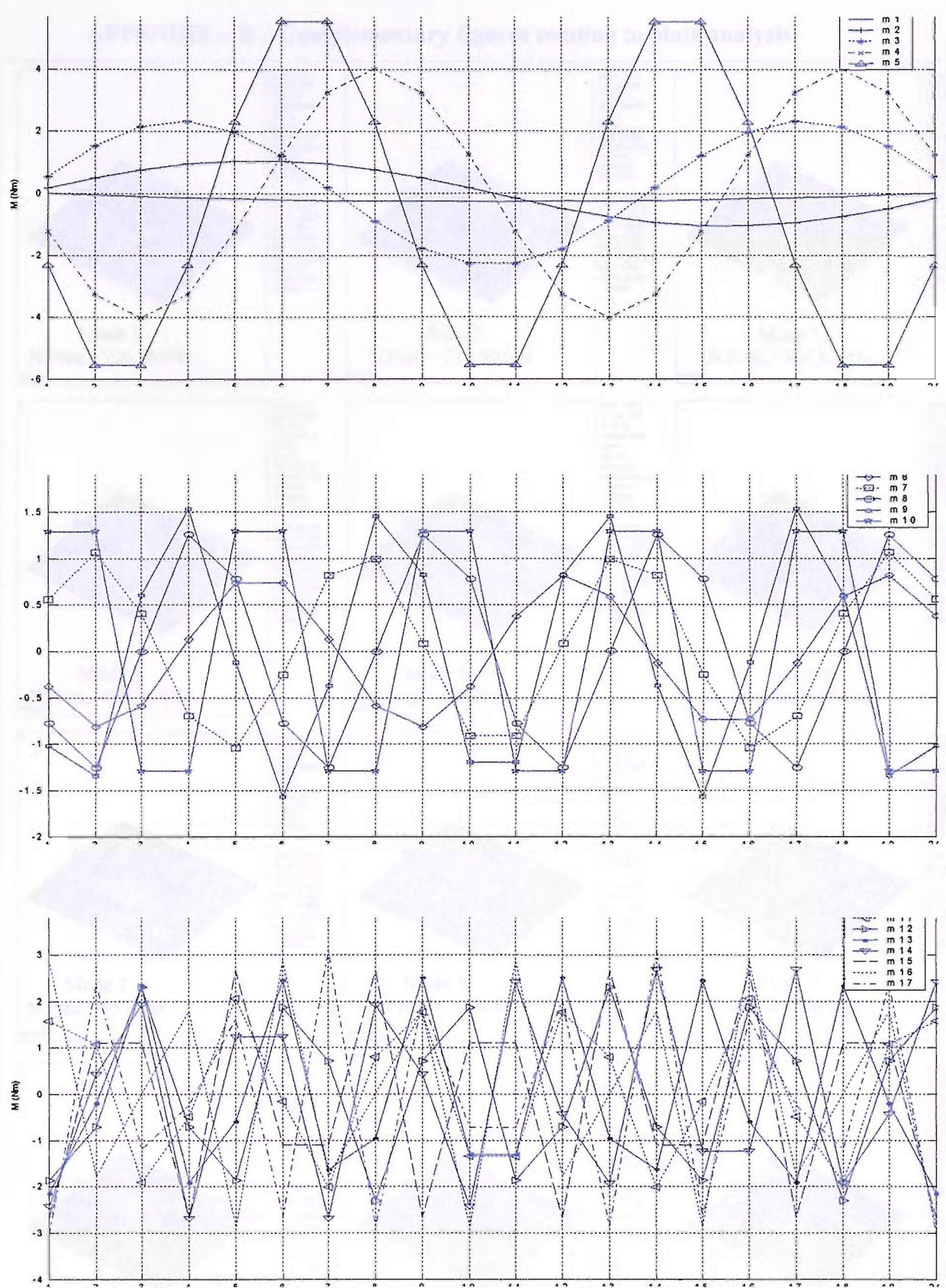


Figure 91 Modal bending moments of the pinned-pinned beam

APPENDIX – B – Complementary figures relating to plate analysis

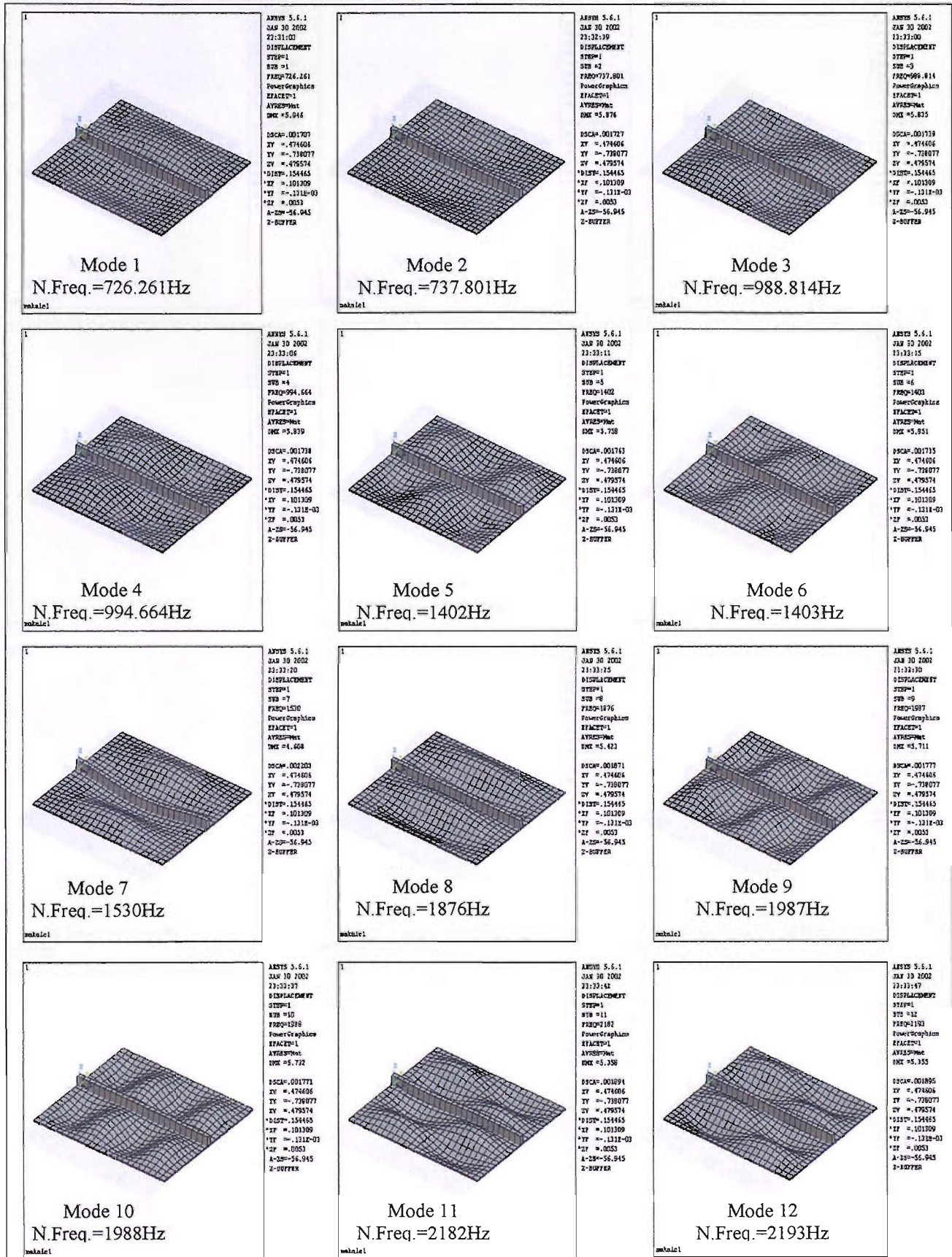


Figure 92 First 12 mode shapes of single stiffened (Beam44) clamped plate-24x24 mesh

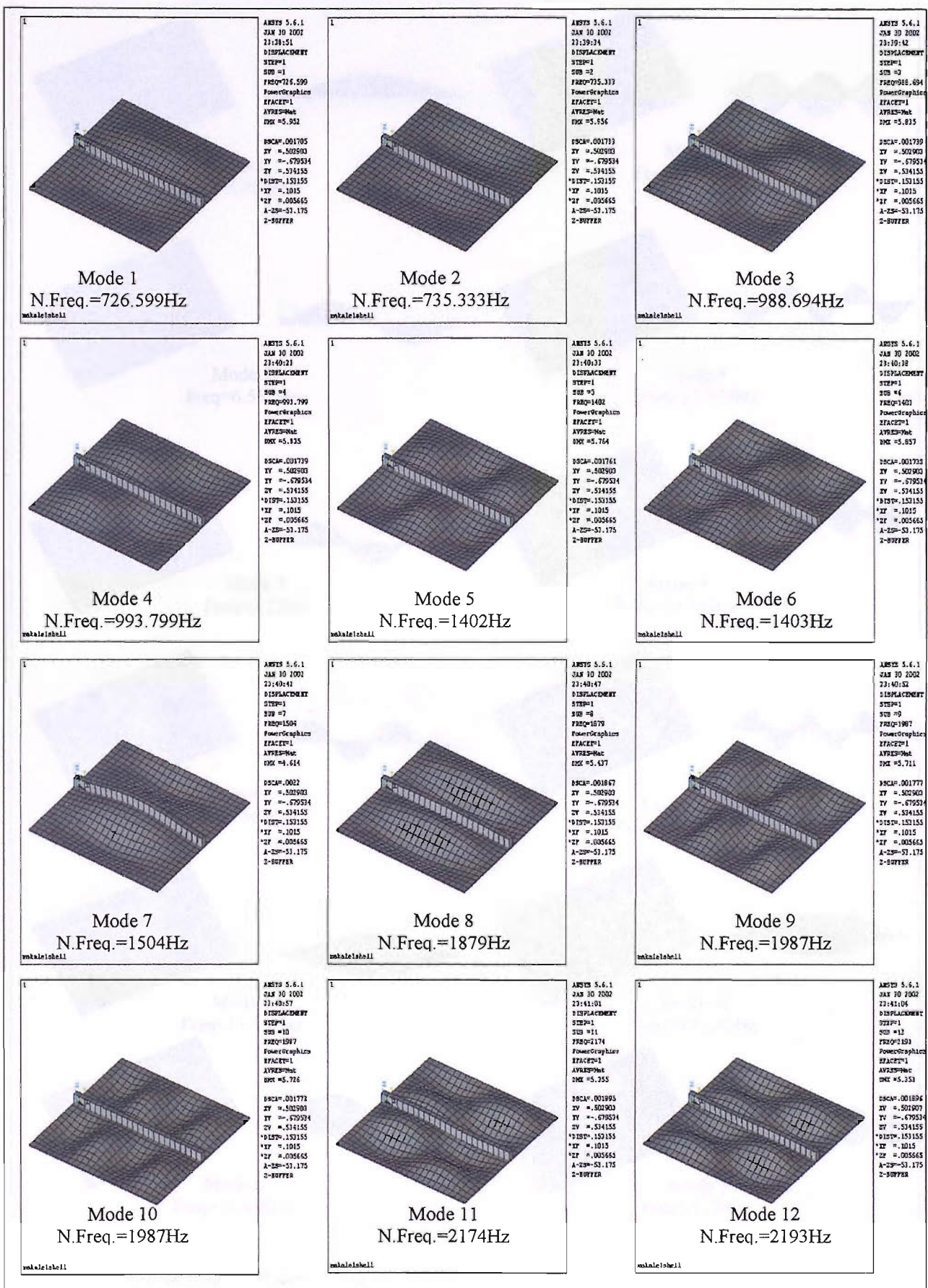


Figure 93 First 12 mode shapes of single stiffened (Shell63) clamped plate-24x24 mesh

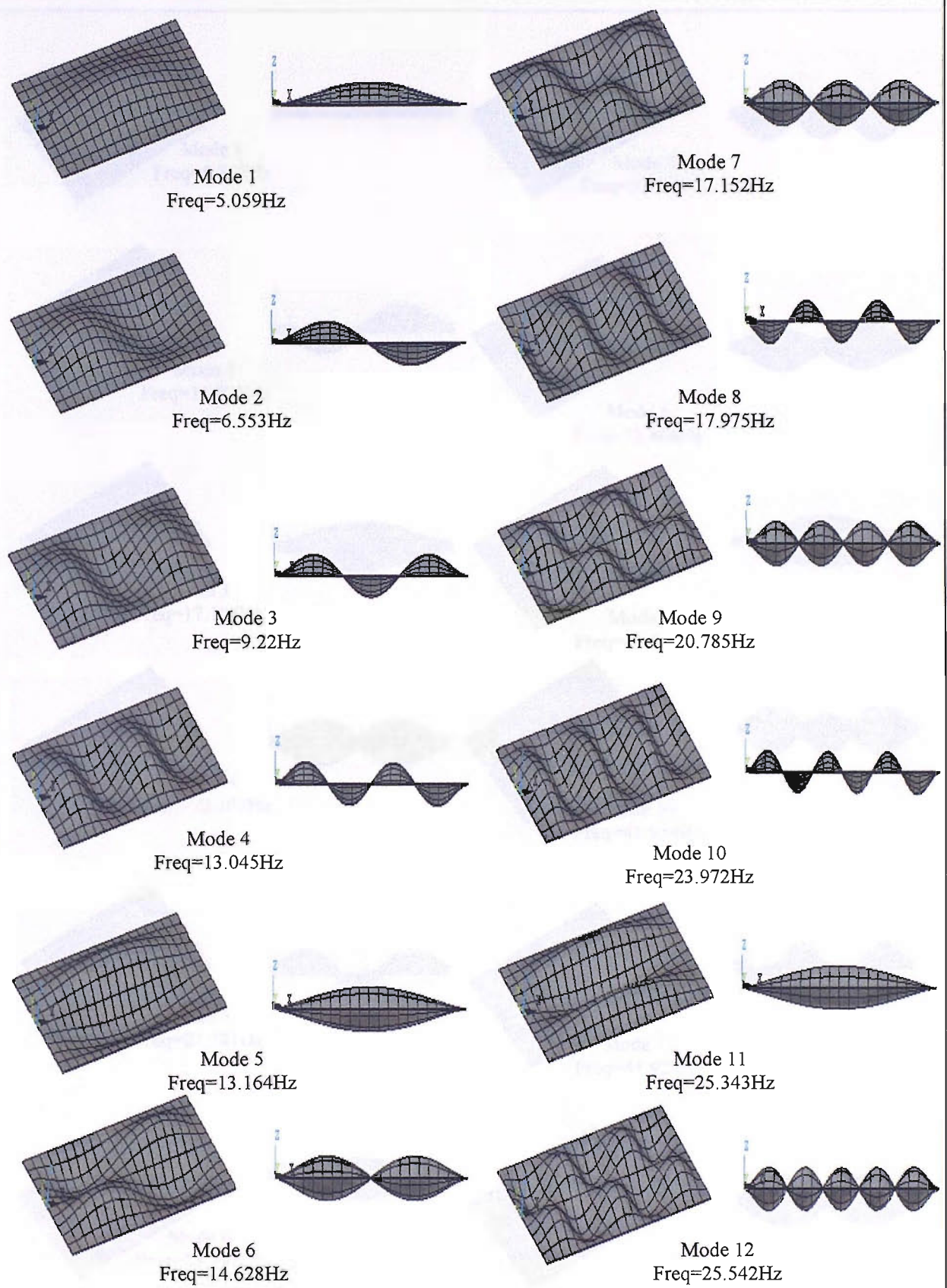


Figure 94 Mode shapes and natural frequencies of the unstiffened flat fixed ended (clamped) plate

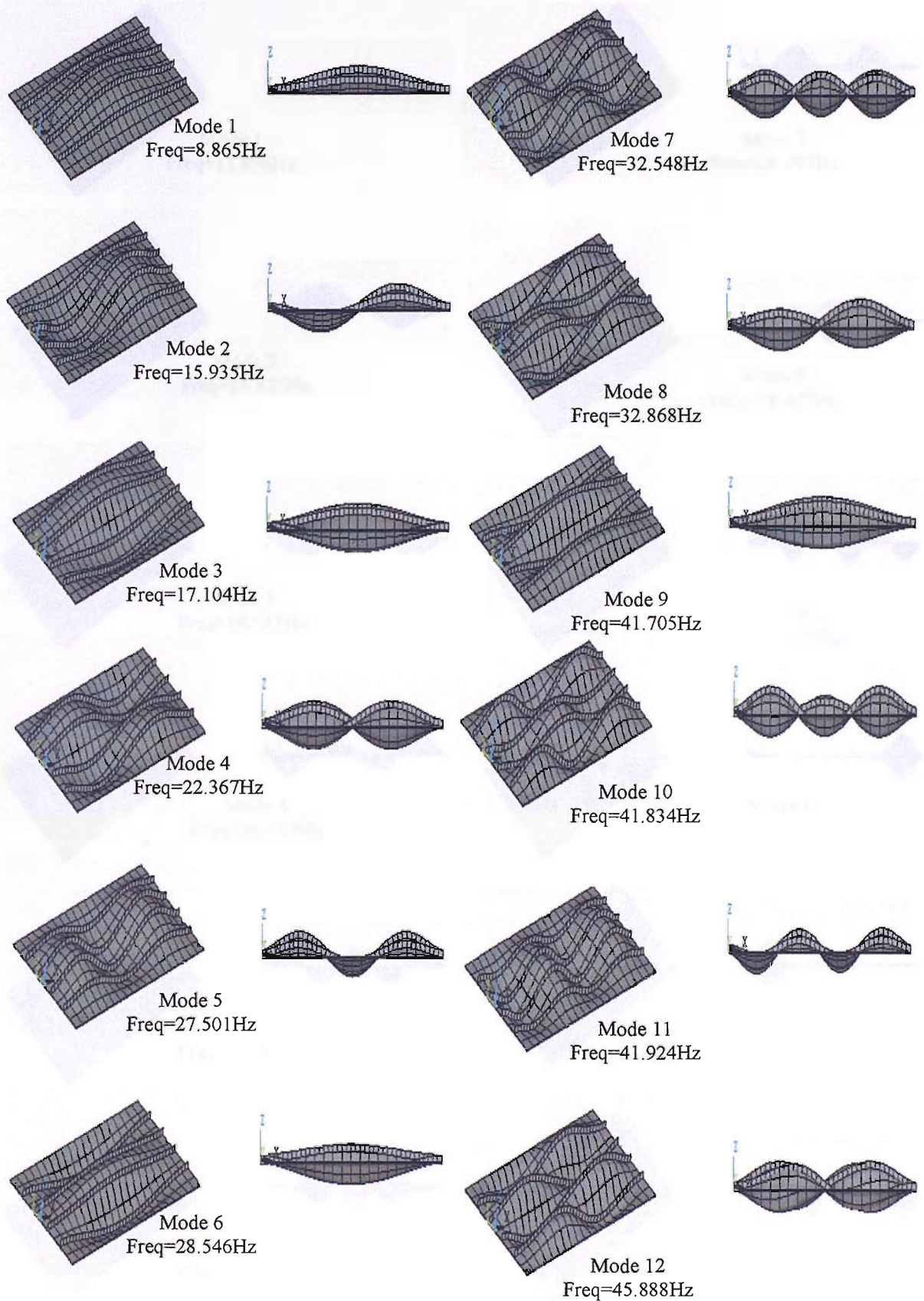


Figure 95 Mode shapes and natural frequencies of the longitudinally stiffened (Shell99-no tripping), fixed end flat plate (Shell99)

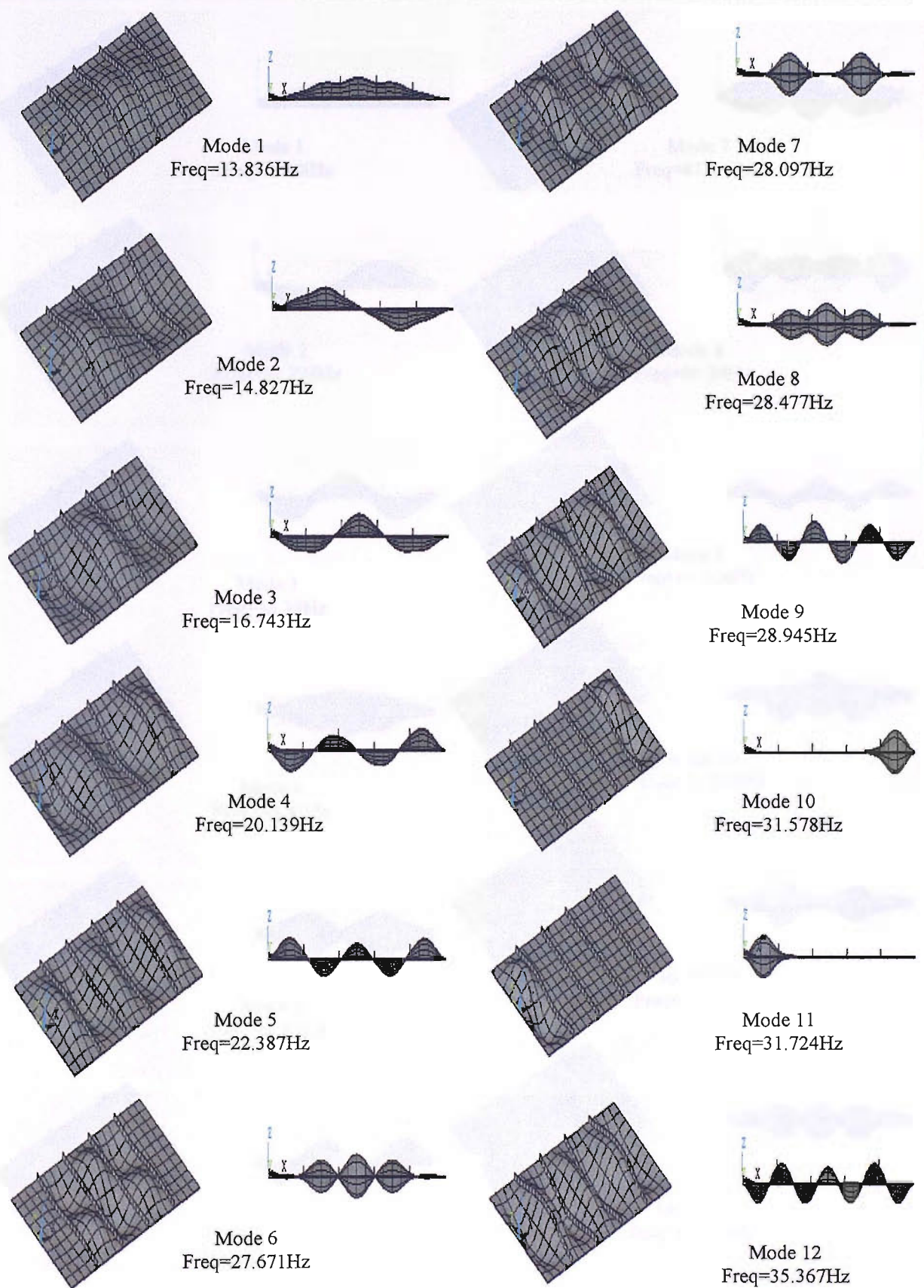


Figure 96 Mode shapes and natural frequencies of the transversely stiffened (Shell99-no tripping), fixed end flat plate (Shell99)

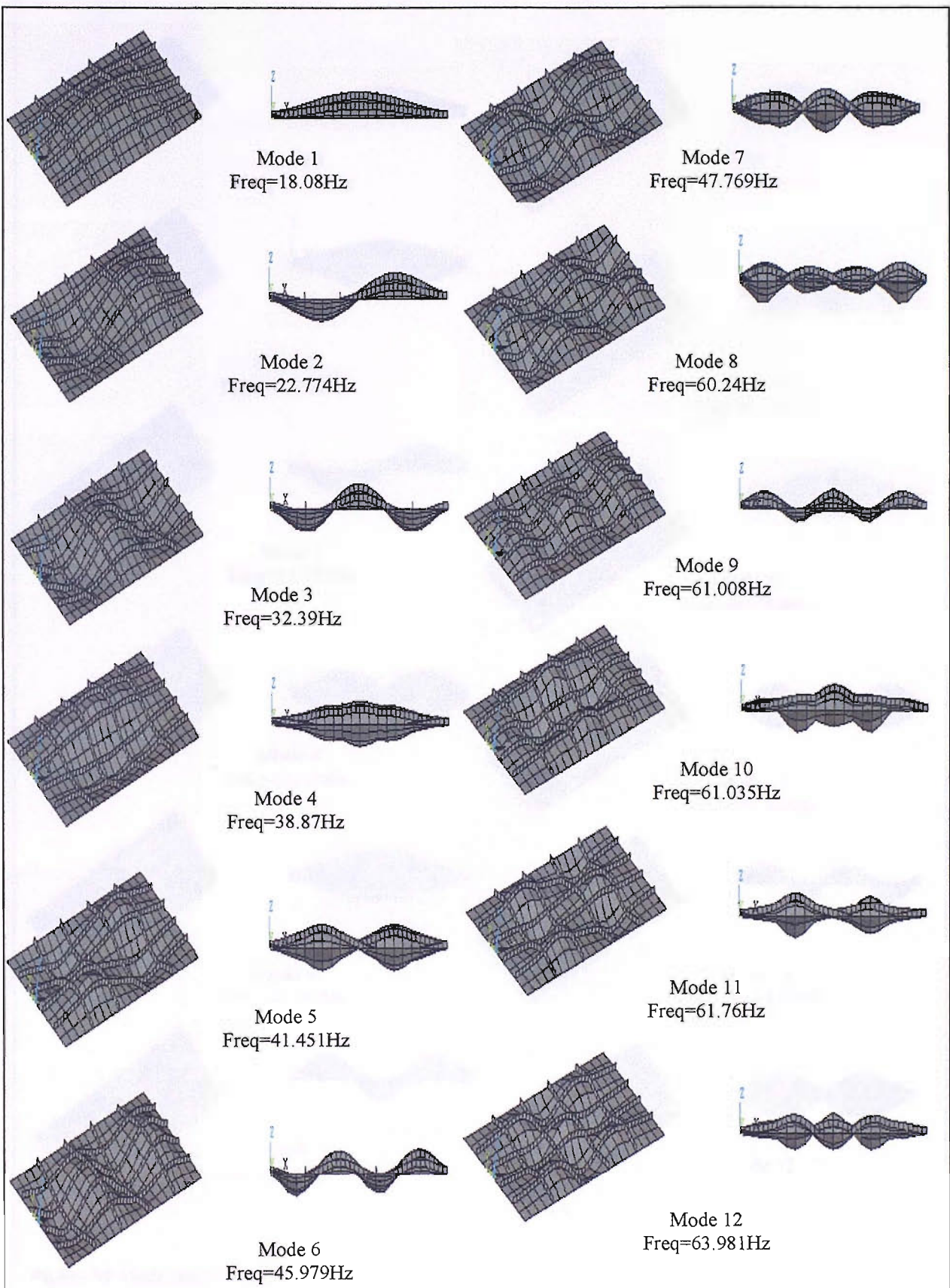


Figure 97 Mode shapes and natural frequencies of the orthogonal stiffened (Shell99-no tripping), fixed end flat plate (Shell99)



Figure 98 Mode shapes and natural frequencies of the longitudinal stiffened (Beam44), fixed end flat plate (Shell99)

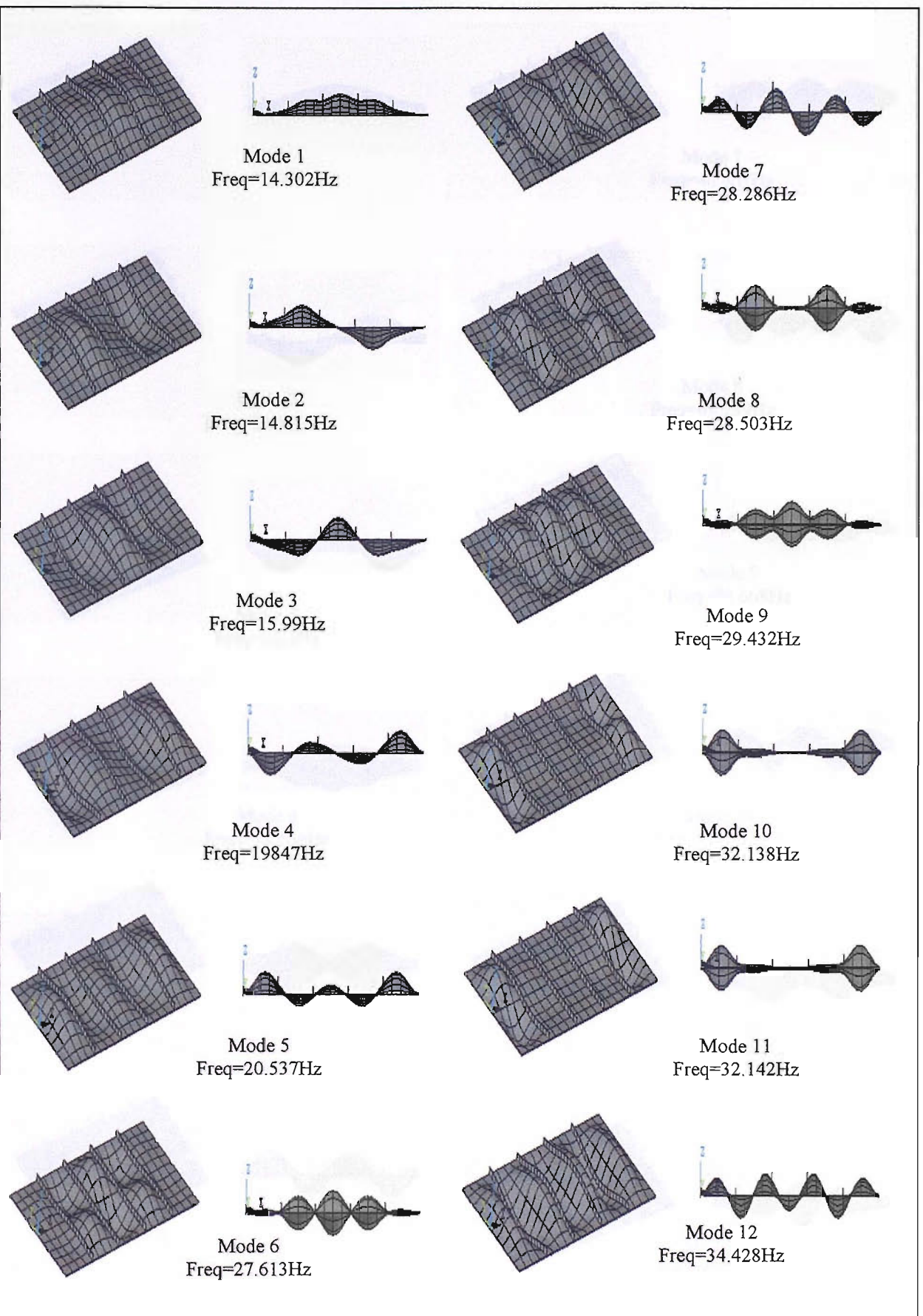


Figure 99 Mode shapes and natural frequencies of the transversely stiffened (Beam44), fixed end flat plate (Shell99)

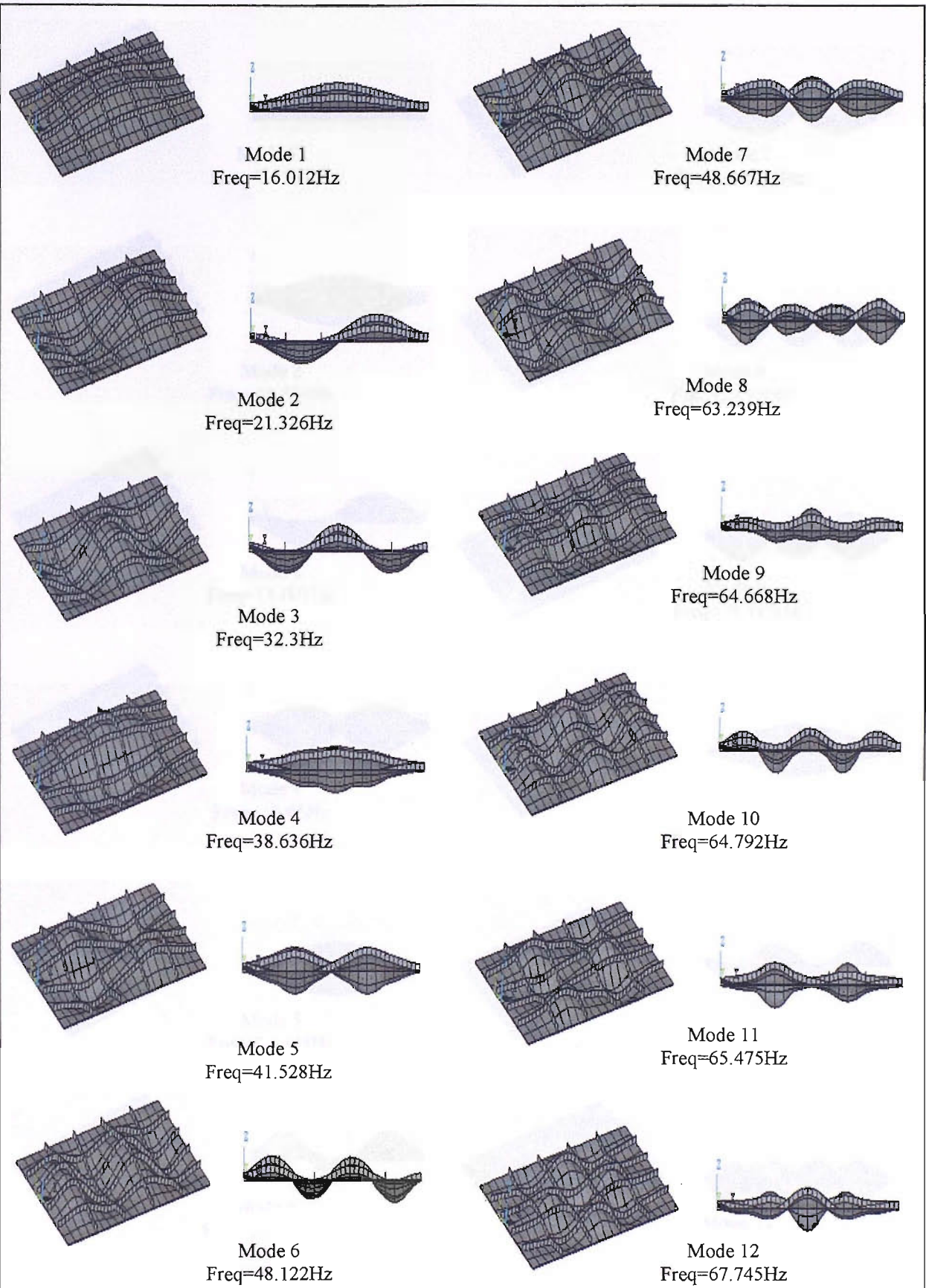


Figure 100 Mode shapes and natural frequencies of the orthogonal stiffened (Beam44), fixed end flat plate (Shell99)

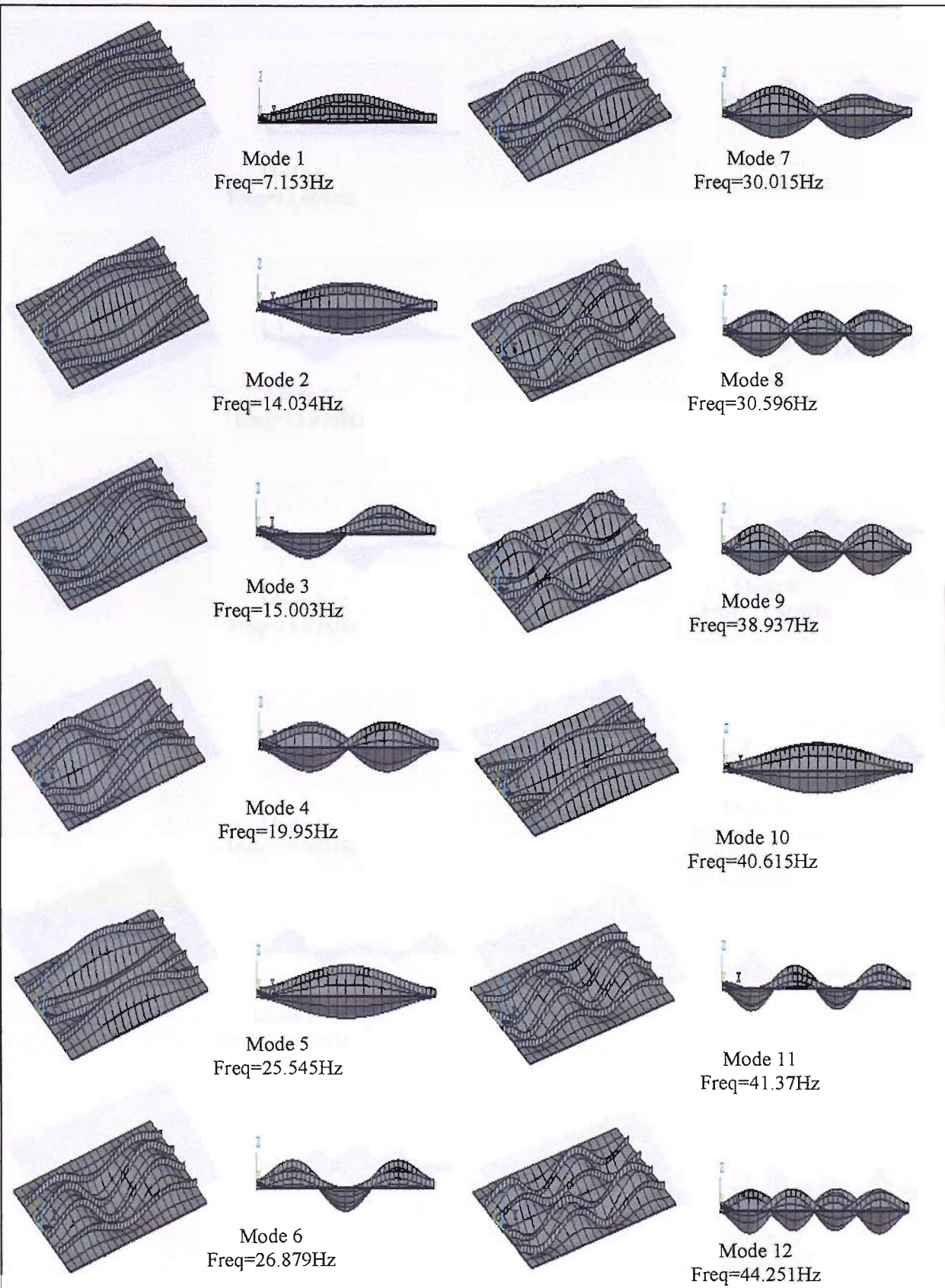


Figure 101 Mode shapes and natural frequencies of the longitudinal stiffened (Shell99), fixed end flat plate (Shell99)

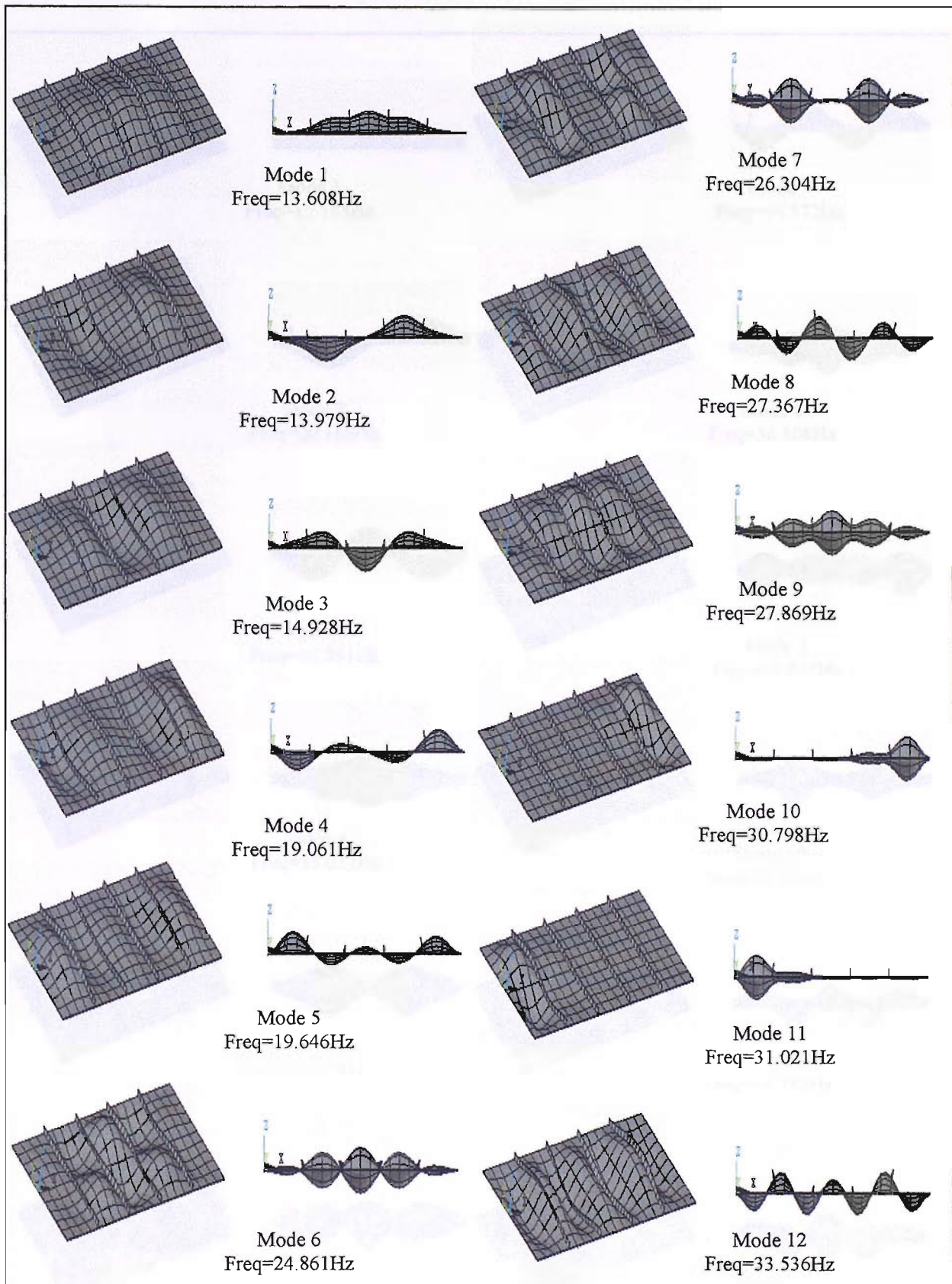


Figure 102 Mode shapes and natural frequencies of the transversely stiffened (Shell99), fixed end flat plate (Shell99)

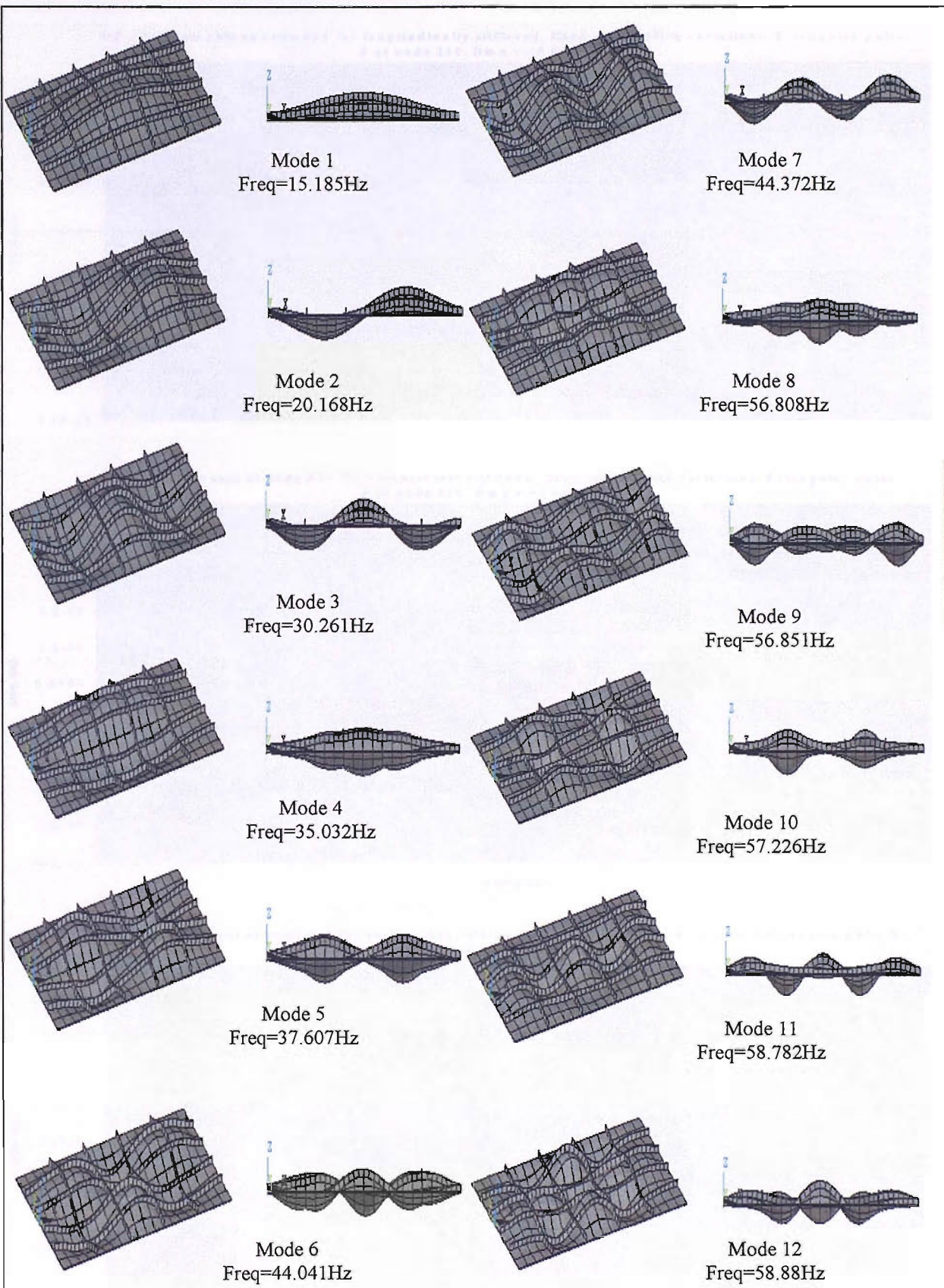
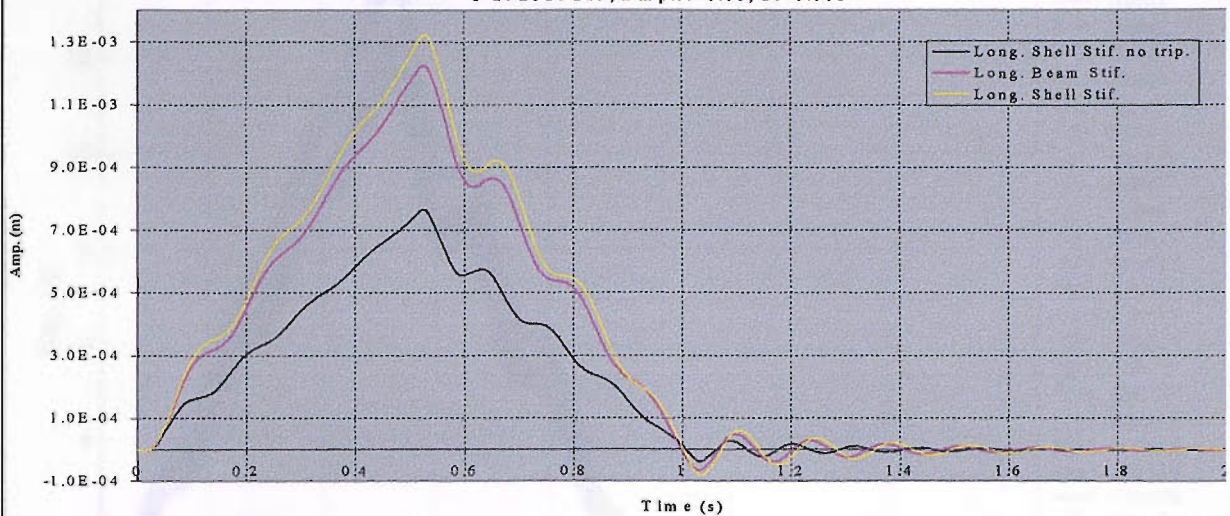
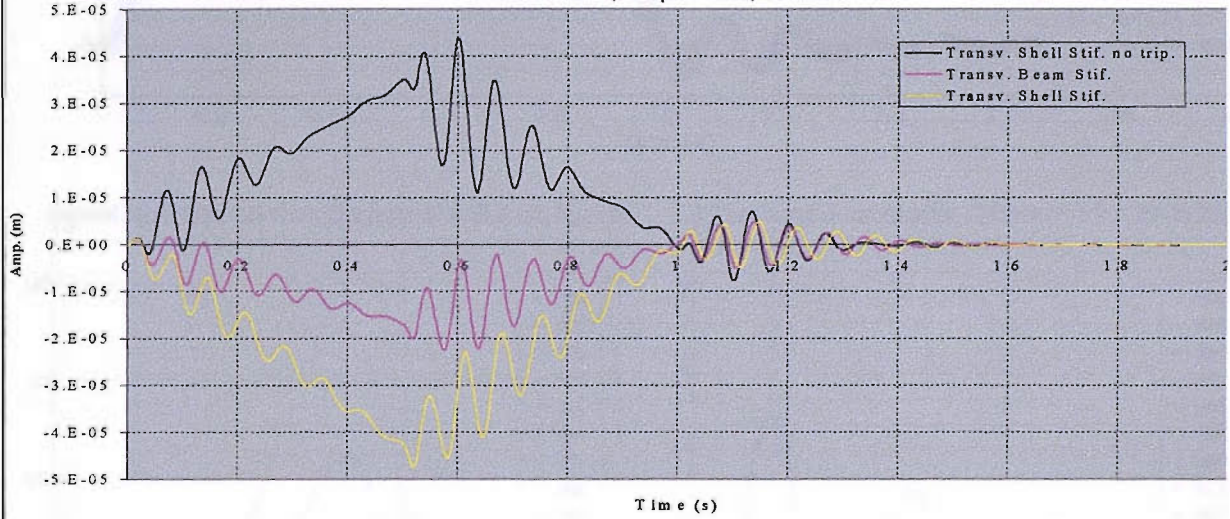


Figure 103 Mode shapes and natural frequencies of the orthogonal stiffened (Shell99), fixed end flat plate (Shell99)

UZ displacements at node 391 for longitudinally stiffened, fixed ended plate variations, Triangular pulse-
 F at node 219, D m p.r.=0.08, dt=0.005



UZ displacements at node 391 for transversely stiffened, fixed ended plate variations, Triangular pulse-
 F at node 219, D m p.r.=0.08, dt=0.005



UZ displacements at node 391 for orthogonal stiffened, fixed ended plate variations, Triangular pulse-F
 at node 219, D m p.r.=0.08, dt=0.005

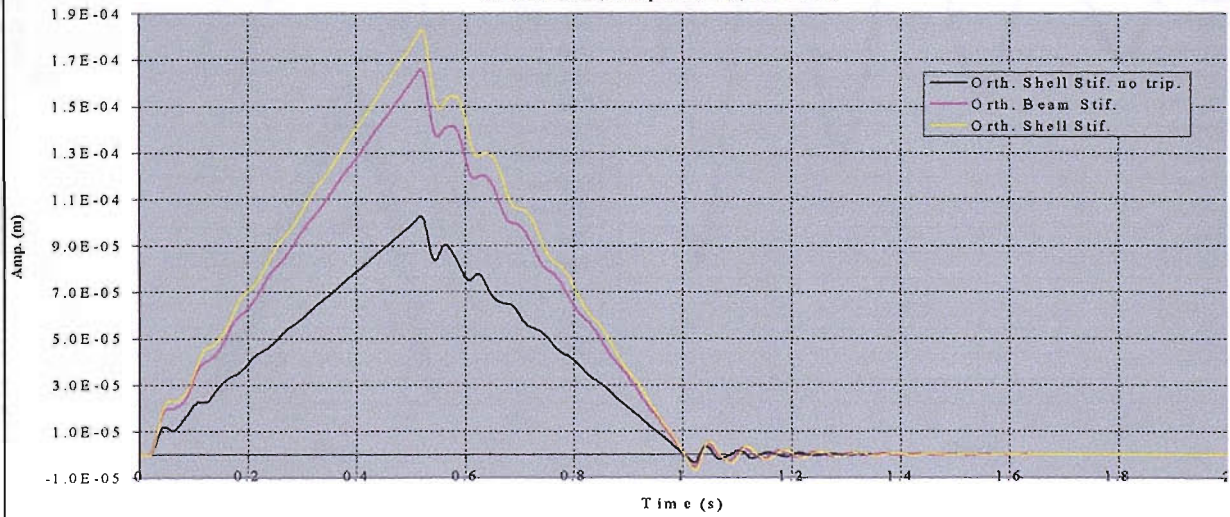
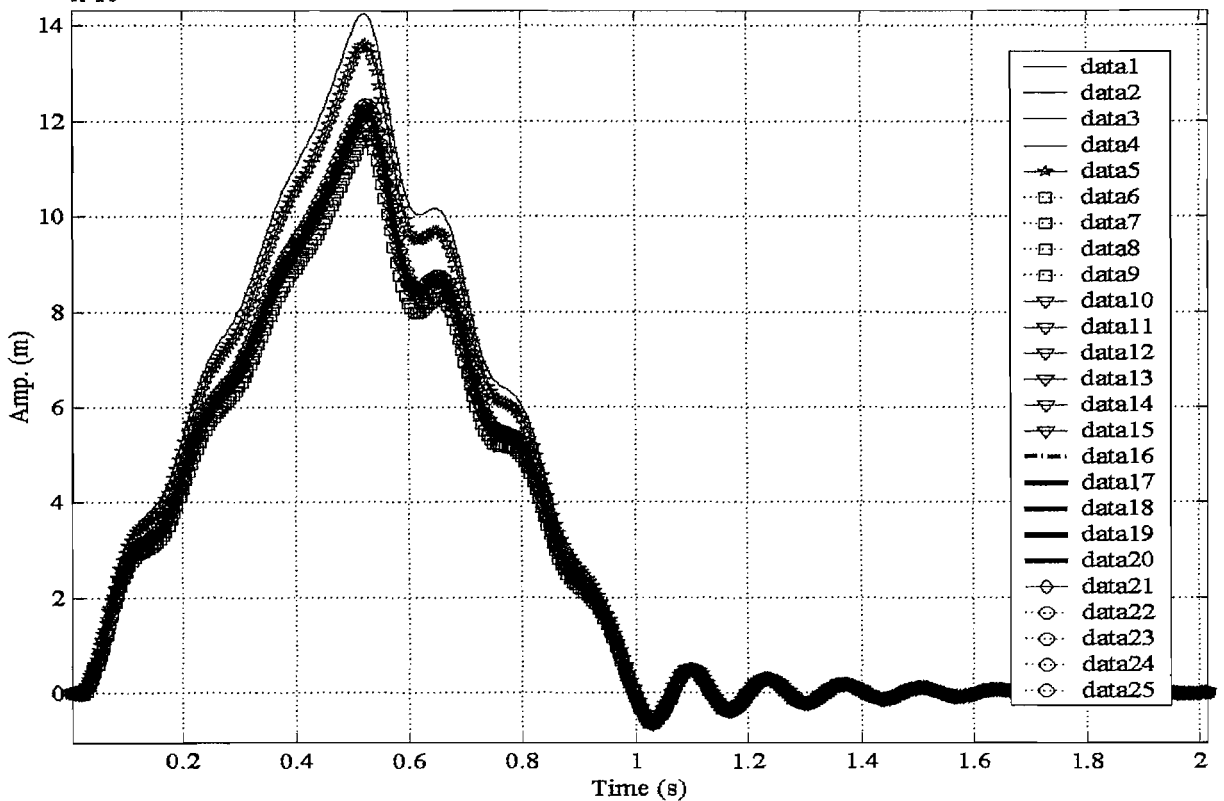
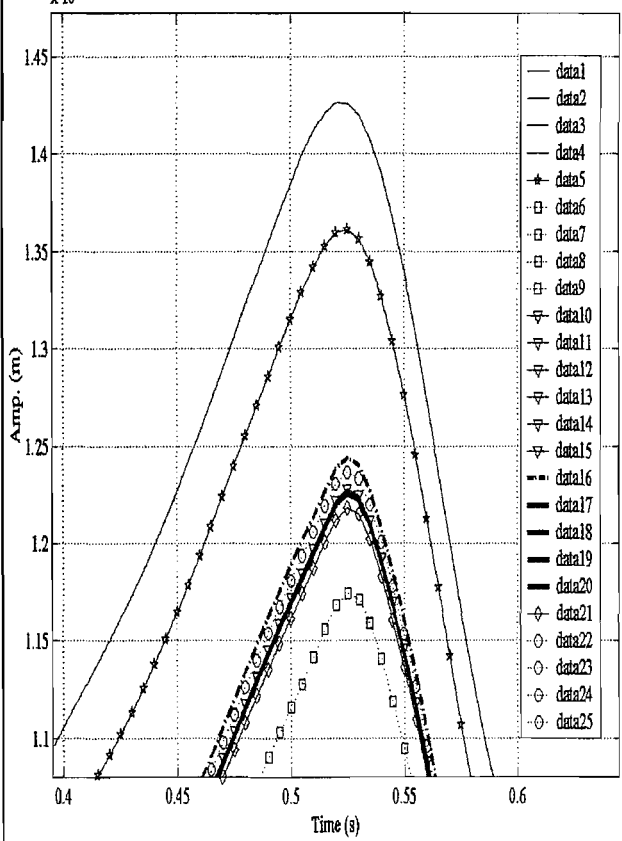


Figure 104 uz-displacements at node 391 for long., transv. and orth. stiffened plates under triangular pulse

Fixed-ended longitudinally beam stiffened plate, UZ-displacement at node 391, $dt=0.005$, $dmp.r.=0.08$



Fixed-ended longitudinally beam stiffened plate, UZ-displacement at node 391, $dt=0.005$, $dmp.r.=0.08$



Fixed-ended longitudinally beam stiffened plate, UZ-displacement at node 391, $dt=0.005$, $dmp.r.=0.08$

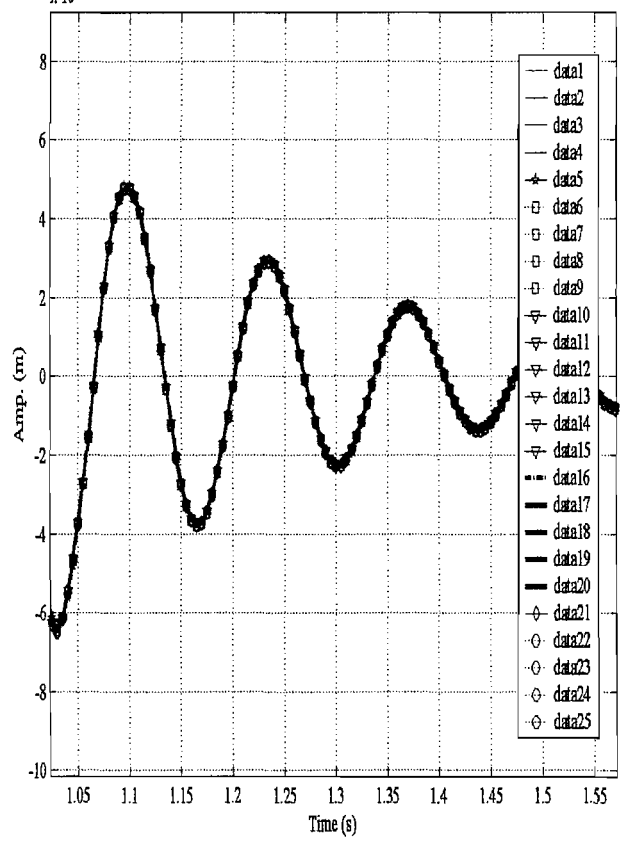
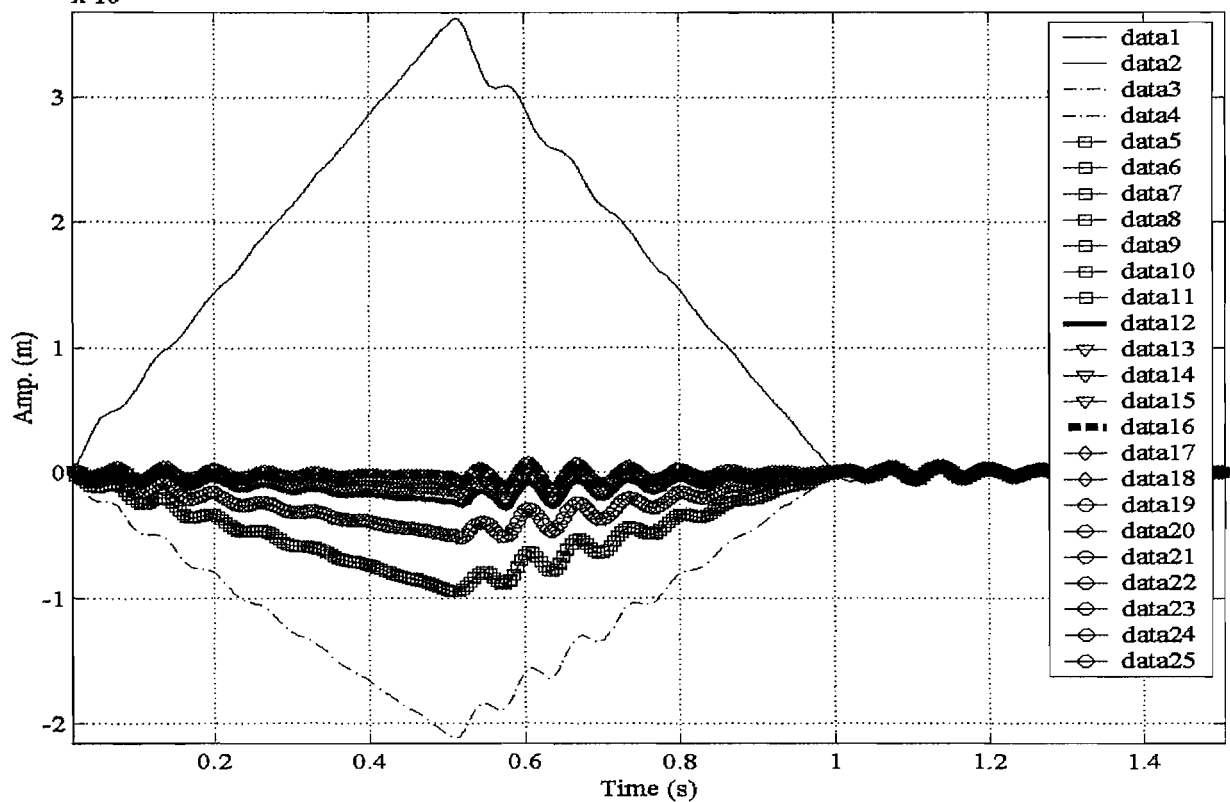


Figure 105 UZ-displacements at node 391 for clamped long. stiffened plate using 1-25 transient mode superposition, $dmp.r.=0.08$, $dt=0.005s$.

Fixed ended transversely beam stiffened plate, UZ-displacement at node 391, dt=0.005, dmp.r.=0.08



Fixed ended transversely beam stiffened plate, UZ-displacement at node 391, dt=0.005, dmp.r.=0.08

Fixed ended transversely beam stiffened plate, UZ-displacement at node 391, dt=0.005, dmp.r.=0.08

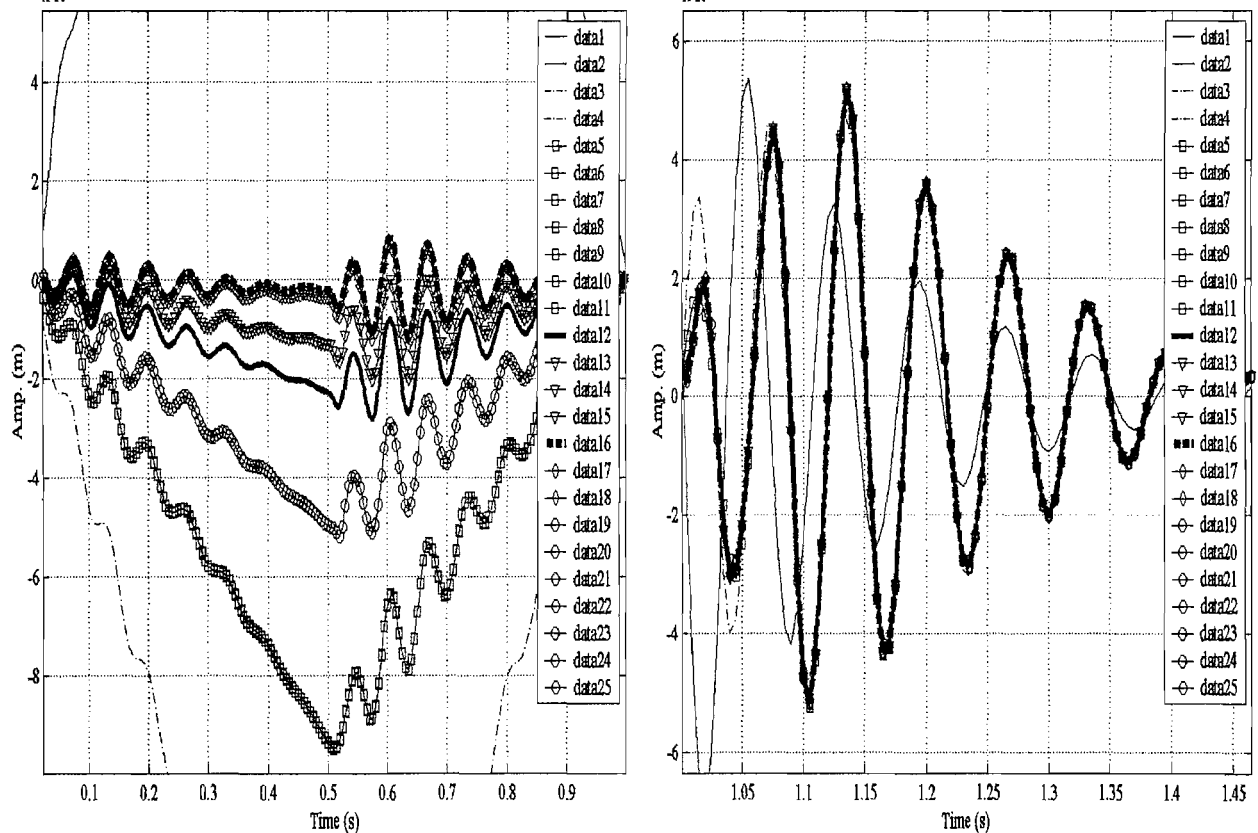
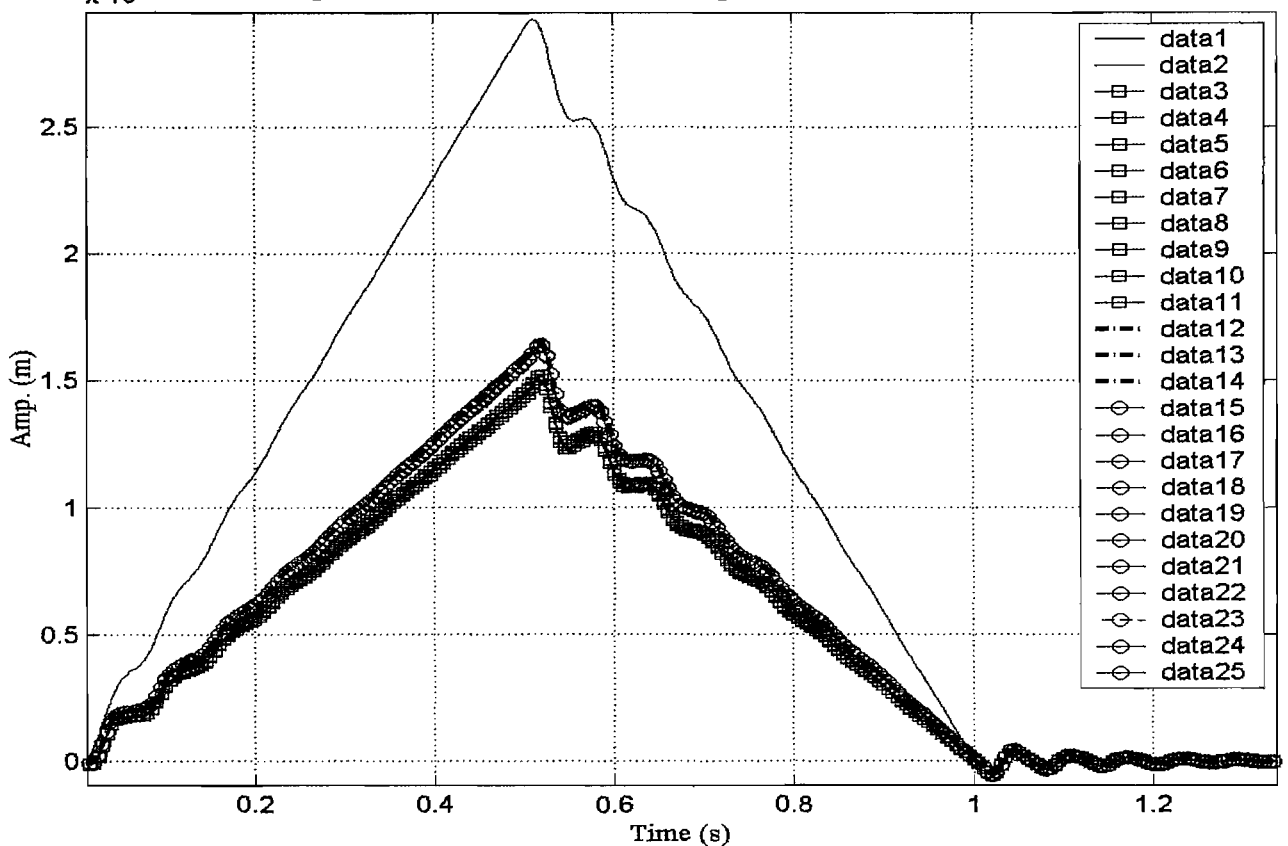
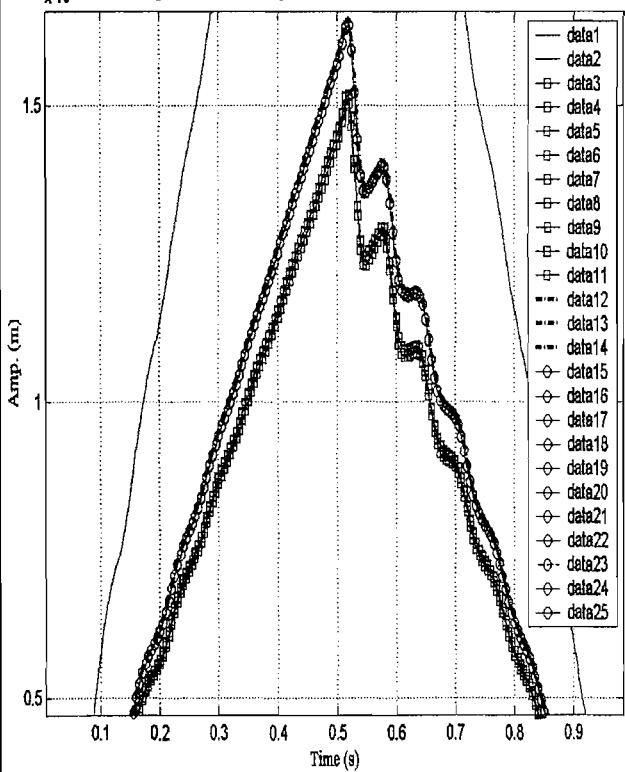


Figure 106 UZ-displacements at node 391 for clamped transv. stiffened plate using 1-25 transient mode superposition, dmp.r.=0.08, dt=0.005s.

Fixed ended orthogonal beam stiffened plate, UZ-displacement at node 391, dt=0.005, dmp.r.=0.08



Fixed ended orthogonal beam stiffened plate, UZ-displacement at node 391, dt=0.005, dmp.r.=0.08



Fixed ended orthogonal beam stiffened plate, UZ-displacement at node 391, dt=0.005, dmp.r.=0.08

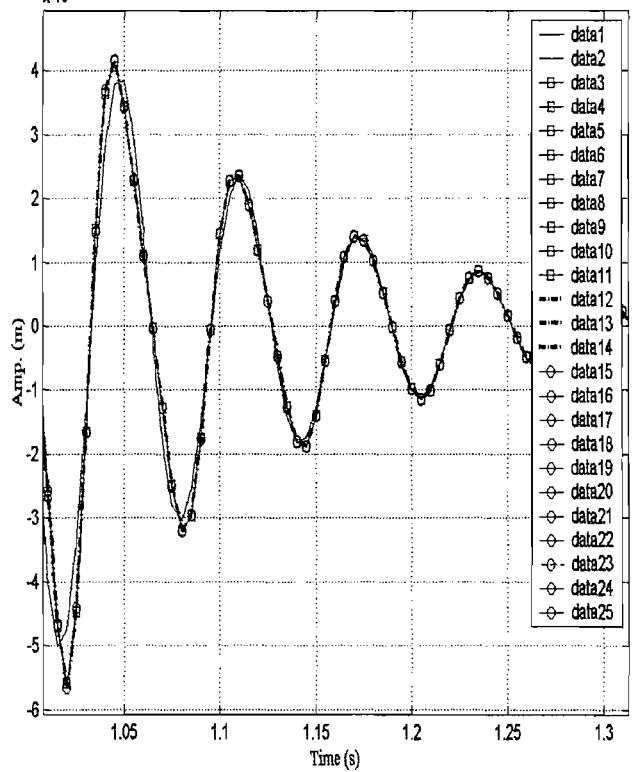


Figure 107 UZ-displacements at node 391 for clamped orth. stiffened plate using 1-25 transient mode superposition, dmp.r.=0.08, dt=0.005s.

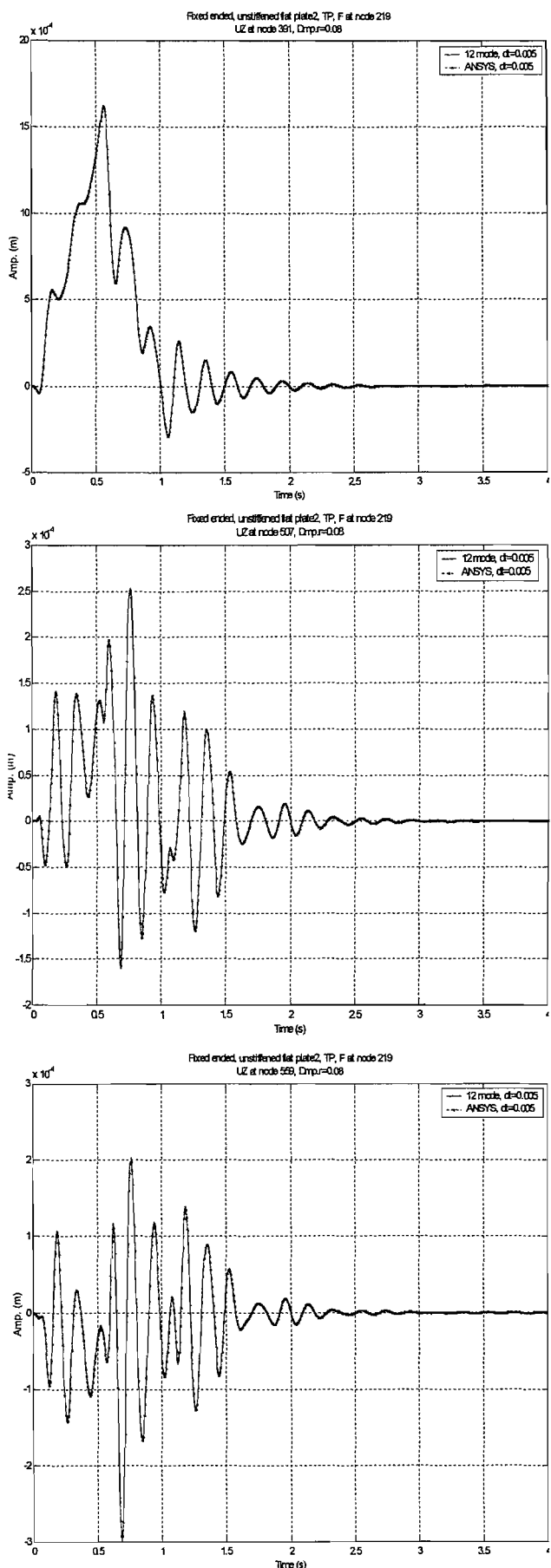


Figure 108 Unstiffened clamped plate uz- amplitudes and sx-stresses for nodes 391, 559,507

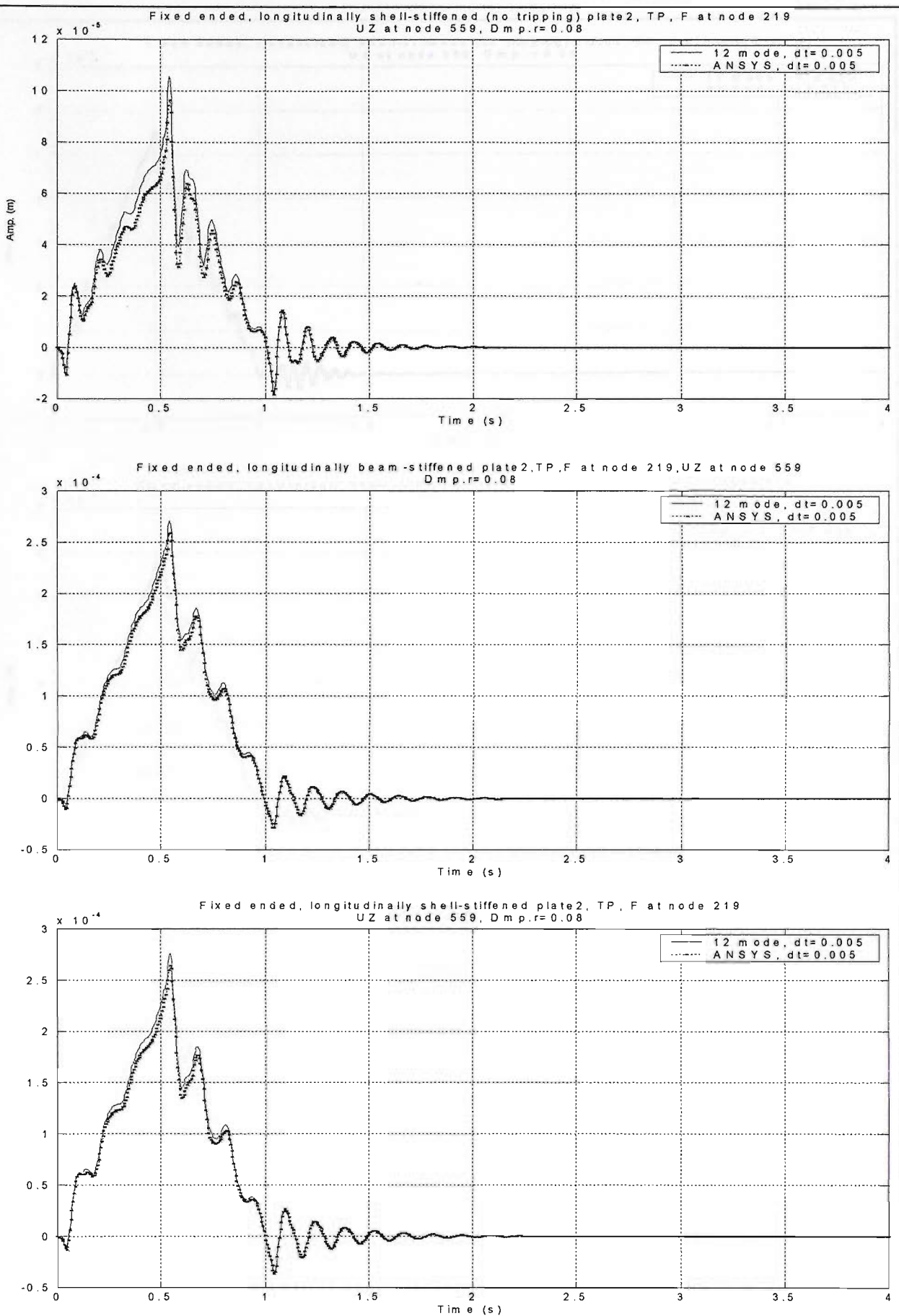


Figure 109 Fixed ended (FE) long. stiffened plate, uz-amplitudes at node 559 for three types of stiffening elements, numerical method $dt=0.005s$.

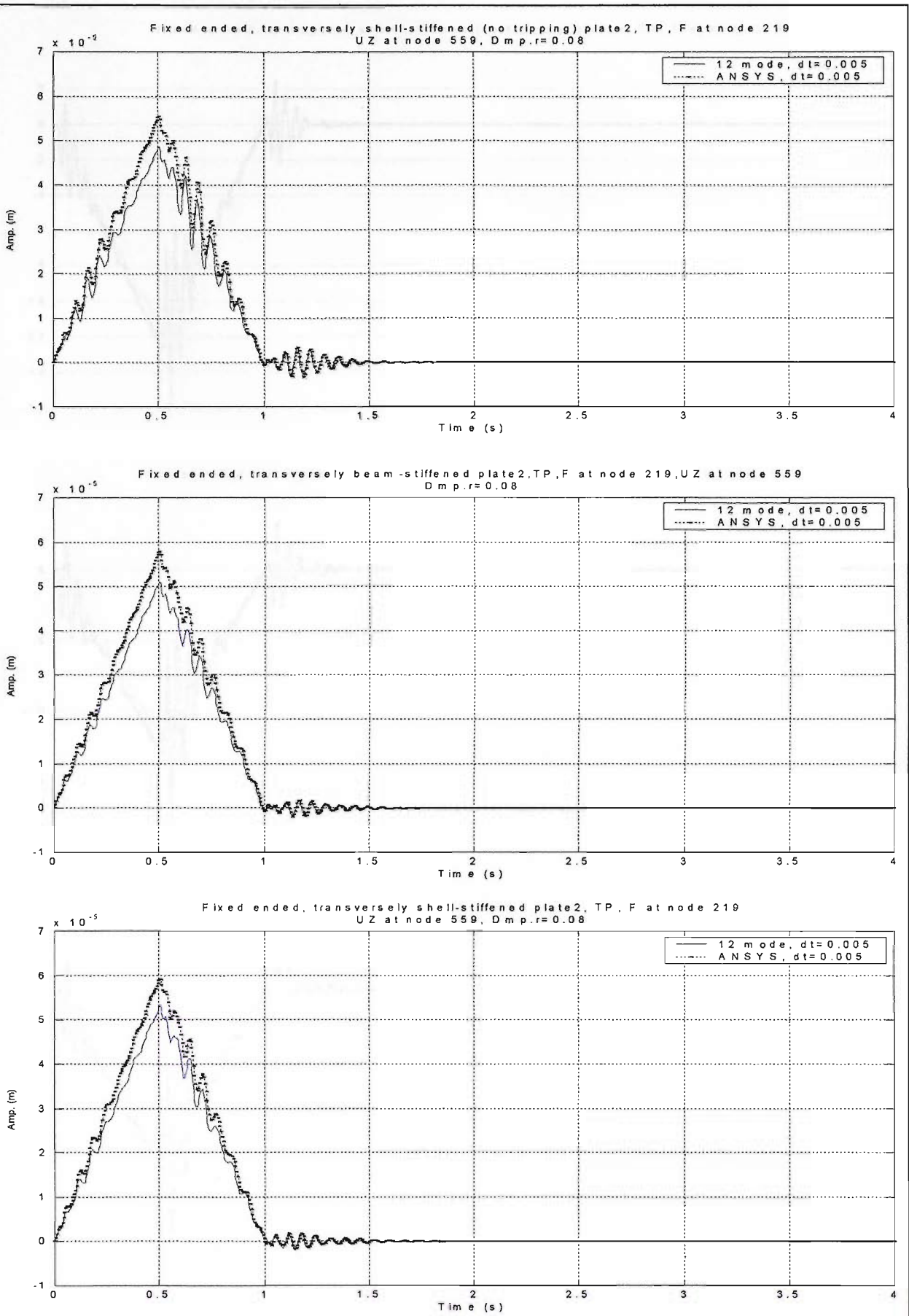
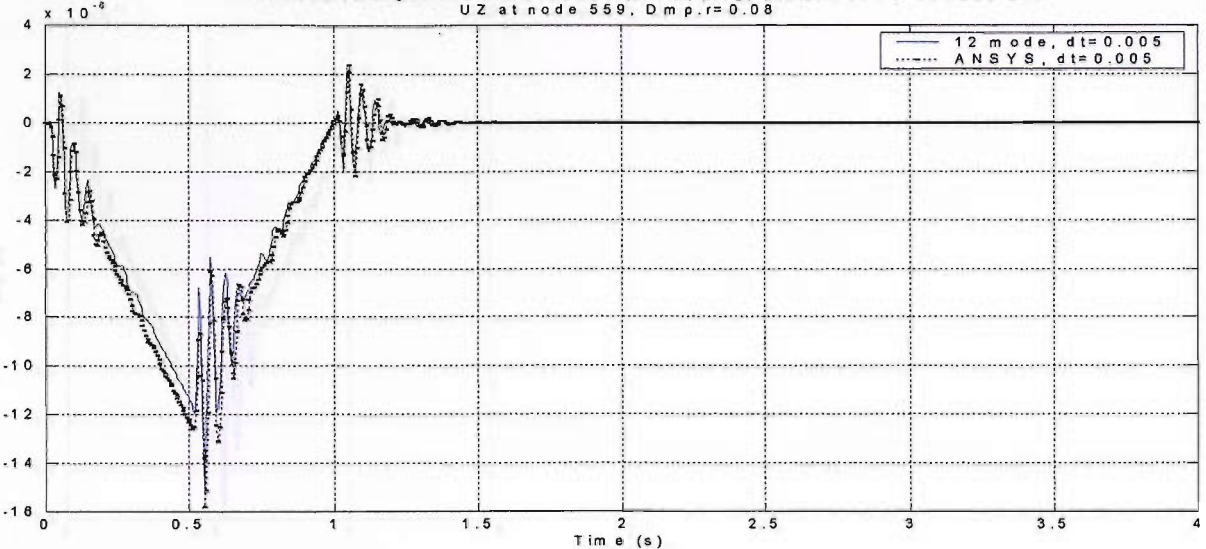
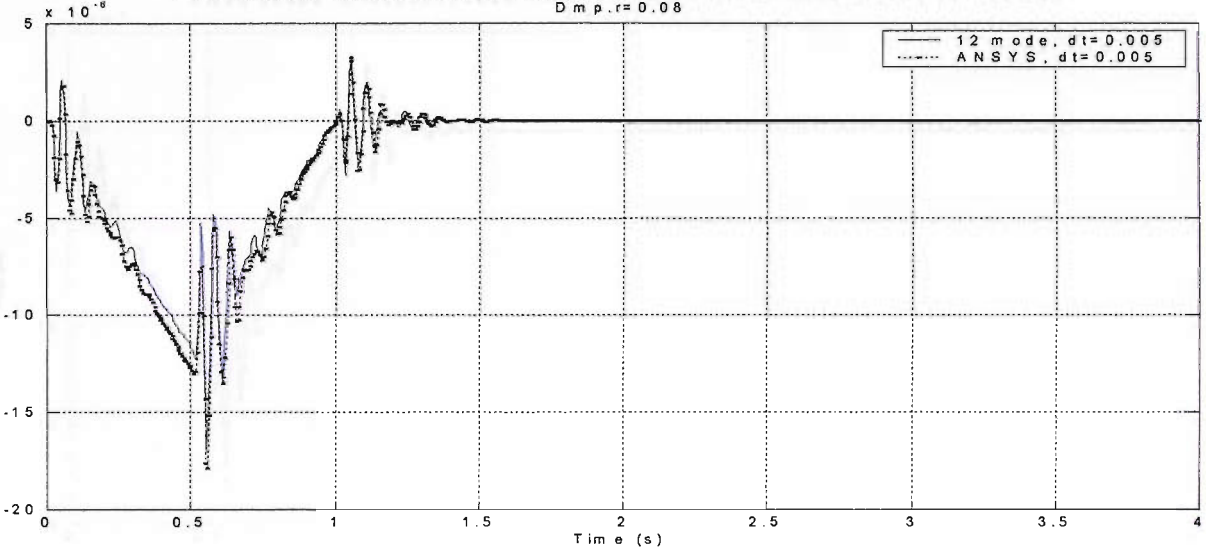


Figure 110 Fixed ended (FE) transv. stiffened plate, uz-amplitudes at node 559 for three types of stiffening elements, numerical method dt=0.005s.

Fixed ended, orthogonal shell-stiffened (no tripping) plate 2, TP, F at node 219
UZ at node 559, Dmp.r=0.08



Fixed ended, orthogonal beam-stiffened plate 2, TP, F at node 219, UZ at node 559
Dmp.r=0.08



Fixed ended, orthogonal shell-stiffened plate 2, TP, F at node 219
UZ at node 559, Dmp.r=0.08

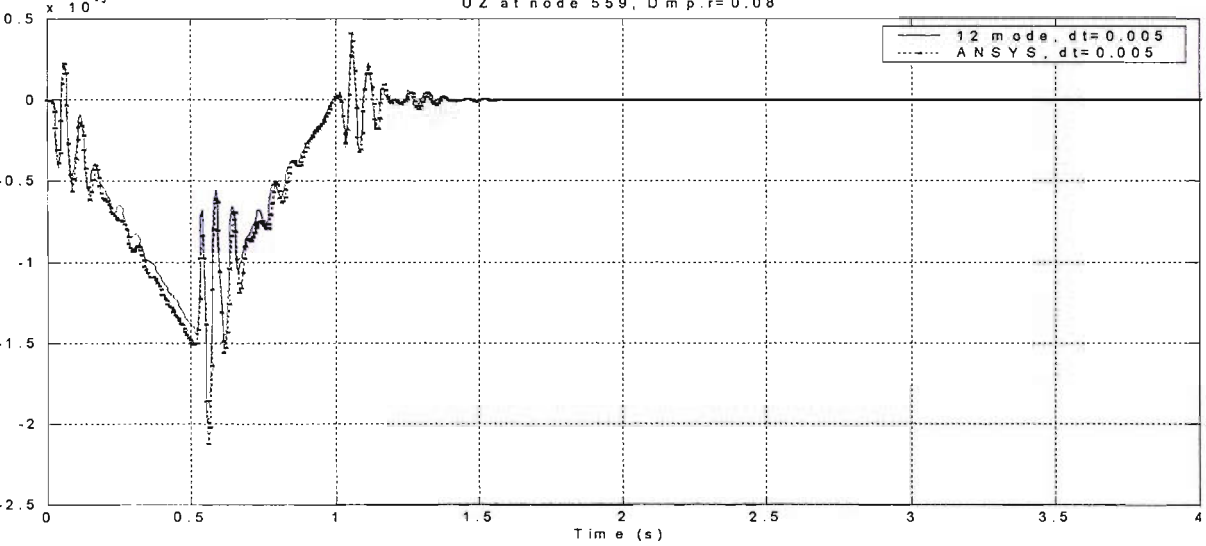
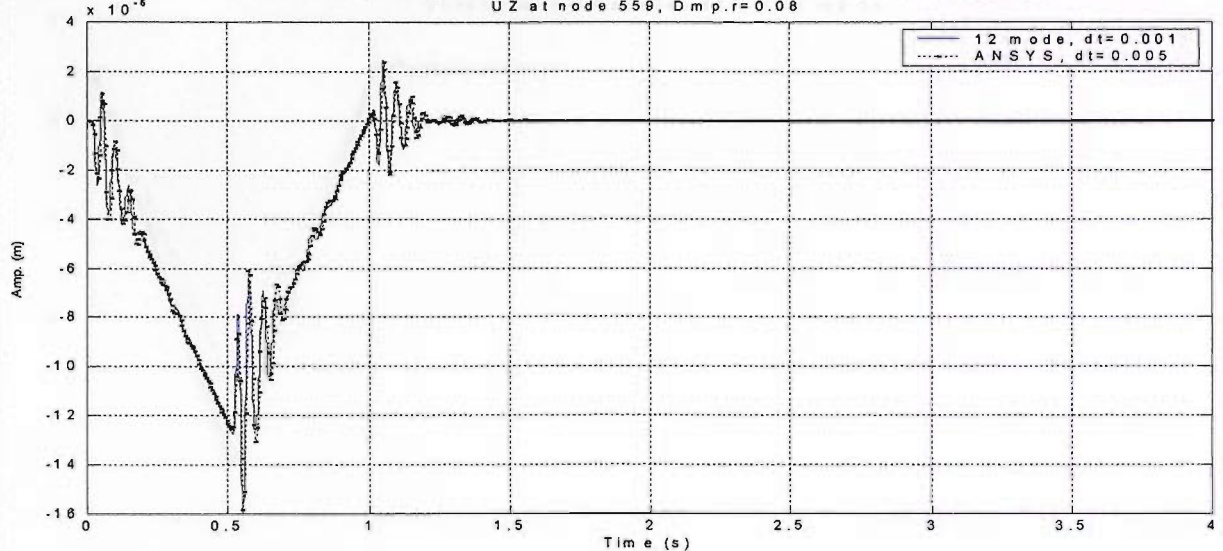
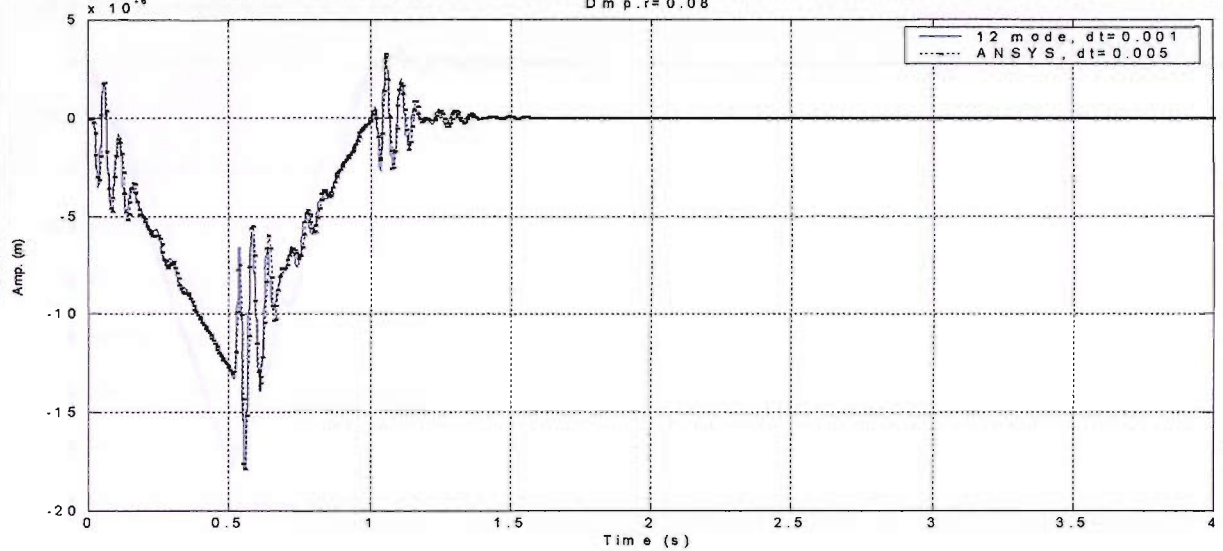


Figure 111 FE orth. stiffened plate, uz-amplitudes at node 559 for three types of stiffening elements,
numerical method dt=0.005s.

Fixed ended, orthogonal shell-stiffened (no tripping) plate2,TP, F at node 219
UZ at node 559, Dmp.r=0.08



Fixed ended, orthogonal beam-stiffened plate2,TP, F at node 219, UZ at node 559
Dmp.r=0.08



Fixed ended, orthogonal shell-stiffened plate2,TP, F at node 219, UZ at node 559
Dmp.r=0.08

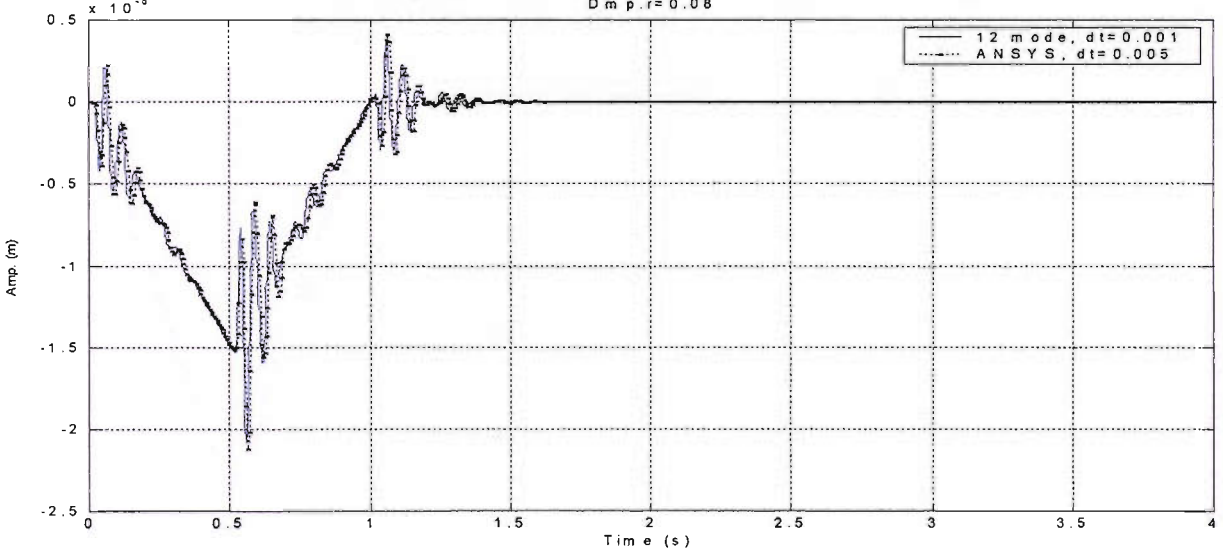


Figure 112 FE orth. stiffened plate, uz-amplitudes at node 559 for three types of stiffening elements,
numerical method dt=0.001s.

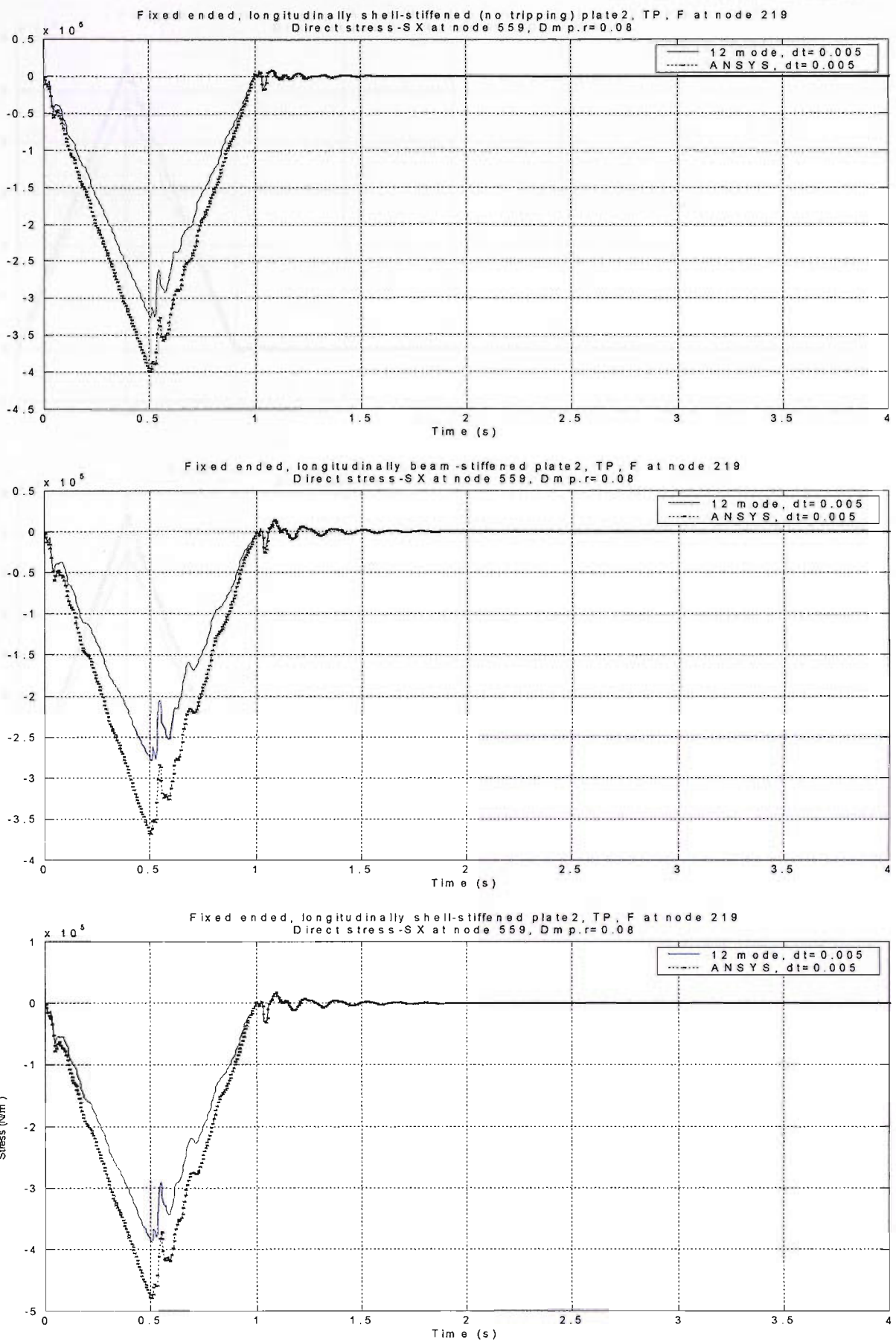
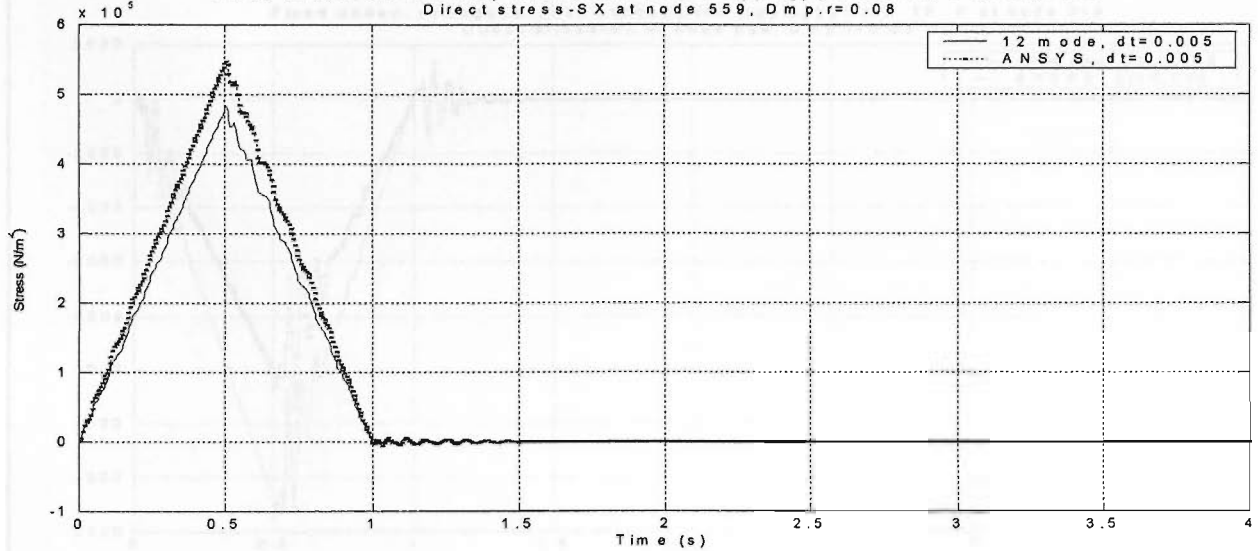
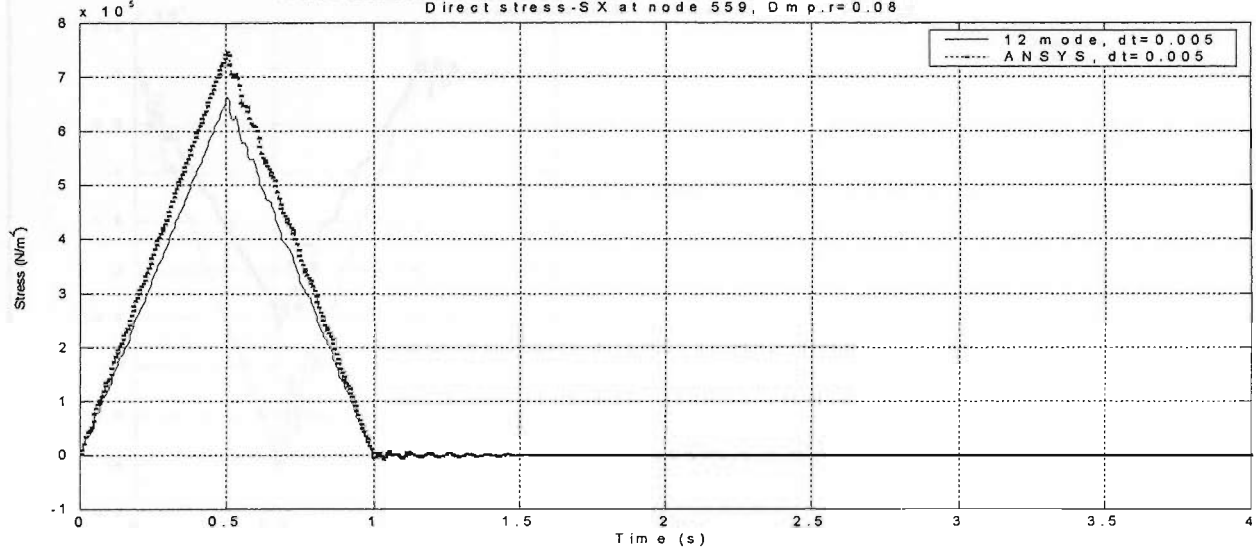


Figure 113 FE long. stiffened plate, sx-stresses at node 559 for three types of stiffening elements, numerical method dt=0.005s.

Fixed ended, transversely shell-stiffened (no tripping) plate2, TP, F at node 219
 Direct stress-SX at node 559, Dmp.r=0.08



Fixed ended, transversely beam-stiffened plate2, TP, F at node 219
 Direct stress-SX at node 559, Dmp.r=0.08



Fixed ended, transversely shell-stiffened plate2, TP, F at node 219
 Direct stress-SX at node 559, Dmp.r=0.08

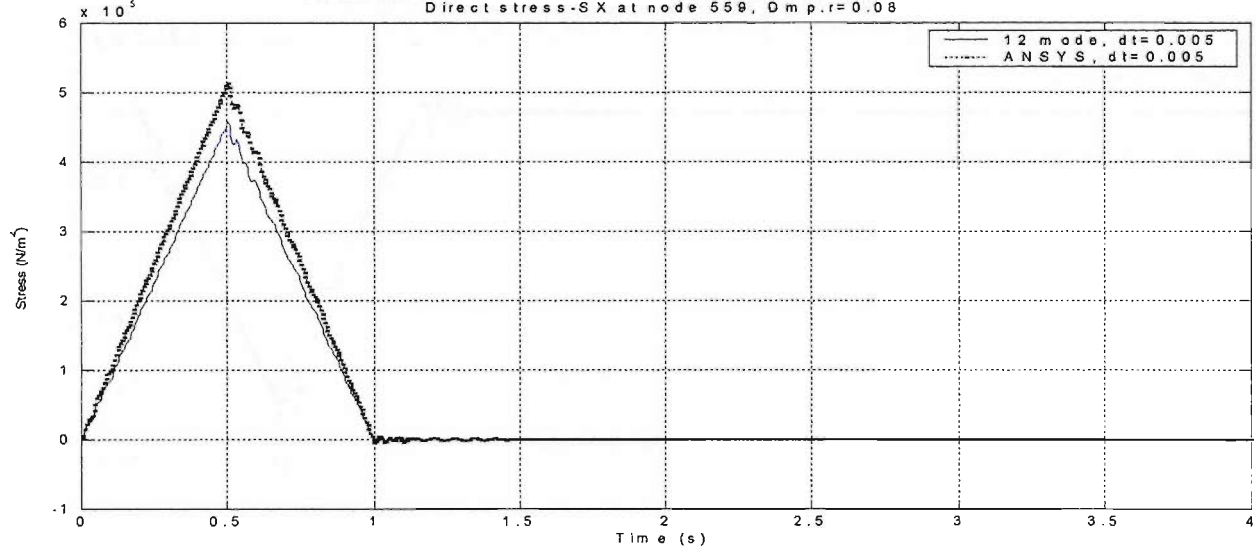
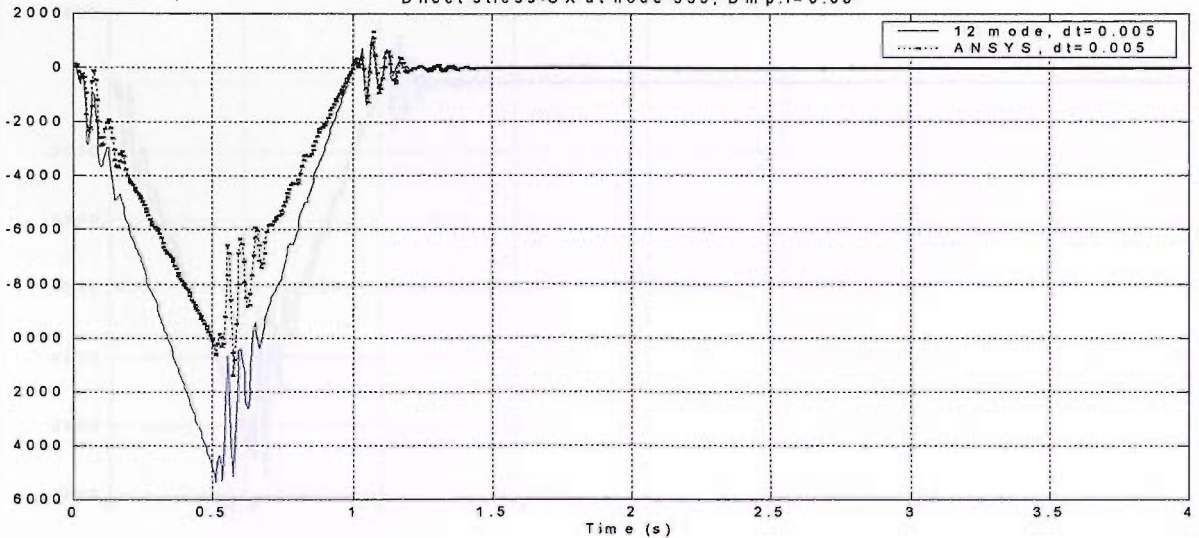
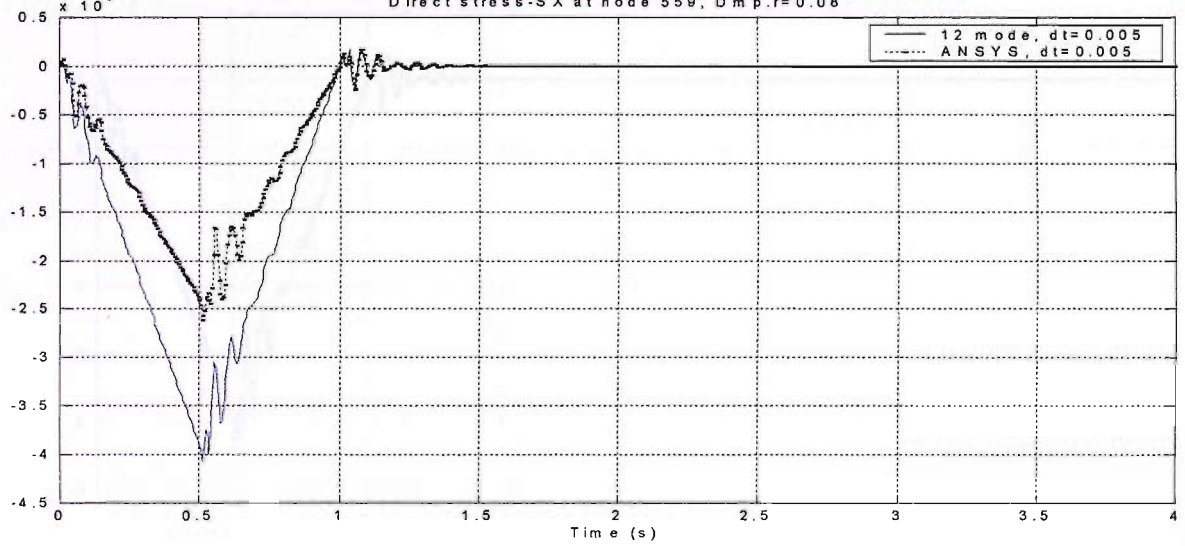


Figure 114 FE transv. stiffened plate, sx-stresses at node 559 for three types of stiffening elements, numerical method $\text{dt}=0.005\text{s}$.

Fixed ended, orthogonal shell-stiffened (no tripping) plate2, TP, F at node 219
Direct stress-SX at node 559, Dmp.r=0.08



Fixed ended, orthogonal beam -stiffened plate2, TP, F at node 219
Direct stress-SX at node 559, Dmp.r=0.08



Fixed ended, orthogonal shell-stiffened plate2, TP, F at node 219
Direct stress-SX at node 559, Dmp.r=0.08

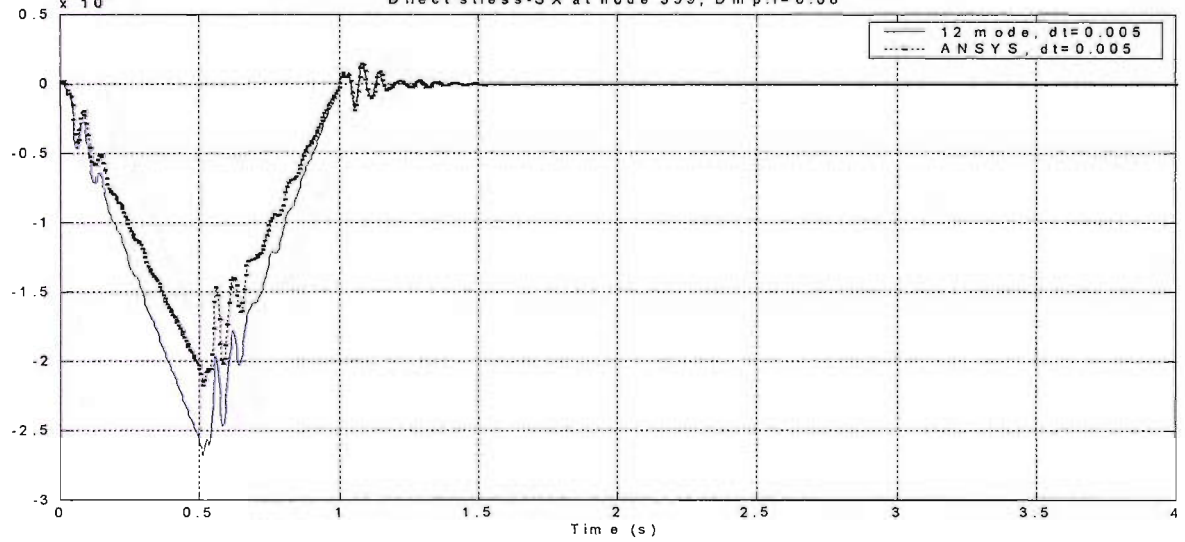


Figure 115 FE orth. stiffened plate, sx-stresses at node 559 for three types of stiffening elements,
numerical method dt=0.005s.

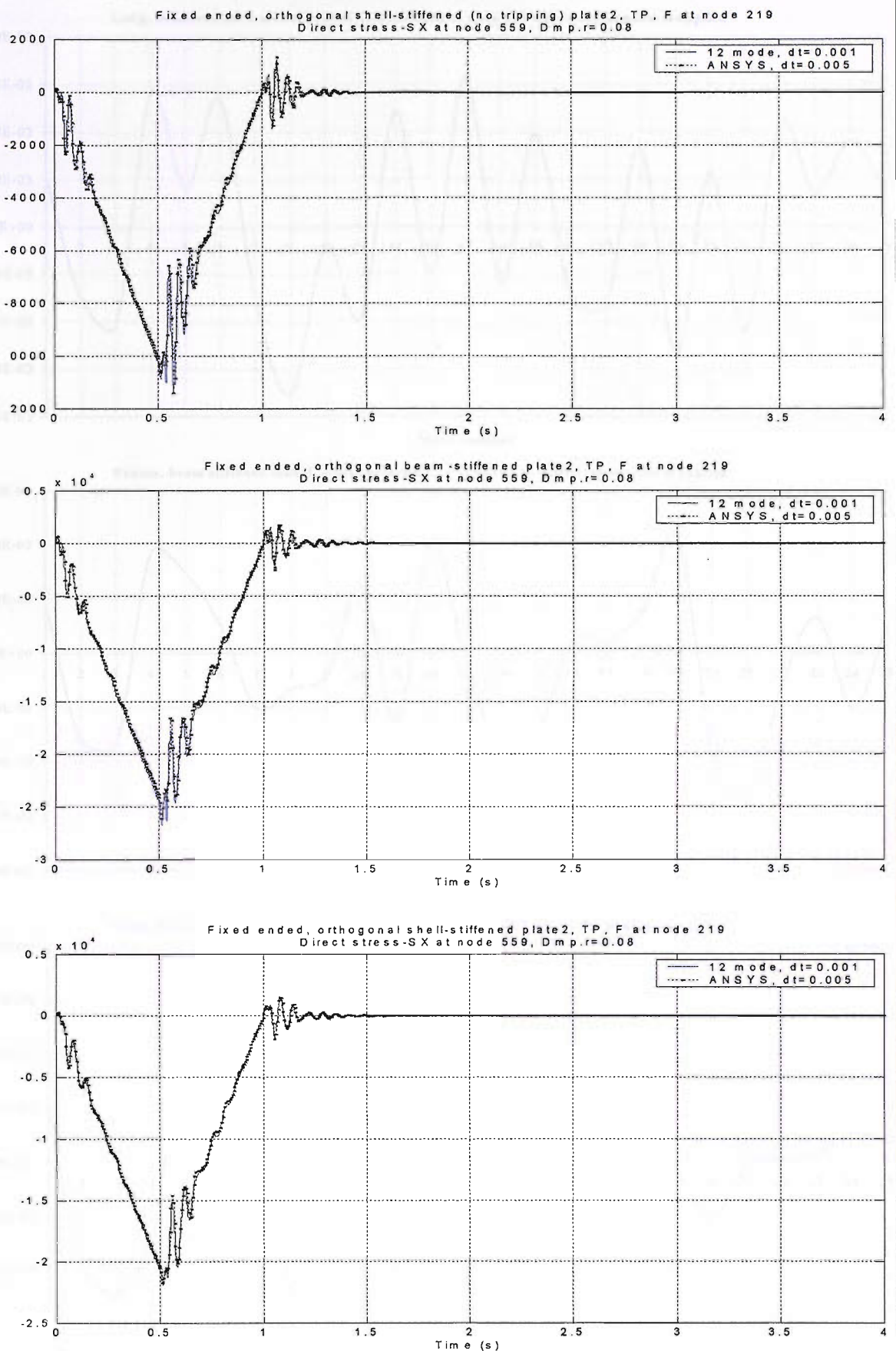


Figure 116 FE orth. stiffened plate, sx-stresses at node 559 for three types of stiffening elements, numerical method dt=0.001s.

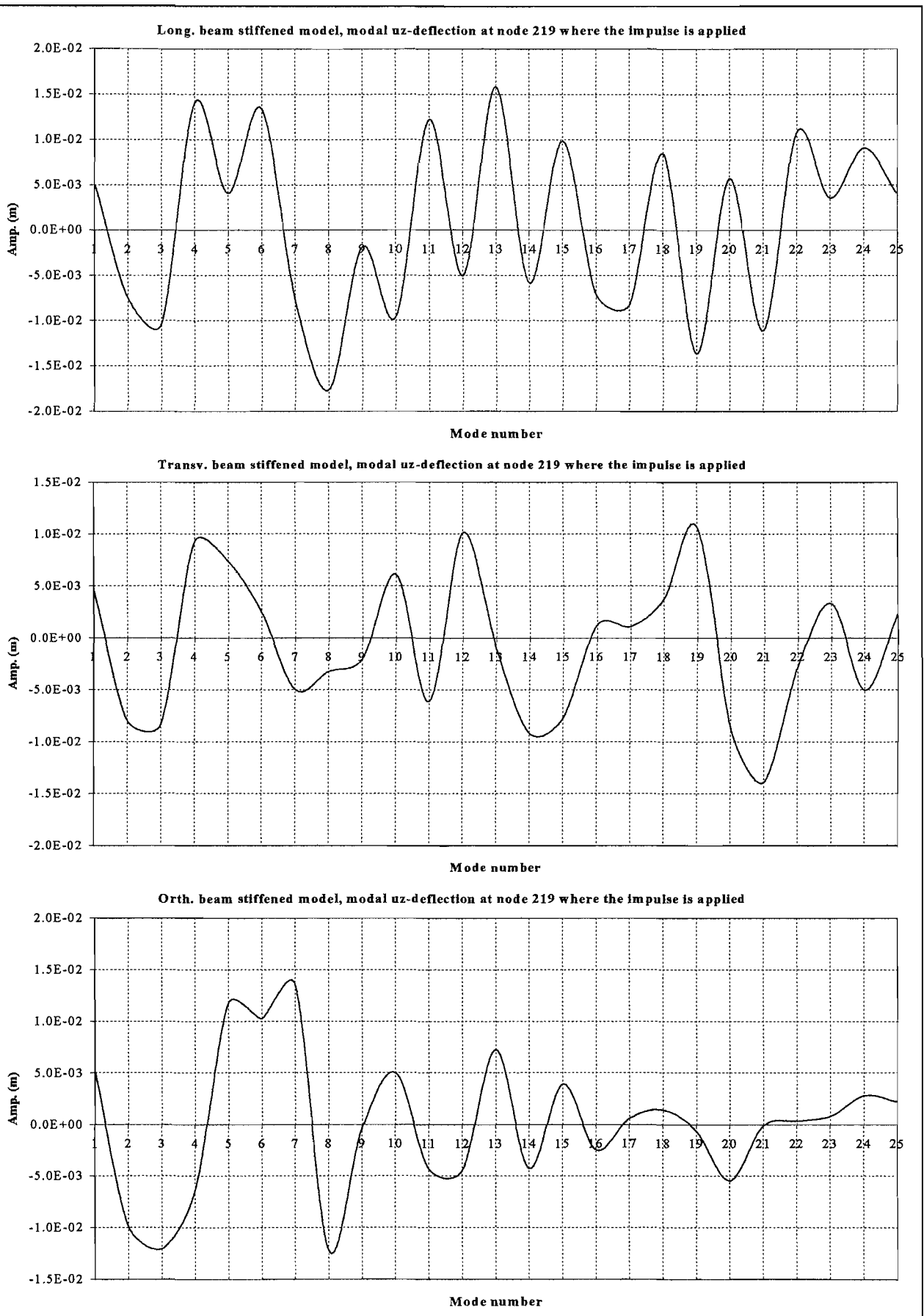


Figure 117 Modal uz-deflections at node 219 for three different stiffening directions

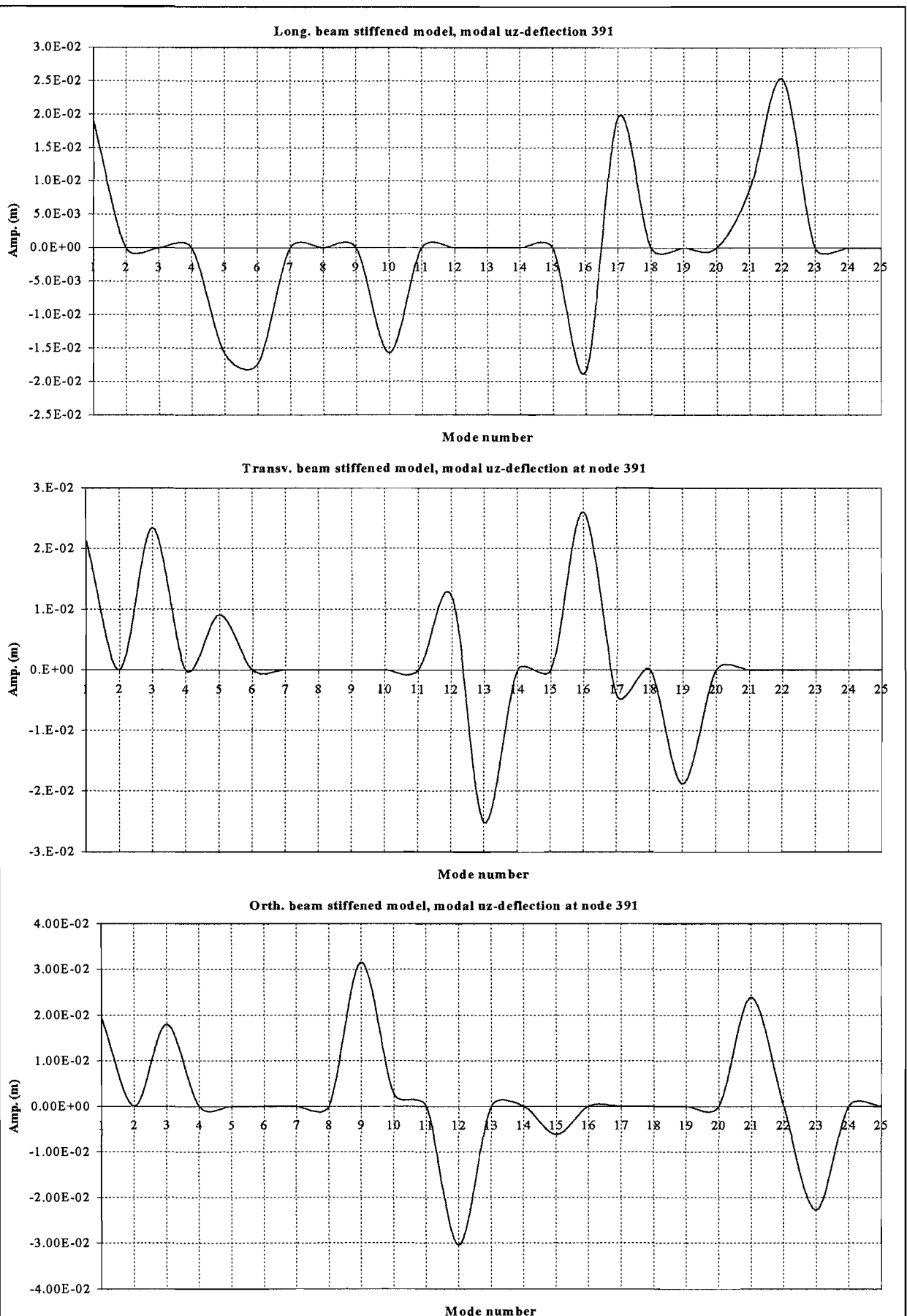


Figure 118 Modal uz-deflections at node 391 for three different stiffening directions

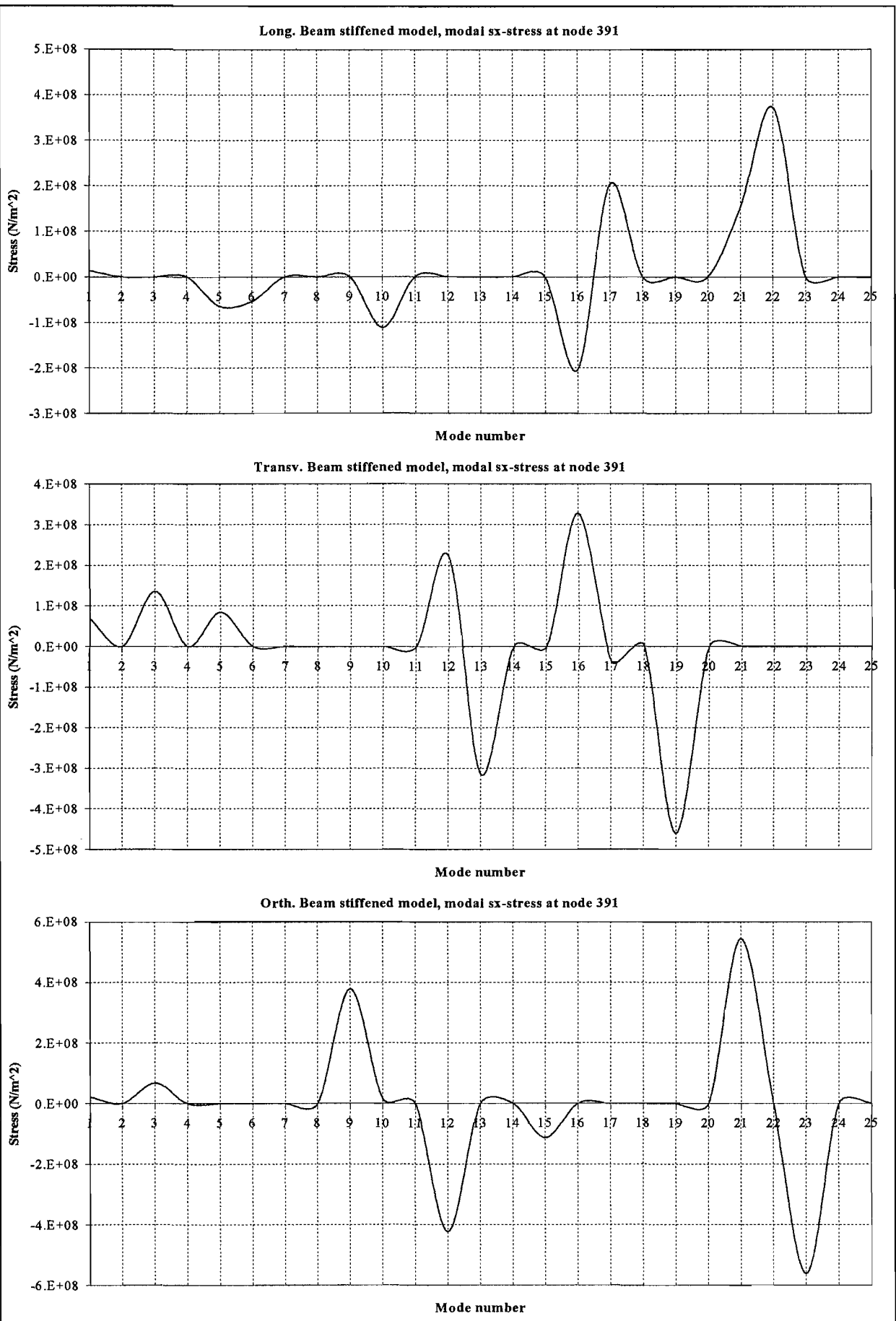


Figure 119 Modal sx-direct stresses at node 391 for three different stiffening directions

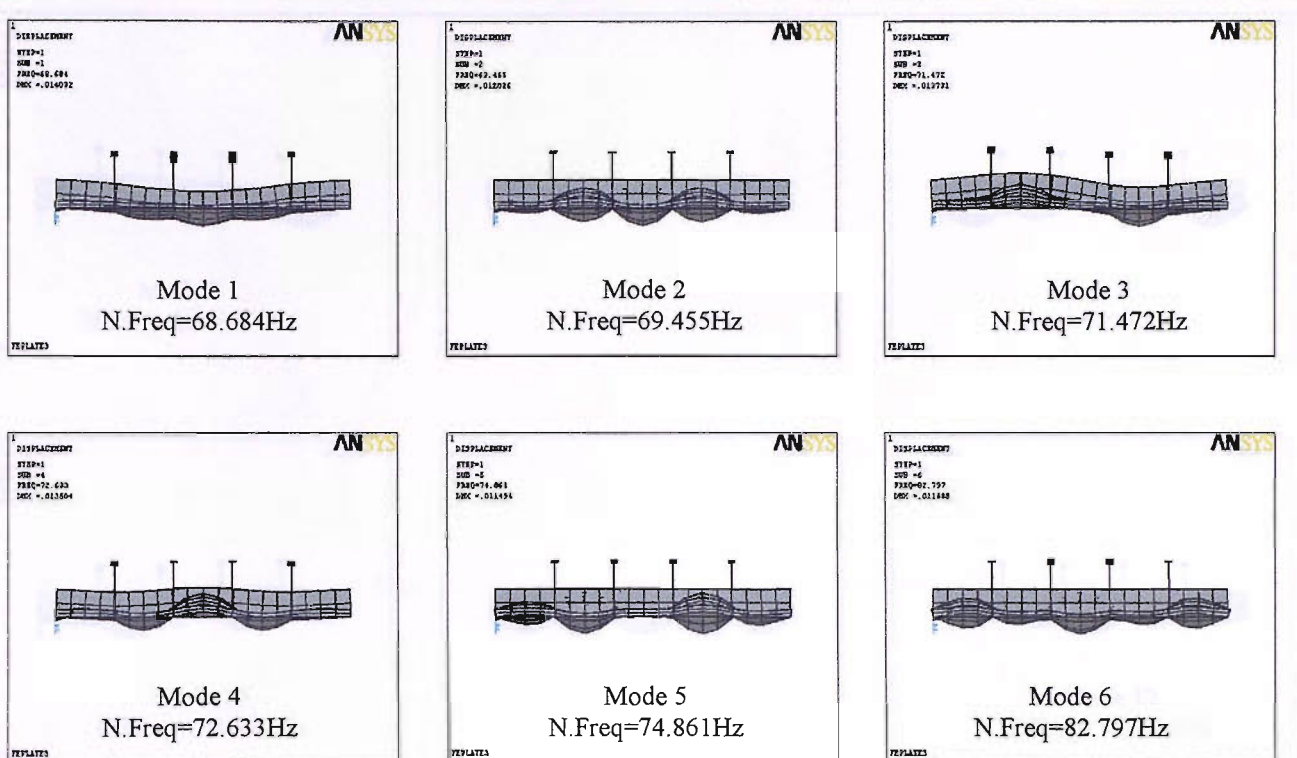


Figure 120 First six mode shapes of the stiffened (Beam-44) tanker plate (Profile view)

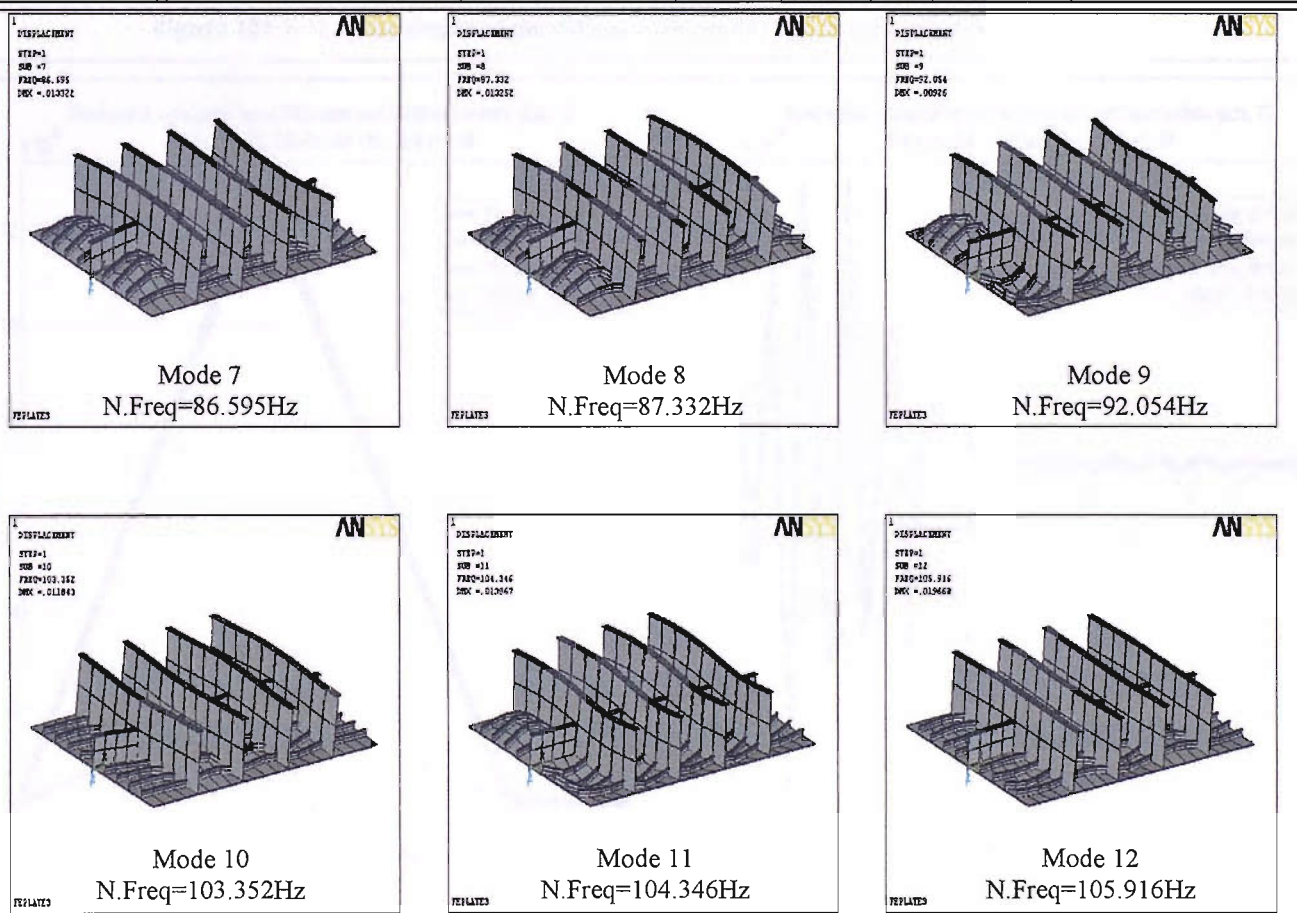


Figure 121 7-12 mode shapes of the stiffened (Beam-44) tanker plate

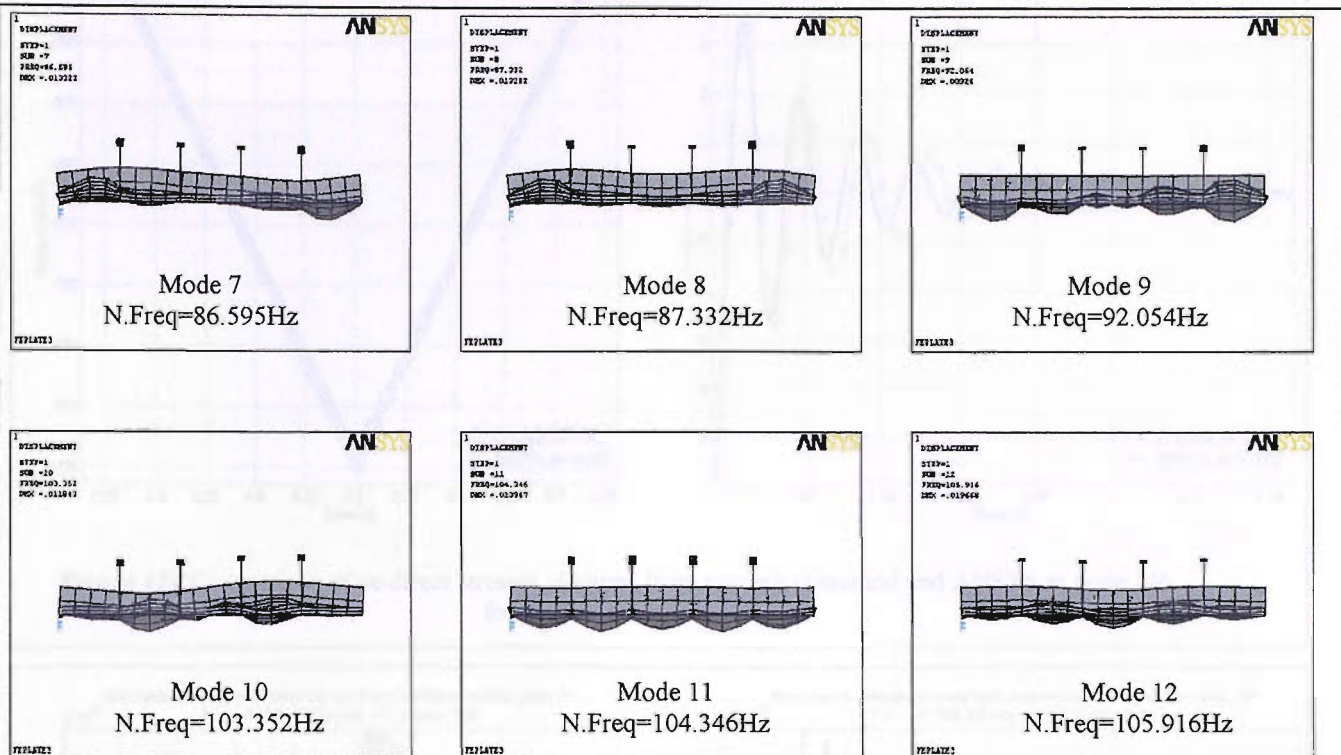


Figure 122 7-12 mode shapes of the stiffened (Beam-44) tanker plate (Profile view)

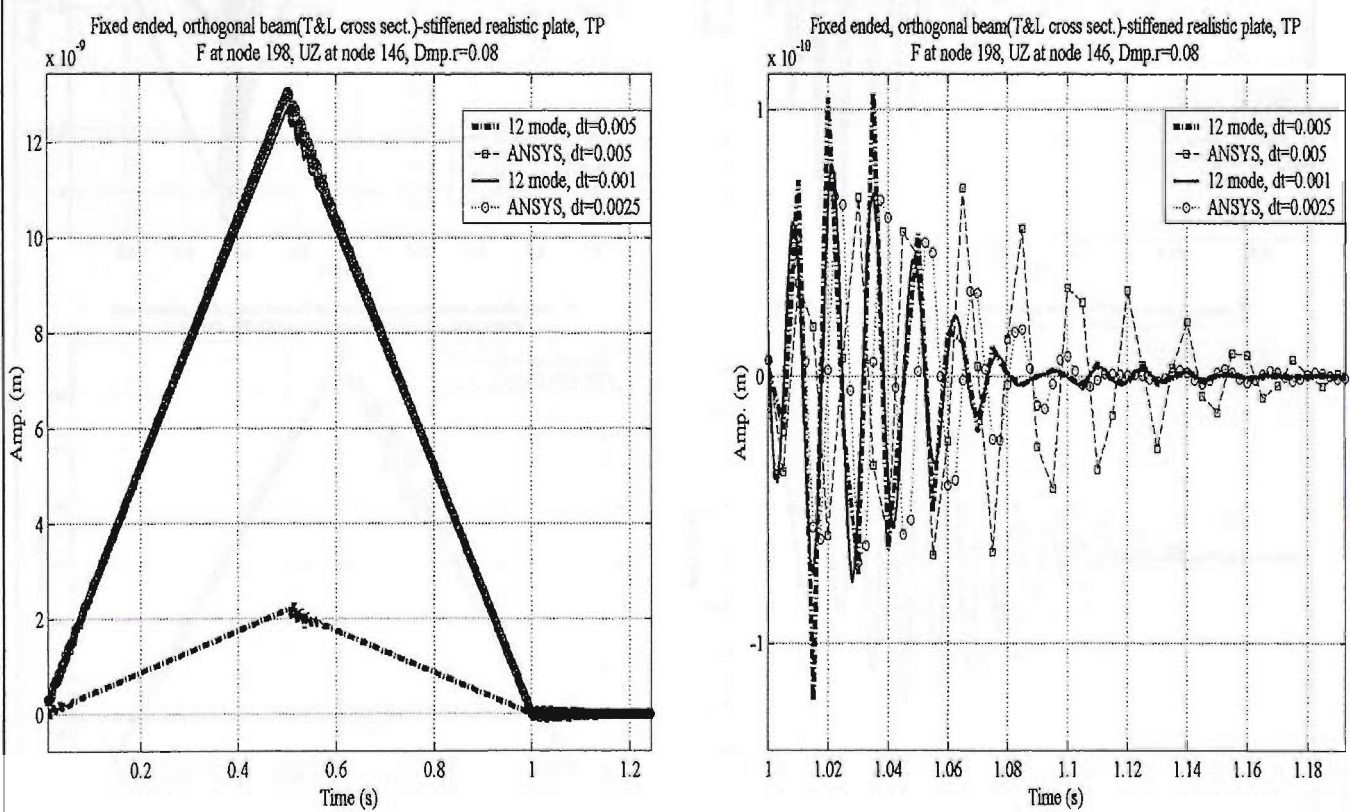


Figure 123 Comparison of uz-displacements obtained from numerical method and ANSYS at node 146 for stiffened tanker plate

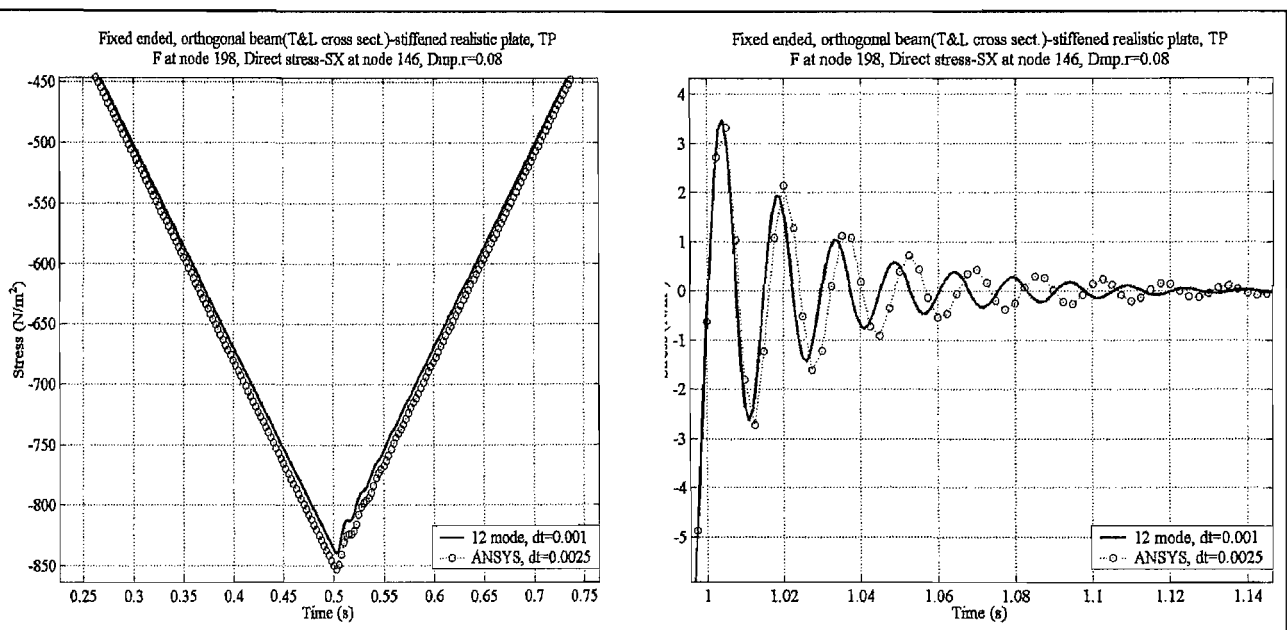


Figure 124 Comparison of sx-direct stresses obtained from numerical method and ANSYS at node 146 for stiffened tanker plate

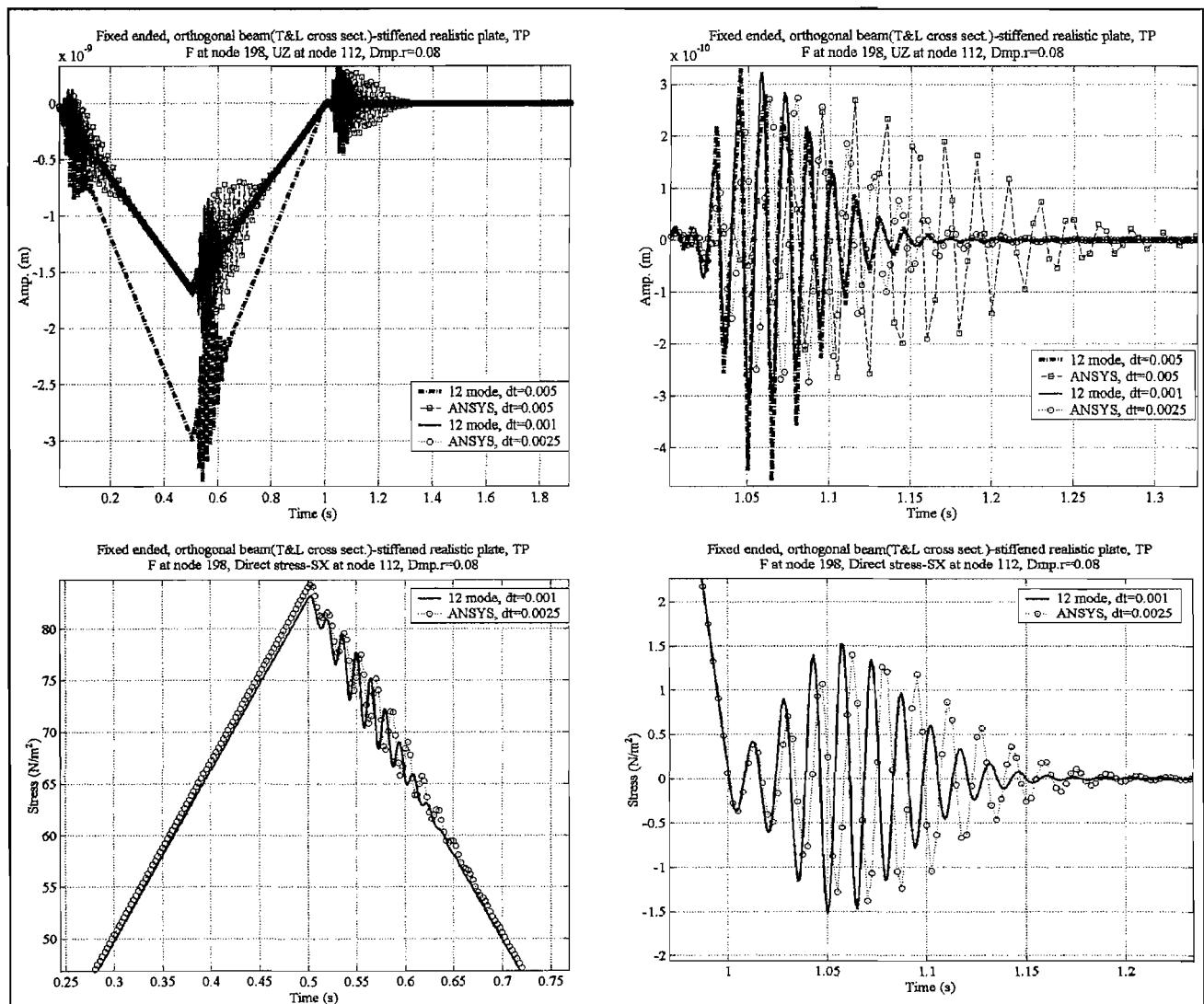
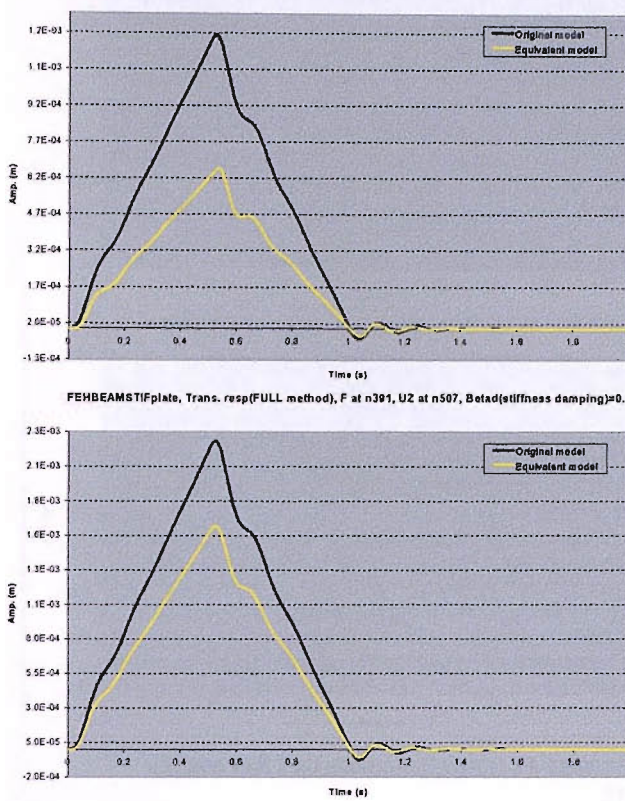
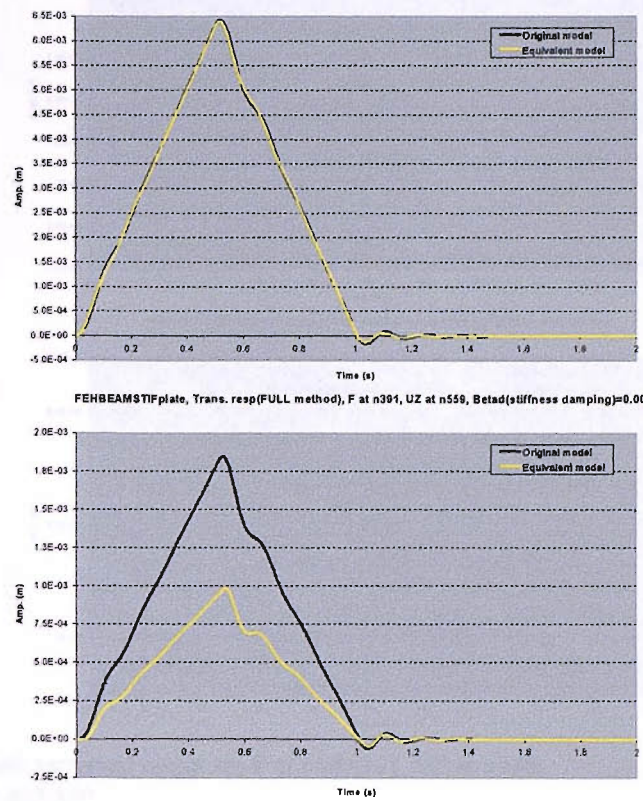


Figure 125 Comparison of uz-displacements & sx-direct stresses obtained from numerical method and ANSYS at node 112 for stiffened tanker plate

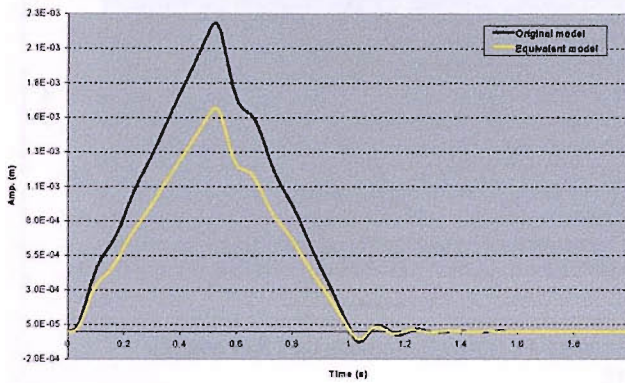
FEHBEAMSTIFplate, Trans. resp(FULL method), F at n391, UZ at n210, Belad(stiffness damping)=0.008



FEHBEAMSTIFplate, Trans. resp(FULL method), F at n391, UZ at n391, Belad(stiffness damping)=0.008



FEHBEAMSTIFplate, Trans. resp(FULL method), F at n391, UZ at n507, Belad(stiffness damping)=0.008



FEHBEAMSTIFplate, Trans. resp(FULL method), F at n391, UZ at n559, Belad(stiffness damping)=0.008

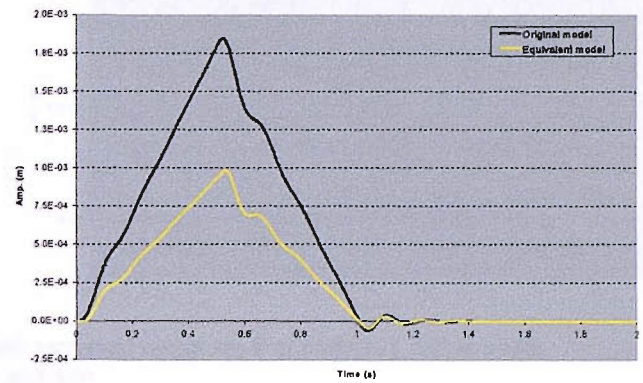
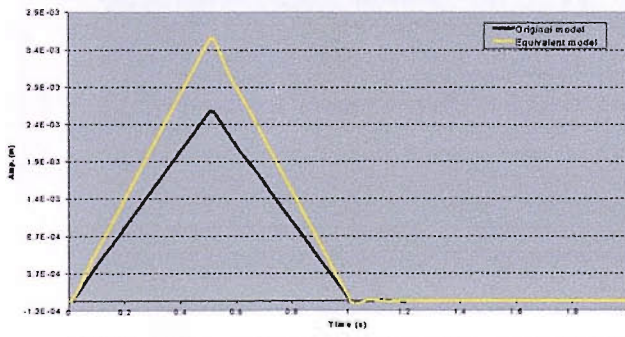
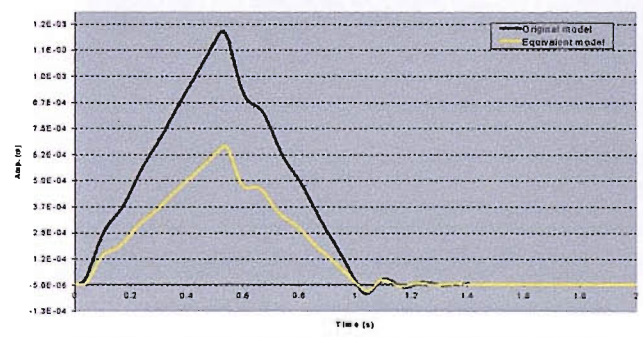


Figure 126 Full method-Original vs equivalent plate transient responses F at node 391, UZ at nodes 219,391,507,559

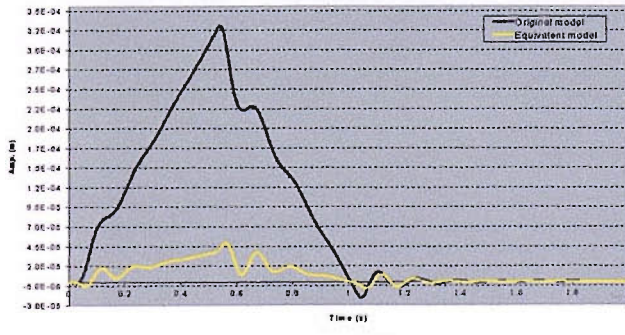
FEHBEAMSTIFplate, Trans. resp(FULL method), F at n219, UZ at n219, Belad(stiffness damping)=0.008



FEHBEAMSTIFplate, Trans. resp(FULL method), F at n219, UZ at n391, Belad(stiffness damping)=0.008



FEHBEAMSTIFplate, Trans. resp(FULL method), F at n219, UZ at n507, Belad(stiffness damping)=0.008



FEHBEAMSTIFplate, Trans. resp(FULL method), F at n219, UZ at n659, Belad(stiffness damping)=0.008

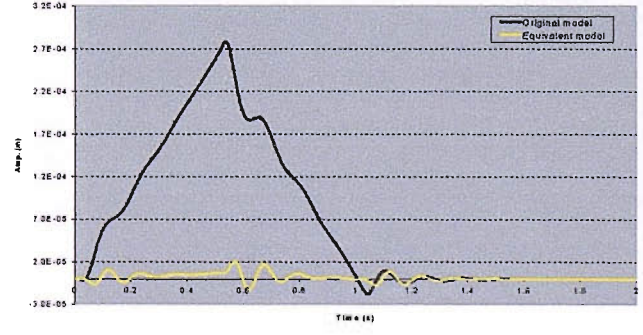


Figure 127 Full method-Original vs equivalent plate transient responses F at node 219, UZ at nodes 219,391,507,559

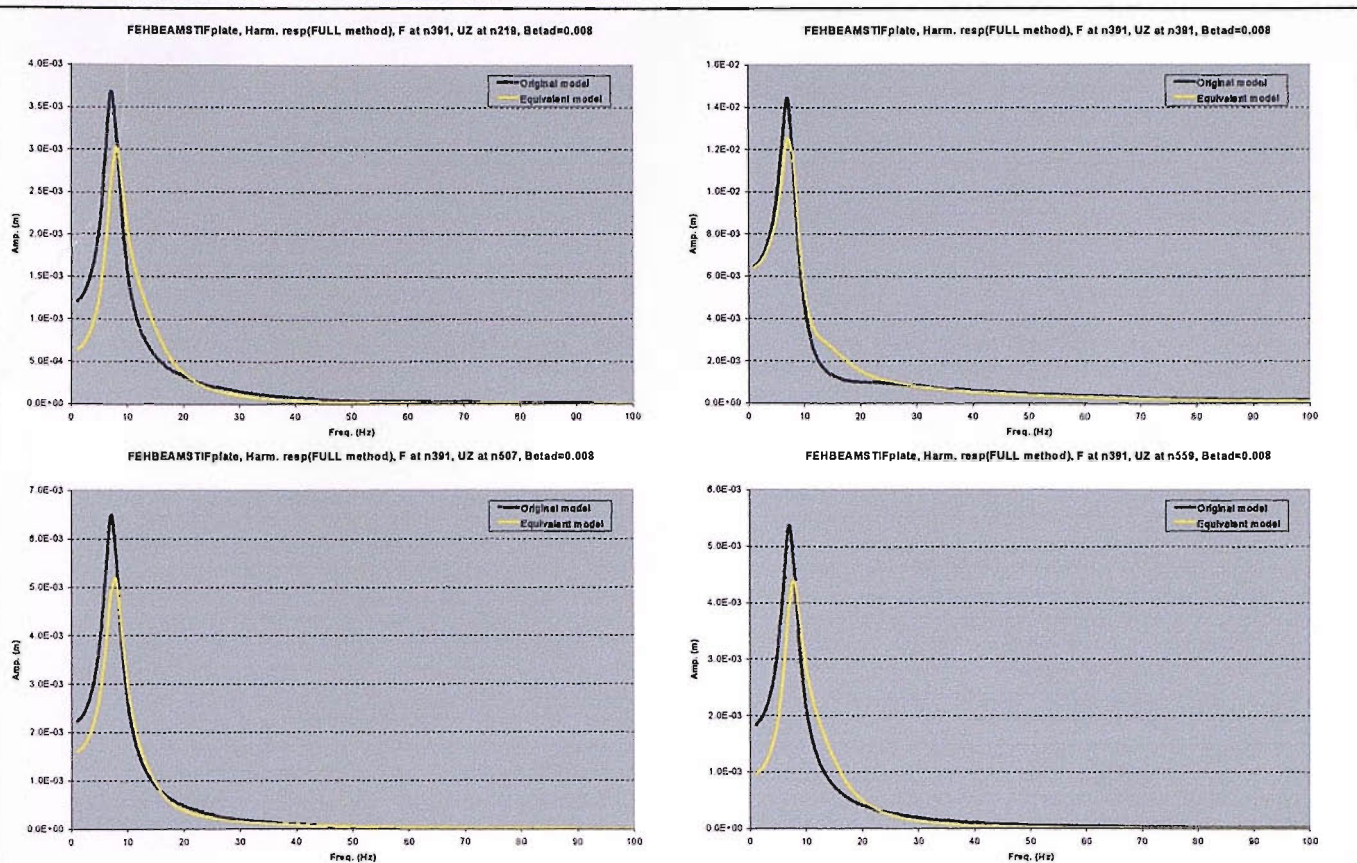


Figure 128 Full method-Original vs equivalent plate harmonic responses F at node 391, UZ at nodes 219,391,507,559

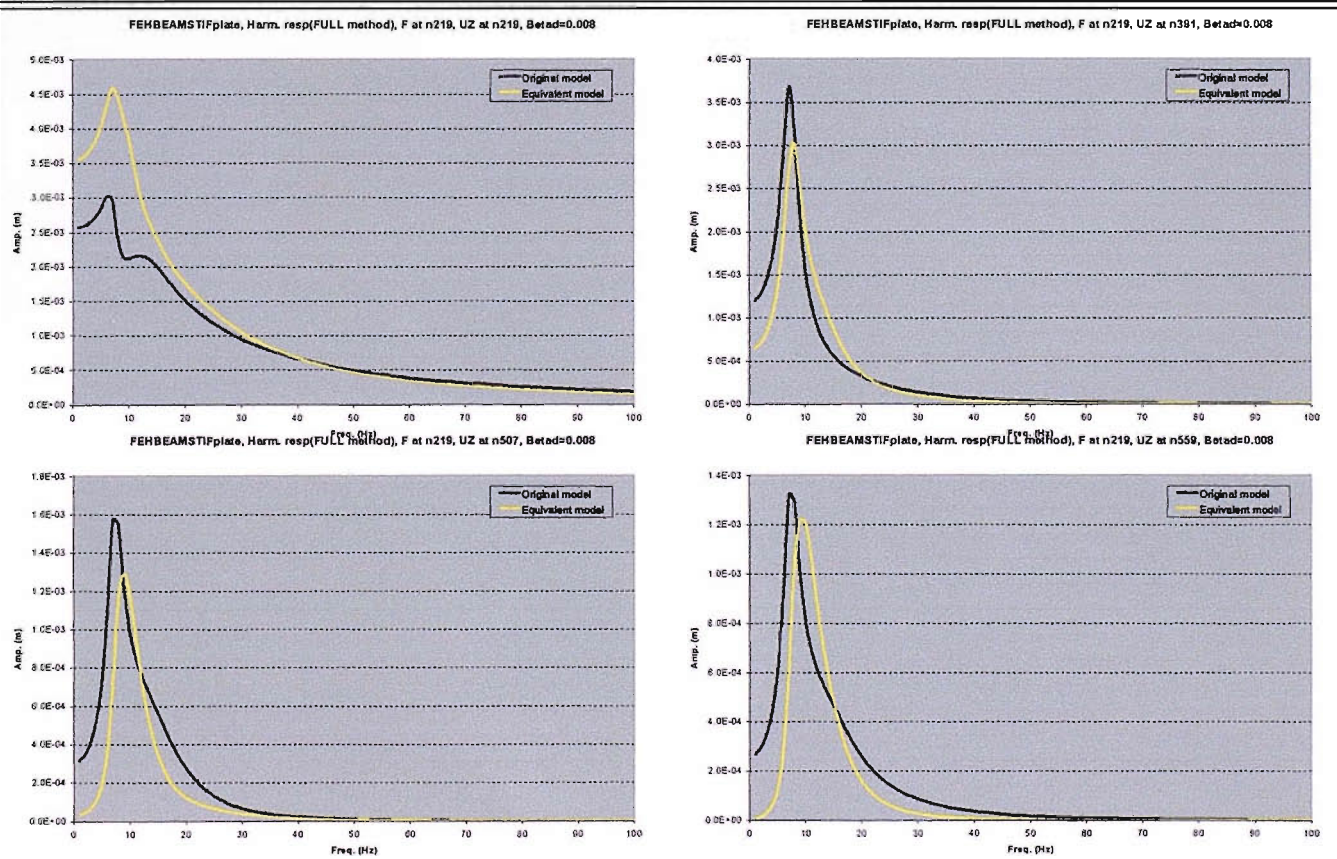


Figure 129 Full method-Original vs equivalent plate harmonic responses F at node 219, UZ at nodes 219,391,507,559